

7 JUNE 1967

3

17

LUNAR DUST DEGRADATION EFFECTS AND REMOVAL/PREVENTION CONCEPTS FINAL REPORT

GPO PRICE \$ _____

CFSTI PRICE(S) \$ _____

VOLUME II - DETAILED RESULTS

Hard copy (HC) 3.00

Microfiche (MF) .65

ff 653 July 65

Prepared for:
NATIONAL AERONAUTICS AND SPACE ADMINISTRATION
GEORGE C. MARSHALL SPACE FLIGHT CENTER
Propulsion And Vehicle Engineering Laboratory

UNDER CONTRACT NAS8-20116

NAS8-21079

FACILITY FORM 602

(ACCESSION NUMBER)

(THRU)

206
(PAGES)

1
(CODE)

94044
(NASA CR OR TMX OR AD NUMBER)

30
(CATEGORY)



NORTRONICS / HUNTSVILLE

NORTHROP CORPORATION

6025 TECHNOLOGY DRIVE, HUNTSVILLE, ALABAMA 35805

TELEPHONE 837-0580

P. O. BOX 1484

Ag 50478

LUNAR DUST DEGRADATION EFFECTS AND
REMOVAL/PREVENTION CONCEPTS

FINAL REPORT

Volume II - DETAILED RESULTS

Northrop/Huntsville Technical Report No. 323

7 June 1967

By

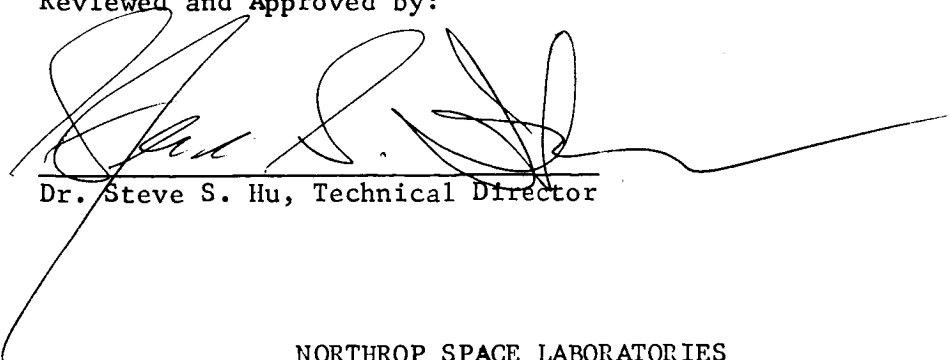
F. B. Tatom
Vanja Srepel
Dr. R. D. Johnson
N. A. Contaxes
J. G. Adams
H. Seaman
B. L. Cline

Prepared for:

NATIONAL AERONAUTICS AND SPACE ADMINISTRATION
GEORGE C. MARSHALL SPACE FLIGHT CENTER
PROPULSION AND VEHICLE ENGINEERING LABORATORY

Under Contract NAS8-20116

Reviewed and Approved by:



Dr. Steve S. Hu, Technical Director

NORTHROP SPACE LABORATORIES
HUNTSVILLE, ALABAMA

FOREWORD

The research effort described in this final report was performed by Northrop Space Laboratories for the Propulsion and Vehicle Engineering Laboratory of George C. Marshall Space Flight Center under Contract NAS8-20116. The report is composed of two volumes. The first volume represents a summary of the results of the investigation. Volume II presents a detailed description of the entire research effort. Mr. W. O. Randolph and Mr. W. B. McAnelly of the Fluid Mechanics and Thermodynamics Branch, Propulsion Division, served as the Contracting Officer's Representatives for the study.

In addition to those personnel appearing as co-authors of this report, several other individuals made significant contributions. Dr. E. Azmon served as an advisor on matters relating to the lunar surface and the characterization and preparation of simulated lunar dust. Mr. C. L. Densmore was responsible for all design work pertaining to the dust removal/prevention concepts and experimental models. Mr. E. W. Bentilla provided suggestions, based on heat transfer considerations, relative to the test apparatus and the design of the experiment.

7 June 1967

TABLE OF CONTENTS

<u>Section</u>	<u>Title</u>	<u>Page</u>
	FOREWORD.	ii
	LIST OF FIGURES	iv
	LIST OF TABLES.	vii
	LIST OF SYMBOLS	viii
I	INTRODUCTION	1-1
II	DUST DEGRADATION OF SURFACES	2-1
	2.1 BACKGROUND	2-1
	2.2 SELECTION OF DUSTS AND SURFACE COATING	2-7
	2.3 DUSTING PROCESS.	2-9
	2.4 MEASUREMENT OF ABSORPTANCE AND EMITTANCE	2-12
III	DUST REMOVAL/PREVENTION CONCEPT	3-1
	3.1 BACKGROUND	3-1
	3.2 MODEL TEST MATERIALS	3-4
	3.3 CONCEPTUAL DESIGN AND ANALYSIS.	3-4
	3.4 WORKING MODEL DESIGN	3-17
	3.5 PERFORMANCE TESTING	3-25
	3.6 ANALYSIS OF TEST DATA.	3-50
IV	CONCLUSIONS AND RECOMMENDATIONS	4-1
V	REFERENCES	5-1
VI	BIBLIOGRAPHY	6-1
	APPENDIX A EXPERIMENTAL DATA ASSOCIATED WITH MEASURE- MENT OF SURFACE SPECTRAL ABSORPTANCE OF DUST-CONTAMINATED THERMAL CONTROL COATINGS	A-1
	APPENDIX B NORTHROP SPACE LABORATORIES PRESENTATION LUNAR DUST REMOVAL/PREVENTION CONCEPT	B-1
	APPENDIX C ORIGINAL TEST DATA FOR DUST REMOVAL/PREVENTION DEVICES	C-1
	APPENDIX D INDEX OF ENGINEERING DRAWINGS.	D-1

7 June 1967

LIST OF FIGURES

<u>Figure No.</u>	<u>Title</u>	<u>Page</u>
2-1	THE GIER-DUNKLE INTEGRATING SPHERE REFLECTOMETER	2-14
2-2	MICROPHOTOGRAPHS OF BASALT DUST ON S-13 COATING.	2-15
2-3	EFFECT OF DUST ON SPECTRAL ABSORPTANCE IN SOLAR SPECTRUM OF S-13	2-18
2-4	VARIATION OF TOTAL SOLAR ABSORPTANCE WITH DUST COVERAGE OF S-13 PLATE	2-20
2-5	VARIATION OF TOTAL SOLAR ABSORPTANCE WITH ANGLE OF INCIDENCE FOR S-13 PLATE WITH AND WITHOUT DUST	2-24
2-6	EFFECT OF DUST ON SPECTRAL ABSORPTANCE OF ALUMINIZED TEFLON.	2-25
2-7	VARIATION OF TOTAL SOLAR ABSORPTANCE WITH DUST COVERAGE OF ALUMINIZED TEFLON PLATE.	2-26
2-8	VARIATION OF TOTAL SOLAR ABSORPTANCE WITH ANGLE OF INCIDENCE FOR ALUMINIZED TEFLON PLATE	2-29
2-9	SPECTRAL ABSORPTANCE IN SOLAR SPECTRUM FOR CLEAR SILICONE	2-31
2-10	PERKIN-ELMER 13 U SPECTROPHOTOMETER	2-32
2-11	SPECTRAL EMITTANCE IN THE INFRARED SPECTRUM FOR S-13 WITH AND WITHOUT BASALT DUST	2-33
2-12	SPECTRAL EMITTANCE IN THE INFRARED SPECTRUM FOR ALUMINIZED TEFLON WITH AND WITHOUT DUST	2-35
3-1	FLAT RADIATOR PANEL CONFIGURATIONS	3-2
3-2	NON-FLAT RADIATOR PANEL CONFIGURATIONS.	3-3
3-3	PRELIMINARY BRUSH CONCEPT	3-8
3-4	PRELIMINARY ELECTROSTATIC CURTAIN CONCEPT.	3-9
3-5	PRELIMINARY ELECTROSTATIC SURFACE CONCEPT.	3-10
3-6	PRELIMINARY JET AND SHIELD CONCEPT	3-11
3-7	PRELIMINARY JET AND SURFACE CONCEPT.	3-12

LIST OF FIGURES (Continued)

<u>Figure No.</u>	<u>Title</u>	<u>Page</u>
3-8	PRELIMINARY SPINNING SHIELD CONCEPT	3-13
3-9	PRELIMINARY VIBRATING SHIELD CONCEPT.	3-14
3-10	PRELIMINARY VIBRATING SURFACE CONCEPT	3-15
3-11	FINAL DESIGN FOR VIBRATING SURFACE DEVICE WITH V-47 VIBRATOR.	3-18
3-12	FINAL DESIGN FOR JET AND SHIELD DEVICE.	3-20
3-13	NOZZLES FOR JET AND SHIELD DEVICE	3-21
3-14	FINAL DESIGN FOR MECHANICAL BRUSH AND SHIELD DEVICE	3-23
3-15	ELECTROSTATIC CURTAIN INSERT.	3-24
3-16	NORTHROP 3.65 x 2.13 METER SPACE CHAMBER	3-26
3-17	CARBON ARC SOLAR SIMULATOR USED WITH SPACE SIMULATION CHAMBER	3-27
3-18	SOLAR SIMULATOR AND SPACE CHAMBER TEST ARRANGEMENT.	3-28
3-19	TEST PLATE ARRANGEMENT.	3-30
3-20	CALIBRATION TEST RUN FOR S-13 PLATE WITH 40% DUST COVERAGE.	3-32
3-21	FINAL DESIGN FOR JET AND PLATE DEVICE	3-34
3-22	TEST ARRANGEMENT FOR DETERMINATION OF OPTIMUM NOZZLE POSITION WITH INHIBISOL	3-38
3-23	FINAL DESIGN OF MECHANICAL BRUSH AND PLATE DEVICE	3-48
3-24a	TEMPERATURE VARIATION WITH HEAT LOAD (SOLAR SIMULATOR OFF) FOR CALIBRATION TEST RUN.	3-52
3-24b	TEMPERATURE VARIATION WITH HEAT LOAD (SOLAR SIMULATOR ON) FOR CALIBRATION TEST RUN.	3-53
3-25a	TEMPERATURE VARIATION WITH HEAT LOAD (SOLAR SIMULATOR OFF) FOR JET AND PLATE TEST RUN (FROZEN INHIBISOL)	3-54
3-25b	TEMPERATURE VARIATION WITH HEAT LOAD (SOLAR SIMULATOR ON) FOR JET AND PLATE TEST RUN (FROZEN INHIBISOL)	3-55

LIST OF FIGURES (Concluded)

<u>Figure No.</u>	<u>Title</u>	<u>Page</u>
3-26a	TEMPERATURE VARIATION WITH HEAT LOAD (SOLAR SIMULATOR OFF) FOR JET AND PLATE TEST RUN (LIQUID INHIBISOL)	3-56
3-26b	TEMPERATURE VARIATION WITH HEAT LOAD (SOLAR SIMULATOR ON) FOR JET AND PLATE TEST RUN (LIQUID INHIBISOL)	3-57
3-27a	TEMPERATURE VARIATION WITH HEAT LOAD (SOLAR SIMULATOR OFF) FOR JET AND GLASS SHIELD TEST RUN (LIQUID INHIBISOL).	3-58
3-27b	TEMPERATURE VARIATION WITH HEAT LOAD (SOLAR SIMULATOR ON) FOR JET AND GLASS SHIELD TEST RUN (LIQUID INHIBISOL).	3-59
3-28a	TEMPERATURE VARIATION WITH HEAT LOAD (SOLAR SIMULATOR OFF) JET AND ARSENIC-TRISULFIDE SHIELD TEST RUN (LIQUID INHIBISOL)	3-60
3-28b	TEMPERATURE VARIATION WITH HEAT LOAD (SOLAR SIMULATOR ON) JET AND ARSENIC-TRISULFIDE SHIELD TEST RUN (LIQUID INHIBISOL)	3-61
3-29a	TEMPERATURE VARIATION WITH HEAT LOAD (SOLAR SIMULATOR OFF) FOR VIBRATING SURFACE TEST RUN.	3-62
3-29b	TEMPERATURE VARIATION WITH HEAT LOAD (SOLAR SIMULATOR ON) FOR VIBRATING SURFACE TEST RUN.	3-63
3-30a	TEMPERATURE VARIATION WITH HEAT LOAD (SOLAR SIMULATOR OFF) FOR MECHANICAL BRUSH TEST RUN	3-64
3-30b	TEMPERATURE VARIATION WITH HEAT LOAD (SOLAR SIMULATOR ON) FOR MECHANICAL BRUSH TEST RUN	3-65
3-31	THERMAL NETWORK	3-69
3-32	CORRELATION OF DIMENSIONLESS PLATE TEMPERATURE θ_p FOR CALIBRATION TEST RUN (SOLAR SIMULATOR ON)	3-75
3-33	CORRELATION OF DIMENSIONLESS PLATE TEMPERATURE θ_p FOR JET AND PLATE TEST RUN (SOLAR SIMULATOR ON)	3-76
3-34	CORRELATION OF DIMENSIONLESS PLATE TEMPERATURE θ_p FOR JET AND ARSENIC-TRISULFIDE SHIELD TEST RUN (SOLAR SIMULATOR ON) .	3-77
3-35	CORRELATION OF DIMENSIONLESS PLATE TEMPERATURE θ_p FOR VIBRATING SURFACE TEST RUN (SOLAR SIMULATOR ON)	3-78
3-36	CORRELATION OF DIMENSIONLESS PLATE TEMPERATURE θ_p FOR MECHANICAL BRUSH TEST RUN (SOLAR SIMULATOR ON).	3-79

LIST OF TABLES

<u>Table No.</u>	<u>Title</u>	<u>Page</u>
2-1	DUST CHARACTERISTICS-SUMMARY OF LITERATURE SURVEY.	2-2
2-2	THERMAL CONTROL PAINT COATINGS.	2-5
2-3	SECOND-SURFACE MIRRORS COATINGS	2-6
2-4	VARIATION OF SOLAR ABSORPTANCE WITH DUST COVERAGE ON S-13 SAMPLES (8-MIL COATING ON ALUMINUM) . . .	2-19
2-5	TOTAL SOLAR ABSORPTANCE OF S-13 AT 20° AND 75° ANGLE OF INCIDENCE.	2-23
2-6	VARIATION OF SOLAR ABSORPTANCE WITH DUST COVERAGE ON ALUMINIZED TEFLON	2-27
2-7	TOTAL SOLAR ABSORPTANCE OF ALUMINIZED TEFLON AT 20° AND 75° ANGLE OF INCIDENCE	2-28
2-8	VARIATION OF TOTAL SOLAR ABSORPTANCE WITH DUST COVERAGE ON CLEAR SILICONE SAMPLES	2-30
2-9	EMITTANCE OF THERMAL CONTROL COATINGS	2-30
3-1	SUMMARY OF SPACE RADIATOR OPERATING CHARACTERISTICS.	3-5
3-2	DATA FOR CALIBRATION TEST RUN	3-33
3-3	OPTIMUM NOZZLE POSITION TEST RESULTS.	3-39
3-4a	DATA FOR JET CONCEPT TEST RUN WITHOUT SHIELD . . .	3-40
3-4b	DATA FOR JET CONCEPT TEST RUN WITHOUT SHIELD . . .	3-41
3-5	DATA FOR JET CONCEPT TEST RUN WITH GLASS SHIELD . . .	3-43
3-6	DATA FOR JET CONCEPT TEST RUN WITH ARSENIC TRISULFIDE SHIELD	3-44
3-7	DATA FOR VIBRATING PLATE TEST RUN.	3-47
3-8	DATA FOR MECHANICAL BRUSH CONCEPT.	3-49
3-9	PLATE TEMPERATURE AFTER CLEANING BY DUST REMOVAL DEVICES	3-66
3-10	RADIATIVE PROPERTIES OF DUST, PLATE, AND SHIELD . . .	3-80

LIST OF SYMBOLS

ENGLISH

<u>Symbol</u>	<u>Definition</u>	<u>Units</u>
A_g	area of shield	sq cm
A_p	area of plate	sq cm
E_p	emissive power of plate	watts/sq cm
E_s	emissive power of solar simulator	watts/sq cm
$E_{g(r)}$	emissive power of shield over $2\mu - \infty$ range	watts/sq cm
$E_{g(s)}$	emissive power of shield over 0- 2μ range	watts/sq cm
$E_{p(r)}$	emissive power of plate over $2\mu - \infty$ range	watts/sq cm
$E_{p(s)}$	emissive power of plate over 0- 2μ range	watts/sq cm
$E_{s(r)}$	emissive power of solar simulator over $2\mu - \infty$ range	watts/sq cm
$E_{s(s)}$	emissive power of solar simulator over 0- 2μ range	watts/sq cm
$E_{w(r)}$	emissive power of chamber walls over $2\mu - \infty$ range	watts/sq cm
$E_{w(s)}$	emissive power of chamber walls over 0 - 2μ range	watts/sq cm
F_{gp}	shape factor for radiation from shield to plate	-
F_{gs}	shape factor for radiation from shield to solar simulator	-
F_{gw}	shape factor for radiation from shield to walls	-
F_{pg}	shape factor for radiation from plate to shield	-

LIST OF SYMBOLS (Continued)

ENGLISH

<u>Symbol</u>	<u>Definition</u>	<u>Units</u>
F_{ps}	shape factor for radiation from plate to solar simulator	-
F_{pw}	shape factor for radiation from plate to walls	-
G_s	solar constant	watts/sq cm
$J_{p(r)}$	radiosity of plate over $2\mu - \infty$ range	watts/sq cm
$J_{p(s)}$	radiosity of plate over $0 - 2\mu$ range	watts/sq cm
$J_{gl(r)}$	radiosity of shield surface no. 1 over $2\mu - \infty$ range	watts/sq cm
$J_{gl(s)}$	radiosity of shield surface no. 1 over $0-2\mu$ range	watts/sq cm
T_p	plate temperature	$^{\circ}K$
q_p	plate power	watts
q_p''	plate power per unit area	watts/sq cm
X	fraction of total plate or shield surface that has dust cover	-

GREEK

$\alpha_{d(r)}$	absorptance of dust over $2\mu - \infty$ range	-
$\alpha_{d(s)}$	absorptance of dust over $0 - 2\mu$ range	-
$\alpha_{g(r)}$	absorptance of shield over $2\mu - \infty$ range	-

LIST OF SYMBOLS (Continued)

GREEK

<u>Symbol</u>	<u>Definition</u>	<u>Units</u>
$\alpha_{g(s)}$	absorptance of shield over 0-2 μ range	-
$\alpha_{g1(r)}$	absorptance of shield surface no. 1 over 2 μ - ∞ range	-
$\alpha_{g1(s)}$	absorptance of shield surface no. 1 over 0-2 μ range	-
$\alpha_{g2(r)}$	absorptance of shield surface no. 2 over 2 μ - ∞ range	-
$\alpha_{g2(s)}$	absorptance of shield surface no. 2 over 0-2 μ range	-
α_s	solar absorptance of thermal control surface	-
$\epsilon_{g1(r)}$	emittance of shield surface no. 1 over 2 μ - ∞ range	-
$\epsilon_{g1(s)}$	emittance of shield surface no. 1 over 0-2 μ range	-
$\epsilon_{g2(r)}$	emittance of shield surface no. 2 over 2 μ - ∞ range	-
$\epsilon_{g2(s)}$	emittance of shield surface no. 2 over 0-2 μ range	-
$\epsilon_p(r)$	emittance of plate over 2 μ - ∞ range	-
$\epsilon_p(s)$	emittance of plate over 0-2 μ range	-
ϵ_r	infrared emittance of thermal control surface	-
θ_p	dimensionless plate temperature = $T_p (\sigma/G_s)^{1/4}$	-
$\rho_{d(r)}$	reflectance of dust over 2 μ - ∞ range	-
$\rho_{d(s)}$	reflectance of dust over 0-2 μ range	-
$\rho_{g(r)}$	reflectance of shield over 2 μ - ∞ range	-
$\rho_{g(s)}$	reflectance of shield over 0-2 μ range	-
$\rho_{g1(r)}$	reflectance of shield surface no. 1 over 2 μ - ∞ range	-

LIST OF SYMBOLS (Concluded)

GREEK

<u>Symbol</u>	<u>Definition</u>	<u>Units</u>
$\rho_{g1(s)}$	reflectance of shield surface no. 1 over 0- 2μ range	-
$\rho_{g2(r)}$	reflectance of shield surface no. 2 over $2\mu - \infty$ range	-
$\rho_{g2(s)}$	reflectance of shield surface no. 2 over 0- 2μ range	-
$\rho_p(r)$	reflectance of plate over $2\mu - \infty$ range	-
$\rho_p(s)$	reflectance of plate over 0 - 2μ range	-
σ	Stefan-Boltzman constant	watts/sq cm °K
$\tau_g(r)$	transmittance of shield over $2\mu - \infty$ range	-
$\tau_g(s)$	transmittance of shield over 0- 2μ range	-
$\tau_{g1(r)}$	transmittance of shield surface no. 1 over $2\mu - \infty$ range	-
$\tau_{g1(s)}$	transmittance of shield surface no. 1 over 0- 2μ range	-
$\tau_{g2(r)}$	transmittance of shield surface no. 2 over $2\mu - \infty$ range	-
$\tau_{g2(s)}$	transmittance of shield surface no. 2 over 0- 2μ range	-

SUBSCRIPTS

d	dust
g	shield
p	plate
s	solar simulator
w	wall
(r)	refers to range of spectrum from 2μ to ∞
(s)	refers to range of spectrum from 0 to 2μ
1	refers to side of shield facing solar simulator
2	refers to side of shield facing plate

SECTION I

INTRODUCTION

A significant problem associated with spacecraft designed for lunar exploration is the dissipation of excess heat generated by the primary power supply, the electronics, and the environmental control system. Finned-tube thermal radiators and similar radiator surfaces represent the most widely accepted means of rejecting or dissipating such heat. Radiator surfaces of this type generally have a thermal control coating with a high value of infrared emittance (~ 0.8) coupled with a low value of solar absorptance (~ 0.2). Changes or degradation of the surface properties of these coatings may increase the value of both infrared emittance and solar absorptance. Such effects can in turn upset the balance of the heat rejection system and jeopardize the entire mission of the spacecraft.

One possible source of degradation of thermal control coatings located near the lunar surface is dust or small particulate debris which may settle on radiator panel surfaces. There has been considerable conjecture concerning the existence of a layer of dust on the lunar surface. The actual presence or absence of such dust on the lunar surface has not been established. However, the most recent results from Surveyor I and III (refs. 1 and 2) indicate a porous, soil-like surface in the vicinity of those spacecraft. Such surface characteristics are certainly compatible with the concept of dust. Furthermore, the manner in which the lunar surface temperature has been observed to vary with time is characteristic of a surface covered by a poor thermal conductor such as dust or powder. If dust is present, whether in a layer one-centimeter deep or 10-meters deep, the possibility of contamination of radiator surfaces will still exist. Thus, until positive evidence

establishes the presence or completely eliminates the possibility of dust, the designer or lunar systems must give consideration to possible dust contamination of radiator surfaces.

Any dust which might settle on a radiator surface will have been displaced from its original location on the lunar surface by some disturbance. This disturbance may be (1) the exhaust from a rocket vehicle such as the Lunar Excursion Module (LEM) or the Manned Flying System (MFS); (2) the wheels or treads of a surface vehicle such as the Mobile Lunar Laboratory (MOLAB) or the Local Scientific Survey Module (LSSM); (3) the movements of astronauts in their walking on the lunar surface; or (4) the impact of micrometeorites, each of which may produce $\sim 10^3$ secondary ejecta from the lunar surface.

Northrop Space Laboratories, Huntsville, Alabama, and Northrop Systems Laboratories, Hawthorne, California, under Contract NAS8-20116 with the Propulsion & Vehicle Engineering Laboratory of Marshall Space Flight Center, have been engaged in a research effort concerned with determining the effect of dust on radiator surfaces and developing methods for preventing or removing accumulations of dust from such surfaces. Section II of this volume provides a detailed discussion of the investigation relating to the degradation of a radiator surface due to dust. Section III describes that portion of the research effort devoted to the development of techniques for preventing or removing dust from a radiator surface in a simulated lunar environment. Conclusions and recommendations based on the results of the investigation are presented in Section IV, with all references cited in Section V. A number of appendixes are also provided which contain the original experimental data.

SECTION II

DUST DEGRADATION OF SURFACES

The first portion of the research effort was directed toward establishing the effects of dust on the thermal properties of representative radiator surfaces. The major objective of this work was to establish the manner in which the spectral and total solar absorptance and infrared emittance varied with the amount of dust contamination. Also, the variation of solar absorptance with angle of incidence was of interest.

2.1 BACKGROUND

A literature survey was conducted to obtain information relative to the effects of dust on radiator surfaces. Aside from data obtained by Northrop during preliminary studies, very little material on this subject was located. The scope of this literature survey is indicated by listings contained in the Bibliography as well as in the References Cited.

Before attempting to establish experimentally the effects of dust on a radiator surface, a thorough understanding of the types of dust which are considered likely to occur on the lunar surface must be acquired. Also an awareness of the current trends in thermal control coatings for space lunar vehicles is necessary.

2.1.1 Lunar Surface Characteristics

A number of previous studies have been carried out concerning the characteristics of the lunar surface (refs. 3 through 12). These studies generally fall into one of two types: One type includes theoretical determination of the nature of the lunar dust, and the second includes laboratory experiments on specific dusts under assumed lunar conditions. Table 2-1 summarizes nine recent studies showing the reference, instrumentation (when applicable), rock identification (composition and texture), degree of vacuum considered or obtained, and type of experiment conducted (if any).

Table 2-1. DUST CHARACTERISTICS SUMMARY OF LITERATURE SURVEY

Author	Date	Reference	Instruments	Rocks			Notes
				Identification	Texture	Vacuum	
Salisbury, J.W. Glaser, F.E. Stein, B.A. Vonnegut, B.	1964	J.F.R. V-1-69 #2, pp. 235-242 Adhesive Behavior of Silicate Powders in Ultrahigh Vacuum.	Oil dif Pumps WC ballmill in dry Argon	Chondrite Tekitte Obsidian Basalt Andesite Dunite Progenite	80% of gr. < 3 μ di 90% < 17 μ 99% < 70 μ	10 ⁻⁹ - 10 ⁻¹⁰ torr	VanderWaals and Electrostatic experiments
Bennett, E.C. Wood, H.L. Jafie, L.D. Martens, R.F.	1963	AIAA Jour. Vol. 1, #6, pp. 1402- 1407 Thermal Properties of Simulated Lunar Material in Air or in Vacuum.	Mechanical + Oil dif pump. 12" glass jar, 11q. N 15 KW heating coil, copper cooling coil	Olivine Basalt Silica Sand	80% < 75 μ 90% < 100 μ 80% < 300 μ 90% < 400 μ	5 x 10 ⁻⁶ torr	Thermal conductivity
Walker, E.R.	1965	AGU 46 Annual Mtg. Lunar Dust Clouds Produced by the Impact of Space Vehicles & Meteoric Bodies	Calculations based on Ranger's No Cloud and Lunic II Cloud	--	50 - 300 μ	(Moon)	
McCracken, C.W. Dubin, M	1963	NASA Technical Note NASA TN D-2100 21 pp. Dust Bombardment on the Lunar Surface	Analysis of Micro- meteorite and meteorite data	(Lunar & Cosmic Composition)	In the order of 10 μ	(Moon)	Abundance of dust apparently present
Ryan, J. A.	1965	OART Contract NAS7-307, 4th qtrly rept. Experimental Investigation of Ultra-High Vacuum Adhesion as related to Lunar Surface	Vacuum Chamber Heater & Cooler (100° - 400°K)	Orthoclase Albite Hypersthene		2-4 x 10 ⁻¹⁰ torr	Load force and temperature effect on vacuum adhesion
Naughton, J.J. Barnes, I.L. Hammond, D.A. (A.D. Little Inc. Cambridge, Mass.)	1965	Science, Vol. 149, pp. 630-631 Rock degradation by Alkali Metal: A possible Lunar erosion mechanism		Basic Acidic	Powder(faster powdering) Powder(slower powdering) Both, Same dia as component crystals	(Vacuum)	Attack by alkali metals Na+K released by melting may cause powdering on the Moon
Gramia, P.D.	1961	NSFC, Huntsville, Ala., Contract NAS8-4377, Study of Cryogenic Storage on the Moon	A surface of diffusely reflecting material	Quartz			α/ϵ ratio increase X 3 by quartz deposit. Bad for cryogenic storage
Stein, B.A. Johnson, P.C.	1964	JGR, Vol. 66, #12, pp. 4293- 4299 Electrostatic Erosion Mechanism on the Moon	Statistical Analysis of charge build up	Silica	Spheres 5- μ dia.	(Vacuum)	Levitation of positively charged particles above the surface & "downhill" gliding
	1964	The Lunar Surface, Material and Charact. Academic Press, 532 pp. Ed. by Salisbury and Glaser. Invest. of Soil Adhesion under High Vacuum. pp. 93-110.	Mechanism for sifting powder inside chamber. Impacting cantilever beams. Heater (100°C)	Olivine Obsidian	100 - 140- μ dia.	(10 ⁻¹¹ torr (in 12 hours) empty 1.3 x 10 ⁻⁹ torr - 6.3 x 10 ⁻¹⁰)	Adhesion to beam. Adhesion function of particle size.

7 June 1967

Based on these preceding studies, certain conclusions can be drawn regarding both the composition and texture of possible lunar dust material. Most of the characteristics described in previous studies would be covered if one acidic rock and one basic rock of terrestrial origin and their extraterrestrial equivalents were selected for investigation. Typical examples of terrestrial rock are granite (acidic) and basalt (basic). Typical examples of extraterrestrial rock are tektite (acidic) and chondrite (basic). Estimates of texture cover a broad range with lower limits ranging from 5 to 50 microns and upper limits from 300 to 500 microns.

In the case of dust generated from basalt, grain size range and distribution appear to have compositional significance as well as mechanical significance. For example, typical basalt is composed of, 1) iron-magnesium silicates such as olivines and pyroxenes and amphiboles, and 2) sodium-calcium-aluminum silicates such as albite and anorthite. The minerals in the first group are more or less ferromagnetic, have higher specific gravity than the second group, and are commonly more abundant in the finer grain size fractions of a dust. The minerals in the second group are nonmagnetic, have lower specific gravity, and are commonly more abundant in the coarser grain size fractions of a dust. Sorting the mixed dust into grain sizes obviously increases the concentration of the iron-magnesium silicates in the finer fractions. On the lunar surface, in the absence of a lunar magnetic field, it is conceivable that such ferromagnetic dust particles will be attracted in the direction of any artificial body that has its own magnetic or electromagnetic field.

2.1.2 Thermal Control Coatings Characteristics

A number of thermal control coatings are currently under consideration for use on lunar vehicles. All of these coatings possess high values of infrared emittance (ϵ_r) and low values of solar absorptance (α_s). In general, these coatings may be

classified as either pigmented compositions (paint) or second-surface mirrors.

Table 2-2 presents a summary of current pigmented coatings while Table 2-3 provides similar data for two promising second-surface mirrors.

The selection of a thermal control coating to be applied to radiator panels in order to evaluate lunar dust removal/prevention concepts is governed by the requirements for specified optical, thermal, and mechanical properties and the stability or minimal changes of these properties under the imposed environmental and operational conditions. In addition to ultraviolet stability, coatings should exhibit minimal erosion due to lunar dust impingement, micrometeoroid and secondary ejecta bombardment, or sputtering and pit formation as a result of low-energy proton impingement.

With the dust removal/prevention problem taken into account, an ideal surface coating should exhibit the following characteristics:

Optical and Thermal Characteristics

1. Low α_s/ϵ_r ratio of the order of 0.22 with an α_s of the order of 0.20 or less.
2. Spectrally selective for heat rejection from the radiator surface at a specified operating temperature.
3. Stable for lunar operation periods extending for 6 months, resulting in an approximate ESH (equivalent sun hours) or exposure of 2000 hours.
4. Minimum degradation of surface due to the thermal-solar (ultra-violet) irradiation conditions, and a known or predictable value of $\Delta\alpha_s$ and of $\Delta\epsilon_r$ due to this effect.
5. Maximum thermal conductivity for heat transmission to the emitting surface.

Physical and Mechanical Properties (Surface and Bulk)

1. Smoothness or low surface roughness to minimize dust entrapment and possible erosion and to provide minimum actual surface area.

Table 2-2. THERMAL CONTROL PAINT COATINGS

<u>No.</u>	<u>Coating</u>	<u>Vehicle</u>	<u>Pigment</u>	α_s	$\epsilon_r @ 294^{\circ}K$	Solar UV Stability 2000 hrs	$(\Delta\alpha_s)$ 4000 hrs
1	S-13 (IIT)	RTV602 (methyl siloxane)	ZnO(SP-500)	0.18	0.89	---	0.02 (also 8000 hrs)
2	Z-93 (IIT)	K silicate	ZnO	0.165	0.86	---	0.014 (4200 hrs)
3	LMSC	K silicate	Li-Al-Silicate (Lithafrax)	0.122	0.91	---	0.17
4	LMSC (Lockpaint) or STL (MT6-2)	K silicate	ZnO ₂	0.127	0.91	---	-- (stable)
5	Dow Corning 9-0090 (Lockheed)	DC92009 (methyl silicone)	TiO ₂	0.166	0.91	.02	.02 (3000 hrs)

Notes: 1) For 6-months storage solar UV exposure is approximately equivalent to 2200 hours (half of full time).

2) TiO₂-Acrylic combinations (Lockheed) show a $\Delta\alpha_s$ of +0.09 from an $\alpha_s = 0.24$ after 436 ESH (equivalent sun hours) exposure indicating inadequate UV stability for the acrylic system.

3) Radiation environment (lunar) due to cosmic rays expected to be about 10^4 (well below 1 megarad level) rads for 1-year exposure. Above coatings are generally qualified to this radiation level. S-13 and Z-93 are expected to be stable in the environment.

4) The Dow Corning formula No. 5 may have special merit for formula modification to improve physical properties because of the 10/1 ratio (relatively high) of resin/catalyst for curing the vehicle.

Table 2-3. SECOND-SURFACE MIRRORS COATINGS

<u>Description</u>	<u>Substrate</u>	<u>Coating</u>	<u>Adhesive</u>	α_s	ϵ
Aluminized, FEP Teflon (Type A)	Aluminum ($\sim 1\mu$ thickness) vacuum-deposited onto coating	Teflon (5 mils thickness)	Q3-0121 (bonds to mirror rad- iator panel)	.19	.85
Clear silicone on aluminum substrate	Alclad 2024 aluminum (radiator panel)	Dow Corning-93022 (3 mils thickness)	Dow Corning 281	.29	$\sim .8$

2. Absence of porosity to provide a cleanable and low dust-collecting surface.
3. High wear or abrasion resistance. For plastics this can be expressed in terms of two parameters: indentation hardness, and extensibility (or toughness). For elastic-isotropic materials hardness bears a relation to Young's modulus. Extensibility reflects both elongation and ultimate tensile strength. The change in hardness and/or toughness characteristics at the generating temperature, especially for coatings with a rubbery polysiloxane matrix, must not impair the function of the dust removal/prevention technique. Scratch resistance is desirable to reduce the appearance of angularity effects which may increase the value of α_s , and to avoid lattice distortion with consequent mechanical yellowing in pigments such as zinc oxide.
4. Low frictional resistance or low adhesion for dust particles due to specific polymeric structure. (e.g., The static coefficient of friction for Teflon in air is 0.04 whereas soft rubbers have a value up to 4 or more).
5. High flexibility, as determined by mandrel bend tests.
6. Good thermal cycling and shock resistance to withstand temperature cycling tests from 111°K to the specified operating temperature.
7. High tensile strength and elongation.
8. Good adhesion of coating or film to substrate, measured by pull or tensile shear test.

2.2 SELECTION OF DUSTS AND SURFACE COATING

The experimental investigation was not designed to cover all possible dust materials and thermal control coatings. The necessity thus arose for selection of representative dust materials and thermal coatings. In this selection process

certain factors had to be considered. These included availability of material, state-of-the-art for fabrication, consistency or reproducibility of characteristics, and compatibility with experimental procedures and objectives.

2.2.1 Dust Material

Because it was expected that dust of either terrestrial or extraterrestrial origin would degrade the radiator performance in a similar manner, only terrestrial dusts were seriously considered for the experimental program. The solar reflectance of basalt is lower than that of granite. Therefore the effect of the basalt dust was regarded as equivalent to that of the "worst" expected contamination by lunar dust. The solar reflectance of basalt (0.12) is also close to the average lunar albedo (0.10, ref. 13). For these reasons basalt was selected for the dust material.

Because of the disparity in available estimates of lunar-dust-particle size and distribution, the decision was made not to attempt to simulate such size and distribution. Instead a well-characterized powder was to be selected from a narrow cut of a specific particle size obtained via conventional sieves and from the finer ill-sorted fraction which passes the smallest available screen size (37 microns).

2.2.2 Thermal Control Coating

Out of the coatings listed in Tables 2-2 and 2-3, four coatings, which were considered representative of the current state-of-the-art, were selected for final evaluation. These four, all of which appeared to be ultraviolet-stable coatings, were S-13, Z-93, aluminized FEP Teflon (type A), and clear silicone (Dow Corning 93-022) cured on a polished aluminum surface. The porous nature of Z-93, combined with certain difficulties associated with its application, resulted in the elimination of Z-93.

Difficulty was encountered in achieving good adhesion to aluminum by the clear silicone (Dow Corning 93-002). This difficulty, coupled with the fact that its solar absorptance is considerably higher than that of the other three coatings, resulted in eliminating this type of second-surface mirror.

Some difficulty was encountered in attaching the aluminized Teflon to the aluminum plate of the radiator. The commercially available aluminized Teflon was easily damaged in handling and the resulting scratches degraded its optical properties. In addition a wide spread of solar absorptance values was obtained from coated samples. For these reasons, aluminized Teflon was not selected as the primary thermal control coating.

The remaining coating, S-13, appeared to have reproducible properties and could be applied to aluminum panels without significant difficulty. These considerations, coupled with the fact that S-13 is nonporous and relatively durable, resulted in the selection of this coating as the primary thermal control coating to be tested.

It should be noted that while aluminized Teflon was not selected as the primary thermal control coating, it demonstrated a minimum tendency to collect dust. The S-13 coating, however, exhibited an unfortunate affinity for dust, which was obviously undesirable. For this reason, and also to provide some basis for a comparison, the decision was reached to carry out a secondary degradation investigation using aluminized Teflon as the thermal control coating. In subsequent portions of this report a limited amount of data is provided describing the effects of dust contamination of aluminized Teflon as well as S-13. A small amount of data relating to contamination of the clear silicone also is included.

2.3 DUSTING PROCESS

Crushed basalt was obtained by means of a grinding operation involving grinding the material against itself in a special rubber-lined mill to minimize any contamination from foreign media. The basalt powder was then sieved by means of a sieve-shaker

apparatus through a series of screens to obtain fraction in specific particle-size ranges. The fractions thus obtained were:

larger than 500 μ ,
500 μ to 250 μ ,
250 μ to 125 μ ,
125 μ to 105 μ ,
105 μ to 74 μ ,
74 μ to 62 μ ,
62 μ to 53 μ ,
53 μ to 44 μ ,
44 μ to 37 μ ,
and smaller than 37 μ .

The largest fraction of dust produced by the grinding method was found to be in the 44 μ to 53 μ size range.

Notice should be taken that complete separation into the fractions listed could not be achieved. The primary reason for this lack of complete separation appeared to be the agglomeration of smaller particle with diameters $\sim 10\mu$ promoted by rapid moisture absorption. Fortunately, early in the experimental work, the percentage of surface covered by dust proved to be the primary factor in the degradation of the surface properties. Neither particle-size distribution nor the total weight of the dust proved to be significant parameters. For this reason, it became unnecessary to control particle-size distribution as an experimental parameter in the measurement of solar absorptance.

Two settling techniques (liquid and dry) were considered as a means of dust application. Liquid settling techniques usually resulted in more uniform particle distribution in the settled layer than that obtained by dry settling. In preliminary work it became evident that due to perfect dispersion of fines (particle size $\leq 2\mu$) present in all lower particle-size cuts, the dust coverage of the sample becomes difficult to determine (particle size is smaller than the resolving limit of the

microscope) and that the even coverage of "colloidal" particles had a stronger effect on reflectivity than "normal" particles. It was also observed, when water was used as the settling medium, that a small part of the dust was soluble in water and a residue remaining after evaporation evenly covered the surface of the sample and contributed to the above described effect of "colloidal" particles.

Dry "dusting," on the other hand, could be conducted in such a way that discrete or agglomerate particles "stuck" to the surface of the coating, which permitted distinguishing, under the microscope, between the surface of the coating and that of dust particles. Thus a meaningful characterization of the dusted coating was possible and a dependence of reflectivity on the proportion of the surface covered by dust could be obtained. For these reasons dry dusting was selected as the means of applying the basalt dust to the S-13 coating.

In the initial dusting attempts basalt powder with particles between 10μ and 100μ was used. In the first test a sample of S-13 silicone coating was dusted with basalt powder through the 74μ screen sieve. The settled dust layer was observed under the microscope. It consisted of particles from 12μ to 74μ with some agglomerates of small particles also present. Two determinations of the area covered by dust were done by two different counting techniques using a calibrated grid of 20 by 20 squares. Two areas, approximately 2.5 mm by 2.5 mm, were selected at random near the center of the sample. One method, based on establishing the part of each square occupied by dust particles and taking the average of all 400 squares, yielded a percent coverage of 23 percent. The other method, based on determining the average particle size and estimating the equivalent number of such "average particles", gave 26-percent coverage. In all subsequent tests the former method was used whenever dust coverage was measured.

In the measurement of solar absorptance, due to the design of the equipment, the dusted sample must be mounted in a vertical position. It was important that no dust be removed from the sample surface during handling after characterization and particularly during the actual measurement process. For this reason it was necessary to artificially increase the adhesion between dust particles and the S-13 coating prior to measurement of solar absorptance. This need for adhesion was especially noticeable in the case of the larger particles (above 100μ) which showed the greatest tendency to fall or roll off the dusted sample. Various solvents (acetone, isopropyl alcohol, toluene, and dimethylformamide) were applied to the cured S-13 to promote better adhesion with basalt powder. No tackiness of the S-13 surface was detected after treatment with these solvents, but some improvement in adhesion was observed after the application of dimethylformamide. It was further established that the latter solvent did not affect the radiative properties of the coating. Accordingly, dimethylformamide was used in all tests involving measurement of the solar absorptance.

While no precise dust removal experiments were conducted as part of the dusting process, a number of general observations were made. It was observed that larger size particles (over 50μ) were easily removed by a slight tap of the sample in the vertical position or by a low-velocity gas jet. It was concluded, on the basis of experimental measurements, that the residual dust contamination, after tapping or blow-off with a gas jet, depended only on the initial amount of fines (particles with diameters below 2μ). For the basalt dust used, the amount of surface covered by fines was generally below 10 percent.

2.4 MEASUREMENT OF ABSORPTANCE AND EMITTANCE

As previously noted in subsection 2.3, the primary parameter affecting solar absorptance of S-13 was found to be the percentage of surface covered by dust. As a

result, dust coverage was the principal experimental parameter which was varied during the measurement of spectral absorptance over the solar spectrum. In addition the effect of angle of incidence was also investigated for the case of solar absorptance. For the case of infrared emittance, the only experimental parameter considered was dust coverage. Because the value of the infrared emittance of the dust (~ 0.88) was only slightly higher than that of the S-13 (~ 0.83), there did not appear much likelihood of drastic changes in the infrared emittance of the S-13 due to dust contamination.

2.4.1 Solar Absorptance Measurements

Spectral absorptance of a number of samples was measured with a Gier-Dunkle integrating sphere, shown in Figure 2-1, in the spectral range from 0.34μ to 2.45μ (which covers 91 percent of the solar energy). Although S-13 was the primary test coating, a limited number of tests were also run with aluminized Teflon and clear silicone. Initial measurements with uncontaminated samples confirmed previous data on S-13 ($\alpha_s \leq 0.2$) and showed that aluminized Teflon had an acceptable absorptance ($\alpha_s = 0.21$) while the sample of clear silicone had a considerably higher value ($\alpha_s = 0.29$).

2.4.1.1 S-13 Solar Absorptance Measurements. In order to obtain a correlation curve between absorptance of a sample and the amount of its contamination (expressed as the proportion of surface covered) a number of samples with S-13 coating (8-mil) were prepared by dusting with basalt powder ($<74\mu$ size) and characterized. Figures 2-2a through 2-2f are microphotographs of six of these samples. Spectral absorptance was measured in the manner already described. Angle of incidence was held at 20° . The tabulated spectral data are provided in Appendix A. Figure 2-3 provides an indication of the variation of spectral absorptance for S-13 with and without dust. Except possibly below 0.4μ , the presence of dust results in an increase in the spectral

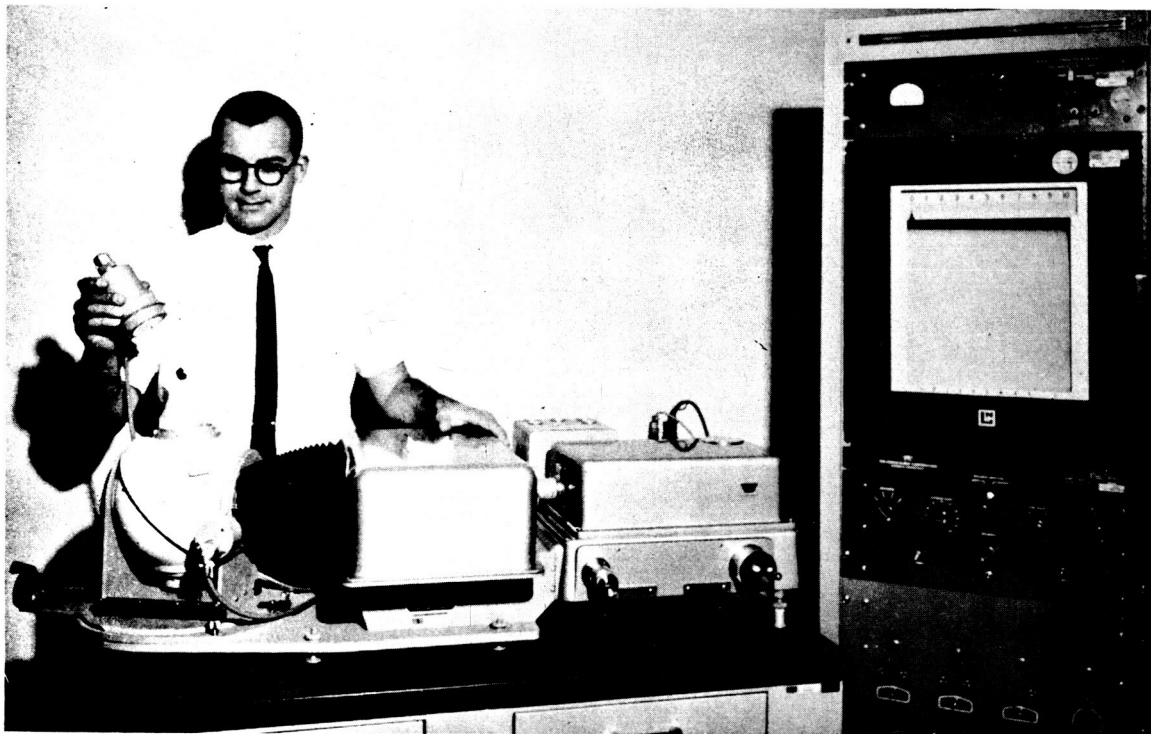
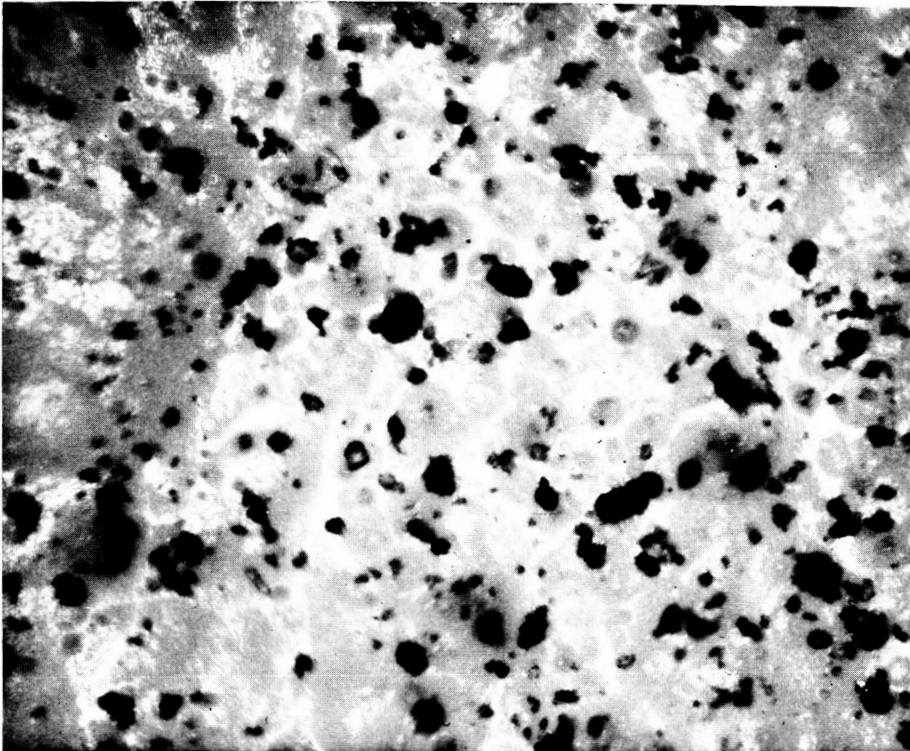
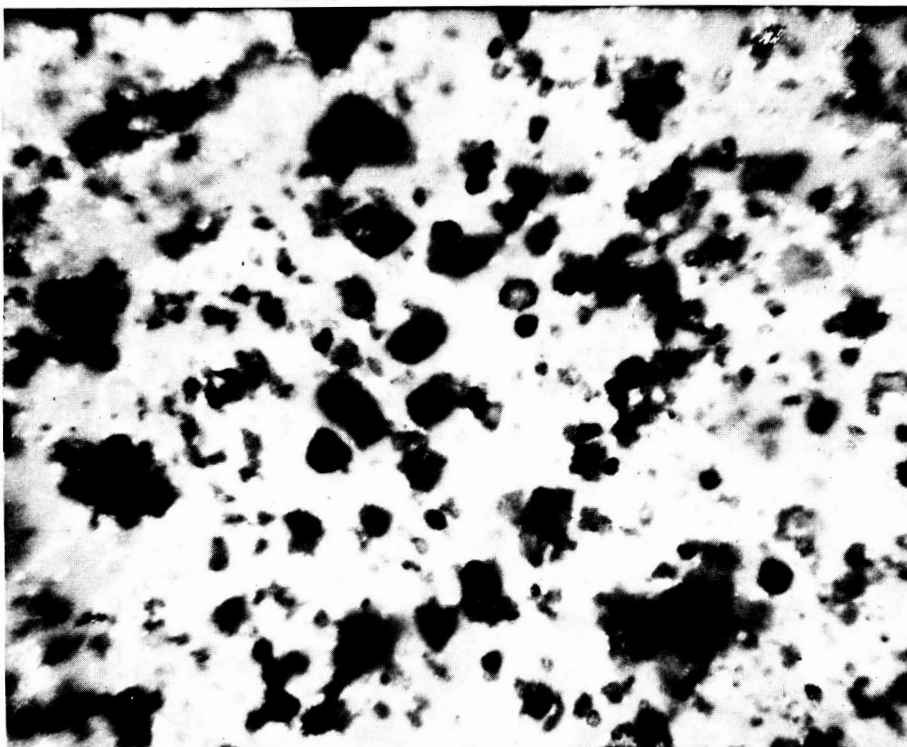


Figure 2-1. THE GIER-DUNKLE INTEGRATING SPHERE REFLECTOMETER

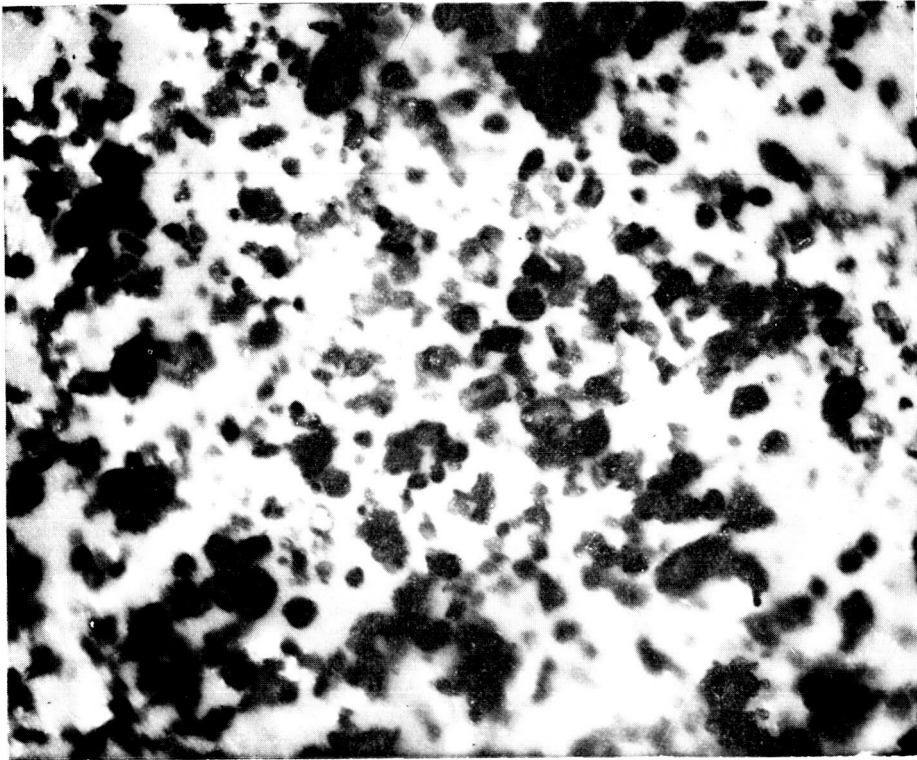


a. SAMPLE #7 - 4.5% DUST COVERAGE

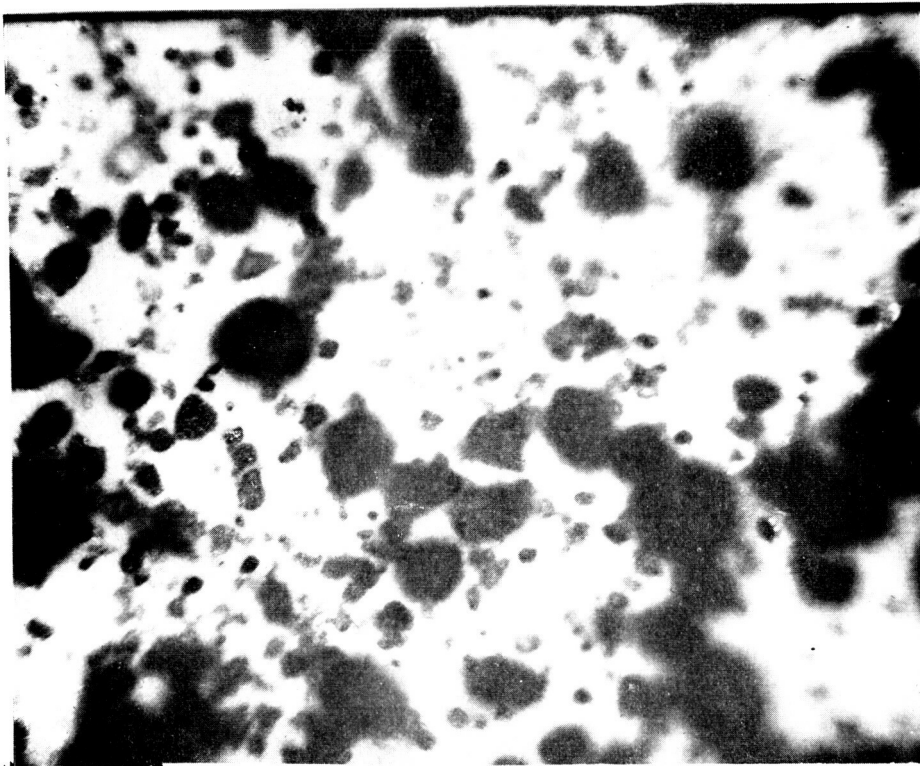


b. SAMPLE #9 - 15.0% DUST COVERAGE

Figure 2-2. MICROPHOTOGRAPHS OF BASALT DUST ON S-13 COATING

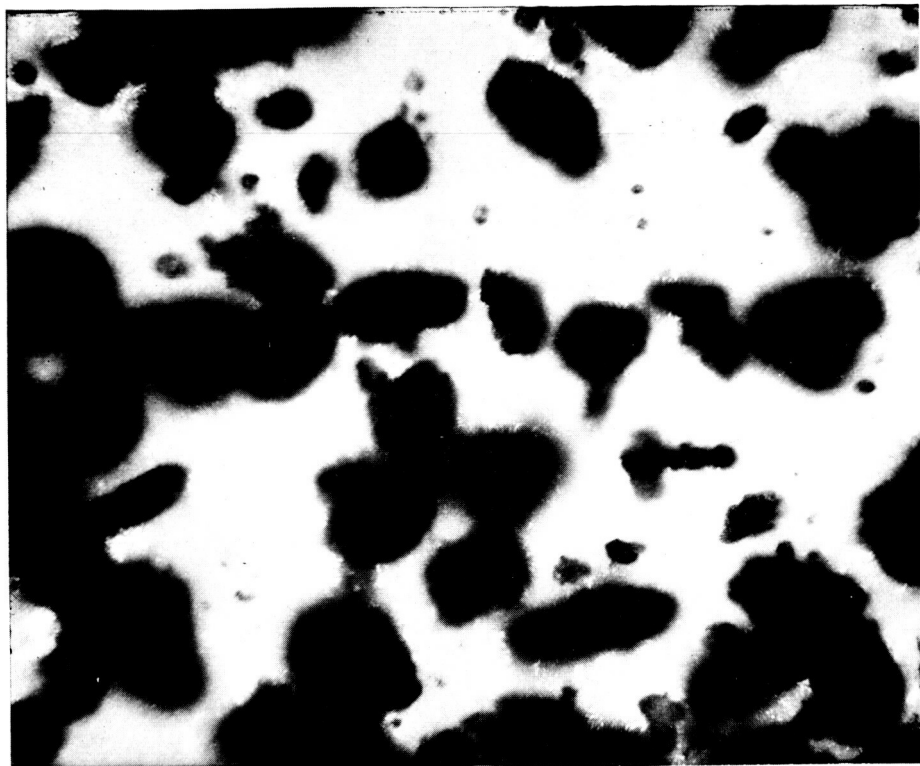


c. SAMPLE #14 - 28.5% DUST COVERAGE

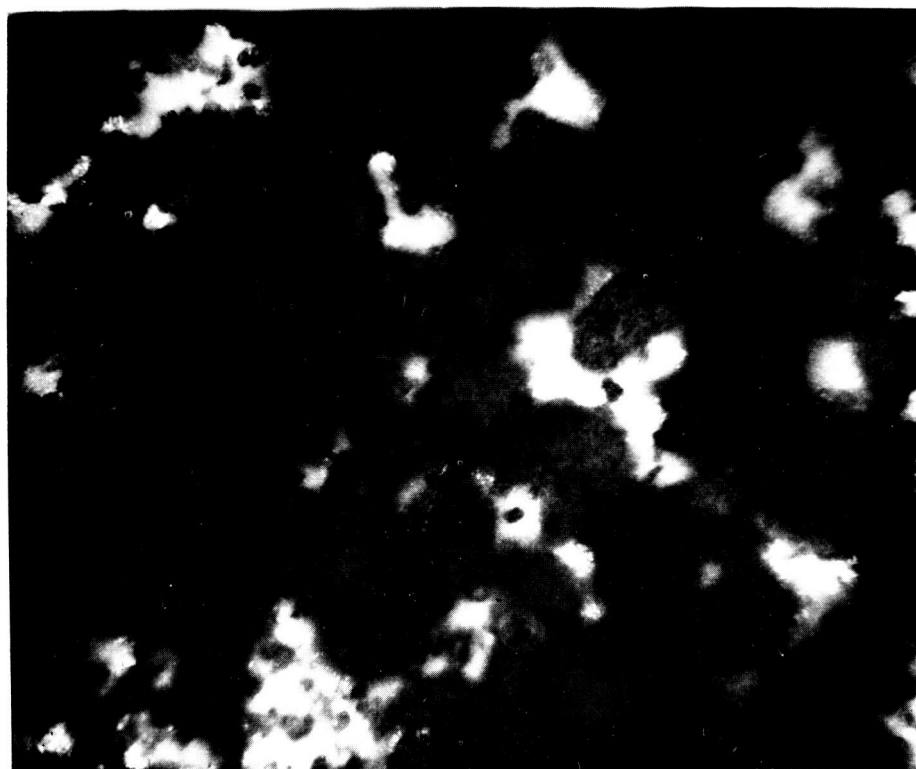


d. SAMPLE #17 - 28.5% DUST COVERAGE

Figure 2-2. MICROPHOTOGRAPHS OF BASALT DUST ON S-13 COATING (CONTINUED)



e. SAMPLE #15 - 35.5% DUST COVERAGE



f. SAMPLE #16 - 80% DUST COVERAGE

Figure 2-2. MICROPHOTOGRAPHS OF BASALT DUST ON S-13 COATING (CONCLUDED)

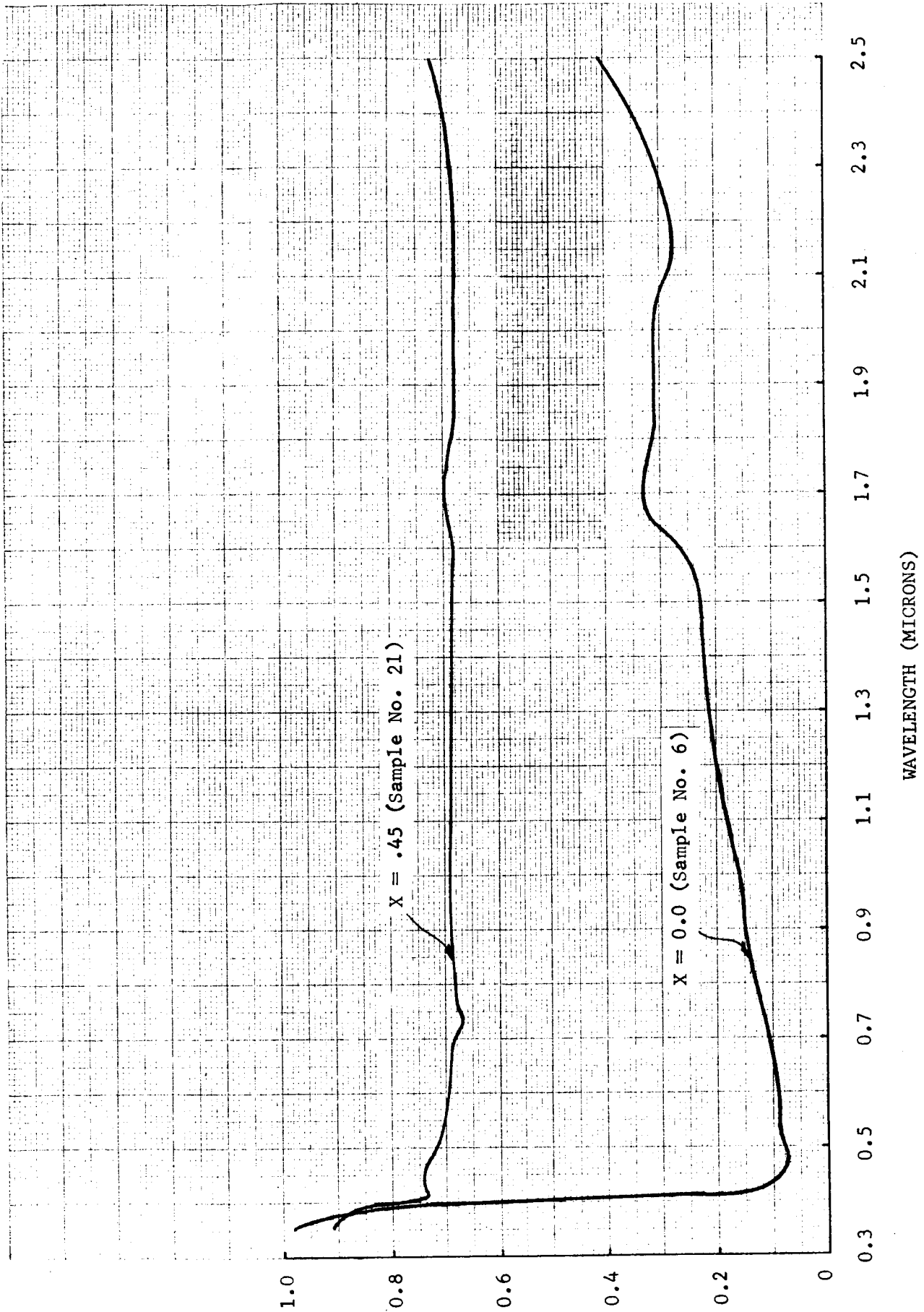


Figure 2-3. EFFECT OF DUST ON SPECTRAL ABSORPTANCE IN SOLAR SPECTRUM OF S-13

absorptance of S-13. Also the presence of the dust results in a relatively constant value of α_s with respect to wavelength. In terms of total absorptance the results of these measurements are presented in Table 2-4 and Figure 2-4. It is noted that the effect of dust contamination on the S-13 coating is nonlinear in nature. Dust coverage of 11 percent can result in an 100-percent increase in the value of solar absorptance.

Table 2-4

VARIATION OF SOLAR ABSORPTANCE WITH DUST COVERAGE ON
S-13 SAMPLES (8-MIL COATING ON ALUMINUM)

<u>Sample</u>	<u>Dust Coverage</u>	<u>Solar Absorptance</u>
6	0	0.195
7	0.045	0.245
8	0.095	0.35
9	0.15	0.49
14	0.285	0.603
19	0.31	0.614
15	0.355	0.625
21	0.45	0.707
20	0.555	0.778
16	~0.80	0.795
22	0.975	0.848

After measurements of the absorptance had been taken for the dusted surface, the dust was blown off with a simple air jet. The gas jet involved nitrogen flowing for 15 seconds at 10-psi nozzle pressure with the nozzle exit positioned approximately one inch above the plate and inclined 20° from the normal to the plate. The spectral absorptance was then measured for 5 samples. The results in terms of total solar absorptance were as follows:

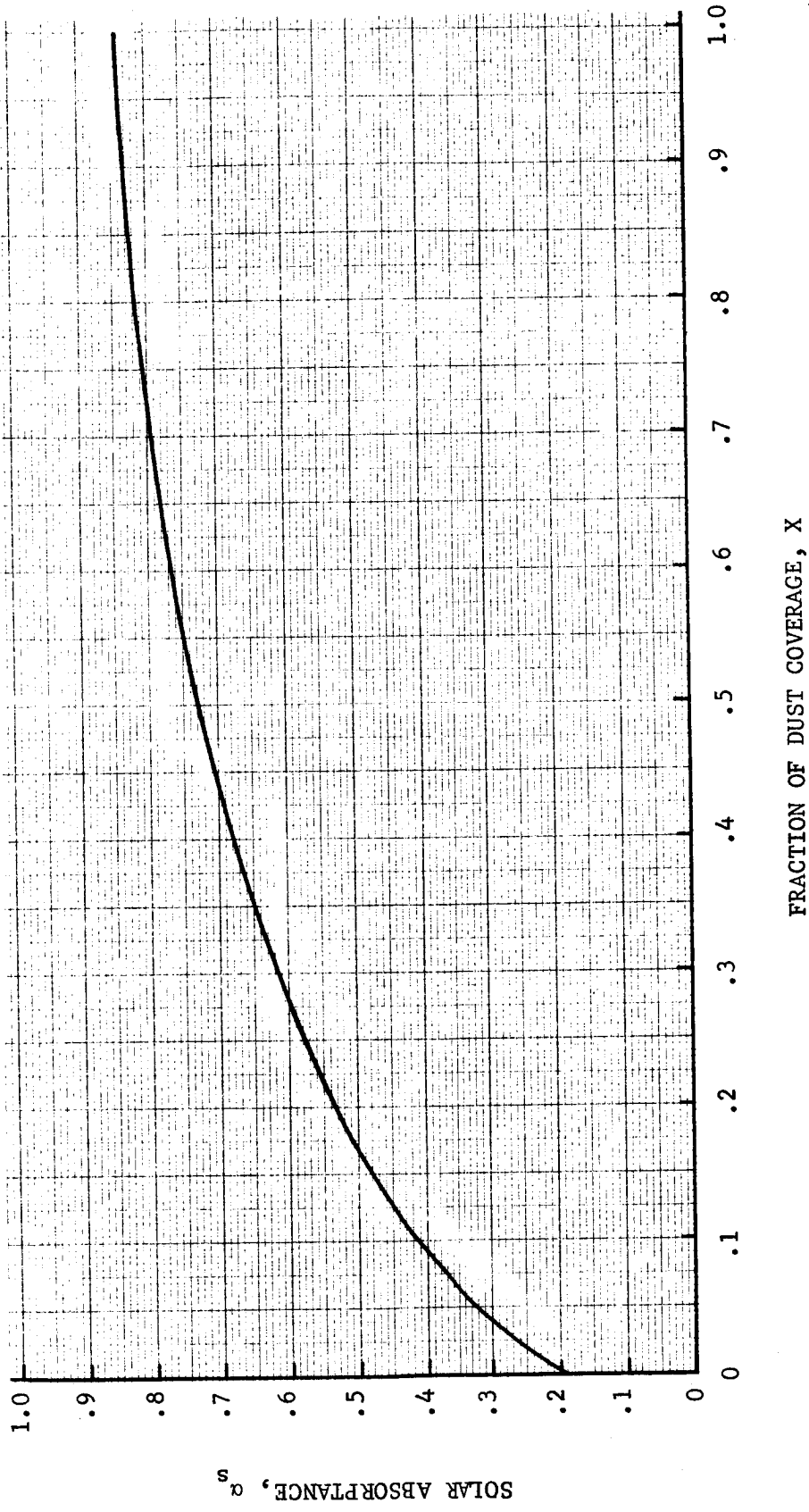


Figure 2-4. VARIATION OF TOTAL SOLAR ABSORPTANCE WITH DUST COVERAGE OF S-13 PLATE

7 June 1967

<u>Sample No.</u>	<u>Particle Type</u>	<u>Initial Dust Coverage</u>	<u>Solar Absorptance</u>	
			<u>Initial</u>	<u>After blow-off</u>
6	None	0.0	0.195	--
7	Fine dust (below 34 μ)	0.045	0.245	0.239
14	Fines in dust	0.285	0.603	0.321
15	Coarse dust (above 50 μ)	0.355	0.625	0.246
21	Fines in dust	0.45	0.707	0.330

It should be noted that in all five cases the solar absorptance after blow-off corresponded to a dust coverage of less than 10 percent (based on Table 2-4).

Furthermore, the more fines present initially, the less reduction in α_s resulted from blow-off.

Four samples were prepared with a new S-13 coating. The new coating was somewhat thinner (5.5 mil) than the first coating (8 mil). Solar absorptance for an uncontaminated sample was therefore higher for the new coating (0.201 as compared with 0.195). Three of the four new samples were dusted in such a manner as to have the same proportion of fines present with various degrees of dust coverage. The initial coverage was established, the dust blown off, and the absorptance measured with the following results:

<u>Sample No.</u>	<u>Initial Dust Coverage</u>	<u>Solar Absorptance After blow-off</u>
29	0.0	0.201
31	0.1	0.281
32	0.5	0.333
30	1.0	0.387

It is apparent that the solar absorptance after blow-off tends to increase with increasing initial dust coverage when the percentage of fines is held constant.

7 June 1967

A third set of tests was performed with an improved S-13 coating dusted with fine basalt powder (below 37μ) without measurement of the surface coverage. The adherence to this smoother and harder coating was weaker and even while dusting with finer particles the residual contamination was found to be less than it was in the case with the first batch of S-13 dusted. The following results were obtained:

<u>Sample No.</u>	<u>Solar Absorptance</u>	
	<u>Initial</u>	<u>After Blow-off</u>
39	0.475	0.249
40	0.581	0.267

In an attempt to establish the relationship between the contamination process and the environment to which the surface was exposed, three identical samples (Nos. 34, 36, and 38) were heated for five hours at 523°K in a bell jar at less than 10^{-6} torr. One sample (No. 34) was dusted before being placed in the bell jar while the other two were dusted after being removed. The dust was then blown off all three samples. In the case of sample No. 36, the dust was blown off while the sample was still hot while sample No. 38 was allowed to cool before the dust was removed. The results were as follows:

<u>Sample No.</u>	<u>Solar Absorptance After Blow-Off</u>
34	.283
36	.250
38	.274

The results indicated that the adhesion of the dust particles to the S-13 surface was not significantly affected by the environment to which the surface was exposed before or after dusting.

Angular dependence of solar absorptance was determined by measurements at angles of incidence of 20° and 75° . The results obtained are shown in Table 2-5 and

Figure 2-5. The uncontaminated S-13 displays a decrease in absorptance with an increase in angle of incidence. The presence of the dust tends to override this trend. Solar absorptance increases with increasing angle of incidence for dusted samples and furthermore this variation is accentuated as the amount of dust coverage increases.

Table 2-5. TOTAL SOLAR ABSORPTANCE OF S-13 AT 20° AND 75° ANGLE OF INCIDENCE

	Dust Coverage	Solar Absorptance		Change in α_s from 20° to 75° Angle of Incidence
		20°	75°	
S-13	0.0	0.219	0.183	-.036
S-13	0.05	0.284	0.312	.028
S-13	0.18	0.523	0.629	.106

At increasing angles of incidence the plate surface area projected to the incident radiation is less; but that of the dust particles, due to their three-dimensional geometry, is much the same. The dust particles, with a much higher solar absorptance than the thermal control coating, thus contribute more and more to the total absorptance with increasing angle of incidence.

2.4.1.2 Aluminized Teflon Solar Absorptance Measurements. Aluminized Teflon samples were dusted with the same basalt powder (particle size below 74μ) used previously on S-13. Spectral measurements for solar absorptance were taken in the same fashion as for S-13. The resulting spectral data is tabulated in Appendix A. An indication of the variation of the solar absorptance of aluminized Teflon with and without dust is provided in Figure 2-6. Similar to S-13, the presence of the dust on aluminized Teflon causes an increase in absorptance at all wavelengths and the resulting curve shows little variation with wavelength. Absorptance values were lower than with S-13, but followed a similar curve in relation to surface coverage as shown in Figure 2-7 and Table 2-6.

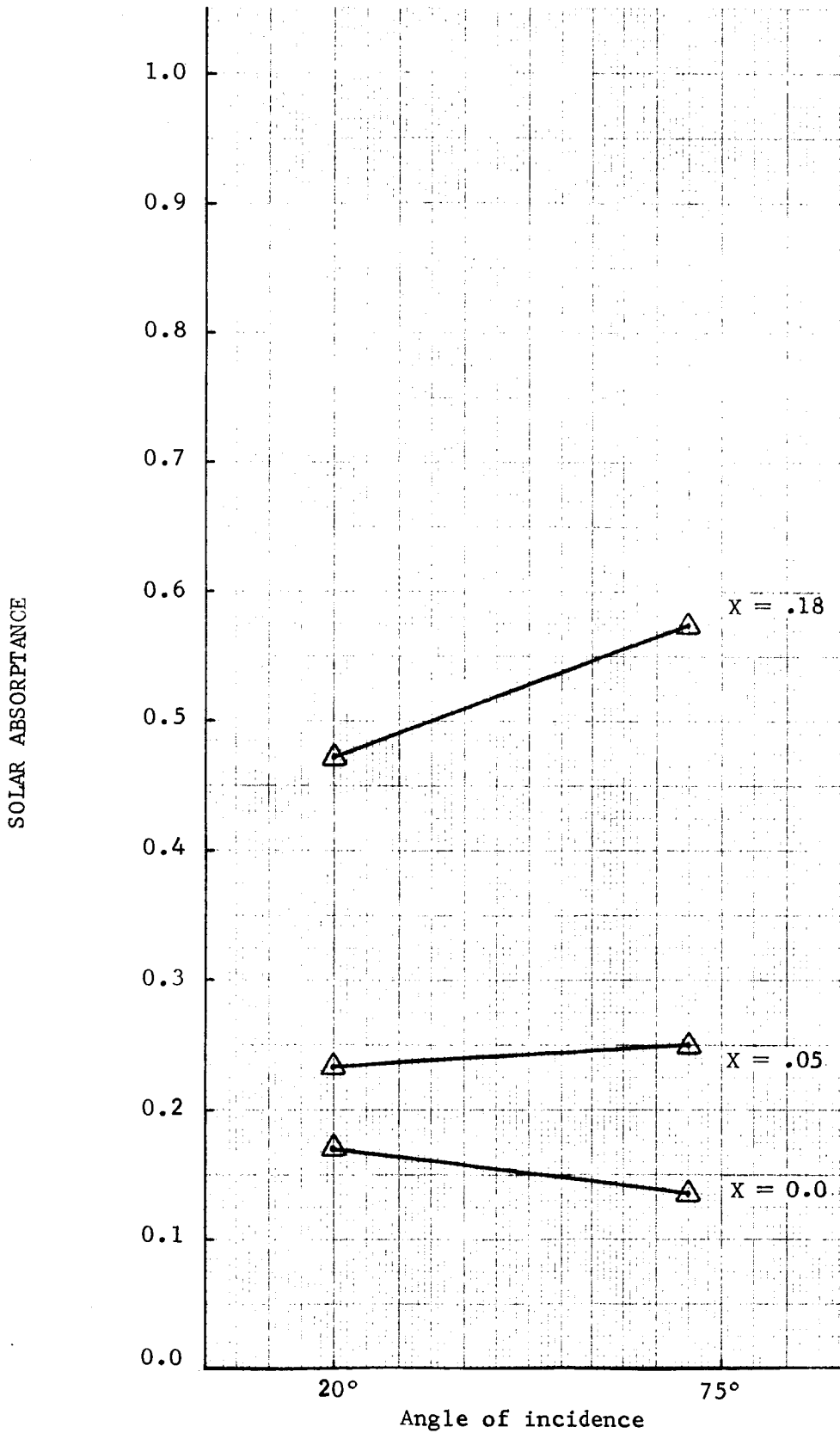


Figure 2-5. VARIATION OF TOTAL SOLAR ABSORPTANCE WITH ANGLE OF INCIDENCE FOR S-13 PLATE WITH AND WITHOUT DUST

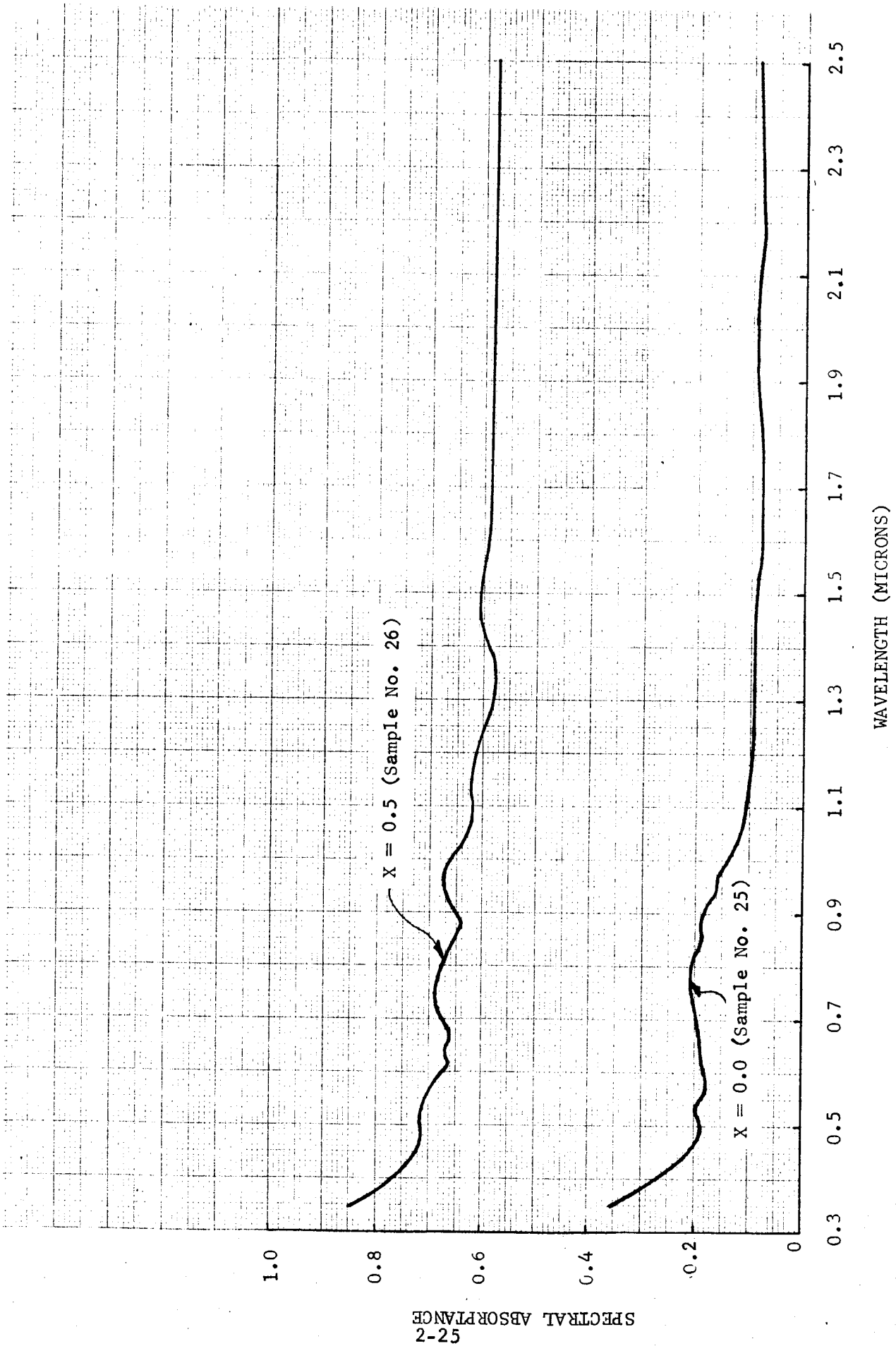


Figure 2-6. EFFECT OF DUST ON SPECTRAL ABSORPTANCE IN SOLAR SPECTRUM OF ALUMINIZED TEFLON

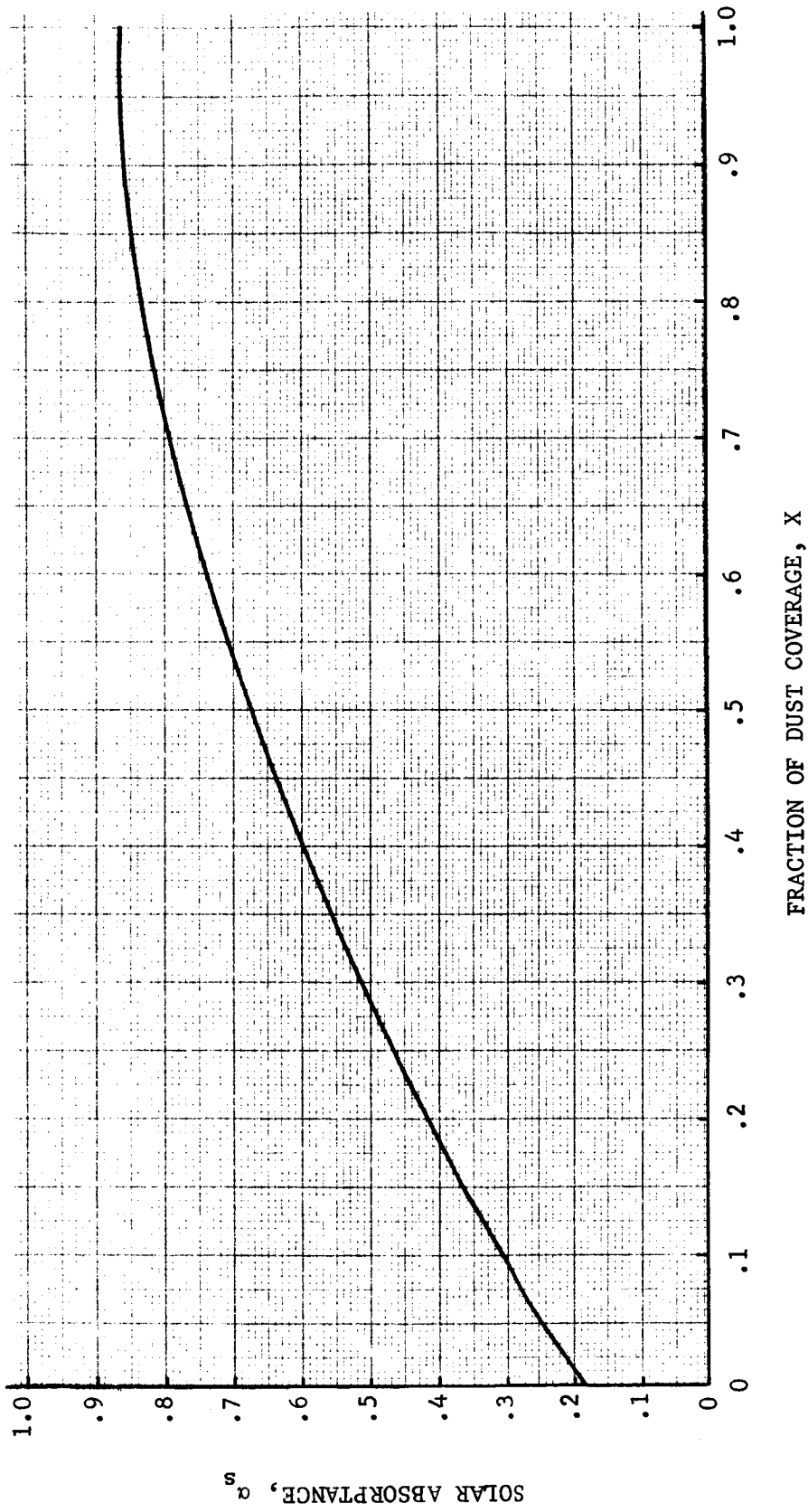


Figure 2-7. VARIATION OF TOTAL SOLAR ABSORPTANCE WITH DUST COVERAGE OF ALUMINIZED TEFLON PLATE

Table 2-6. VARIATION OF SOLAR ABSORPTANCE WITH DUST COVERAGE ON ALUMINIZED TEFLON

<u>Sample No.</u>	<u>Dust Coverage</u>	<u>Solar Absorptance</u>
23	0.0	0.185
25	0.0	0.174
27	0.265	0.481
26	0.5	0.67
28	0.6	0.739
24	1.0	0.864

Some difficulty was encountered in dusting the Teflon surface for purposes of measuring solar absorptance. Fines adhered to the surface but larger particles had a tendency to roll off when the sample was mounted in the vertical position.

Removal of the dust from the aluminized Teflon by simple gas jet was accomplished on samples No. 26 and 28 with the following results

<u>Sample No.</u>	<u>Initial Dust Coverage</u>	<u>Solar Absorptance</u>	
		<u>Initial</u>	<u>After Blow-Off</u>
26	0.5	0.481	0.191
28	0.6	0.739	0.163

These results indicate that for the case of aluminized Teflon the dust removal by a gas jet was quite effective. There is also an indication, based on this data along with that of Table 2-6, that the values of solar absorptance for the uncontaminated (or decontaminated) aluminized Teflon display a significant spread from sample to sample (all of which were taken from the same panel).

Three samples of aluminized Teflon (Nos. 33, 35, and 37) were tested in the same manner as that described for S-13 samples No. 34, 36, and 38. Sample No. 33 was dusted before being put in the bell jar, while samples No. 35 and 37 were dusted after

being removed from the bell jar. The dust was removed from all three samples with sample No. 35 still hot and sample No. 37 cool. The results were as follows:

<u>Sample No.</u>	<u>Solar Absorptance After Blow-Off</u>
33	0.202
35	0.196
37	0.194

As with S-13, these results indicated the adhesion of the dust to the aluminized Teflon surface was not appreciably affected by the environment to which the surface was exposed before or after dusting.

Solar absorptance for aluminized Teflon was measured at angles of incidence of 20° and 75°. The results are shown in Table 2-7 and Figure 2-8.

Table 2-7. TOTAL SOLAR ABSORPTANCE OF ALUMINIZED
TEFLON AT 20° AND 75° ANGLE OF INCIDENCE

<u>Dust Coverage</u>	<u>Solar Absorptance</u>		Change in α_s from 29° to 75° <u>Angle of Incidence</u>
	<u>20°</u>	<u>75°</u>	
0.0	0.196	0.287	0.091
0.0	0.213	0.295	0.082
~0.5	0.667	0.875	0.208

For the uncontaminated sample an increase in solar absorptance is observed with an increase in angle of incidence. The presence of the dust appears to cause greater increase in solar absorptance for a given increase in angle of incidence.

2.4.1.3 Clear Silicone Solar Absorptance Measurements. Only two data points were obtained for the solar absorptance of clear silicone as a function of dust coverage. These are as follows:

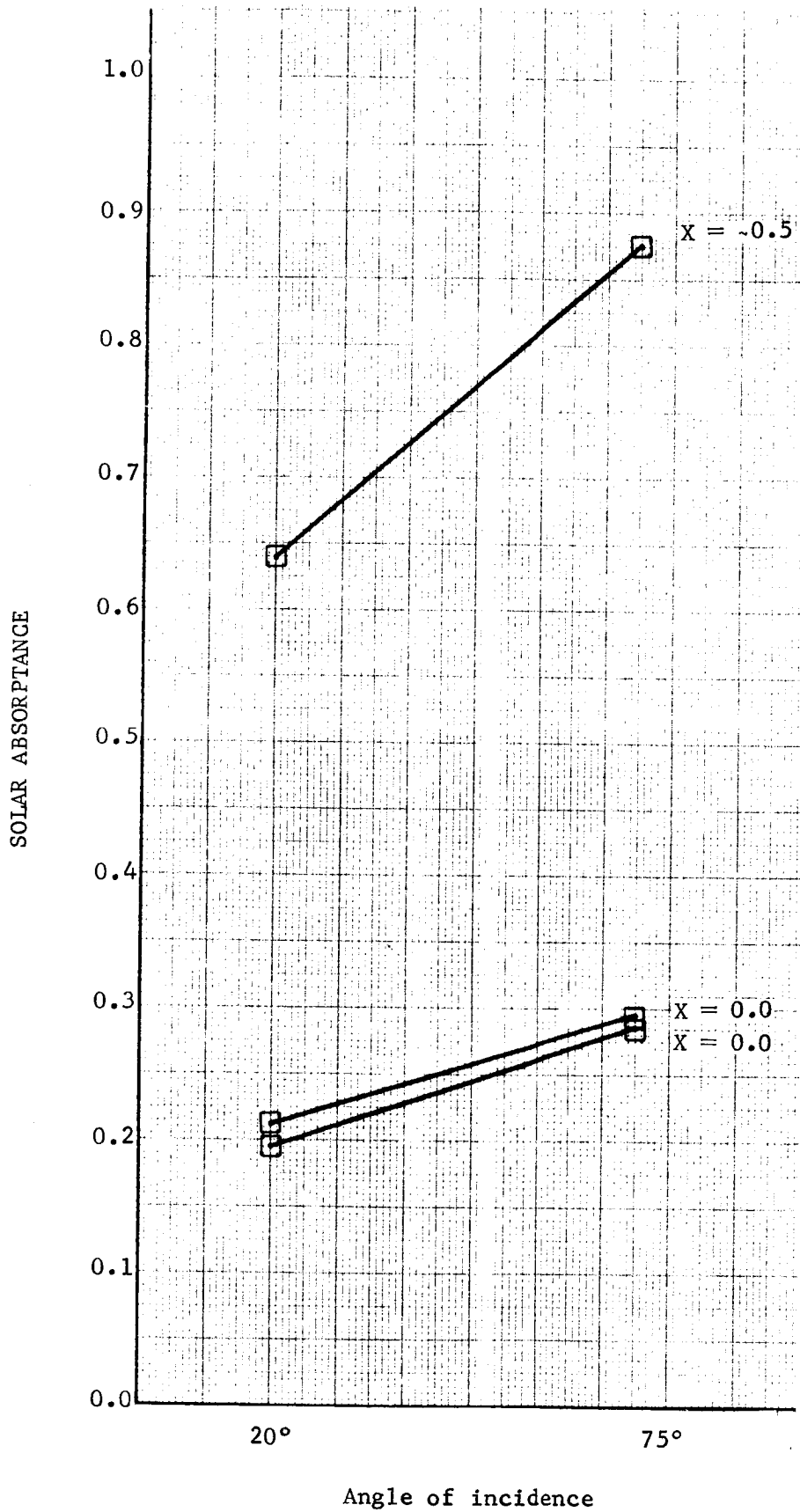


Figure 2-8. VARIATION OF TOTAL SOLAR ABSORPTANCE WITH ANGLE-OF-INCIDENCE FOR ALUMINIZED TEFLON PLATE

Table 2-8. VARIATION OF TOTAL SOLAR ABSORPTANCE WITH DUST COVERAGE ON CLEAR SILICONE SAMPLES

<u>Dust Coverage</u>	<u>Solar Absorptance</u>
0.0	0.29
0.37	0.581

The uncontaminated spectral data is presented in Figure 2-9. It is noted that while the uncontaminated clear silicone has a higher value of solar absorptance than uncontaminated S-13 or aluminized Teflon, the effect of dust contamination on clear silicone is not so severe as is the case with the other two coatings.

2.4.2 Infrared Emittance Measurements

The infrared emittance of test samples of S-13 and aluminized Teflon was measured with a Perkin-Elmer 13U Spectrophotometer shown in Figure 2-10 with a black body source temperature of 523°K. The value of emittance was calculated for a black body energy distribution at 395°K (peak at 7.3 μ). The spectral range measurements (2 μ -14 μ) cover 70 percent of the radiant energy. The contribution of emittance above 14 μ should not substantially change the calculated value, because only slight variations in emittance are to be expected in this wavelength range. The measured values of total normal emittance for clean and dusted samples are listed in Table 2-9.

Table 2-9. EMITTANCE OF THERMAL CONTROL COATINGS

	<u>Clean</u>	<u>Dusted</u>	<u>Dust Coverage</u>
S-13	0.83	0.88	1.00
Aluminized Teflon	0.85	0.92	~0.9

A monochromatic emittance curve for S-13 with and without basalt dust is shown in Figure 2-11. Tabulated spectral data is found in Appendix A. S-13 shows a strong absorption band with a peak at 3.12 μ (attributed to -OH groups) and a strong

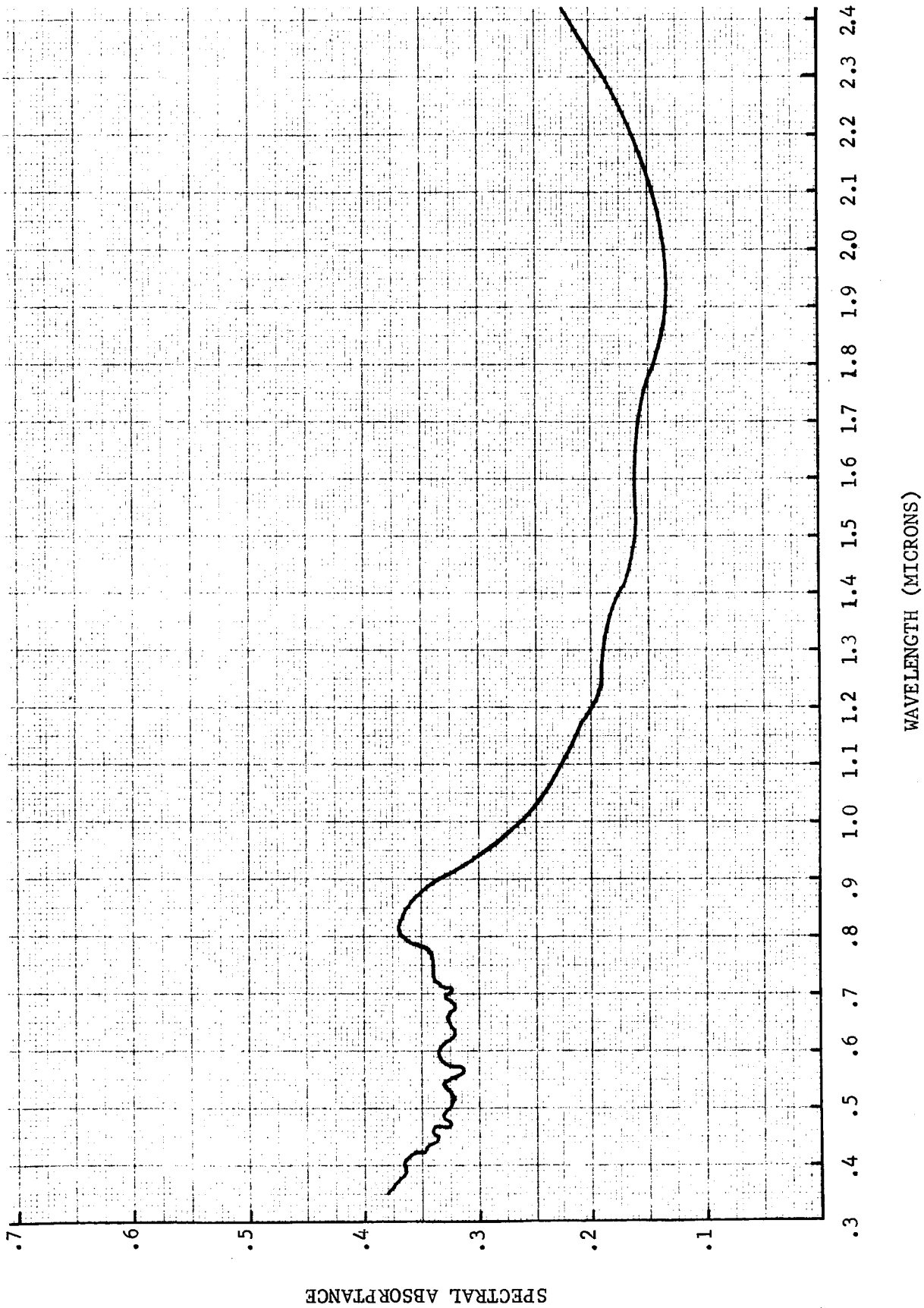


Figure 2-9. SPECTRAL ABSORPTANCE IN SOLAR SPECTRUM FOR CLEAR SILICONE

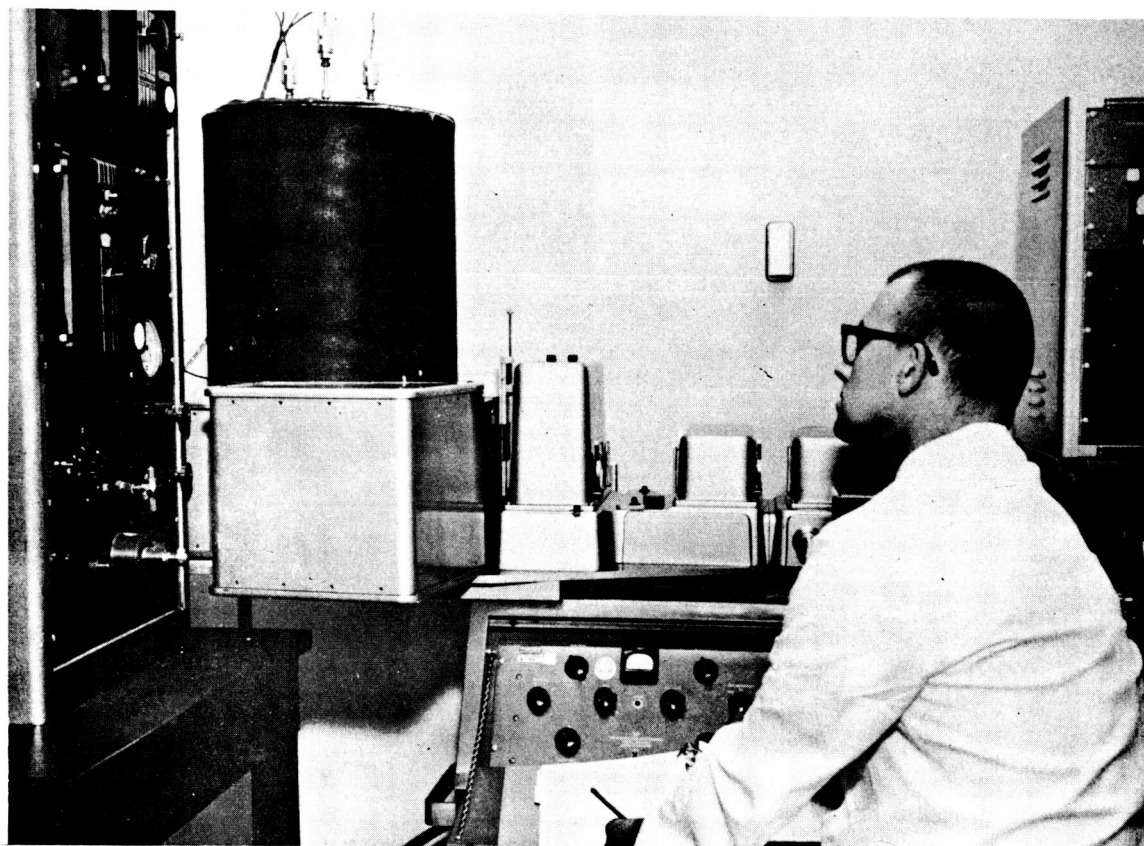


Figure 2-10. THE PERKIN ELMER 13U SPECTROPHOTOMETER

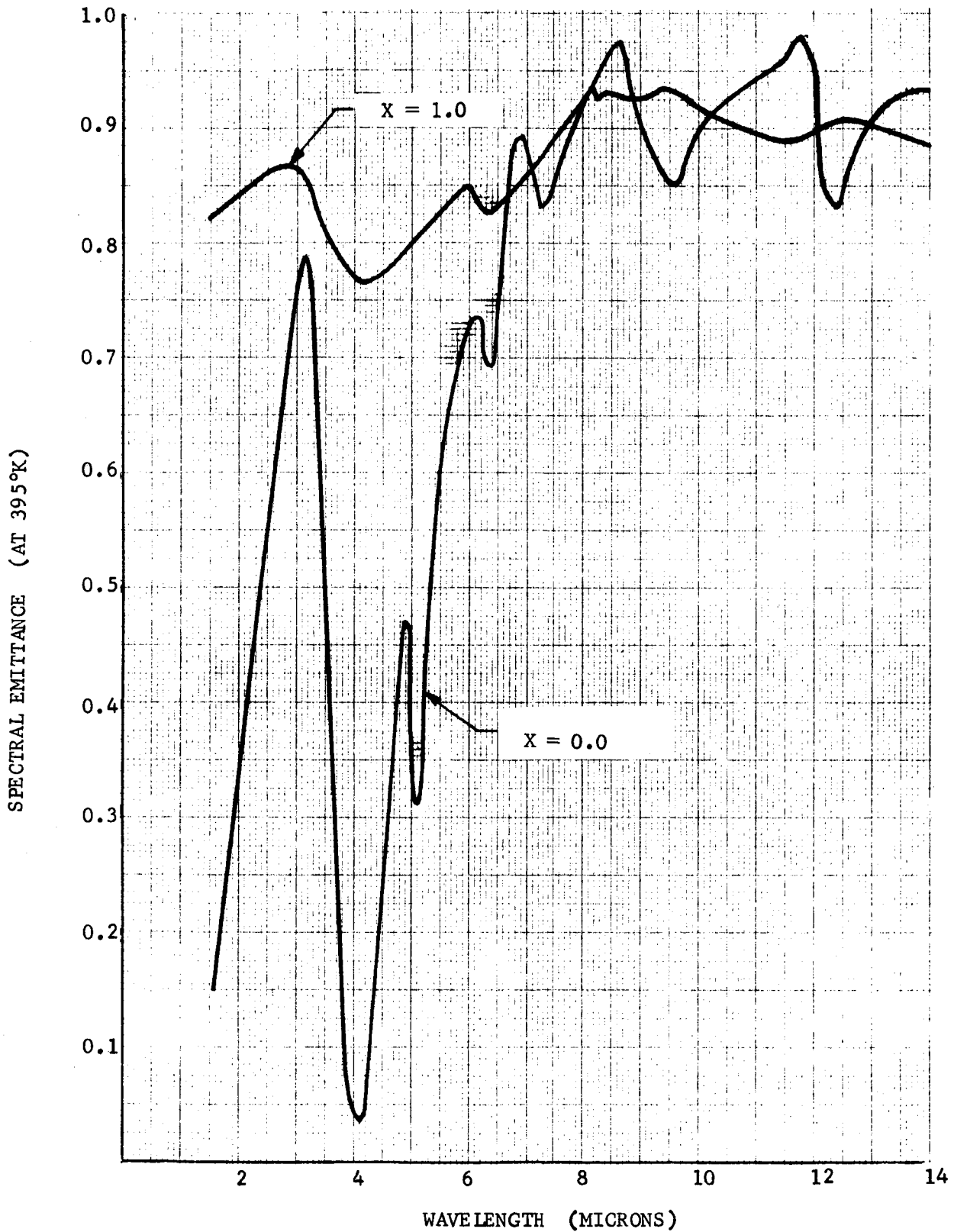


Figure 2-11. SPECTRAL EMITTANCE IN THE INFRARED SPECTRUM FOR S-13 WITH AND WITHOUT BASALT DUST

reflectance at 4.1μ . At longer wavelengths the emittance gradually increases to a maximum at 8.6μ (attributed to the Si-O absorption band at 7.9μ), with another maximum at 11.75μ . With basalt dust present these features are strongly attenuated and the spectral absorptance becomes more uniform over the $2-14\mu$ spectral range.

It was not possible to work with an aluminized Teflon sample covered completely by basalt dust as with the S-13 sample. However, even with incomplete coverage (~ 0.9) as shown in Figure 2-12, the same trend was observed; i.e., the spectral absorptance is more uniform over the wavelength range ($2-14\mu$) when the sample is covered by dust.

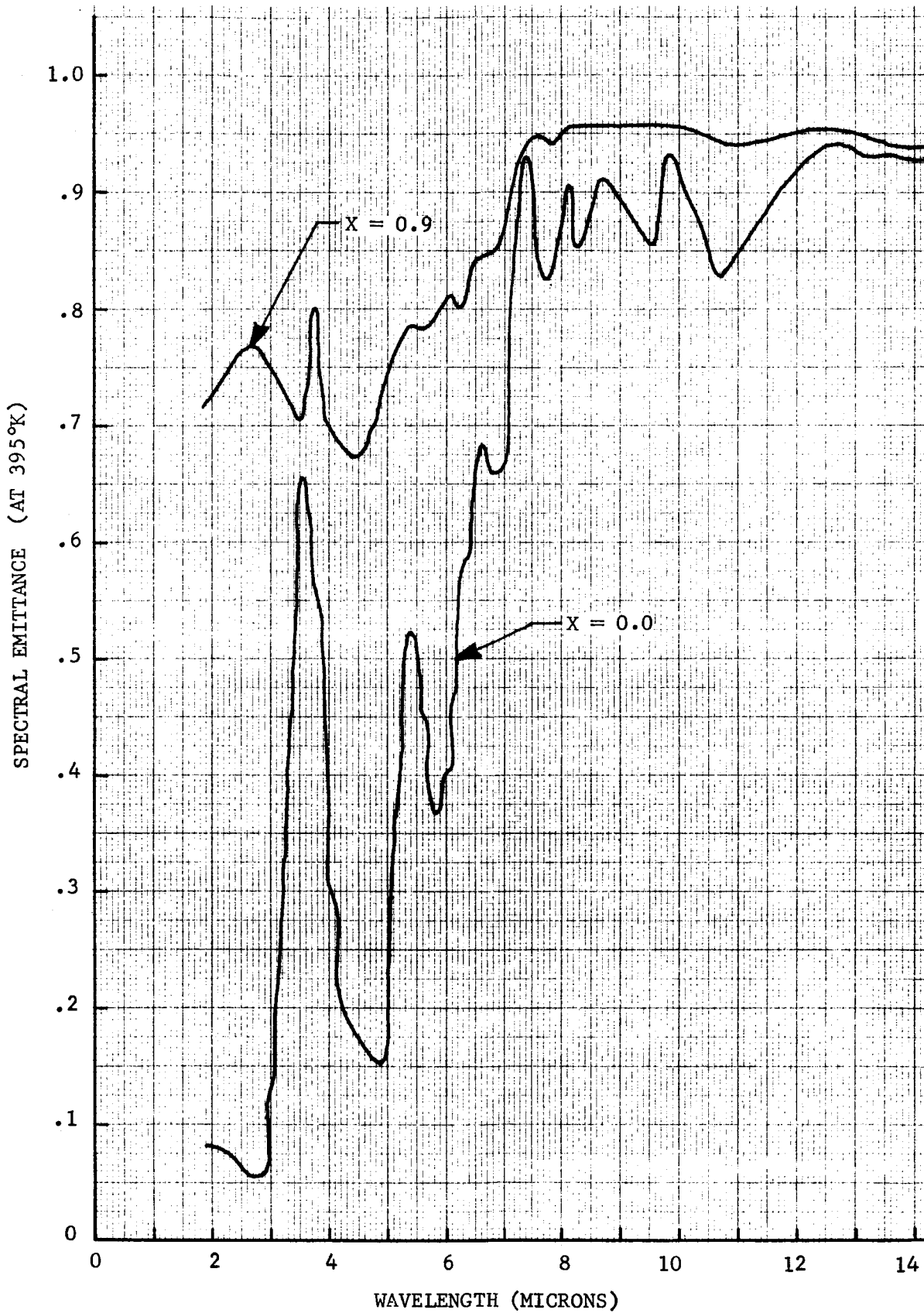


Figure 2-12. SPECTRAL EMITTANCE IN THE INFRARED SPECTRUM FOR ALUMINIZED TEFLON WITH AND WITHOUT DUST

SECTION III

DUST REMOVAL/PREVENTION CONCEPT

During the second phase of the research effort, the primary objective was to investigate the most promising techniques for removing or preventing the accumulation of dust on radiator surfaces. The subsections which follow provide a detailed account of this investigation.

3.1 BACKGROUND

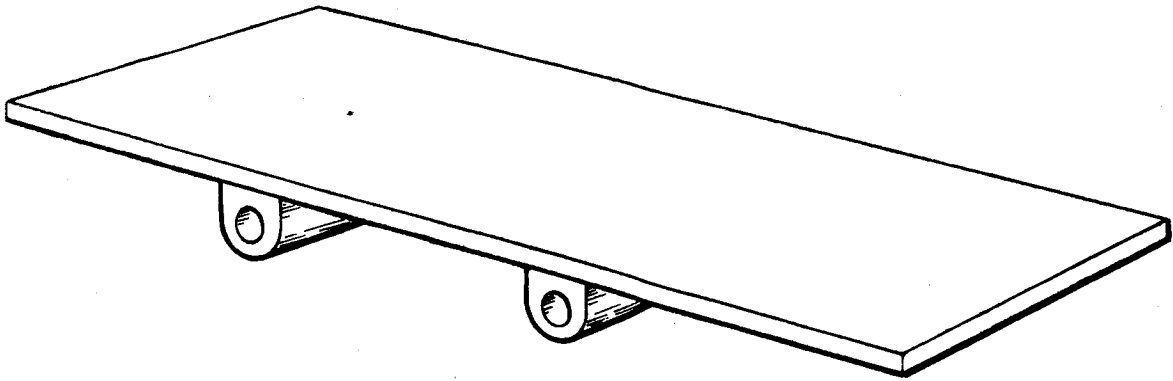
In order to realistically approach the problem of the removal/prevention of dust, an awareness of current trends in thermal radiator designs for space systems is necessary. Also, an understanding of the results of any past studies relating to dust removal in an environment similar to that of the Moon is useful.

3.1.1 Thermal Radiator Characteristics

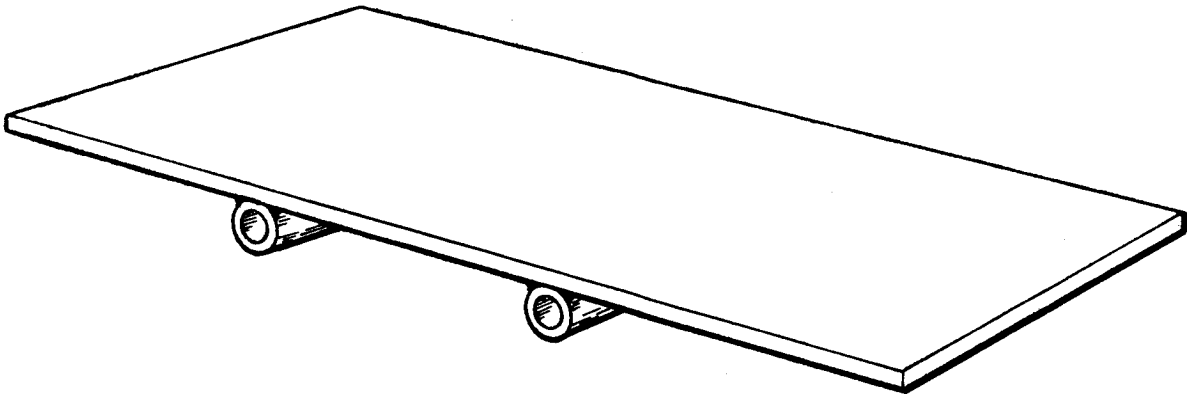
Thermal radiators generally consist of a plate with tubes carrying the coolant fluid. For the case of a flat radiator panel these tubes are brazed or welded to the non-radiating side of the plate. Three such configurations are shown in Figure 3-1. The radiator panel need not be completely flat. For example, free-standing vertical radiators radiating from both sides have been considered, in which the panels are arranged in a plane through the tube centerline. This and other possible configurations in which the surface is not completely flat are shown in Figure 3-2. The tubes may be circular or flat depending on internal pressure, manufacturing techniques, and meteoroid protection requirements.

A literature survey was carried out to establish the thermal radiator characteristics for typical space systems. Systems studied included SNAP 50/SPUR

(a) SINGLE SHEET EXOTIC TUBE



(b) SINGLE SHEET



(c) SINGLE EMBOSSSED

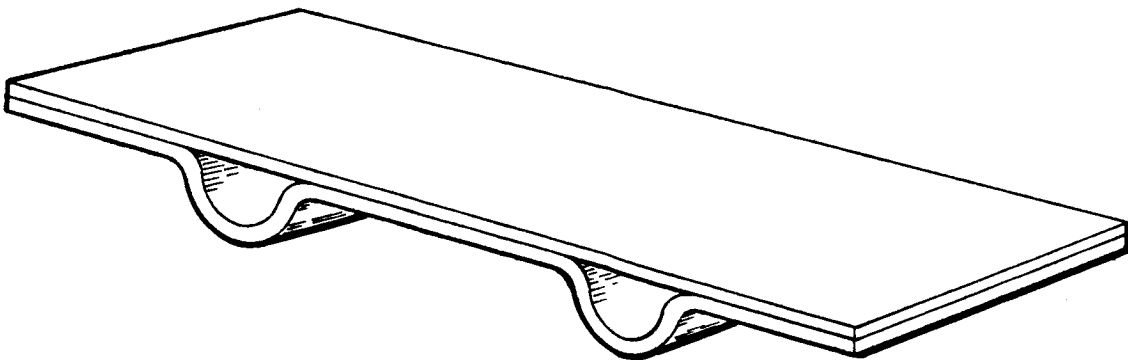
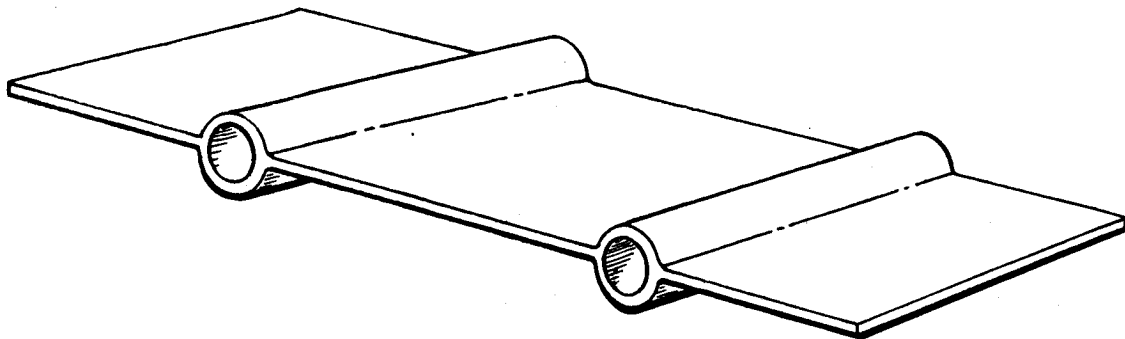
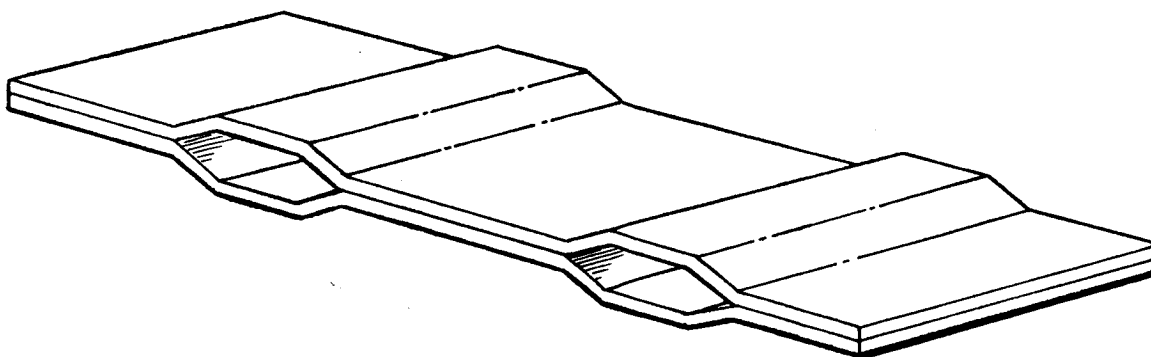


Figure 3-1. FLAT RADIATOR PANEL CONFIGURATIONS

(a) FIN & TUBE TYPE



(b) DOUBLE EMBOSSED (NON-CIRCULAR)



(c) SINGLE SHEET FORMED

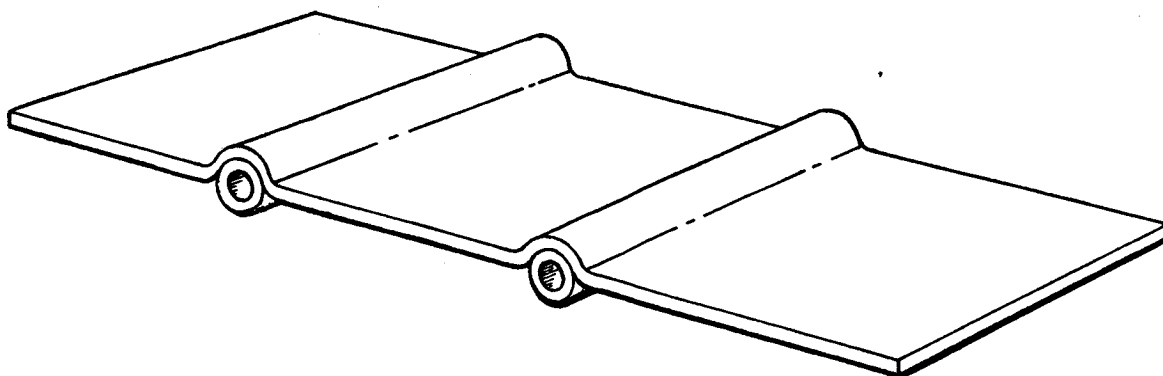


Figure 3-2. NON-FLAT RADIATOR PANEL CONFIGURATIONS

(ref. 14), Lunar Exploration Systems for Apollo (refs. 15 and 16), MOLAB (ref. 17), Lunar Shelter/Rover (ref. 18), and Northrop's Lunar Drill (ref. 19), as well as several other systems (refs. 20 and 21). All radiator designs involved either flat or convex radiator surfaces. Surface temperature ranged from 278°K to 952°K. A summary of the results of the literature survey is provided in Table 3-1.

3.1.2 Previous Dust Removal/Prevention Concepts

Very little information is available in current literature relating to dust removal concepts in a simulated lunar environment. In the literature survey associated with the current study, reference 6 provided the only pertinent data. This report described the use of vibratory motion to shake dust off surfaces in a vacuum. For basalt particle 3 μ to 70 μ in diameter, a frequency of 3000 cycles per second was required to overcome the adhesive forces occurring in a vacuum of 4.8 to 9 x 10⁻¹⁰ torr. An impact device was used to cause the vibration of the surface.

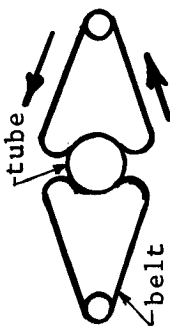
3.2 MODEL TEST MATERIALS

Based on the results of the first phase of the research effort described in Section II, S-13 was selected as the thermal control coating for the second phase. Basalt dust with particle size below 53 μ was selected for the dust. Aluminum alloy 2024T4 was chosen for the radiator panel material. A square, flat surface was established as the standard shape with a finned-tube radiator panel surface to be tested for any concept which appeared sensitive to radiator surface geometry.

3.3 CONCEPTUAL DESIGN AND ANALYSIS

Preliminary conceptual design efforts were directed toward establishing the size and configuration of radiator panels and the dust removal/prevention models

TABLE 3-1. SUMMARY OF SPACE RADIATOR OPERATING CHARACTERISTICS

<u>SYSTEMS/REFERENCE</u>	<u>GEOMETRY</u>	<u>COOLANT</u>	<u>AREA</u>	<u>MATERIAL</u>	<u>TEMPERATURE</u>
1) Radiators for SNAP 50/SPUR, Technical Report AF APL-TR-64-143, Airesearch Man. Co.		K and NaK	8.35m ²	Stainless steel with stainless clad copper fins with emission coating	812° - 950°K
2) Engineering Study Multipurpose Engine and Fuel System, LESA Final Report Vol. 5; WANL-PR(S)-006-B		H ₂ O	Optimized for 1 KW segments	Aluminum or Beryllium	200° - 610°K
3) Apollo Logistic Support Systems MOLAB Studies, Section 6 Task Report on Radiator Study NASA Tech. Memo. X-53032.6, R. H. Hansen and O. R. Kosfeld	---	---	---	---	2 cases 345° and 534°K Coolant Inlet Temperature
4) Feasibility Investigation of a Moving Belt Radiator, ASD-TDR-63-551		K	Optimized	Several investigated	812° - 922°K
5) Lunar Drill Radiator, Internal Northrop Data	---	---	---	---	Inlet: 562°K Outlet: 422°K
6) Compact Lunar Power Station, MTP-ASTR-A-63-8	---	---	---	---	Secondary coolant at 1260°K and Contact with Lunar Surface as Heat Sink

to be fabricated and tested. The basic guidelines were:

- The radiator panel should be designed such that it can be tested with several different removal/prevention systems.
- The radiator panel with a removal/prevention system attached should fit easily into either a 46- by 77-cm bell jar or a 0.90- by 1.52-m space chamber.
- The Northrop carbon-arc solar simulator produces a beam of uniform intensity in a region ~30 cm in diameter.
- Each removal/prevention system should be capable of several consecutive tests in the vacuum chamber without the need for breaking the vacuum.
- The radiating surface should be isothermal.

With these guidelines, the conclusion was reached that a radiator panel approximately 15.4 cm square was the most suitable for the experimental work.

A total of eight different concepts were considered for application to the program. These concepts were as follows:

- Brush - The surface is wiped clean of dust by the sweeping action of a moving brush.
- Electrostatic Curtain - An electrostatically charged curtain sweeps over the surface lightly and removes the dust particles if they possess an electrostatic charge.
- Electrostatic Surface - Charged particles are driven off the surface by a continuously varying sinusoidal electrostatic force field which is generated by electrical conductors embedded in the thermal control coating.

- Jet and Shield - A transparent shield prevents dust from collecting on the radiator surface and a high-velocity gas jet blows the dust particles off the shield.
- Jet and Surface - A high-velocity gas jet blows the dust particles off the radiator surface.
- Spinning Shield - A spinning transparent shield prevents dust from collecting on the radiator surface while its spinning action slings the dust off its own surface.
- Vibrating Shield - A vibrating transparent shield prevents collection of dust on the radiator surface and is kept free of dust by the vibrating action which tends to bounce the dust particles off the shield.
- Vibrating Surface - The radiator surface itself is vibrated and this action tends to bounce the dust particles off the radiator surface.

Figures 3-3 through 3-10 provide sketches of these initial concepts. As part of the basic design philosophy, as indicated in these figures, the devices were compatible to one another with regard to interchange of parts or possible combination of devices. This philosophy permitted greater flexibility and efficiency during model fabrication and testing. Figures 3-3 through 3-10 also give evidence to the fact that all of the dust removal/prevention concepts were originally conceived as experimental laboratory devices, as opposed to operational systems.

Performance factors for grading or comparing the eight concepts were established. A presentation of the relative merits of the eight concepts was made to MSFC personnel on 29 June 1966. Attending this meeting were representatives from the Propulsion and Vehicle Engineering Laboratory, Aero/Astrodynamic Laboratory, and Advanced Systems Office, along with Northrop/Huntsville and Northrop/Hawthorne personnel. Sketches of

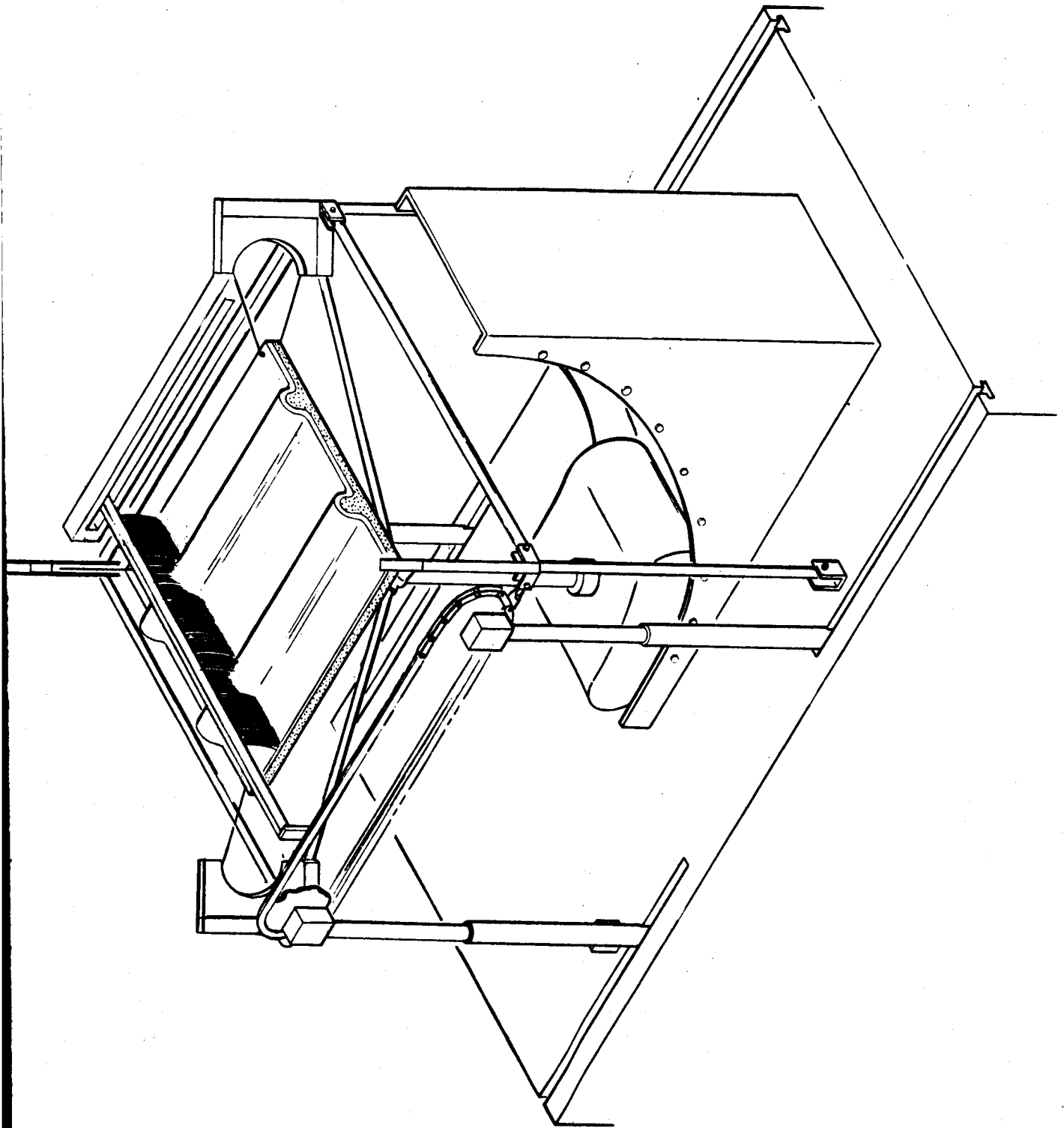


Figure 3-3. PRELIMINARY BRUSH CONCEPT

TR-792-7-207B
7 June 1967

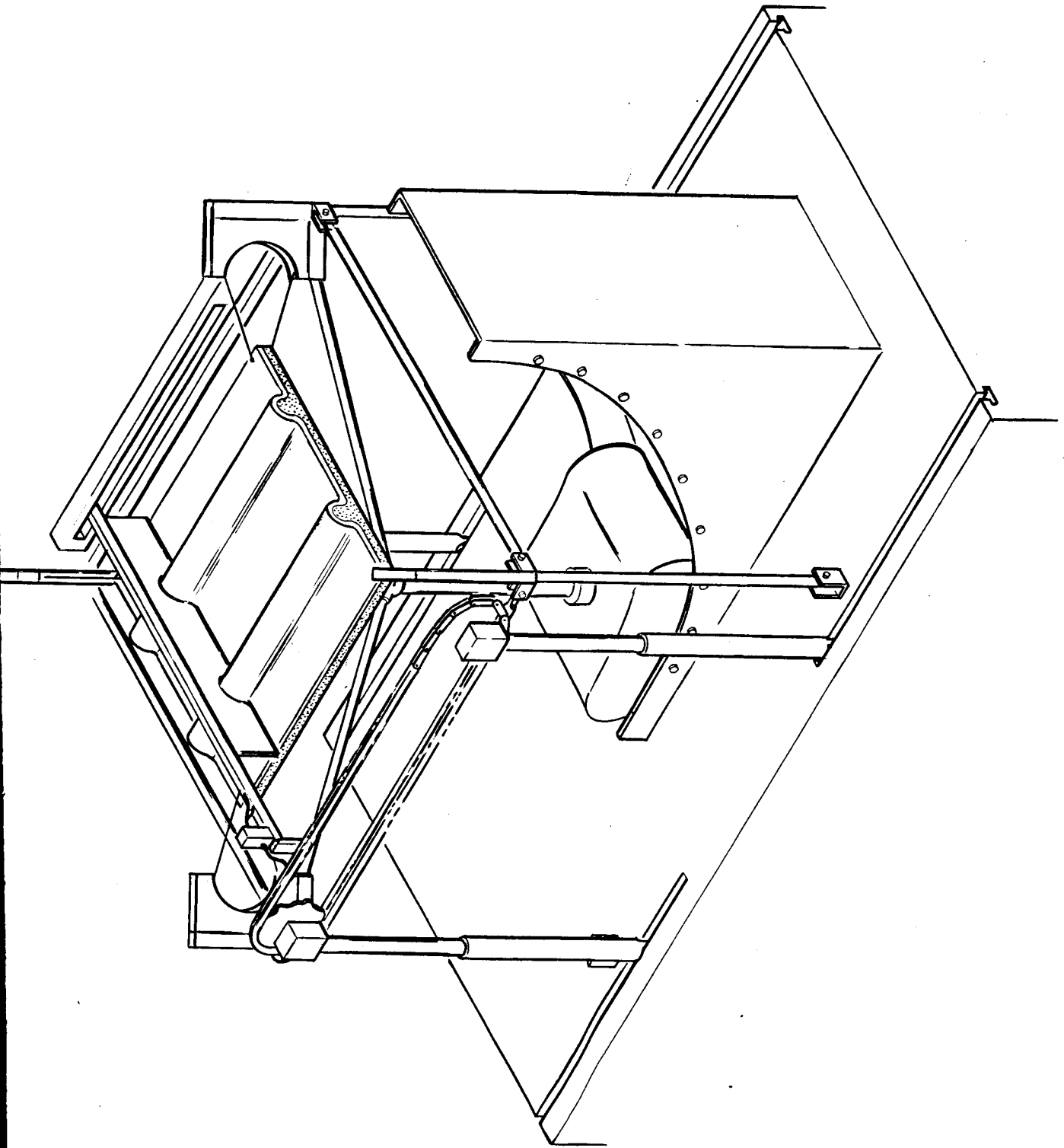


Figure 3-4. PRELIMINARY ELECTROSTATIC CURTAIN CONCEPT

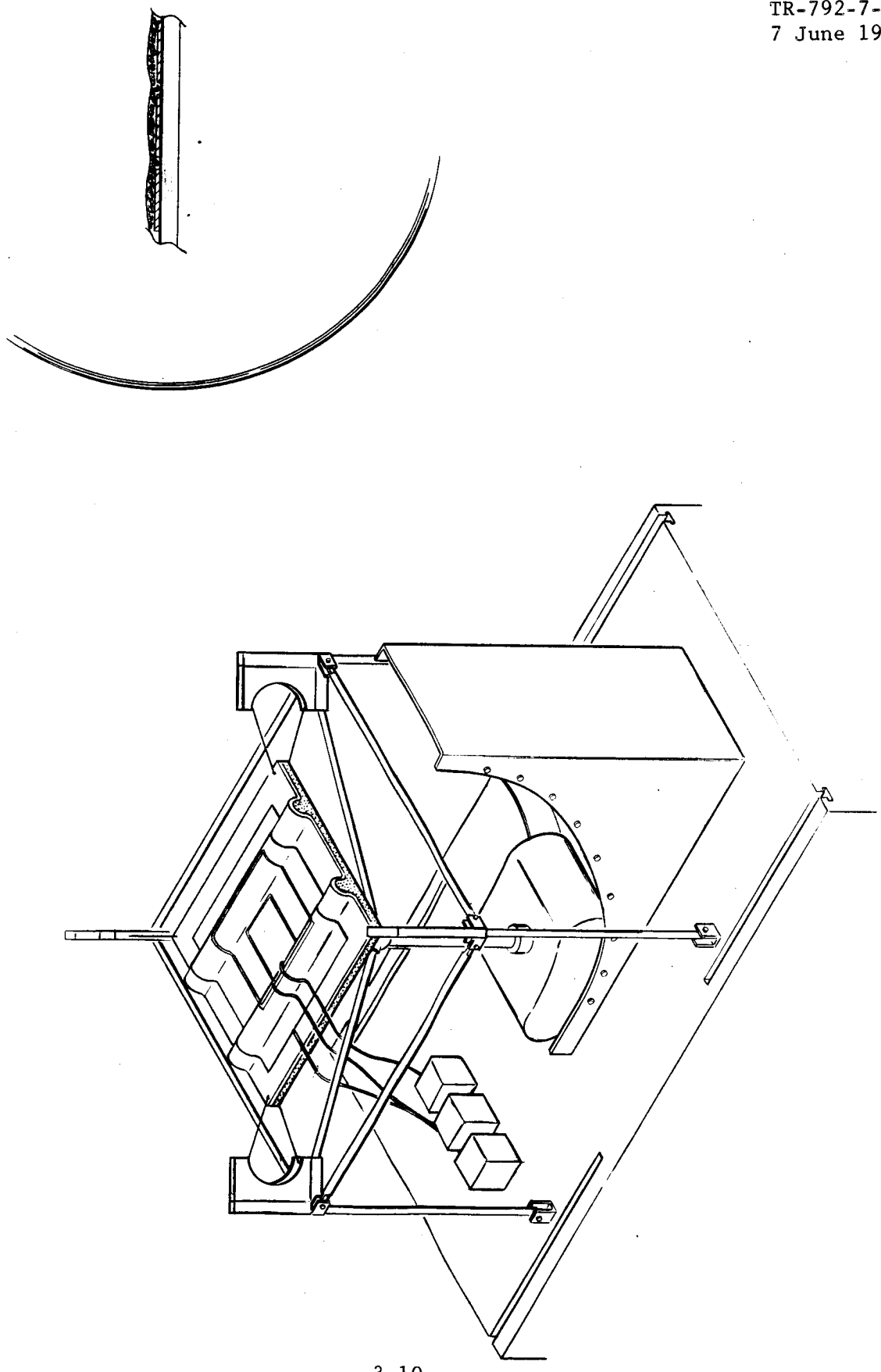


Figure 3-5. PRELIMINARY ELECTROSTATIC SURFACE CONCEPT

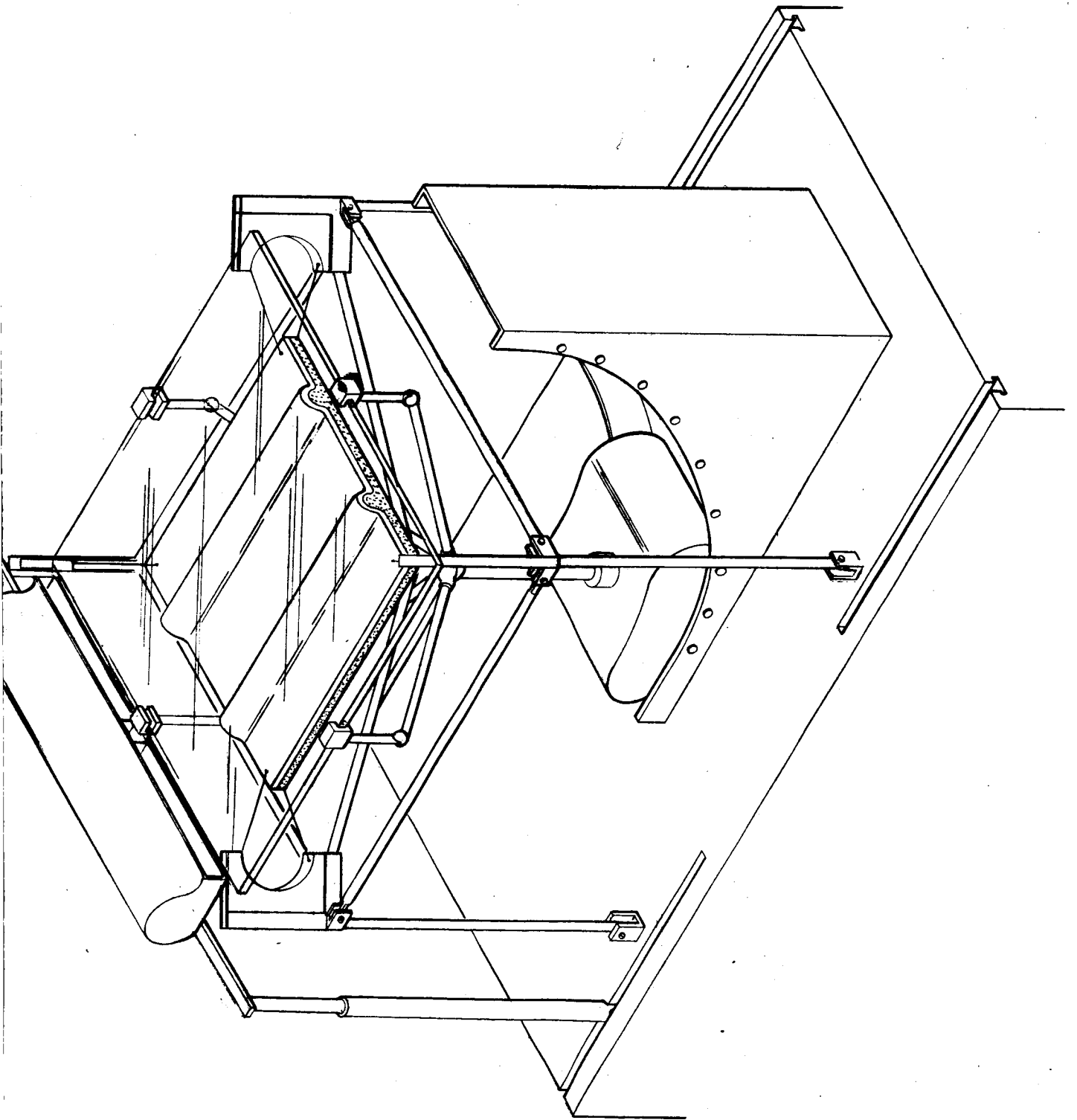


Figure 3-6. PRELIMINARY JET AND SHIELD CONCEPT

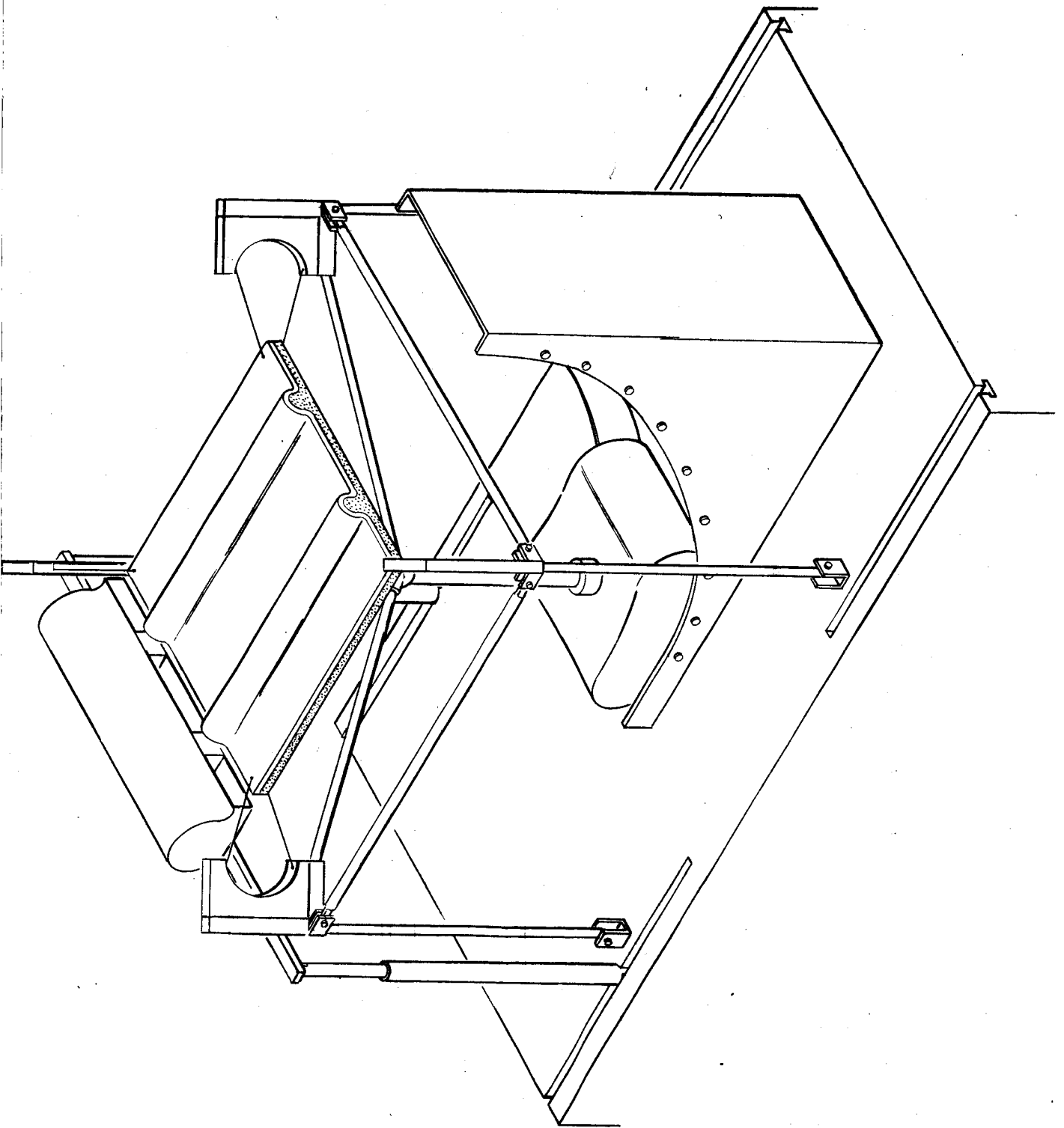


Figure 3-7. PRELIMINARY JET AND SURFACE CONCEPT

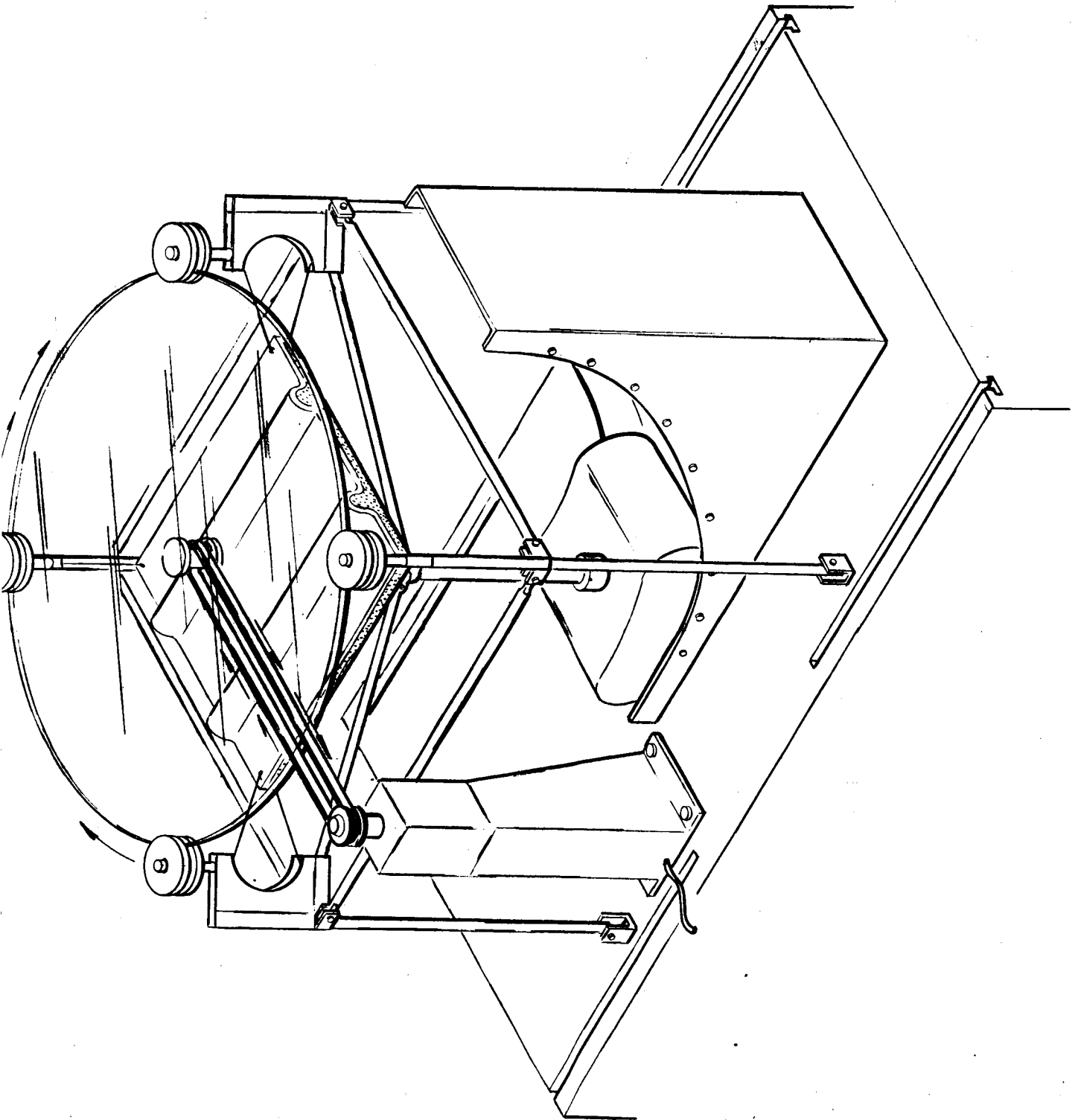


Figure 3-8. PRELIMINARY SPINNING SHIELD CONCEPT

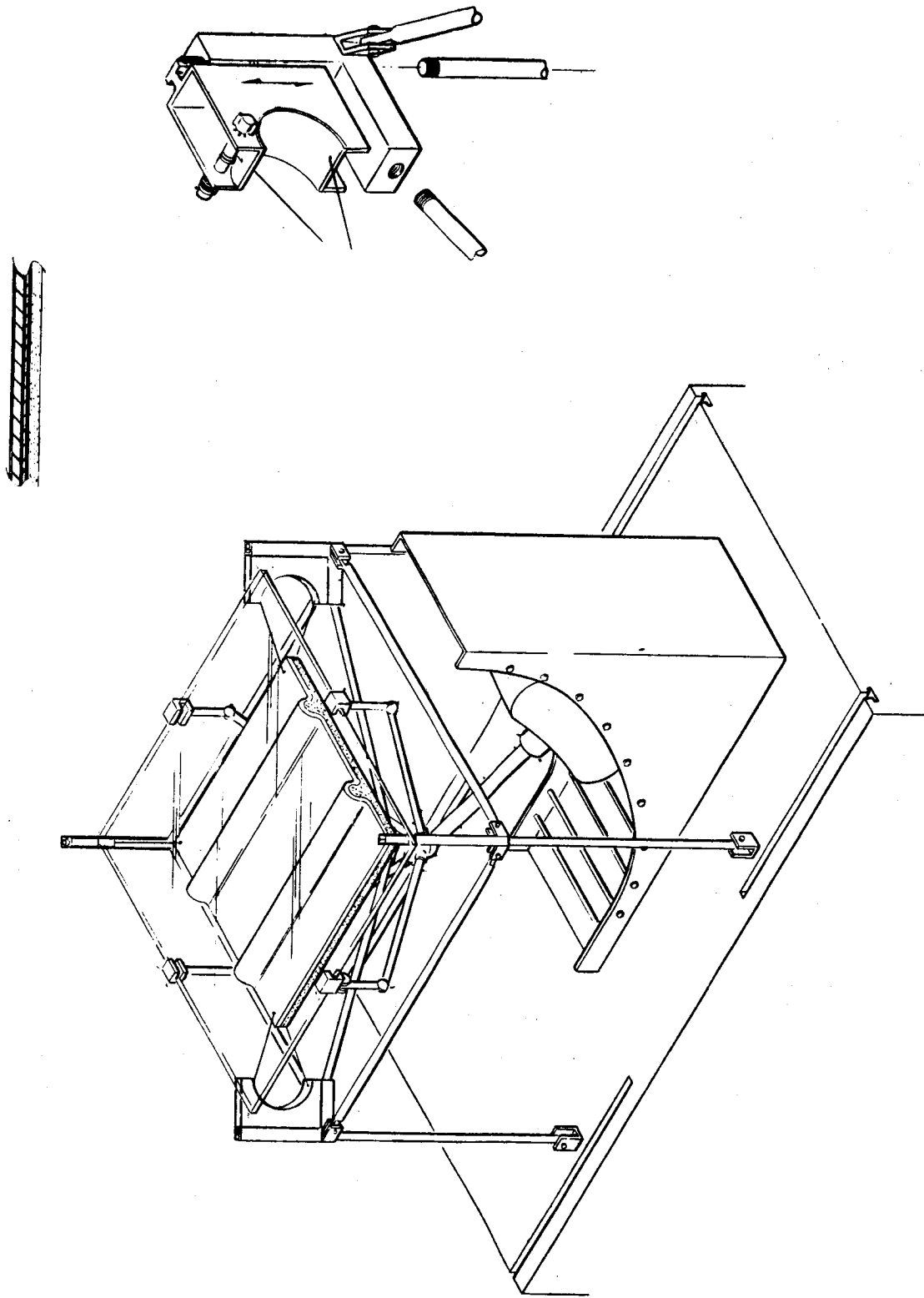


Figure 3-9. PRELIMINARY VIBRATING SHIELD CONCEPT

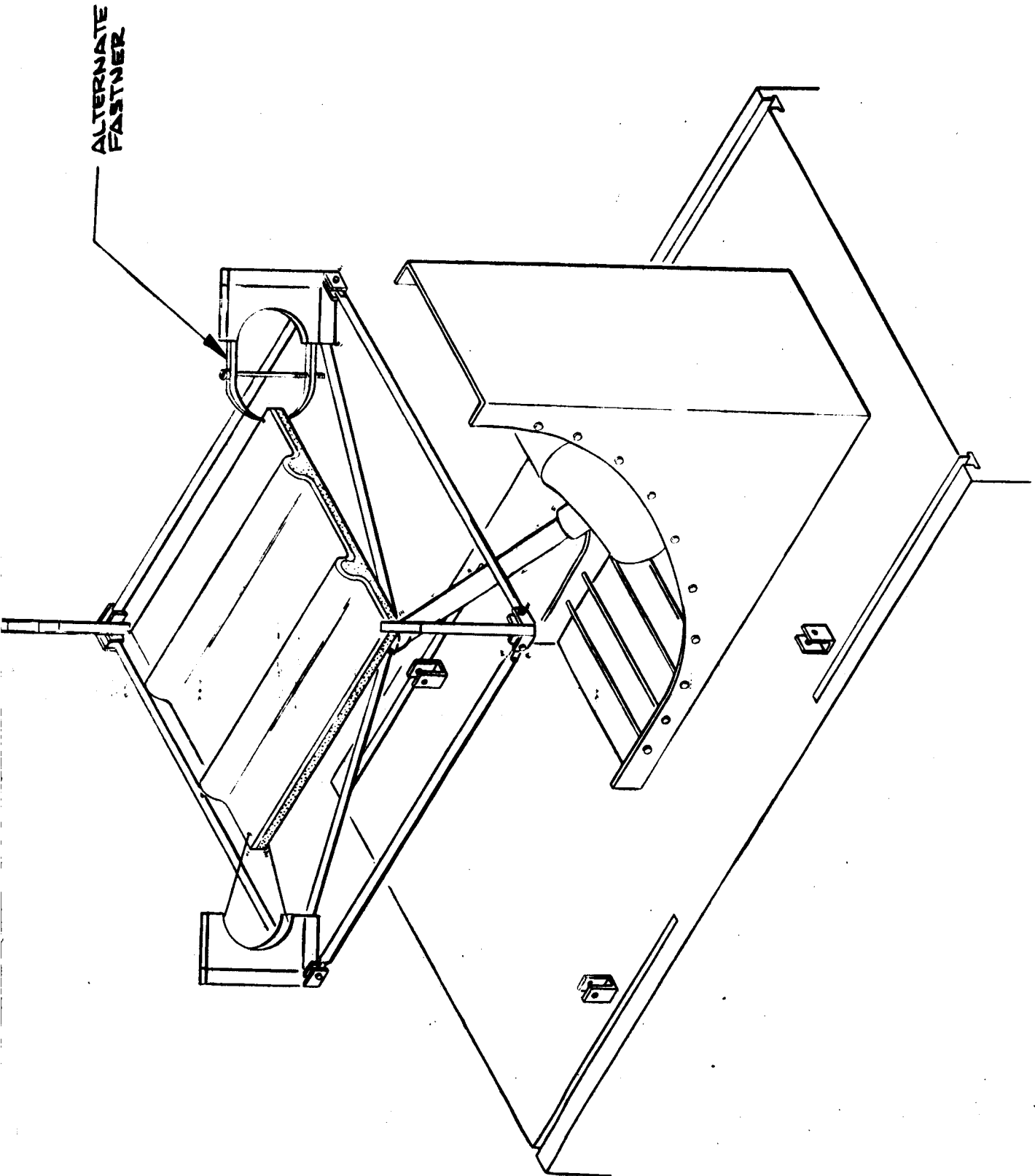


Figure 3-10. PRELIMINARY VIBRATING SURFACE CONCEPT

all eight concepts were delivered to the NASA Technical Representative at this meeting. The charts used in the presentation are provided in Appendix B along with a discussion of their development. Chart 1 provides the basic philosophy for the conceptual design of any of the devices. Chart 2 summarizes the available forces for removing the dust. The eight devices and the force associated with each are summarized in Chart 3. The performance parameters were divided into two categories; experimental and operational. The experimental parameters which are shown in Chart 4 reflect the feasibility of carrying out a test program with experimental models of the concepts. The operational parameters, presented in Chart 5, are concerned with the practicality of a particular concept for an operational system on the Moon. These parameters were subdivided into two groups: operational factors and operational considerations. Essentially the operational factors were those parameters which were more quantitative in nature, while the operational considerations were those which were more qualitative. It should be noted that astronaut maintenance, implying astronaut extravehicular activity (EVA), was one of the operational factors. The avoiding of astronaut EVA was one of the basic guidelines for the entire research effort.

Performance matrices were developed to present the grades assigned to each device for each parameter. These matrices are presented in Charts 6 through 9. Mass and power requirements were regarded as important enough to have a separate chart (Chart 9) devoted to the calculated values for the various systems. The data presented in this chart were based on the mass or power associated with cleaning or shielding 0.093 square meter of radiator surface in one second. In those cases where the overall size of the radiator surface affected the calculations, a 3.04- by 3.04-meter surface was used. It was assumed that $0.00159 \frac{\text{kg}}{\text{watt}}$ was the powerplant mass per power produced, and this factor multiplied by the power requirement for each system gave the "mass for power." Including this as part of the system weight was not necessarily appropriate as the system will not operate continuously and the power supply used for it can be used for

other purposes as well. The "mass for power" in every case, however, was negligible in comparison with the mass of the entire system, and thus this additional mass had no significant effect on the relative operational merit of the concepts.

A summary matrix is provided in Chart 10 to indicate the relative merit of the various concepts and to indicate the order of priority for design, fabrication, and test. As this chart indicates, the vibrating surface was assigned priority no. 1. The jet and shield was assigned priority no. 2, while the brush operating on the transparent shield was given priority no. 3. These three devices were definitely to be tested. The electrostatic curtain, which was fourth in priority, was to be tested providing time and funds permitted. The selection of the two devices involving shields was motivated by a desire to avoid imposing excessive handicaps on concepts due to the affinity of S-13 for dust.

3.4 WORKING MODEL DESIGN AND FABRICATION

Based on the priority established in the preceding subsection, working drawings were developed for the first three concepts. A list of these drawings is provided in Appendix D.

For the vibrating surface, provision was made for either a mechanical vibrator or a piezoelectric oscillator to be used as the source of vibration. A Goodman V-47 vibrator was selected for the mechanical vibrator. The design, as shown in Figure 3-11, called for the shaft of the V-47 vibrator to be positioned on the lower face of the test plate so that vibration could be induced either by continuous motion with the shaft attached to the plate or by impact with the shaft unattached to the plate. For piezoelectric vibration, piezoelectric crystals (Type 10D4 HDT-31) 10.24 cm in diameter and 0.256-cm thick were ordered from Gulton Industries, Inc. The design called for one crystal to be bonded to the lower face of the test plate. The crystal

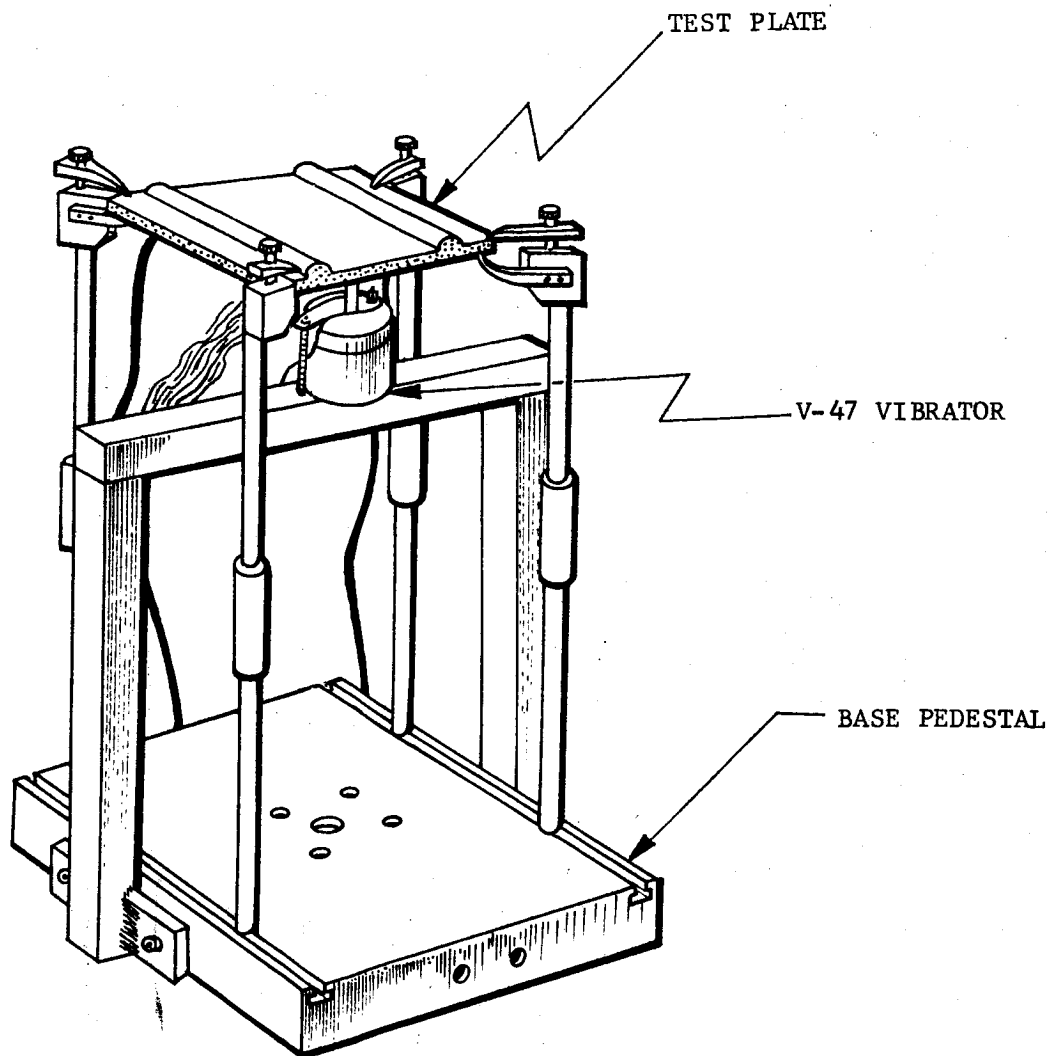


Figure 3-11. FINAL DESIGN FOR VIBRATING SURFACE
DEVICE WITH V-47 VIBRATOR

was to oscillate in the radial mode causing the plate to vibrate in a similar manner. The frequency of oscillation was to be varied to remove dust located in a nodal area (corresponding to a specific frequency) on the plate.

The final version of the jet and shield device is shown in Figure 3-12.

Preliminary test results indicated that for a compressible fluid a simple converging nozzle produced a jet with shearing stresses equal to those obtained with a converging-diverging nozzle. Several different sizes of converging nozzles (hemispherical slit models 3/8" TTL, TTP, TTQ, TTR, TTU, and TTV) were obtained from Spraying Systems Company. These nozzles are shown in Figure 3-13(a). Provision was also made for the use of an incompressible fluid in the jet and shield concept. For this case special nozzles (Models 1/4" P5010, 3/8" P5025, and 3/8" P5040) from Spraying System Company, designed for use with incompressible fluids, were selected. The incompressible flow nozzles are shown in Figure 3-13(b). As noted in Figure 3-10, the position of the nozzles relative to the plate or shield was adjustable.

A number of different materials were considered for the transparent shield. These included potassium chloride (KCl), sodium chloride (NaCl), arsenic trisulfide ($As_2 S_3$), and arsenic modified selenium glass. The ideal characteristics of such a shield would be high transmittance in the infrared spectrum and high reflectance in the solar spectrum. Evaluation of the relative performance of the four materials listed was hampered by lack of available data concerning their values of transmittance and reflectance in both the solar and infrared regions. Based on the available data plus cost and time considerations, arsenic-trisulfide glass manufactured by Servo Corporation of America under the trade name Servofrax was chosen.

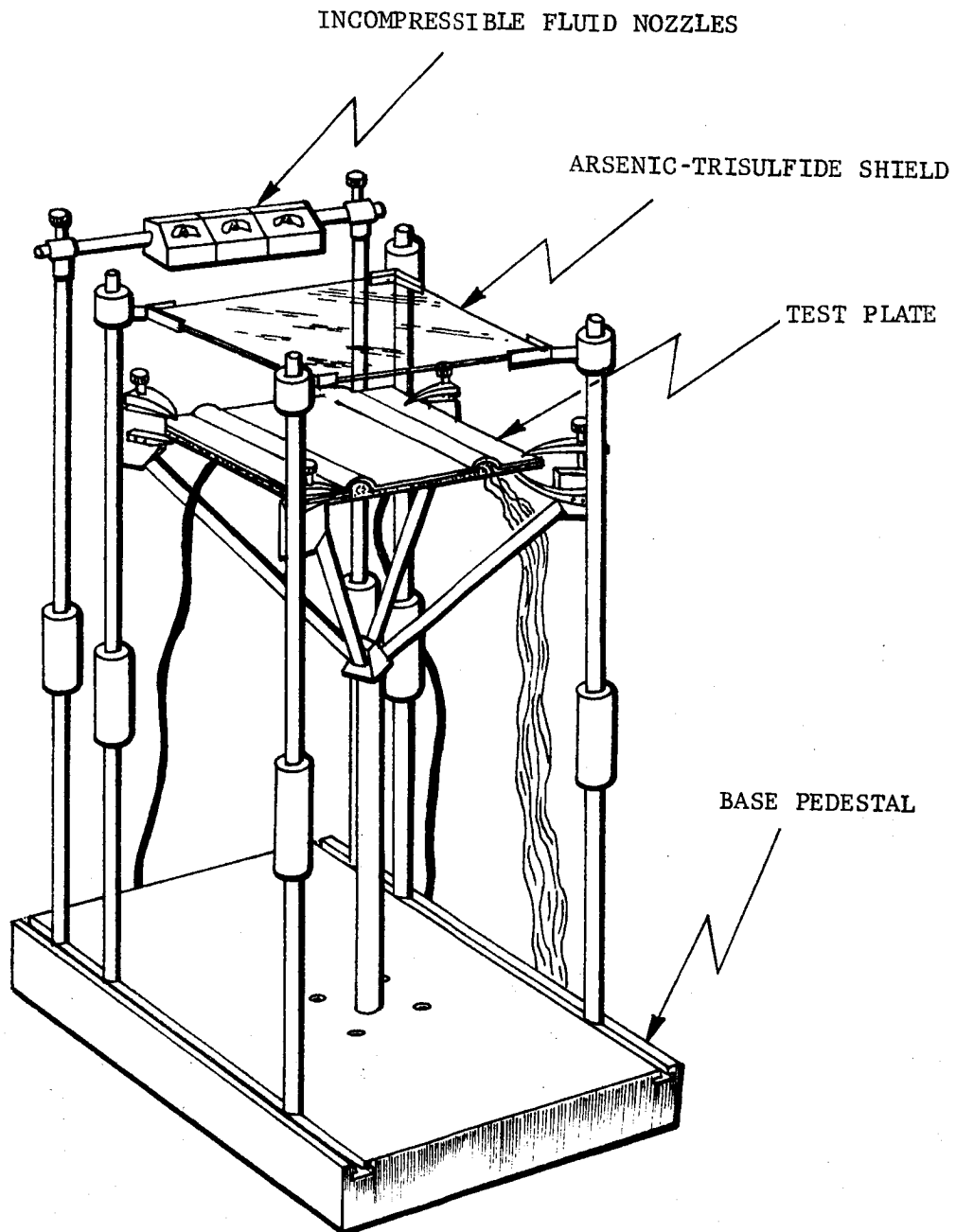
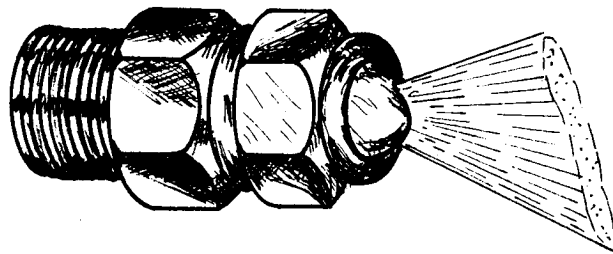
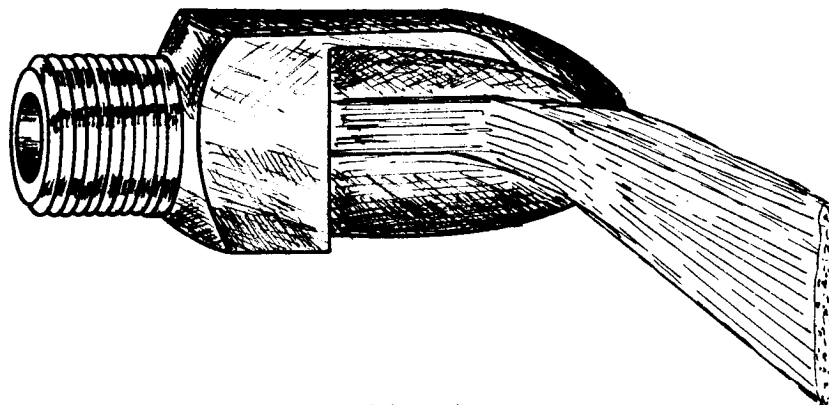


Figure 3-12. FINAL DESIGN FOR JET AND SHIELD DEVICE



a. Compressible Flow



b. Incompressible Flow

Figure 3-13. NOZZLES FOR JET AND SHIELD DEVICE

The final mechanical brush design, shown in Figure 3-14, involved a worm gear drive system which pushed the brush frame forward and back like a piston. The brush was attached to the frame by means of a slotted insert. The use of slotted inserts permitted the testing of more than one brush material for wiping the test plate or shield. Brush materials selected included bristles, cheesecloth, and styrofoam.

The electrostatic curtain design was so similar to that for the mechanical brush that no design drawings were necessary. Basically a special slotted insert was to be used with the mechanical brush design. This insert, which was to be connected to a high-voltage electrostatic generator, consisted of three parts as shown in Figure 3-15. The center was an electrical conducting wire or rod. The upper portion, where the insert joined the brush frame, was composed of an electrical insulator. The lower face of the insert, which was to be in contact with the dusted plate or shield, was dielectric material.

As previously noted in subsection 3.3, 15.4-cm square aluminum plates 0.103-cm thick were selected for use as the radiator panel. These plates were of two types, flat and non-flat. The non-flat plates had 2 half-cylindrical humps on their surface to simulate the top of a fin-tube radiator surface. The design of these test plates called for the upper face to be coated with S-13 paint while the lower face was to be coated with a spray-on resistance heating material 0.04- to 0.05-cm thick.

Fabrication of the first three concepts was performed by Metal Research, Inc. The spray-on resistance heater plates were applied by Electrofilm, Inc. The S-13 coatings for the same plates were applied by Northrop. Because of lack of funds the electrostatic device was never fabricated.

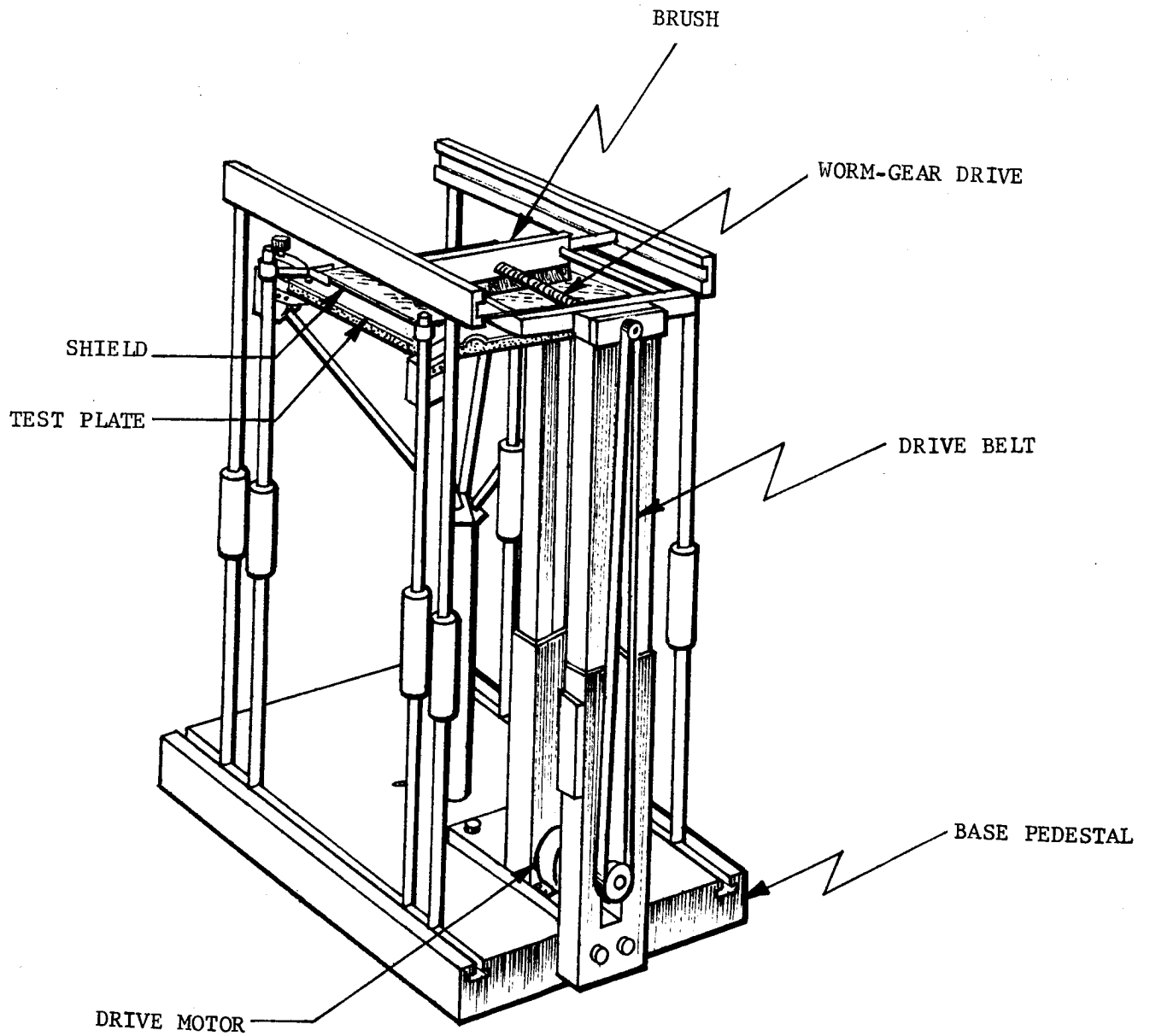


Figure 3-14. FINAL DESIGN FOR MECHANICAL BRUSH AND SHIELD DEVICE

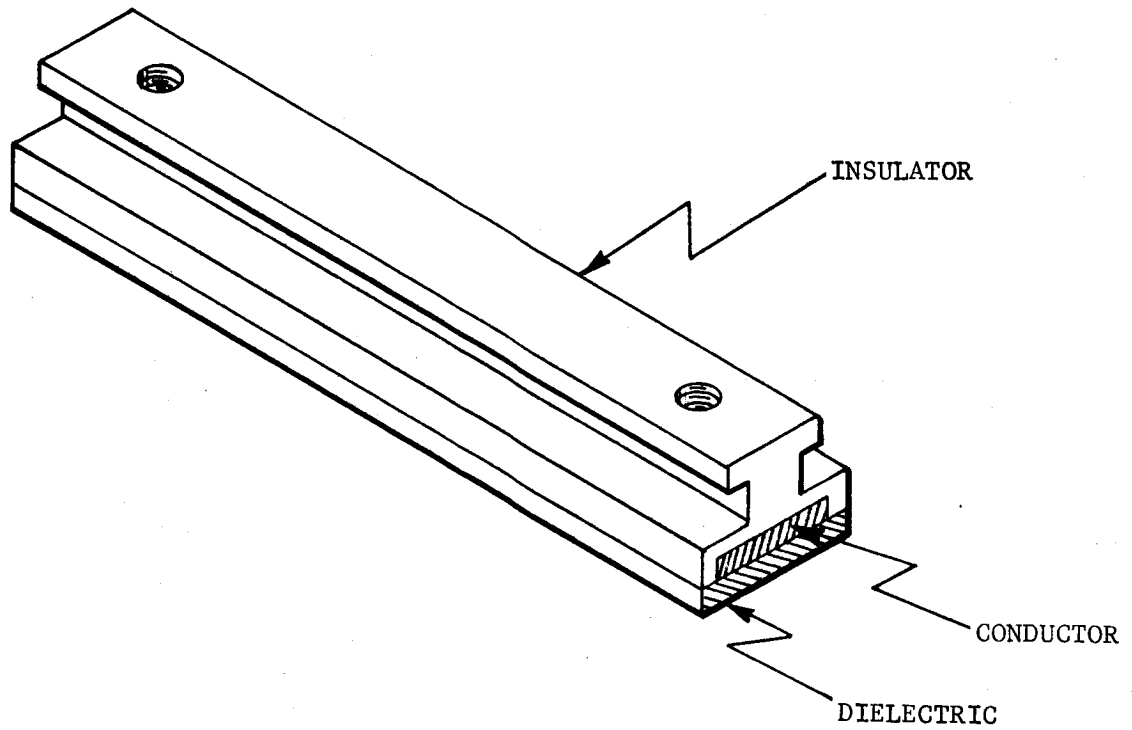


Figure 3-15. ELECTROSTATIC CURTAIN INSERT

3.5 PERFORMANCE TESTING

In testing the dust removal/prevention devices, the basic philosophy was to carry out simple preliminary tests under atmospheric conditions, followed by tests at low pressure without a heat load in a bell jar or vacuum chamber. Based on the results from these two types of tests, the final tests of each device were carried out in a vacuum chamber with a heat load. Because of delays encountered in receiving certain parts of the apparatus, the actual order of testing was:

- 1) Jet concept
- 2) Vibrator concept
- 3) Brush concept
- 4) Electrostatic concept (preliminary only).

3.5.1 General Test Arrangement and Procedure

The final tests for each device were carried out in Northrop's 3.65 x 2.13-meter space chamber shown in Figure 3-16. Chamber wall temperature for each test was maintained at 80°K by means of liquid nitrogen. Chamber pressure ranged from 10^{-6} to 10^{-5} torr.

The solar simulation was supplied by a Strong Electric Corporation carbon-arc lamp (Model 75000-1) shown in Figure 3-17. This lamp was placed outside the chamber and aimed at an 18-cm diameter port in the chamber wall. The beam was then deflected 90° downward, by a first-surface aluminum mirror, onto the test specimen. The lamp was positioned such that the intensity of the beam when focused on the test specimen was one sun. Figure 3-18a and 3-18b provide general views of the space chamber and solar simulator during the tests. The beam was approximately 23 cm in diameter at the plane of the test specimen. Radiometers (Model # P-1401-B-03-000-072 from Hy-Cal Engineering) were used to monitor the radiation intensity during test runs.

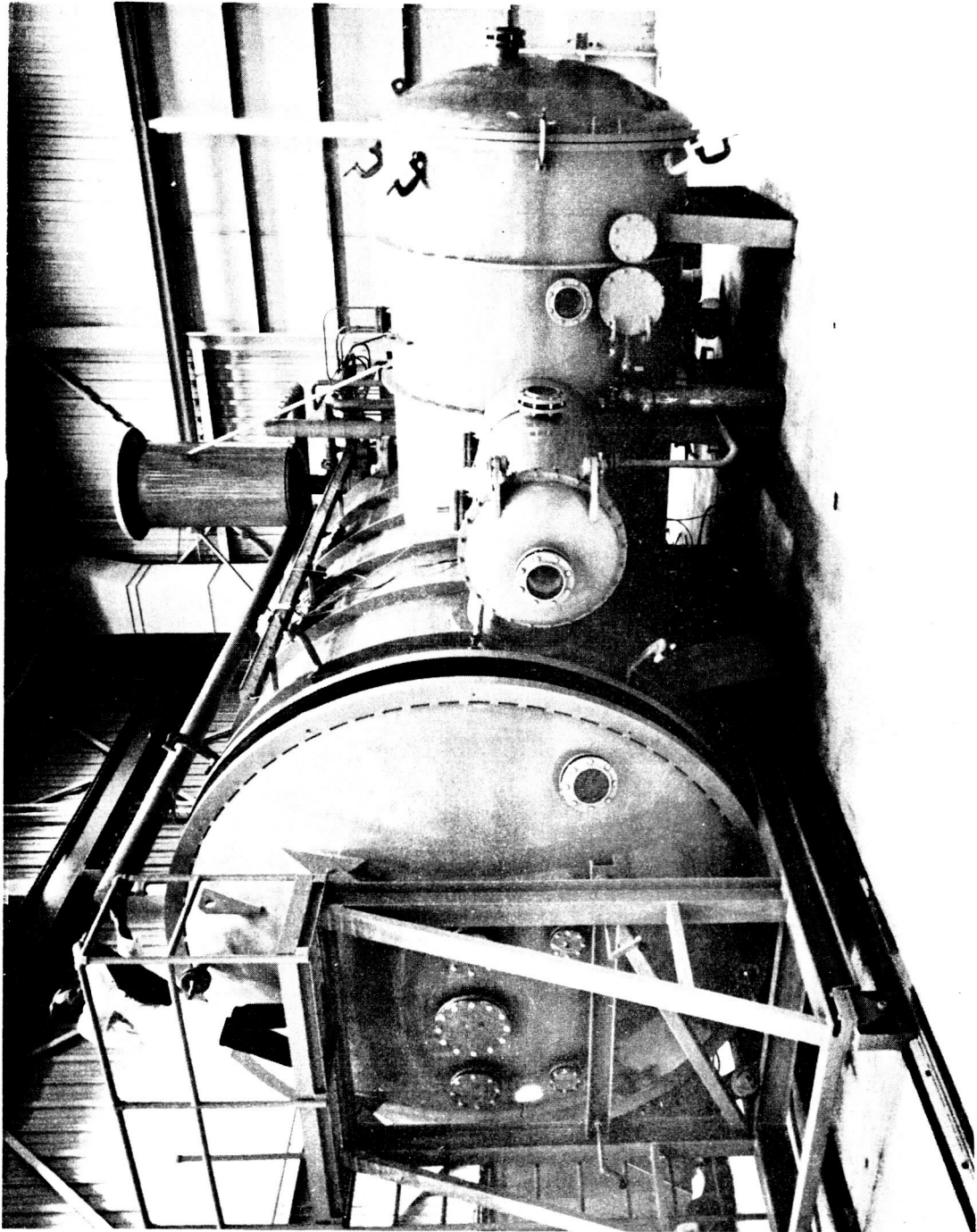
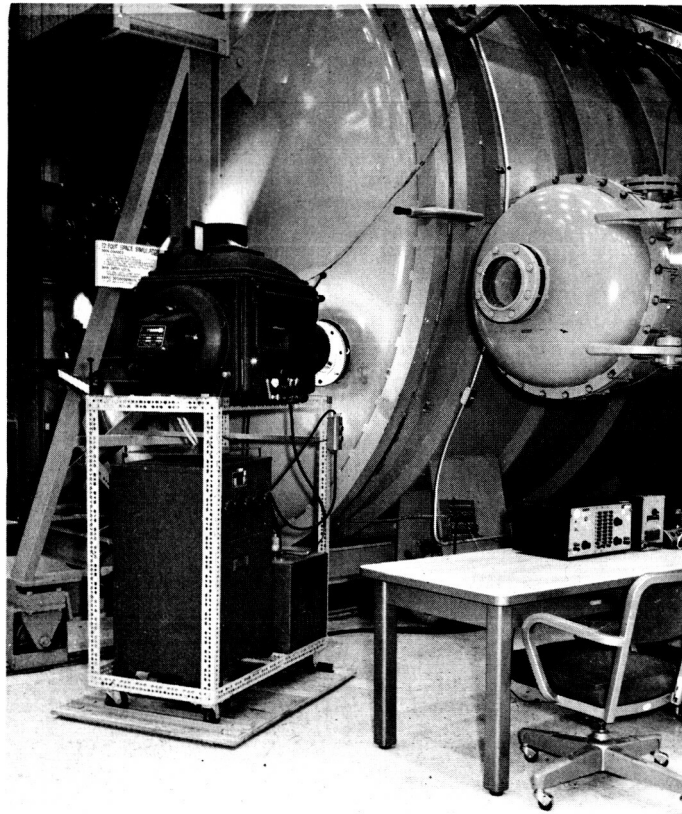


Figure 3-16. NORTHROP'S 3.65- X 2.13-METER SPACE CHAMBER

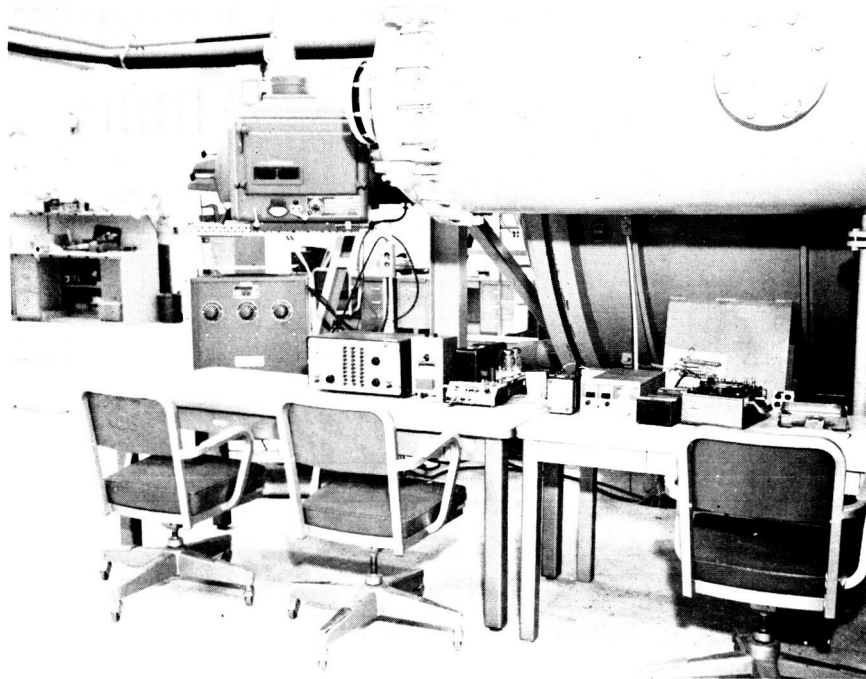
TR-792-7-207B
7 June 1967



Figure 3-17. THE CARBON ARC SOLAR SIMULATOR USED WITH THE SPACE SIMULATION CHAMBER



(a)



(b)

Figure 3-18. SOLAR SIMULATOR AND SPACE CHAMBER TEST ARRANGEMENT

7 June 1967

Power was supplied to the resistance heater coating by means of a regulated DC power supply, Model LH 131 FM, manufactured by Lambda Electronics Corp. A Weston portable standard wattmeter, Model 310 was used to measure the power expended. The test plate was mounted in the apparatus as shown in Figure 3-19. The nylon tips on the support tongs proved effective in minimizing heat leakage. The underside of the test plate was insulated with aluminized fiberglass mat 0.48-cm thick.

The test samples were instrumented with chromel-constantan thermocouples to measure equilibrium temperatures of the samples. The thermocouples were made using 40-gauge wire to keep heat conduction losses to a minimum. Five thermocouples were attached to the underside of each test sample, one at each corner and one in the center. Holes were provided in the heating element coating to allow the thermocouples to be attached directly to the aluminum plate.

When used, the shield was mounted above the plate at a distance of 4.5 cm. The shield temperature was measured by means of chromel-constantan thermocouples attached on the edge of the shield.

3.5.2 Calibration Test Runs

Initial equilibrium temperature calibration tests were carried out with one of the test plates. Temperature readings from 4 of the 5 thermocouples attached to the panel were recorded with varying dust coverage and different ambient conditions. The thermocouples were attached at the center and near three of the four corners of the panel. The fourth corner of the test plate was damaged and no temperature measurements were recorded from that thermocouple. Because the temperatures from the other three corners were almost identical, the lack of temperature data for one corner did not warrant repeating the calibration test. There was, however, some

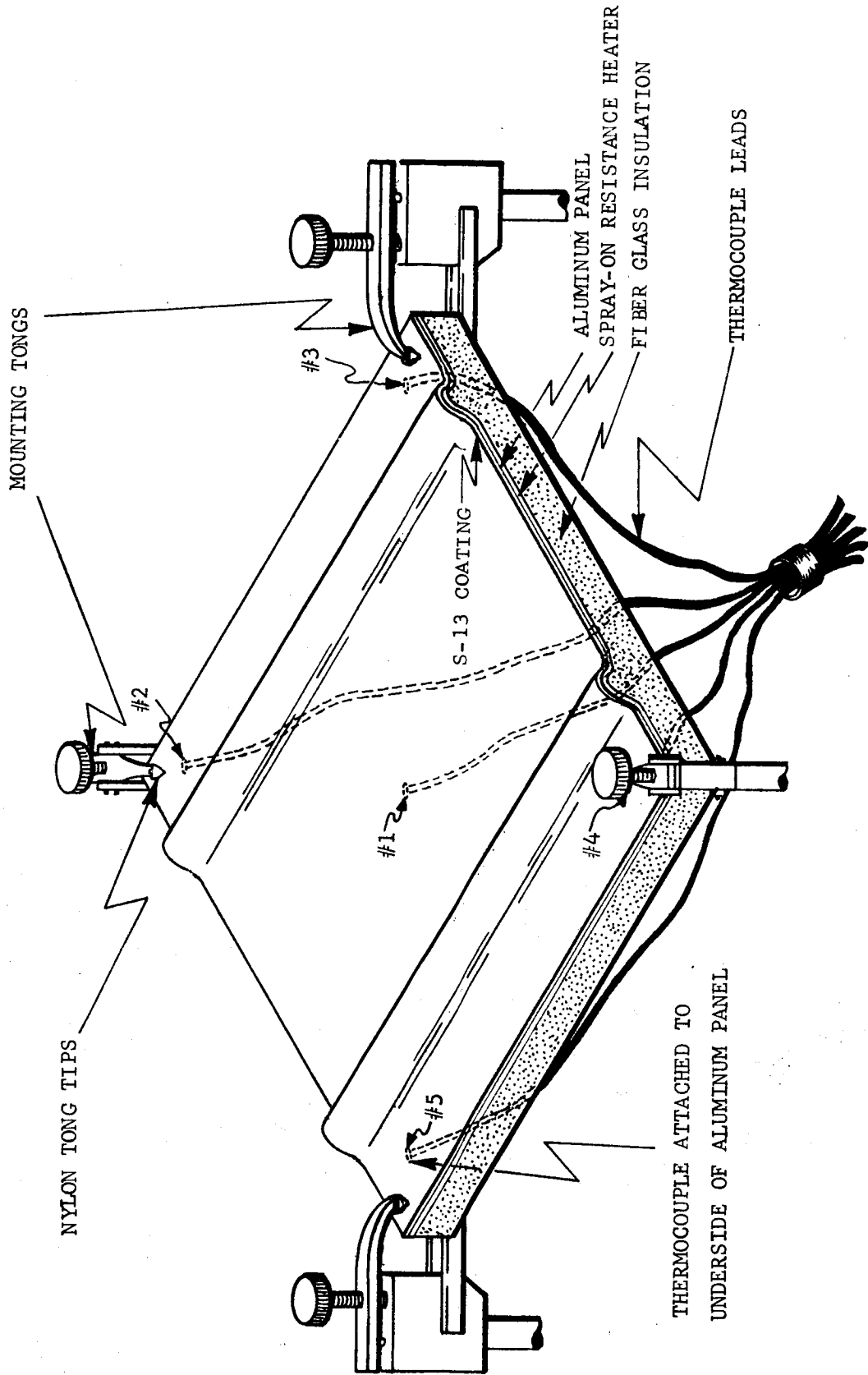


Figure 3-19. TEST PLATE ARRANGEMENT

heat leakage from the corners as shown by slightly higher temperatures at the center of the plate. The general test arrangement is shown in Figure 3-20.

A summary of the runs is presented in Table 3-2. For the first run a clean S-13 coated plate was used. For the second run the same plate was covered with basalt powder with particle size of 50μ (44μ to 53μ fraction) by sieving the dust on the surface of S-13. The amount of dust on this heavily dusted plate was not determined under the microscope, but the coverage was visually estimated to be 40 percent. The dusted plate is shown in Figure 3-20. After the measurements, the dust was blown off and the plate with the remaining fines, estimated to represent 3- to 4-percent coverage, was used for the third run. Finally, the plate was cleaned with toluene and used for the fourth run.

The environmental conditions for all tests were the same. The vacuum was in the order of 10^{-5} torr and the chamber walls were cooled by liquid nitrogen to $\sim 80^{\circ}\text{K}$. The intensity of irradiation falling on the sample from the solar simulator was 1 solar constant or 0.14 watt/cm^2 . To heat the plate in the vacuum to 366°K required 25 watts of power input to the Electrofilm heating elements, and about 32.5 watts to bring the temperature to 394°K .

3.5.3 Jet Concept Testing

As originally conceived, the jet concept was to be applied to cleaning the transparent shield. Because of the design of the experimental device, however, it was possible to conduct tests with the jet cleaning either the shield or the plate. As a result test runs for both combinations were carried out. The final version of the jet and plate model is shown in Figure 3-21.

TR-792-7-207B
7 June 1967

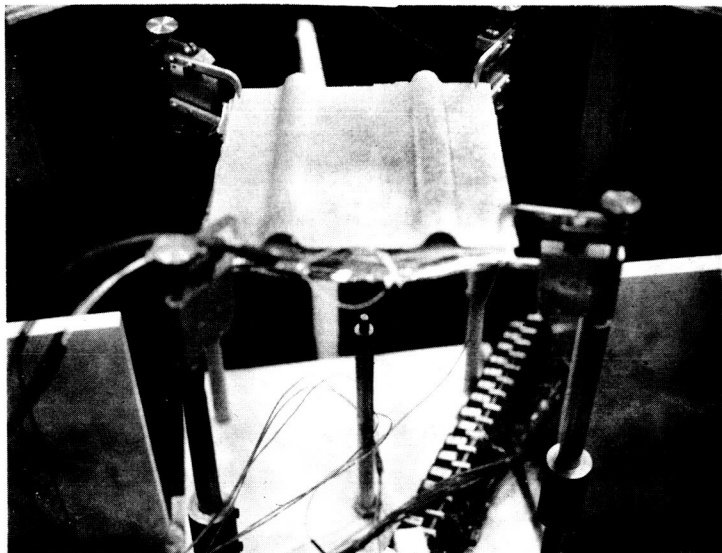


Figure 3-20. CALIBRATION TEST RUN FOR S-13 PLATE WITH 40-PERCENT DUST COVERAGE

Table 3-2. DATA FOR CALIBRATION TEST RUN

Surface: S-13 Coated Aluminum

Solar Simulator	Heat Load ($\frac{\text{watts}}{\text{cm}^2}$)	S-13 Temp ($^{\circ}\text{K}$) Thermocouple #					Test Set-up	Dust Coverage*
		1	2	3	4	5		
OFF	.0976	370	-	369.5	369.5	369.5	Clean S-13	0.0
OFF	.127	395	-	394	394	394		
ON	.0976	392	-	391	391	391		
OFF	.0976	379	-	378.5	378.5	378	Dusted S-13	0.40
ON	0	326.5	-	324	324	325		
ON	.0976	422	-	422	422	422		
OFF	.0976	366.5	-	365.5	365.5	365.5	Jet Cleaned S-13	0.03 - 0.04
OFF	.131	395.5	-	393	393.5	393.5		
ON	0	301	-	300	301	301		
ON	.0976	396	-	393	394	394		
ON	.131	421	-	415	418	418		
OFF	.0976	370	-	369	369	369	Toluene Cleaned S-13	~0.0
OFF	.128	395	-	393.5	393.5	393.5		
ON	0	276	-	275	275	275		
ON	.0976	391	-	389.5	389.5	389.5		
ON	.128	415.5	-	411	411	411		

* based on visual inspection.

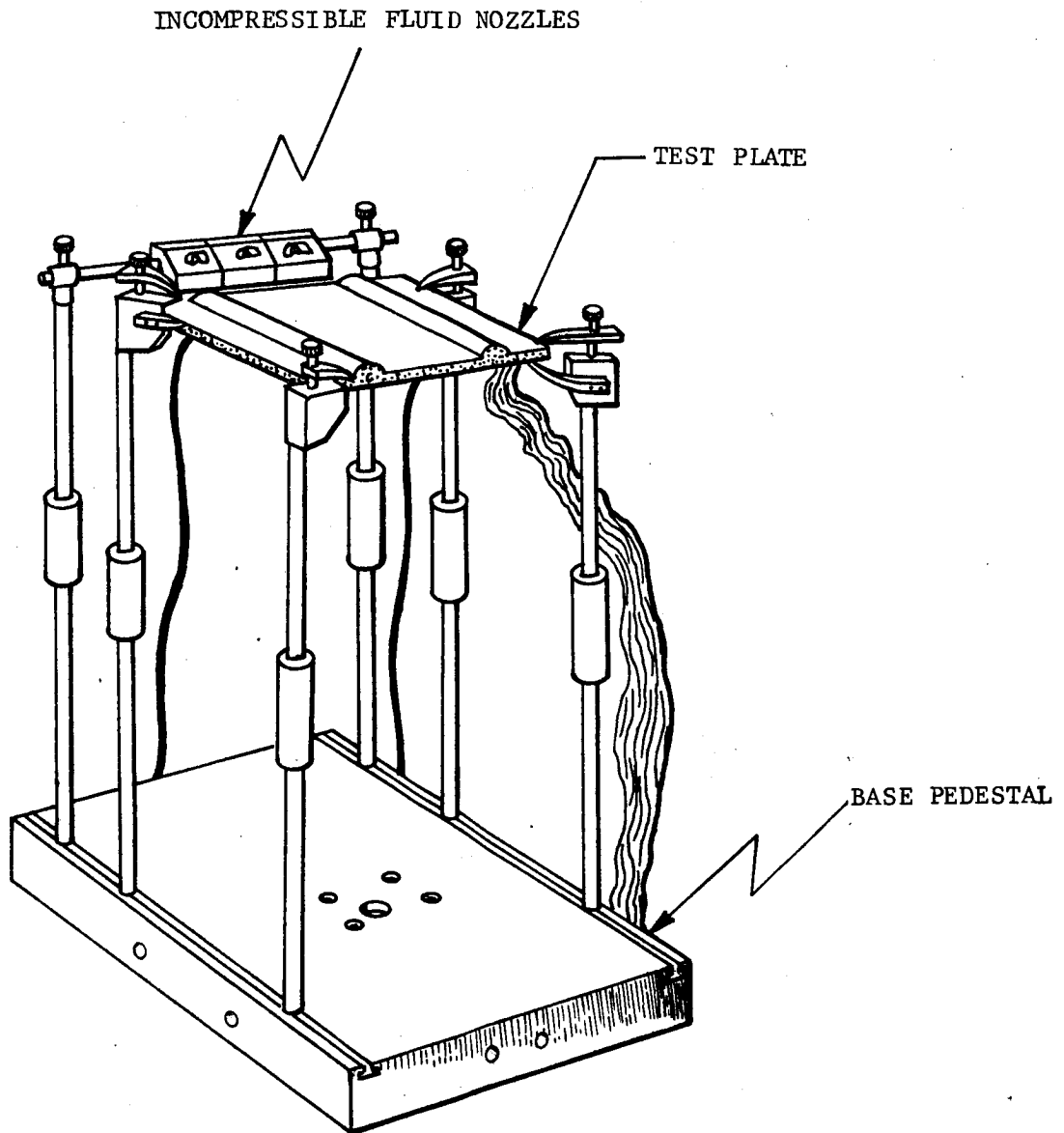


Figure 3-21. FINAL DESIGN FOR JET AND PLATE DEVICE

3.5.3.1 Preliminary Jet Testing. Before arrival of the special nozzle from Spraying Systems Company, preliminary tests both under atmospheric conditions and in the space chamber at 10^{-4} torr were carried out using several makeshift converging nozzles. Nitrogen gas at pressure ranging from 0.68 to 68 atmos. was used. These preliminary tests indicated that the effectiveness of the jet cleaning concept decreases with decreasing ambient pressure. In general with the nozzle located approximately 2.6 cm from the dusted surface, a significant amount of dust was removed only from that portion of the surface within 3 cm of the leading edge. In this region the residual dust was 2 to 3 percent. In general, large angles of incidence (relative to the normal) proved most effective.

3.5.3.2 Establishment of Working Fluid. Both compressible and incompressible fluids were used in the jet and shield tests. In all tests the shield was completely covered uniformly with basalt dust of particle size in the 44μ to 53μ fraction. Because of delays associated in the delivery of the arsenic-trisulfide glass, initial runs were carried out with ordinary plate glass (18.2 x 18.2 x 0.32 cm).

For compressible fluid gaseous nitrogen was used at 20.5 atmos. Three different hemispherical slit nozzles (models TTU, TTQ, and TTL) from Spraying Systems Company were tested. Chamber pressure was 2×10^{-4} torr.

Dust remained on the glass test plate with 2-percent (at the nozzle) to 75-percent coverage. This test with the three nozzles was repeated at ambient atmospheric pressure and resulted in less than 3-percent dust remaining on the plate. An additional test was run in vacuum with 1.28-cm baffles erected at the edges of the plate and parallel to the gas stream. The only effect of the baffles was to change the dust pattern without substantially changing its coverage.

7 June 1967

These tests confirmed preliminary test results indicating that a compressible jet was ineffective for dust removal from the experimental apparatus in a vacuum.

The first incompressible fluid tested with the jet and shield concept was water. The water pressure was 4.44 atmos. and flow was controlled (on-off) by a solenoid valve at each of three nozzles. The nozzles were all "flatjets" made by Spraying Systems Company. Three sizes were used: 1/4" P5010, 3/8" P5025, and 3/8" P5040. The nozzles were located as close as possible to the top of the glass plate with the nozzle axis parallel to the plate. Under atmospheric pressure, this was the position providing the most effective sweep of the glass. The spray was about 45° from the nozzle axis.

There was no noticeable difference in the cleaning effect of the three nozzles. Chamber pressure was 10^{-6} torr at the beginning of the test. The water froze immediately on leaving the nozzle and flakes of ice were visible 50 milli-seconds after the valve was opened. During this test, the valve was open 0.5 second. For this entire period, ice left the nozzle area in random sizes. Some pieces were about 2 cm across, but all were very thin in cross section. It is possible that the water froze in these thin sheets on striking the nozzle deflector. There was a partial removal of dust, but the glass plate was not cleaned. After the ice sublimed from the glass, there was a mottled residue of dust remaining on the glass plate. This residue possibly resulted in part from impurities in the water.

The second incompressible fluid tested was benzene which, at a pressure of 3.4 atmos., was sprayed onto the test plate. Chamber pressure was in the 10^{-6} torr range. The nozzle, a Spraying Systems Company 3/8" P5025 flatjet was located 18 cm above the edge of the test plate with the nozzle axis parallel to the plate surface.

The spray was activated for about 0.5 second and the test plate then examined for dust coverage. The remaining dust coverage was 2 percent at the minimum (near the nozzle) to 20 percent at the maximum.

The third incompressible fluid tested was inhibisol (methyl chloroform). The initial tests with inhibisol were carried out in the same manner as described previously for benzene. Dust remaining after the test varied from 4 percent to 10 percent. The test was run again for confirmation and resulted in 5-percent to 10-percent dust coverage remaining.

During the initial tests with nitrogen and the three liquids mentioned, high-speed (100 frames/sec) cinematography was utilized to record results. Based on an analysis of the resulting films, as well as an examination of the dusted surfaces after each test, inhibisol was selected as the most promising working fluid for further testing.

The next series of tests was designed to determine the optimum position of the nozzle relative to the dusted surface with inhibisol as the working fluid. A 3/8" P5025 nozzle was used. The test arrangement is shown in Figure 3-22. In all cases the inhibisol was at a pressure of 3.4 atmos. and chamber pressure was less than 10^{-5} torr. The spray was activated for 0.5 to 1.0 second. Test results are tabulated in Table 3-3. Test No. 5 indicates that the inhibisol jet can satisfactorily clean the S-13 surface as well as glass. Dust coverage was determined under the microscope and by measuring solar absorptivity of a representative area. The dusted "sample" had $\alpha_s = 0.236$, indicating 3.5-percent coverage (see Table 2-4). For a clean sample $\alpha_s = 0.186$.

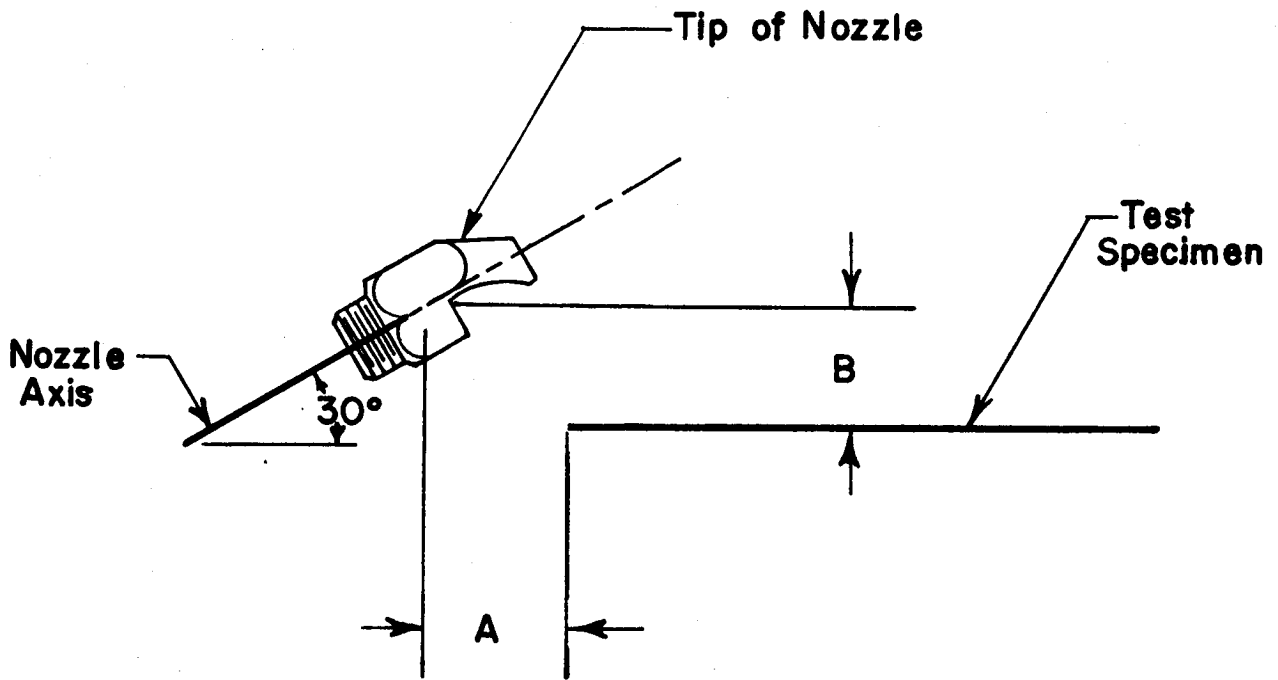


Figure 3-22. TEST ARRANGEMENT FOR DETERMINATION OF OPTIMUM NOZZLE POSITION WITH INHIBISOL

Table 3-3. OPTIMUM NOZZLE POSITION TEST RESULTS

<u>Test No.</u>	<u>Specimen</u>	<u>A. (cm)</u>	<u>B. (cm)</u>	<u>Dust Coverage - Remaining</u>
1	glass	7.68	1.28	0.10
2	glass	3.84	3.84	0.02 - 0.10
3	glass	3.84	6.40	0.02
4	polished aluminum	3.84	6.40	0.01
5	S-13 coated aluminum	3.84	6.40	0.35

3.5.3.3 Final Jet Tests. The final tests with the inhibisol jet concept involved the use of the solar simulator and the resistance heater and was carried out in three parts. First the jet was used to clean a dusted S-13 plate without a shield. Second, the jet was applied to a dusted glass shield covering the S-13 plate. Finally the jet was used to clean a dusted arsenic-trisulfide shield covering the S-13 plate. The glass and As_2S_3 shields were placed 4.5 cm above the test plate. The glass shields measured 18.2 by 18.2 by 0.32 cm while the arsenic trisulfide was 17.9 by 17.9 by 0.64 cm. In all runs chamber pressure was $\sim 10^{-6}$ torr. The methyl chloroform spray was activated in the first test with chamber wall temperature at 150°K. This resulted in the inhibisol freezing in the feed line to the nozzle and produced a frozen particle spray which left a dust residue of from zero to twenty percent. This test was repeated with the chamber walls at room temperature during the dust-cleaning portion of the test. This resulting in the inhibisol remaining in a liquid form as it traveled from the nozzle to the plate. The results obtained in terms of plate temperature for both the frozen inhibisol and the liquid inhibisol are shown in Tables 3-4a and 3-4b. The original test data for these runs are found in Appendix C.1.

Table 3-4a. DATA FOR JET CONCEPT TEST RUN WITHOUT SHIELD

Surface: S-13 coated aluminum
Spray: Frozen methyl chloroform (inhibisol)

Solar Simulator	Heat Load ($\frac{\text{watts}}{\text{cm}^2}$)	S-13 Temp (°K)	Test Set-Up	Dust Coverage*
OFF	.078	366	Dusted S-13 Without Shield	0.25
OFF	.078	366		
OFF	.101	393		
OFF	.101	391		
ON	.078	414		
ON	.101	431		
OFF	.0351	294	Spray Cleaned S-13 Without Shield	0.075
OFF	.078	357		
OFF	.117	393		
ON	0	298		
ON	.117	418		

*based on visual inspection

Table 3-4b. DATA FOR JET CONCEPT TEST RUN WITHOUT SHIELD

Surface: S-13 coated aluminum
Spray: Liquid methyl chloroform (inhibisol)

Solar Simulator	Heat Load ($\frac{\text{watts}}{\text{cm}^2}$)	S-13 Temp (°K)	Test Set-Up	Dust Coverage*
OFF	.0663	360	Dusted S-13 Without Shield	0.25
OFF	.078	376		
OFF	.117	416		
OFF	.156	449		
ON	0	361		
ON	.0585	419		
ON	.078	433		
ON	.0975	449		
ON	.117	458		
ON	.137	471		
ON	.156	484		
OFF	.0351	294	Spray Cleaned S-13 Without Shield	0.03
OFF	.0585	331		
OFF	.0975	373		
OFF	.156	417		
ON	0	294		
ON	.0624	373		
ON	.0975	401		
ON	.156	437		

* based on visual inspection

For the tests involving the shields, the inhibisol spraying process was carried out with the chamber walls at room temperature and a liquid spray resulted. The results obtained for these tests involving the shields are provided in Tables 3-5 and 3-6. The original test data for these runs are found in Appendixes C.2 and C.3.

Unfortunately, a network of hairline cracks appeared in the As_2S_3 shields during testing. To what extent these cracks impaired the performance of the shields is difficult to establish. These As_2S_3 shields did not, however, appear to have performed in accordance with the performance specifications provided by the manufacturer.

3.5.4 Vibrator Concept

Two sources of vibration were utilized in conducting the vibration tests, mechanical and piezoelectric. For the mechanical vibrator, two methods of transferring the vibration to the test plate were considered. The first involved transfer by direct linkage or bonding. The second involved transfer by impact.

3.5.4.1 Preliminary Vibrator Tests. A 300V oscillator was assembled for the vibration tests. It consisted of a Krohn-Hite Model 440A oscillator connected to a McIntosh 75-watt amplifier. The output of the amplifier passed through a 115V to 700V step-up transformer yielding an output of 0-340V over a frequency range of 50-2000 cps.

Preliminary tests were performed with the V-47 vibrator. This vibrator has a frequency range of 10 to 2000 cps with a maximum displacement of 0.256 cm and a maximum force of 4.45×10^5 dynes. In the first of the preliminary tests under

Table 3-5. DATA FOR JET CONCEPT TEST RUN WITH GLASS SHIELD

Surface: S-13 coated aluminum
Shield: Glass
Spray: Liquid methyl chloroform (inhibisol)

Solar Simulator	Heat Load ($\frac{\text{watts}}{\text{cm}^2}$)	S-13 Temp (°K)	Shield Temp (°K)	Test Set-Up	Dust Coverage*
OFF	.0195	266	---	Clean S-13 Coated Aluminum No Shield	0.0
OFF	.0234	273	---		
OFF	.0897	369	---		
OFF	.121	396	---		
ON	0	272	---		
ON	.0897	389	---		
ON	.121	412	---		
OFF	.0585	350	256	Clean Glass Shield Over Specimen	0.0
OFF	.0897	387	276		
ON	.0585	381	289		
ON	.0897	408	307		
OFF	.0741	368	261	Dusted Glass Shield Over Specimen	0.25
OFF	.101	399	280		
ON	.0741	396	314		
ON	.101	423	327		
OFF	.0585	353	256	Spray-Cleaned Glass Shield Over Specimen	< 0.05
OFF	.0897	387	275		
ON	.0585	382	290		
ON	.0897	412	304		
ON	.101	422	310		

*based on visual inspection.

Table 3-6. DATA FOR JET CONCEPT TEST RUN WITH ARSENIC TRISULFIDE SHIELD

Surface: S-13 coated aluminum
Shield: Arsenic trisulfide (As_2S_3)
Spray: Liquid methyl
chloroform (inhibisol)

Solar Simulator	Heat Load ($\frac{\text{watts}}{\text{cm}^2}$)	S-13 Temp (°K)	Shield Temp (°K)	Test Set-Up	Dust Coverage *
OFF	.0059	216	---	Clean S-13 Coated Aluminum No Shield	0.0
OFF	.0078	227	---		
OFF	.0117	247	---		
OFF	.0351	301	---		
OFF	.078	358	---		
OFF	.137	408	---		
OFF	.195	445	---		
ON	.0585	358	---		
ON	.0897	388	---		
ON	.121	411	---		
OFF	.078	370	249	Clean As_2S_3 Shield Over Specimen	0.0
OFF	.137	420	270		
ON	.0585	374	319		
ON	.137	437	335		
OFF	.0585	349	255	Dusted As_2S_3 Shield Over Specimen	0.25
OFF	.0897	387	277		
OFF	.137	426	295		
ON	.078	391	320		
ON	.137	440	342		
OFF	.0897	384	262	Spray-Cleaned As_2S_3 Shield Over Specimen	<0.05
OFF	.137	423	280		
OFF	.183	451	295		
ON	.078	395	327		
ON	.137	437	338		

* based on visual inspection.

atmospheric conditions the shaft of the vibrator was bonded to a 15.4- by 15.4-cm aluminum plate. Mechanical transfer to the plate was good except at higher amplitudes with lower frequencies. The dust could be removed fairly well from a clean aluminum plate. However, finer dust remained in a spiral path from the center out, following a nodal area located in a circle about half-way between the center and the edges of the plate. The dust could not be vibrated from the S-13 coating on an identical aluminum plate.

In a second test, the shaft of the vibrator was not attached to the plate. A 2.56-cm diameter aluminum disc was attached to the V-47 head and placed 0.005 cm below the test plate and set into vibration. With the test system tilted 15°, the polished aluminum plate was cleaned to within 2-percent residual dust coverage. Results with an S-13 coated plate were less satisfactory. Approximately 15-percent dust coverage remained.

In testing the piezoelectric vibrator, the crystal was bonded to a 15.4- by 15.4-cm plate of aluminum, and was then excited by a wide range of voltages (up to 800 volts) at frequencies throughout and above the audio range. In the initial test the aluminum plate was resting on a laboratory table top and was tilted at various angles to the horizontal during crystal excitation, with marked improvements in performance as angle of tilt increased. As expected, excitation at the resonant frequency gave the best results, but adequate dust removal was not achieved by this method. An excessive residue of fines remained, even after extended periods of vibration. Because these initial tests were carried out under atmospheric pressure, the results obtained were not considered conclusive.

Subsequent tests with the piezoelectric crystal were conducted using different clamping and suspension techniques. The 15.4- by 15.4-cm aluminum plate was:

(1) suspended by clamps at the four corners, (2) clamped along all four edges, (3) clamped on two opposite edges, and (4) clamped along one edge. In each case the crystal was excited up to 800 volts at frequencies throughout and above the audio range. Dust removal was not satisfactory.

Based on the results of these preliminary tests, the decision was reached to utilize the V-47 shaker for the final series of tests of the vibrator concept.

3.5.4.2 Final Vibrator Tests. The tests utilizing the V-47 Goodman shaker were conducted in Northrop's 3.65- by 2.13-meter chamber with wall temperature at 79°K and pressure in the low 10^{-6} torr range. The axis of the shaker was normal to the test plate and located at the center of the plate. The shaker head was separated from the test plate a distance of 0.005 cm in the rest condition. The assembly was tilted 15° and the shaker excited at 100 cycles/sec for about 3 seconds to remove the dust. The test was run two times. The validity of the first data must be questioned because the dust removal appeared poor and the shaker head adhered to the test plate. The test results are presented in Table 3-7. The original test data is provided in Appendix C-4.

3.5.5 Brush Concept

Initially plans called for testing the mechanical brush in conjunction with the As_2S_3 shield. Because of the disappointing performance of the latter, however, the decision was made to test the brush concept with the S-13 plate. The final arrangement for this device is shown in Figure 3-23.

A number of different brush materials were considered for use with the mechanical brush concept. For practical reasons, however, it was necessary

Table 3-7. DATA FOR VIBRATING PLATE TEST RUN

Surface: S-13 coated aluminum
 Vibrator: Goodman V-47
 Frequency: 100 cycles/sec
 Tilt Angle: 15°

Solar Simulator	Heat Load ($\frac{\text{watts}}{\text{cm}^2}$)	S-13 Temp (°K)	Test Set-Up	Dust Coverage*
OFF OFF OFF OFF ON ON ON ON	.0234 .0624 .0975 .156 0 .0624 .0975 .156	275 337 372 416 275 365 393 431	Clean S-13 Coated Aluminum	0.0
OFF OFF OFF ON ON ON ON	.0624 .975 .156 0 .0624 .975 .156	352 390 438 348 413 437 472	Dusted S-13 Coated Aluminum	0.25
OFF OFF OFF OFF ON ON ON ON	.078 .113 .156 .195 .078 .117 .156 .195	359 390 422 447 415 440 462 482	Vibrator Cleaned First Test	0.24
OFF OFF OFF ON ON ON	.0975 .125 .156 .0585 .0918 .125	372 395 417 396 419 436	Vibrator Cleaned Second Test	0.23

* based on visual inspection

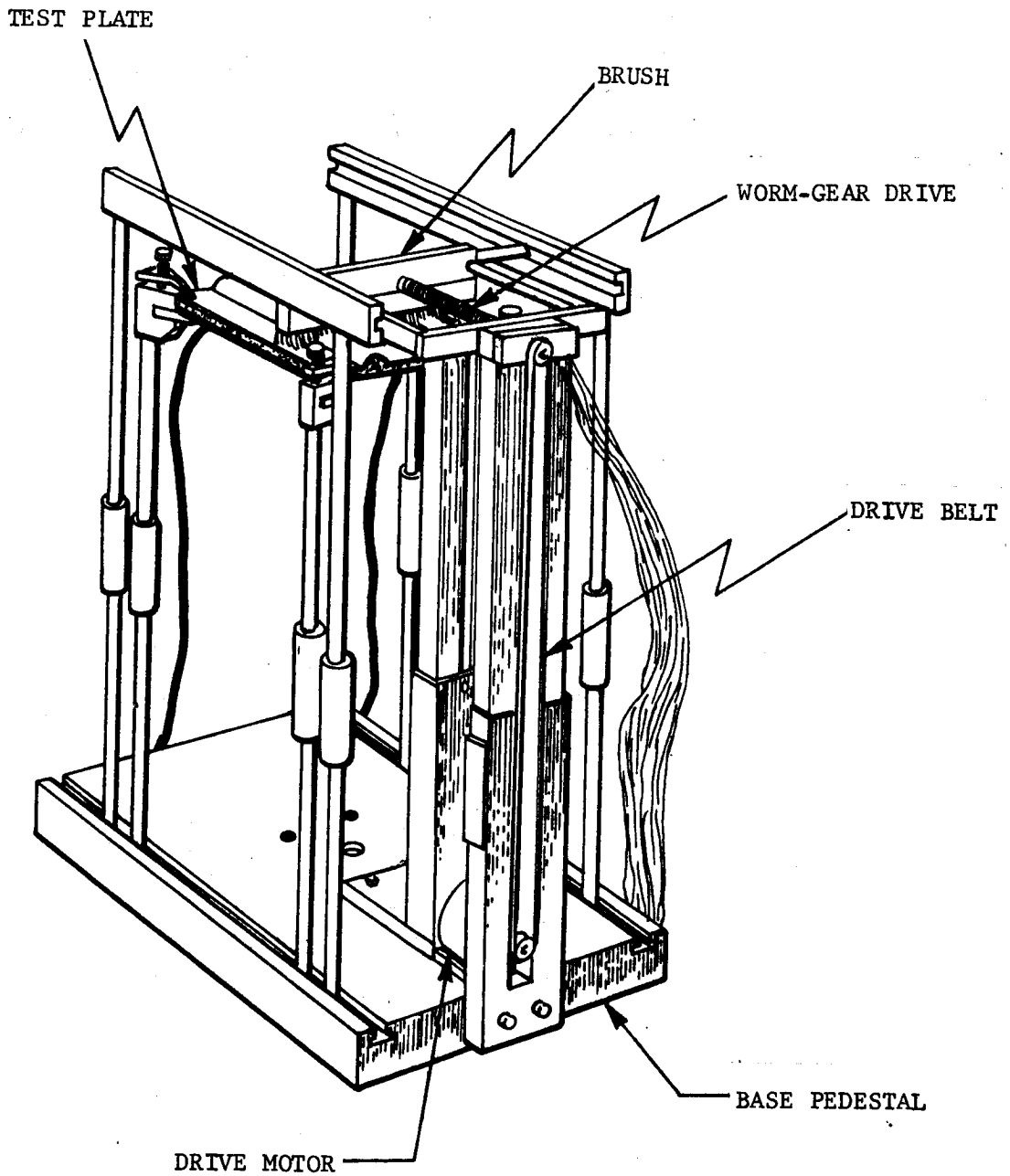


Figure 3-23. FINAL DESIGN OF MECHANICAL BRUSH AND PLATE DEVICE

7 June 1967

to select three representative and readily available materials: bristle brush, cheese cloth, and styrofoam.

3.5.5.1 Preliminary Brush Test. Initial tests under atmospheric conditions were carried out with the previously mentioned materials. Of these the cheesecloth appeared to be the most effective when applied with even pressure to the surface. Obtaining a uniform pressure with cheesecloth proved quite difficult. As a result the styrofoam brush which produced more uniform results, and which out performed the bristle brush, was selected for further testing.

3.5.5.2 Final Brush Test. The test was carried out in the Northrop 12-foot chamber with wall temperature at 78°K and a chamber pressure of the order of 10^{-6} torr. A formed styrofoam brush was swept over the specimen five times (3 sweeps in one direction and 2 sweeps in the opposite). The results of the test are presented in Table 3-8. The original test data is provided in Appendix C-5.

Table 3-8. DATA FOR MECHANICAL BRUSH CONCEPT

Surface: S-13 Coated Aluminum
Brush Material: Styrofoam

SOLAR SIMULATOR	HEATER LOAD (WATTS) (CM ²)	S-13 TEMP (°K)	TEST SET-UP	DUST* COVERAGE
OFF	.0975	401	DUSTED S-13	0.25
OFF	.156	450		
ON	.0975	445		
ON	.156	481		
OFF	.0975	373	BRUSH CLEANED S-13	0.17
OFF	.156	417		
ON	.0975	405		
ON	.133	429		

*based on visual inspection

3.5.6 Electrostatic Concept

Time and fund restrictions prevented a complete series of tests with the electrostatic concept. Preliminary testing of the electrostatic removal concept, however, was conducted. For charging the dust particles, two experiments were performed. In the first test the dust was sieved and allowed to fall in close proximity to a charged Van de Graaf sphere (0.304-meter diameter) capable of potentials in excess of 10^5 volts. However, the charge leakage in air, both in the laboratory (50-percent relative humidity) and in the environmental chamber (30-percent relative humidity), was considerable. The dust particles apparently did not acquire sufficient charge to produce any effect. No movement was observed during the fall or in contact with a charged plate (low voltage). Another test was performed in an attempt to charge the plate (the standard 15.4- by 15.4-cm aluminum panel) by contact with the Van de Graaf sphere without success. Only if the dust particles fell directly on the charged Van de Graaf sphere would some of the fines fly away, apparently repulsed after having acquired a sufficient charge. Based on the described experimental observations it appeared that a very high potential is required to charge the basalt particles to the point where they can be thrown off a charged plate.

3.6 ANALYSIS OF TEST DATA

The test data collected from the dust removal tests covered a wide variety of conditions involving a large number of experimental parameters. To avoid undue complexity, analysis of test data was restricted to graphical representation of data and to comparison of the measured surface temperature of the plate with predicted plate temperatures, taking into account the degradation of the radiative

properties of the surface due to dust. This approach also provided a means of comparing values of dust coverage based on visual observation with dust coverage (based on the results of the first phase of the study) necessary to produce the measured surface temperatures.

3.6.1 Graphical Representation of Data

The use of dimensional plots, provides the simplest way of observing the general data trends. Figures 3-24 through 3-30 provide such plots for all calibration and test runs previously described. Because of plotting limitations, individual data points are not shown. Instead the curves are drawn through the data points to indicate the trend of the data and to allow interpolation or extrapolation. Notice should be taken that some variation in radiant intensity of the solar simulator occurred during test runs. This produces some irregularities in these dimensional plots. For each test run two sets of curves are available. One corresponds to the case with the solar simulator turned off and the other with the simulator on. The general shape of the curves is characteristic of radiating bodies with the emitted radiation proportional to the fourth power of temperature. It is noted that for a clean S-13 surface, the presence of solar radiation, corresponding to a lunar noon, is equivalent to an internal heat load of ~ 0.025 watts/cm².

The presence of dust on the S-13 surface, with the solar simulator turned off (Figures 3-24a through 3-30a), produces a temperature profile only slightly different from that of a clean surface. This is due to the fact that the infrared emissivity of basalt dust (0.88) is quite close to that of the S-13 (0.83). Actually the presence of the dust in small amounts tends to lower the temperature profile. With increasing amounts of dust, however, an insulating effect occurs which causes the surface temperature of the plate to increase.

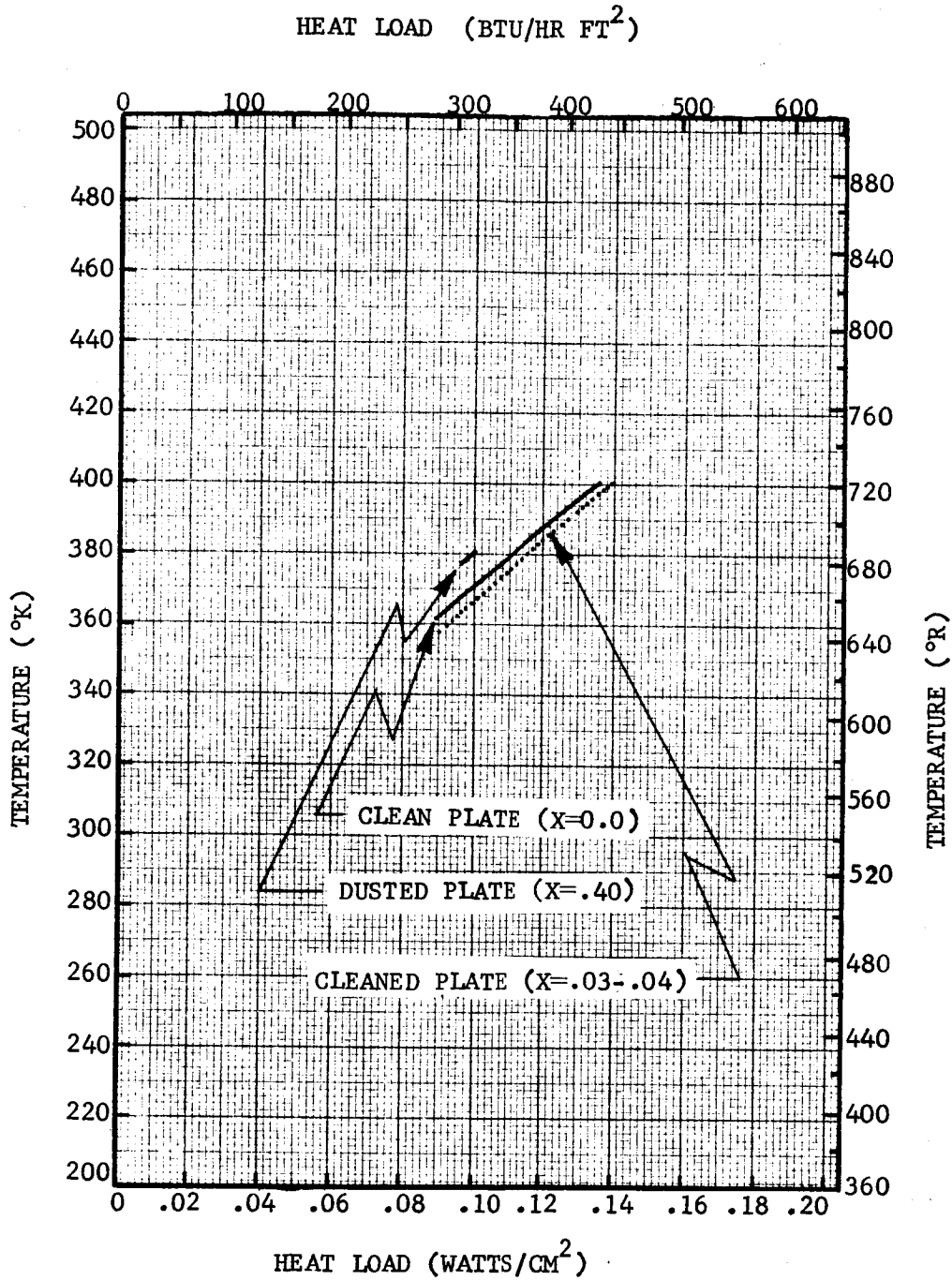


Figure 3-24a. TEMPERATURE VARIATION WITH HEAT LOAD (SOLAR SIMULATOR OFF)
FOR CALIBRATION TEST RUN

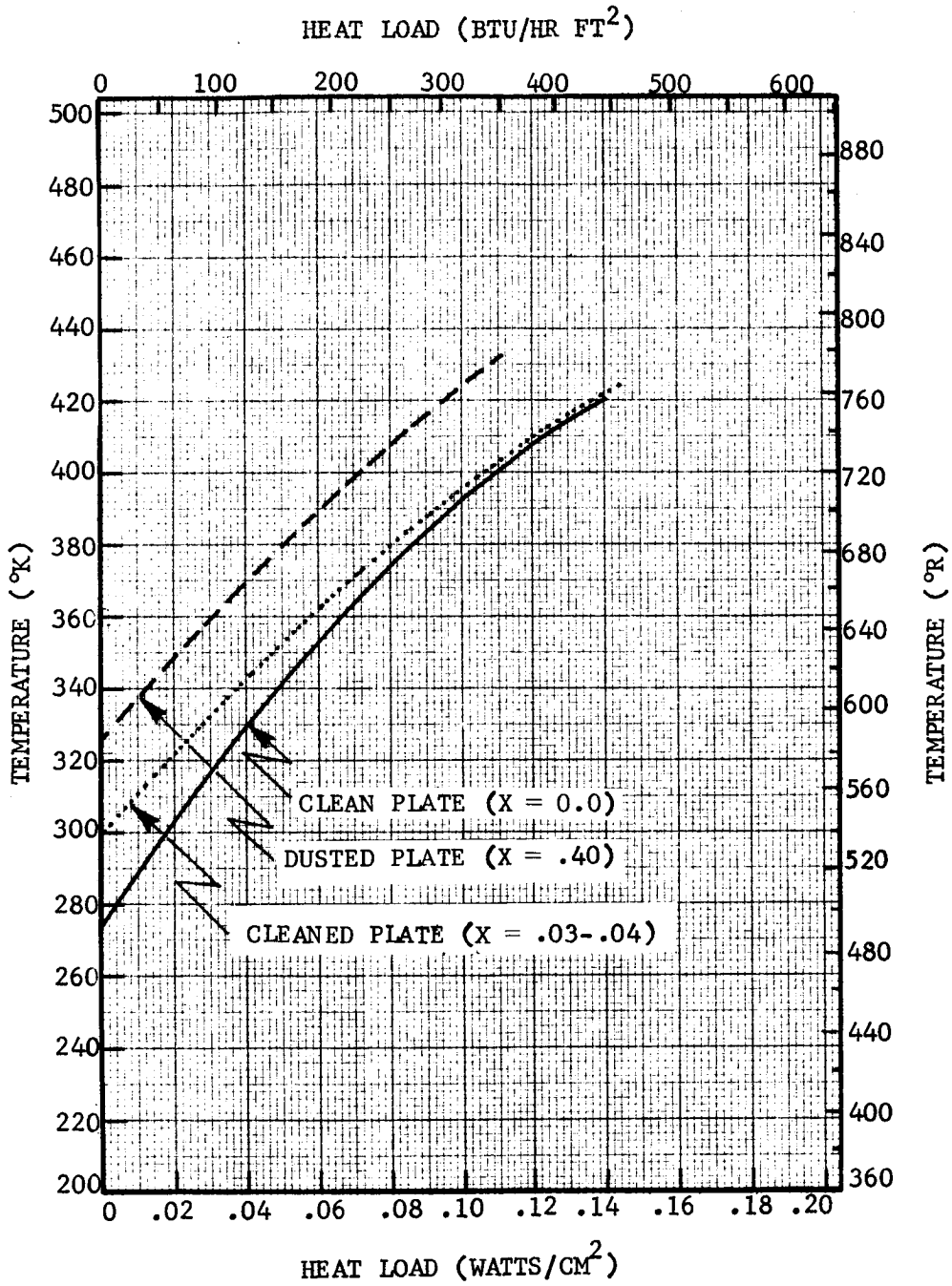


Figure 3-24b. TEMPERATURE VARIATION WITH HEAT LOAD (SOLAR SIMULATOR ON) FOR CALIBRATION TEST RUN

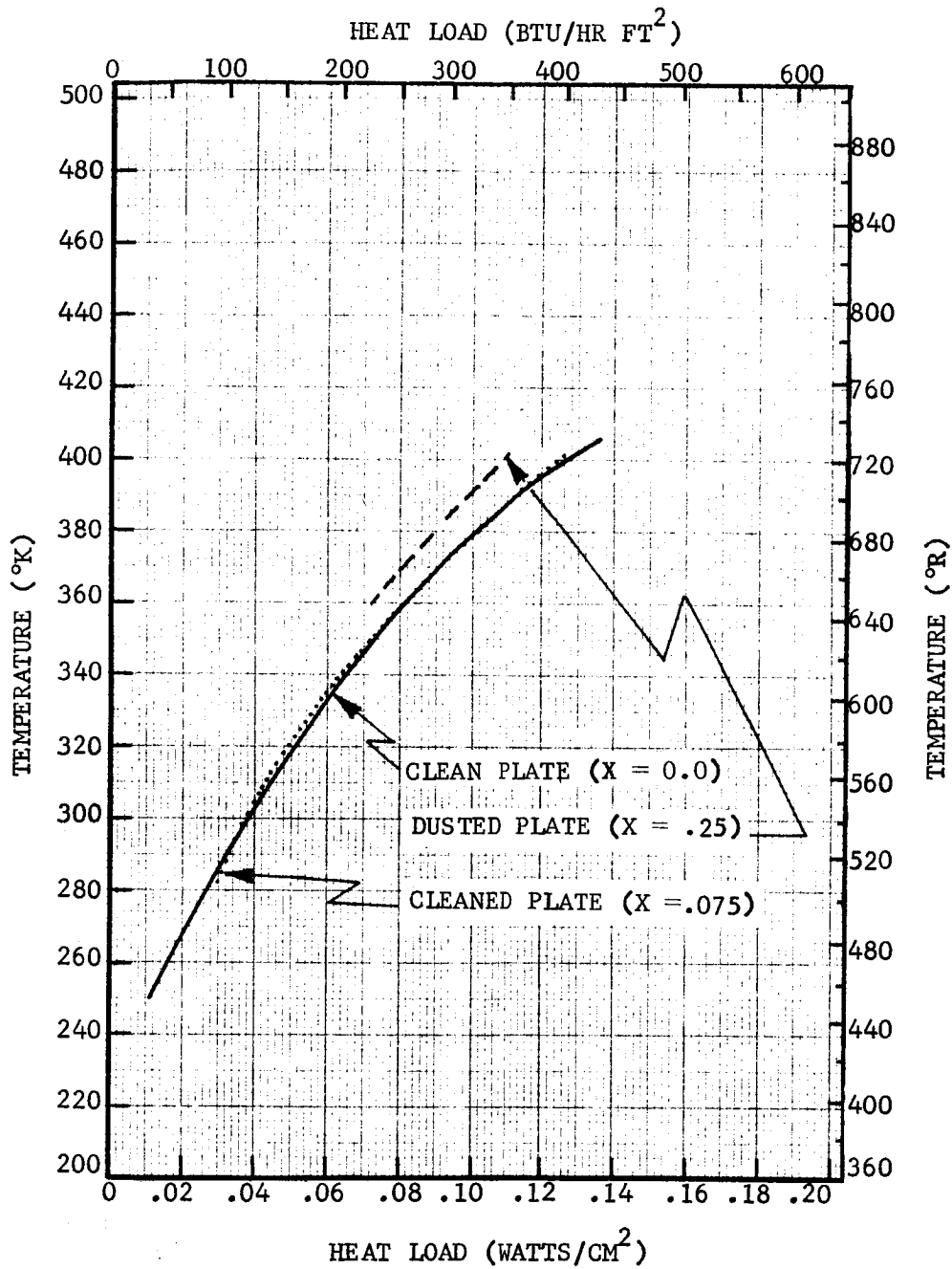


Figure 3-25a. TEMPERATURE VARIATION WITH HEAT LOAD (SOLAR SIMULATOR OFF) FOR JET AND PLATE TEST RUN (FROZEN INHIBISOL)

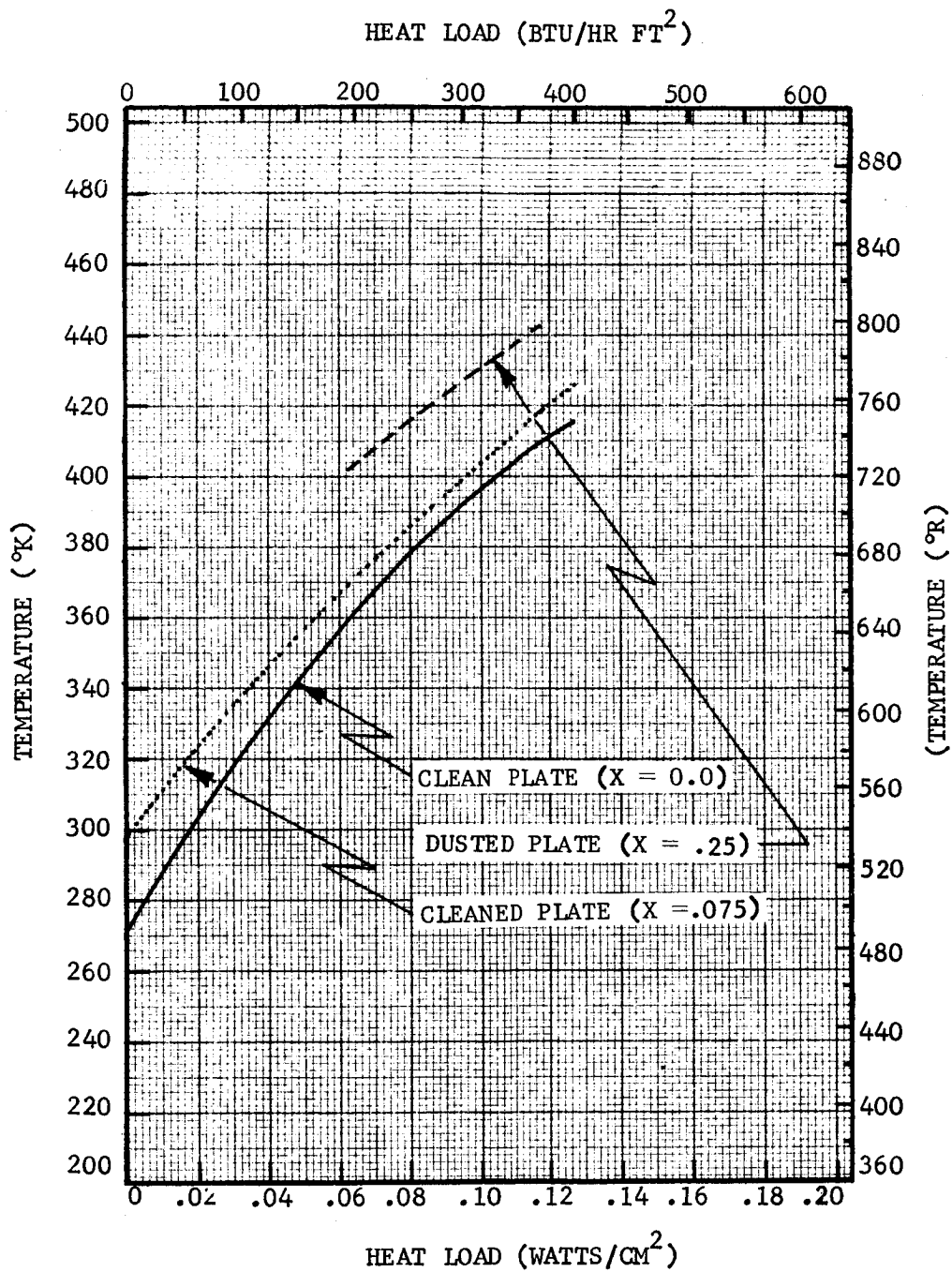


Figure 3-25b. TEMPERATURE VARIATION WITH HEAT LOAD (SOLAR SIMULATOR ON)
FOR JET AND PLATE TEST RUN (FROZEN INHIBISOL)

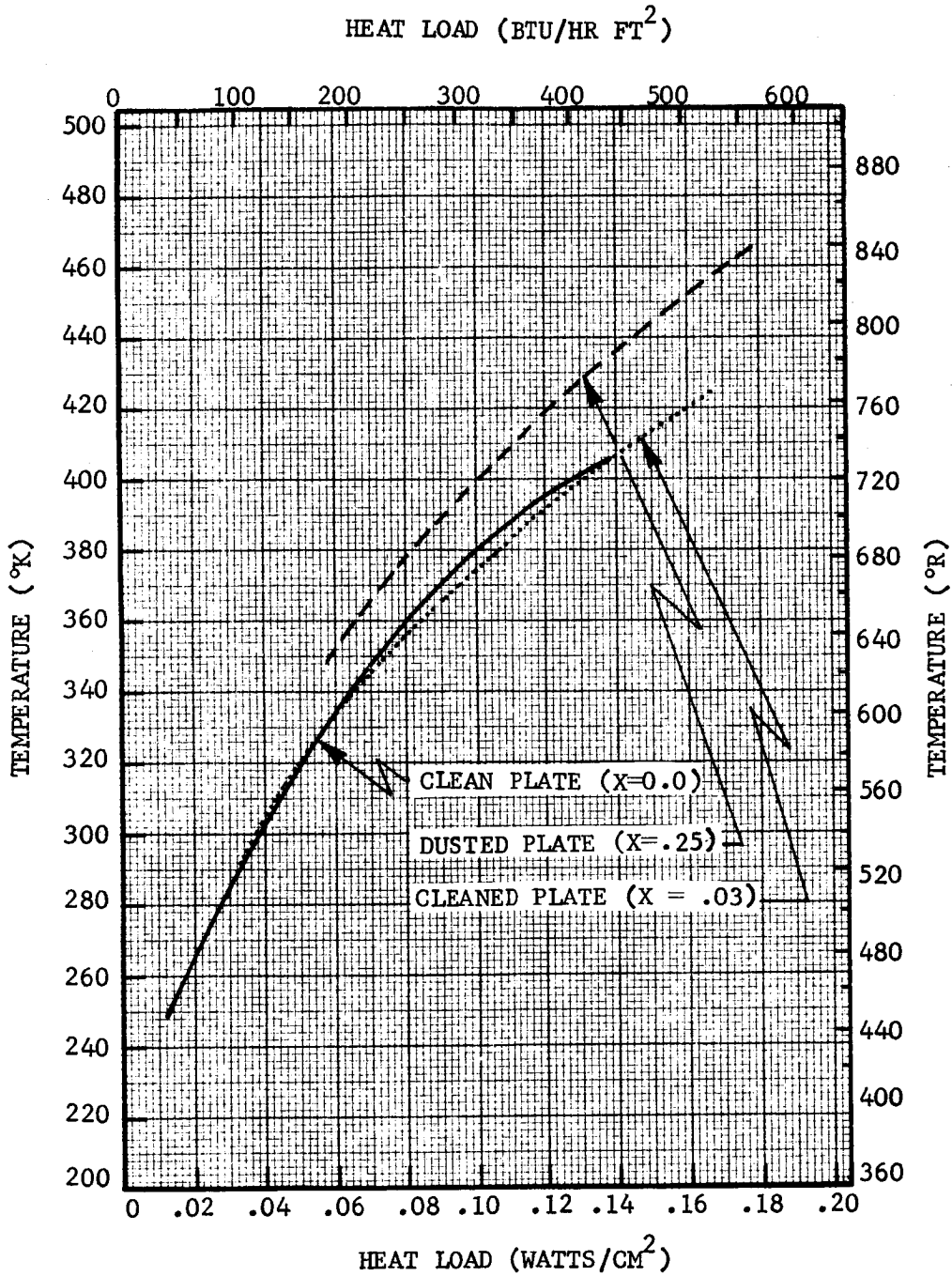


Figure 3-26a. TEMPERATURE VARIATION WITH HEAT LOAD (SOLAR SIMULATOR OFF) FOR JET AND PLATE TEST RUN (LIQUID INHIBISOL)

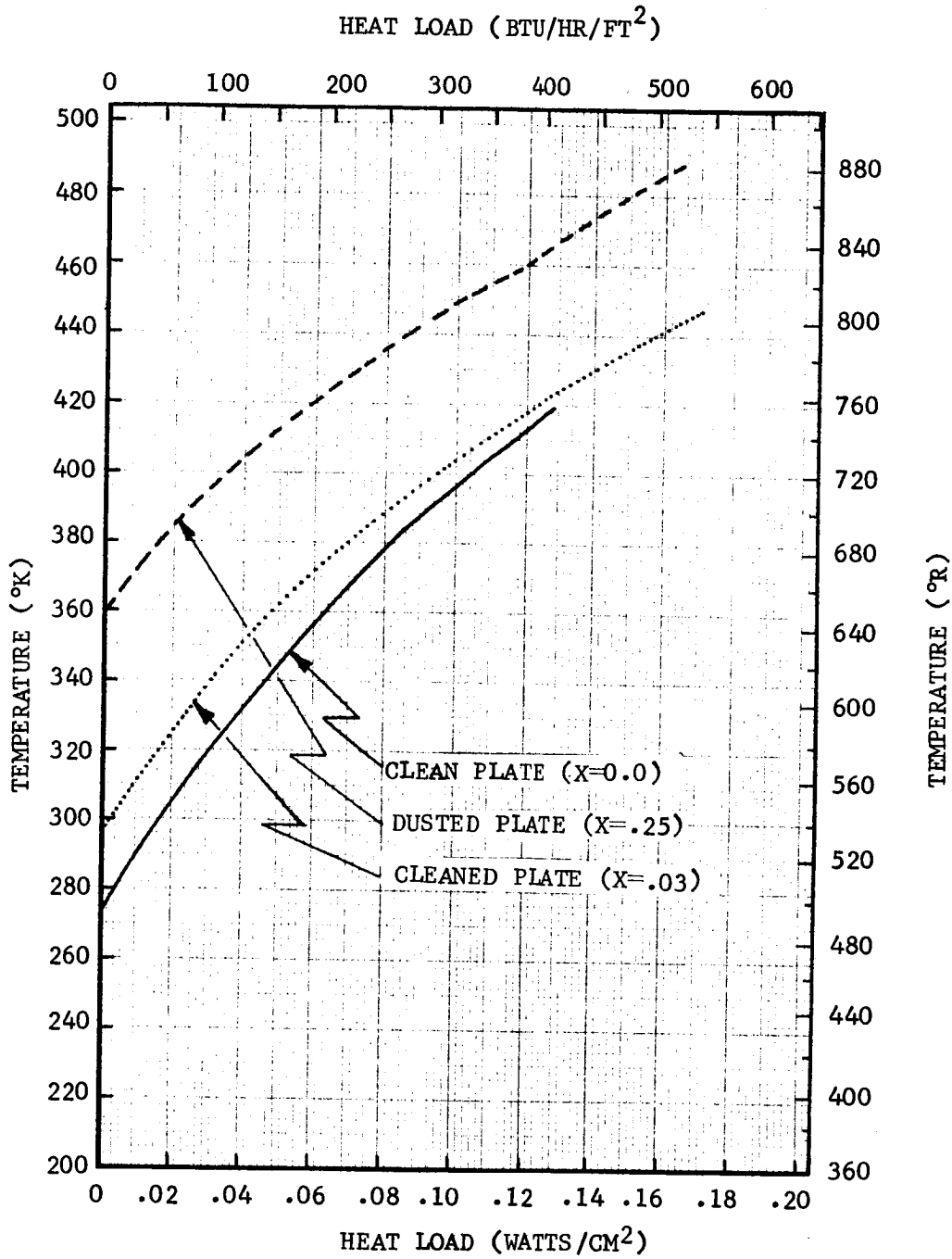


Figure 3-26b. TEMPERATURE VARIATION WITH HEAT LOAD (SOLAR SIMULATOR ON) FOR JET AND PLATE TEST RUN (LIQUID INHIBISOL)

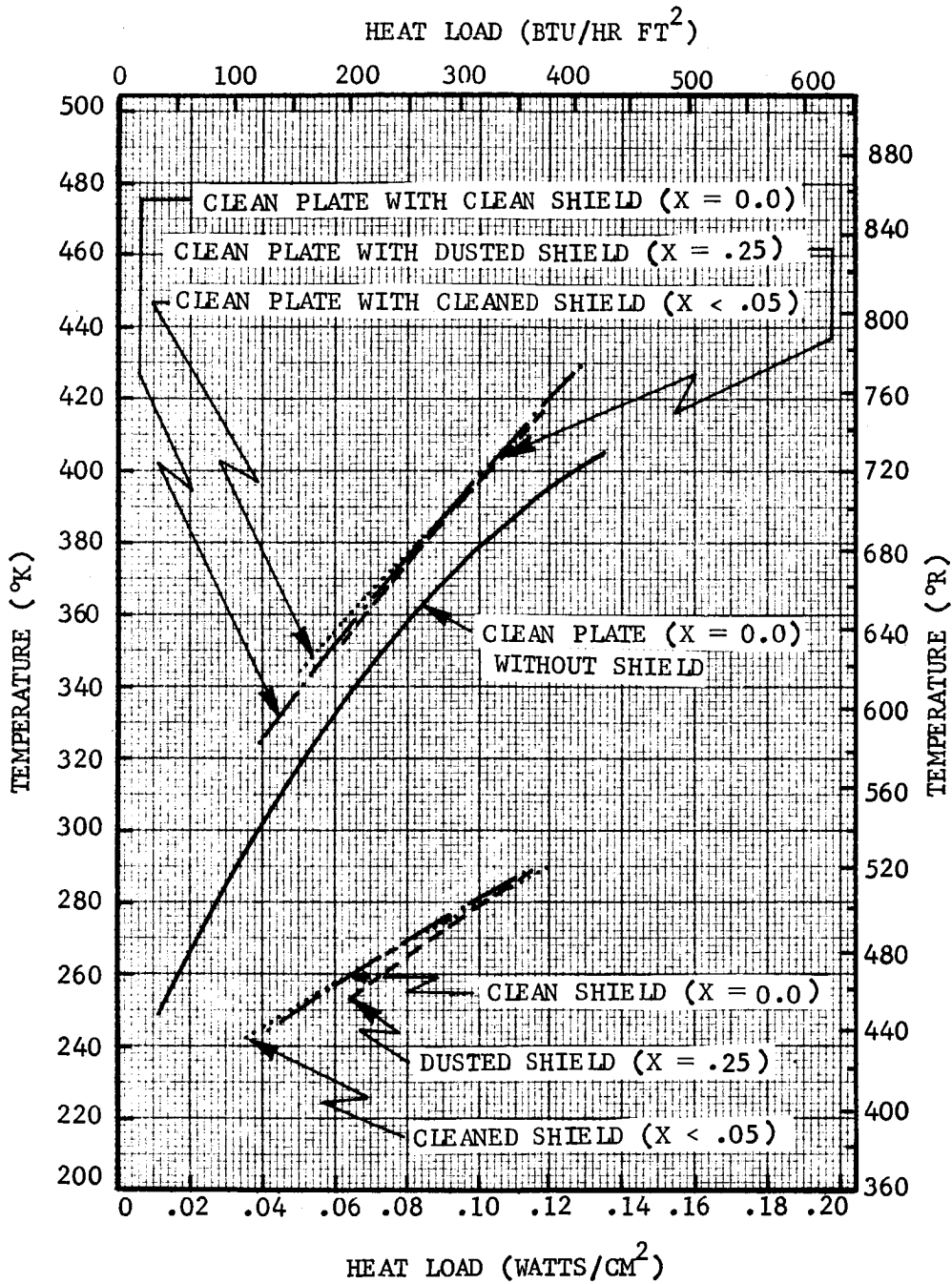


Figure 3-27a. TEMPERATURE VARIATION WITH HEAT LOAD (SOLAR SIMULATOR OFF)
FOR JET AND GLASS SHIELD TEST RUN (LIQUID INHIBISOL)

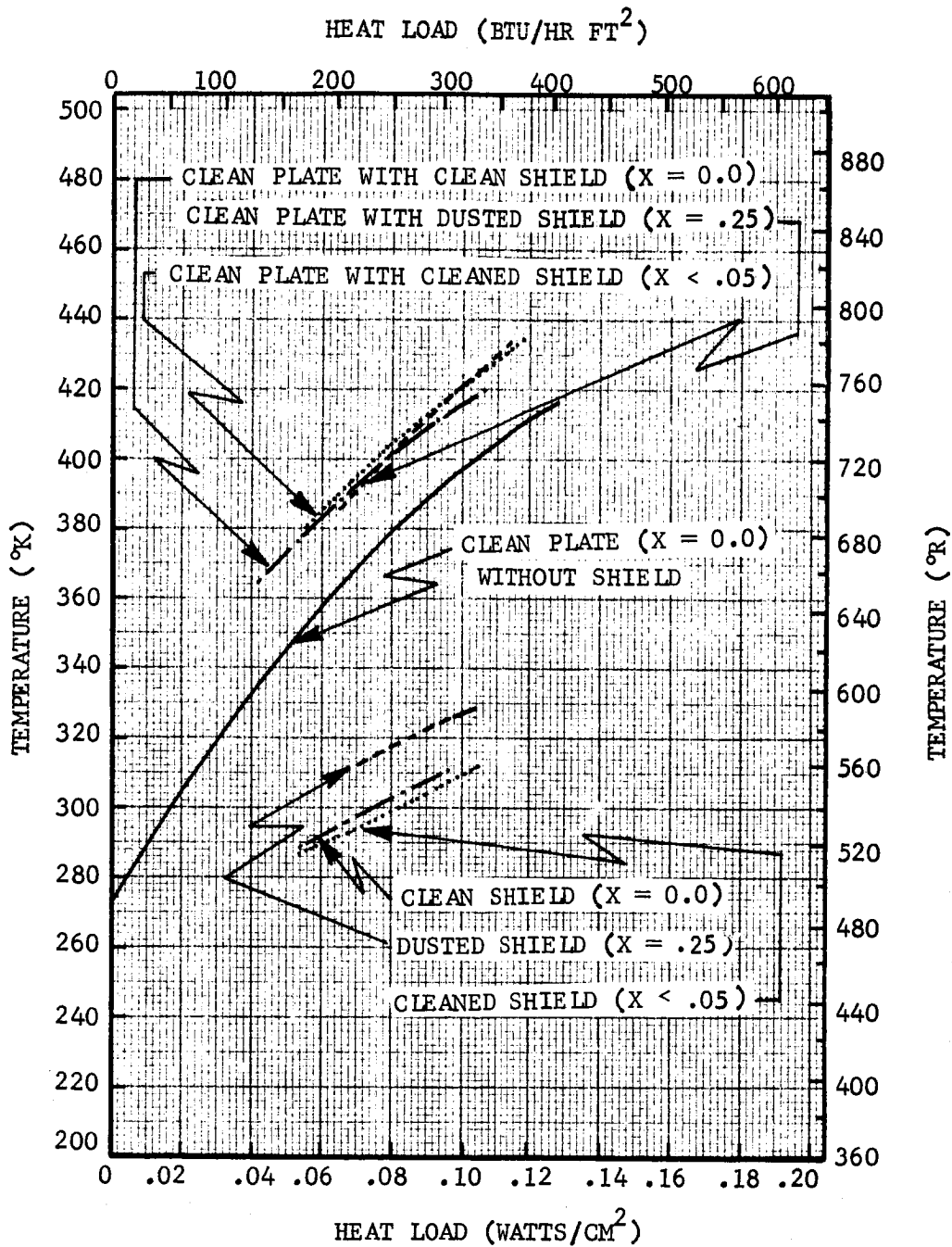


Figure 3-27b. TEMPERATURE VARIATION WITH HEAT LOAD (SOLAR SIMULATOR ON) FOR JET AND GLASS SHIELD TEST RUN (LIQUID INHIBISOL)

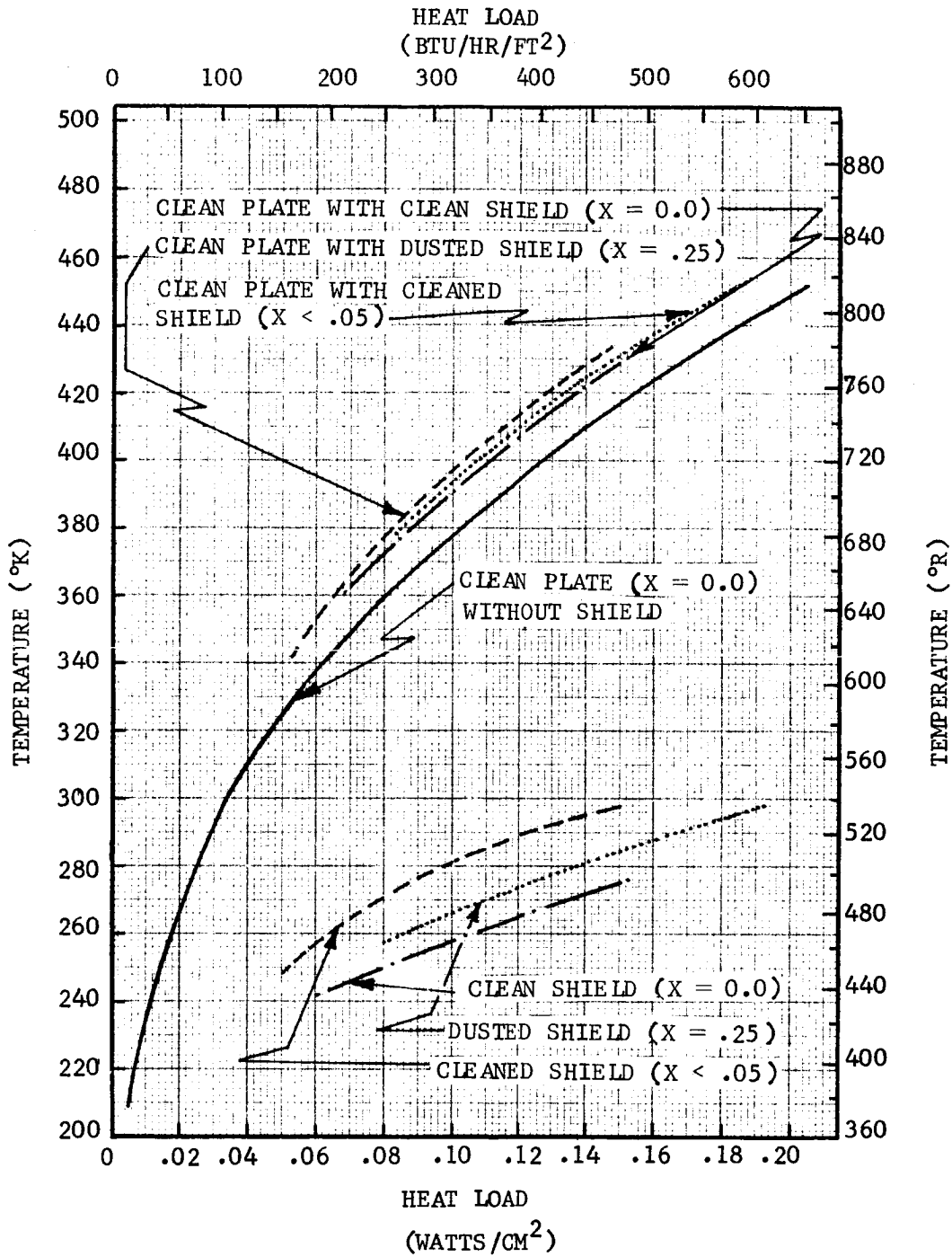


Figure 3-28a. TEMPERATURE VARIATION WITH HEAT LOAD (SOLAR SIMULATOR OFF) FOR JET AND ARSENIC-TRISULFIDE SHIELD TEST RUN (LIQUID INHIBISOL)

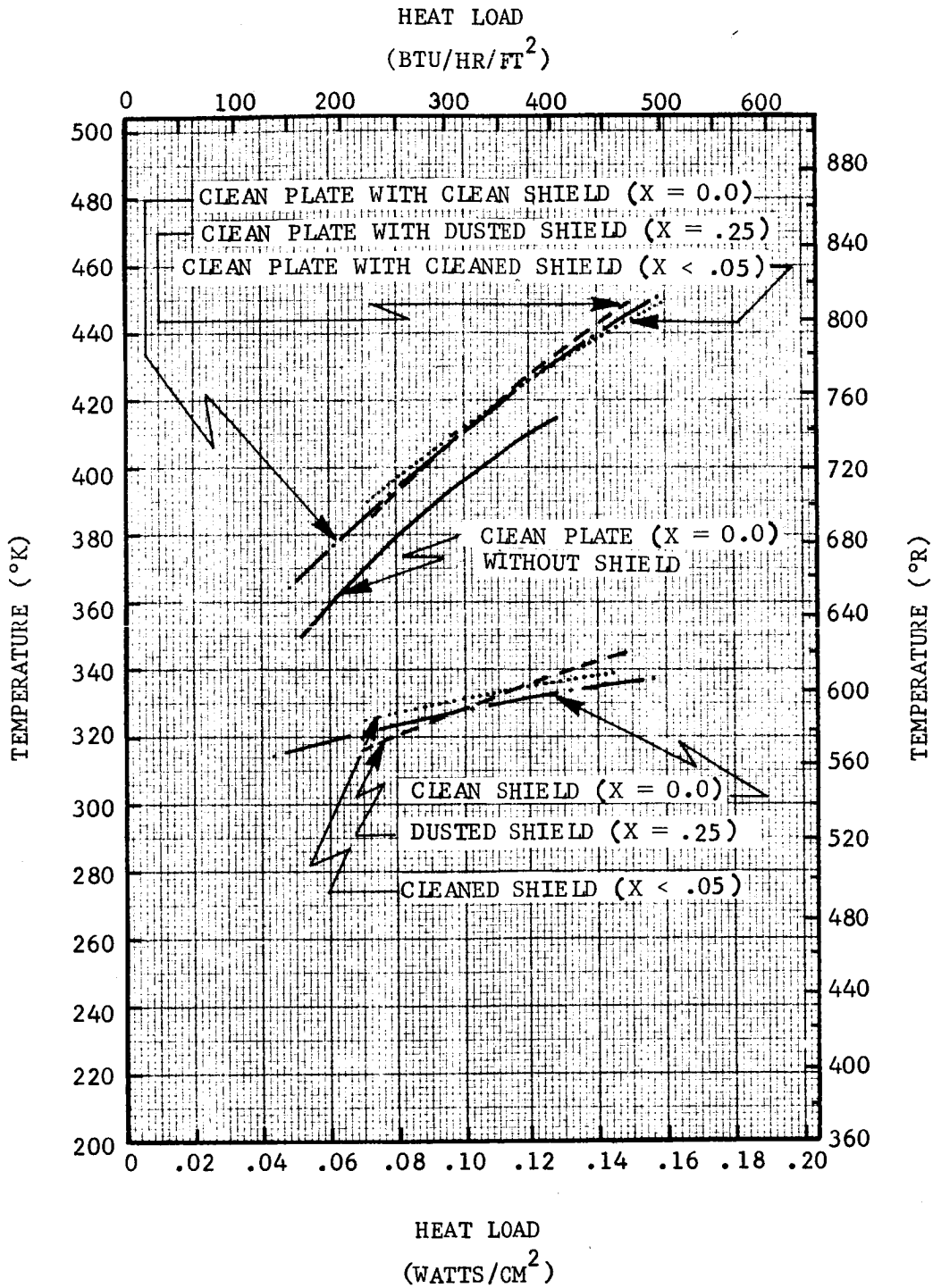


Figure 3-28b. TEMPERATURE VARIATION WITH HEAT LOAD (SOLAR SIMULATOR ON) FOR JET AND ARSENIC-TRISULFIDE SHIELD TEST RUN (LIQUID INHIBISOL)

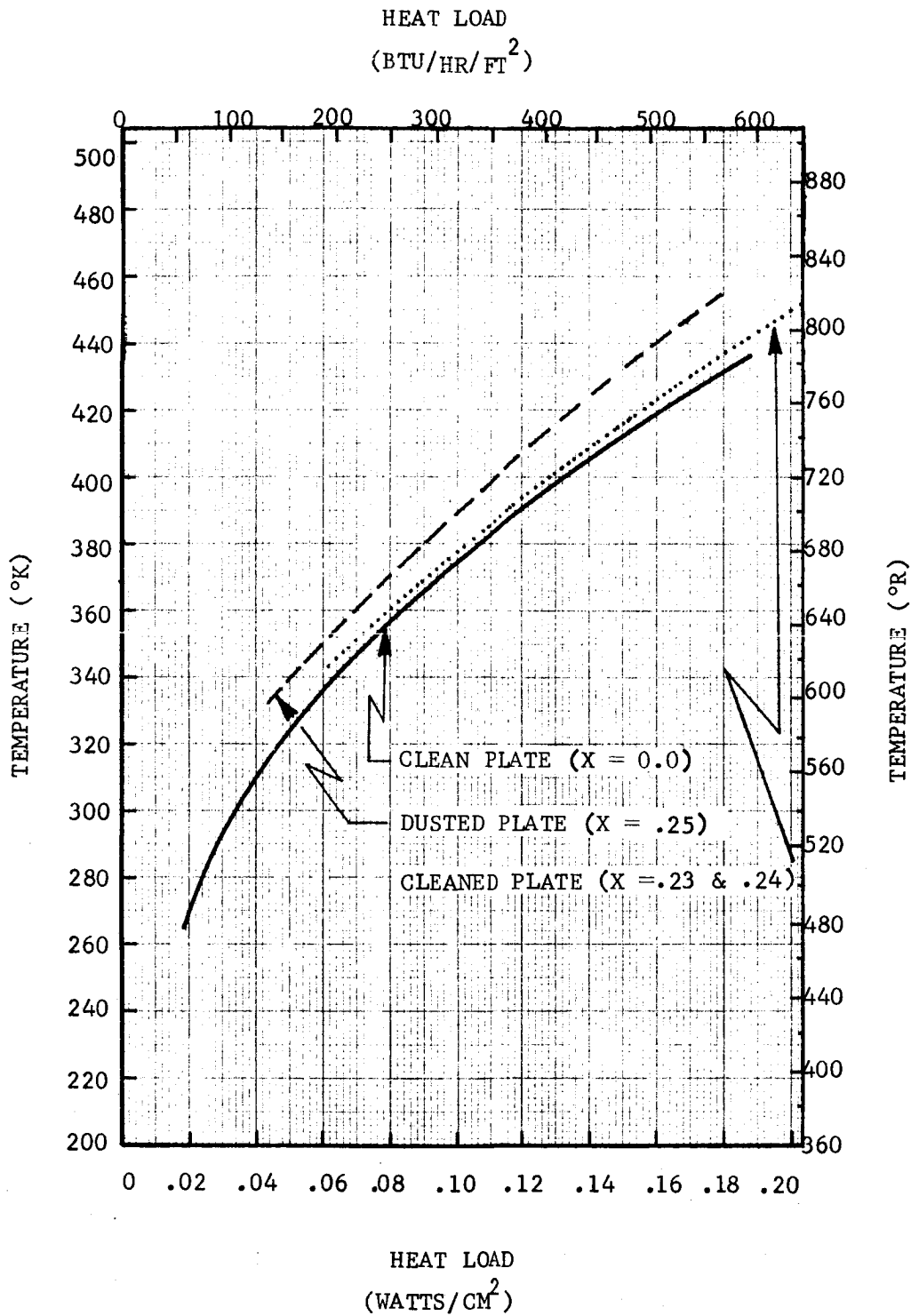


Figure 3-29a. TEMPERATURE VARIATION WITH HEAT LOAD (SOLAR SIMULATOR OFF) FOR VIBRATING SURFACE TEST RUN

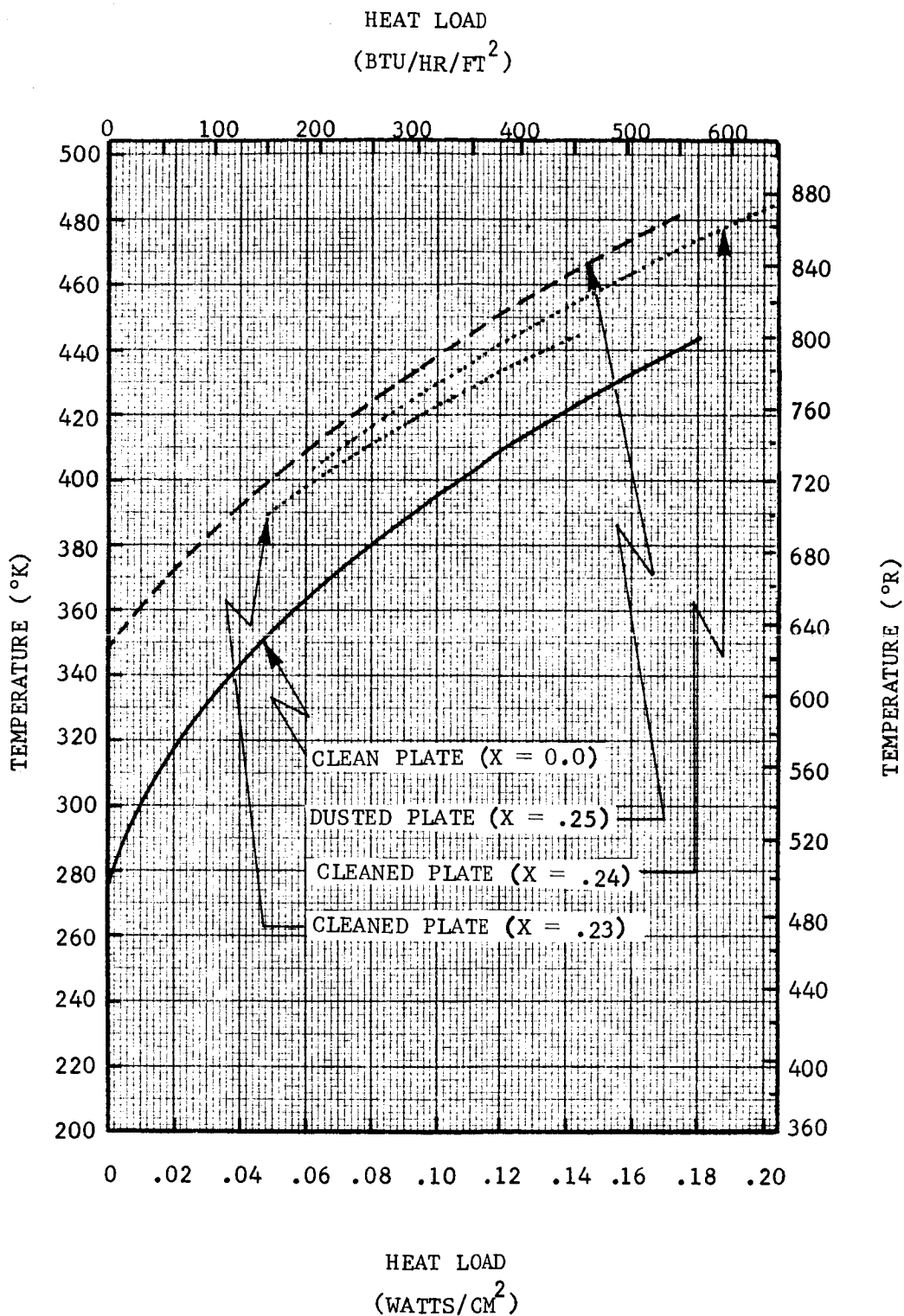


Figure 3-29b. TEMPERATURE VARIATION WITH HEAT LOAD (SOLAR SIMULATOR ON) FOR VIBRATING SURFACE TEST RUN

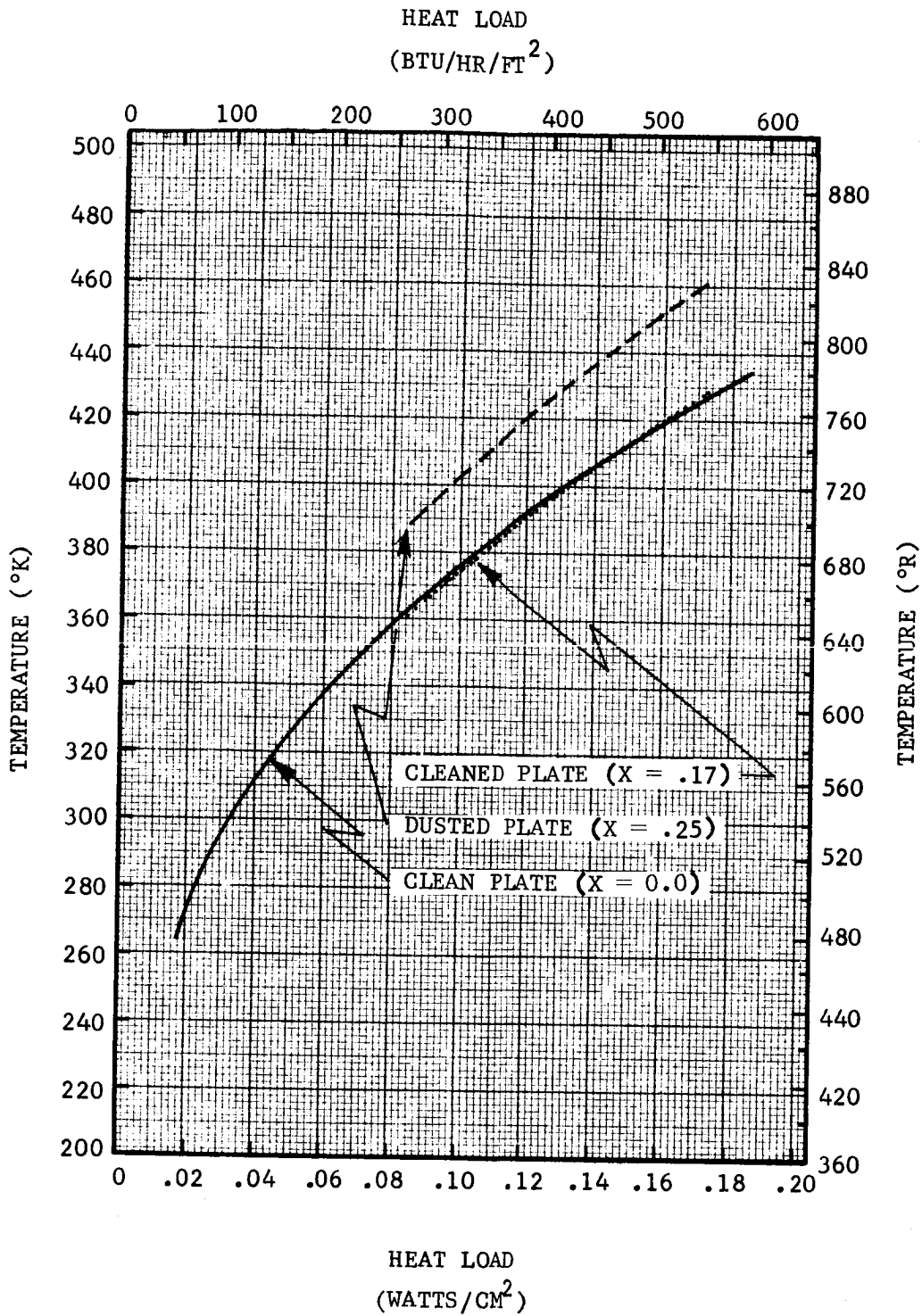


Figure 3-30a. TEMPERATURE VARIATION WITH HEAT LOAD (SOLAR SIMULATOR OFF) FOR MECHANICAL BRUSH TEST RUN

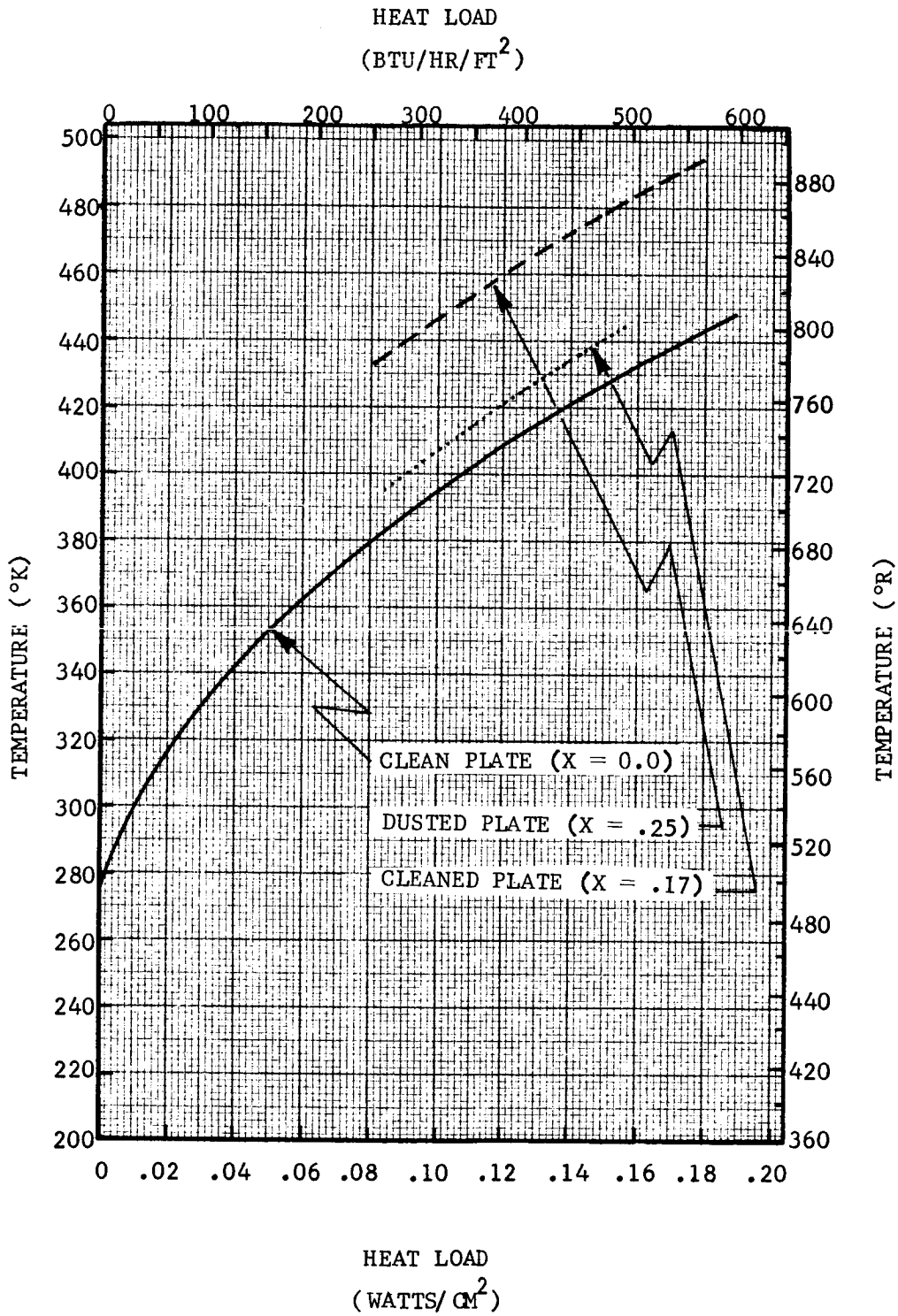


Figure 3-30b. TEMPERATURE VARIATION WITH HEAT LOAD (SOLAR SIMULATOR ON) FOR MECHANICAL BRUSH TEST RUN

The cleansing effect of the various devices is difficult to determine from these figures with the solar simulator off because of the small changes in temperature involved. The temperature profile of the contaminated surface with the solar simulator on (Figures 3-24b through 3-30b) is significantly higher than the corresponding profile for the clean surface. This difference is the result of the increase in the solar absorptance of the S-13 due to the presence of the dust. Also with sizeable amounts of dust coverage the insulating effect already mentioned contributes to the temperature increase. The relative performance of the various dust removal concepts is most clearly indicated in the figures with the solar simulator on. Based on Figures 3-25b through 3-30b, corresponding to a heat load of 0.12 watts/cm², the following table can be constructed:

Table 3-9. PLATE TEMPERATURE AFTER CLEANING BY DUST REMOVAL DEVICES

Device	Figure	Plate Temperature (°K)	Heat Load ($\frac{\text{watts}}{\text{cm}^2}$)	Solar Simulator
Jet and Plate (Frozen Inhibisol)	3-25b	420	0.12	ON
Jet and Plate (Liquid Inhibisol)	3-26b	417	↓	↓
Jet and Glass Shield (Liquid Inhibisol)	3-27b	436		
Jet and As ₂ S ₃ Shield (Liquid Inhibisol)	3-28b	426		
Vibration Plate (Second Test)	3-29b	433		
Mechanical Brush	3-30b	421		

Based on the results of Table 3-9, which appears representative for the entire test program, the order of ranking the devices (in terms of minimizing plate temperature) is as follows:

1. Jet and Plate (liquid inhibisol)
2. Jet and Plate (frozen inhibisol)
3. Mechanical Brush
4. Jet and As_2S_3 Shield (liquid inhibisol)
5. Jet and Glass Shield (liquid inhibisol)
6. Vibrating Plate.

Of special interest is the manner in which the plate temperature varies when protected by a shield. The presence of the clean glass shield with the solar simulator on produces a plate temperature profile which is higher ($\sim 19^\circ\text{K}$) than that produced by the clean plate without the shield. For the arsenic-trisulfide shield the increase in plate temperature is $\sim 12^\circ\text{K}$. The fact that the ordinary glass appears to produce plate temperatures only 7°K hotter than the arsenic trisulfide is somewhat surprising. For a given increase in dust coverage the shielded (As_2S_3) plate displays a smaller temperature increase than the unshielded plate. This can be seen by comparing plate temperature after contamination but before cleaning. The trend of the data in this respect would indicate that with a level of dust coverage above ~ 20 percent the As_2S_3 shielded plate would have a lower temperature than the unshielded plate.

3.6.2 Correlation of Data

The most straightforward correlation of data involves prediction of the surface temperature of the plate and comparing the predicted values with the experimental data. In order to predict the surface temperature of the plate a thermal radiation model must be established.

3.6.2.1 Thermal Radiation Model. In radiation problems of the type under study, use of electrical circuit analogy as discussed in reference 22 proves useful. The original concept of such a thermal network was designed to handle either opaque black or gray bodies. In the present investigation, the absorptance of the thermal control surface with respect to most of the incoming radiation is not equal to the emittance of the surface. Likewise, for the tests involving the arsenic-trisulfide shield, the value of the shield transmittance, absorptance, and reflectance vary with wavelength. Thus the need arises for developing a network analogy including non-gray opaque and transparent surfaces. The desired analogy can be achieved with reasonable accuracy by dividing the electromagnetic spectrum into two parts: 0 to 2.0μ (solar spectrum) and above 2.0μ (infrared spectrum). The spectrum is divided at this point because all bodies at temperatures below 500°K emit less than 0.03 percent of their total thermal radiation below 2.0μ .

In constructing the network for each spectrum, care must be taken to distinguish between fixed and floating potential. In the present analysis the Sun (represented by the solar simulator) and the Universe (represented by the space chamber wall) are fixed potentials of known value. The plate is a floating potential subjected to controllable load which is known. The shield is a floating potential.

The thermal network developed in accordance with the preceding discussion is presented in Figure 3-31. Notice should be taken that heat conduction effects within the plate and shield are neglected in the network. By means of this thermal network, a set of equations can be derived based on the analogy between heat transfer and electric current. For each node of unknown potential in each network, one equation exists. In addition there are the heat balance equations at the surface of the plate and within the shield. Thus there are six linear algebraic equations as follows:

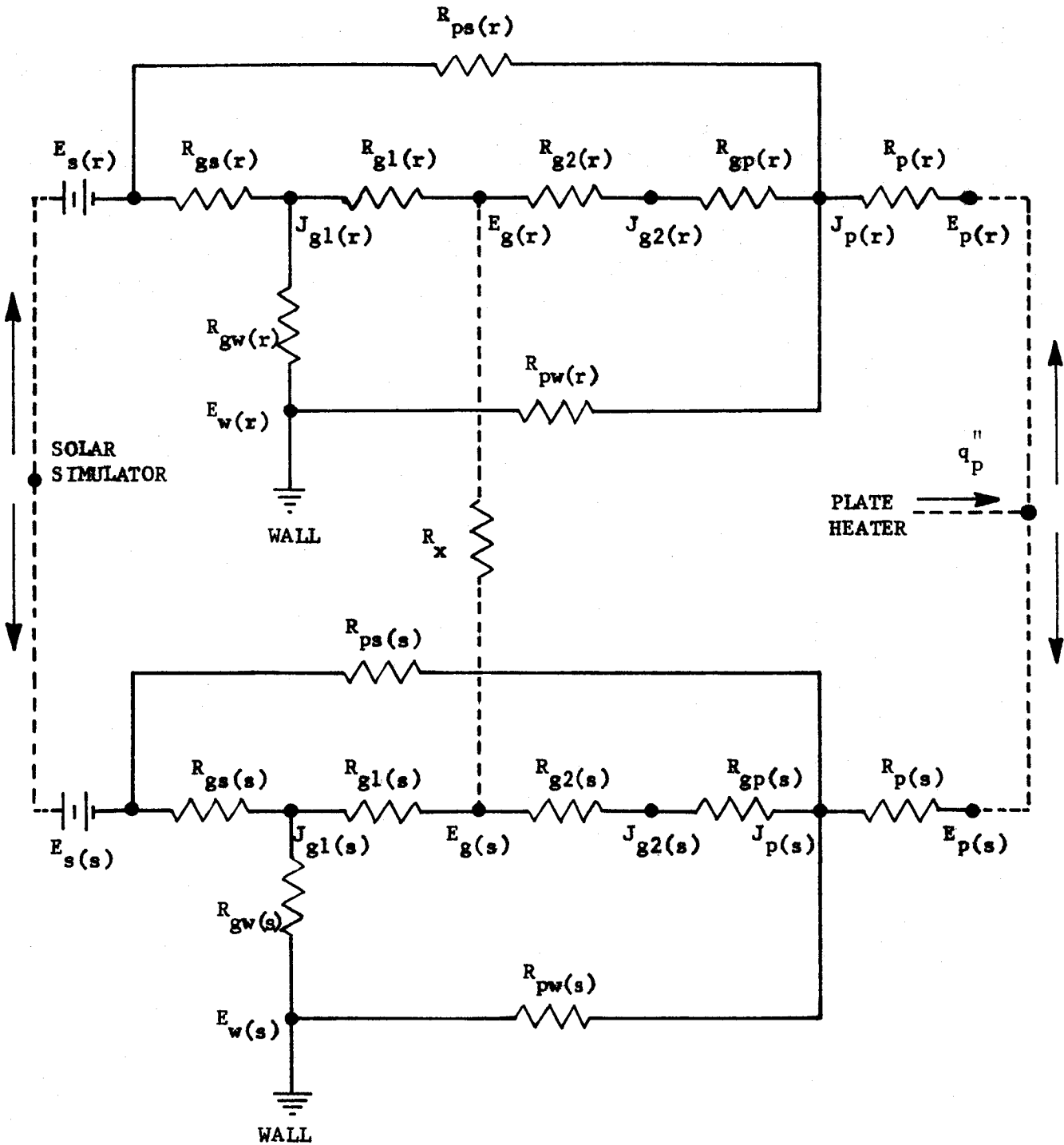


Figure 3-31. THERMAL NETWORK

$$\frac{E_{g(s)} - J_{gl(s)}}{R_{gl(s)}} + \frac{E_{s(s)} - J_{gl(s)}}{R_{gs(s)}} + \frac{E_{w(s)} - J_{gl(s)}}{R_{gw(s)}} = 0 \quad (3-1)$$

$$\frac{E_{g(r)} - J_{gl(r)}}{R_{gl(r)}} + \frac{E_{s(r)} - J_{gl(r)}}{R_{gs(s)}} + \frac{E_{w(r)} - J_{gl(r)}}{R_{gw(s)}} = 0 \quad (3-2)$$

$$\frac{E_{p(s)} - J_{p(s)}}{R_{p(s)}} + \frac{E_{s(s)} - J_{p(s)}}{R_{ps(s)}} + \frac{E_{w(s)} - J_{p(s)}}{R_{pw(s)}} + \frac{E_{g(s)} - J_{p(s)}}{R_{gp(s)} + R_{g2(s)}} = 0 \quad (3-3)$$

$$\frac{E_{p(r)} - J_{p(r)}}{R_{p(r)}} + \frac{E_{s(r)} - J_{p(r)}}{R_{ps(r)}} + \frac{E_{w(r)} - J_{p(r)}}{R_{pw(r)}} + \frac{E_{g(r)} - J_{p(r)}}{R_{gp(r)} + R_{g2(r)}} = 0 \quad (3-4)$$

$$\frac{E_{p(s)} - J_{p(s)}}{R_{p(s)}} + \frac{E_{p(r)} - J_{p(r)}}{R_{p(r)}} = q_p'' A_p \quad (3-5)$$

$$\frac{E_{g(s)} - J_{gl(s)}}{R_{gl(s)}} + \frac{E_{g(s)} - J_{p(s)}}{R_{gp(s)} + R_{g2(s)}} + \frac{E_{g(r)} - J_{gl(r)}}{R_{gl(r)}} + \frac{E_{g(r)} - J_{p(r)}}{R_{gp(r)} + R_{g2(r)}} = 0 \quad (3-6)$$

where

$$R_{p(s)} = \frac{\rho_{p(s)}}{\epsilon_{p(s)} A_p}$$

$$R_{gw(s)} = \frac{1}{A_g F_{gw} (1 - \tau_{gl(s)})}$$

$$R_{gl(s)} = \frac{\rho_{gl(s)}}{A_g \epsilon_{gl(s)} (1 - \tau_{gl(s)})}$$

$$R_{pw(s)} = \frac{1}{A_p F_{pw} \tau_{gl(s)}}$$

$$R_{g2(s)} = \frac{\rho_{g2(s)}}{A_g \epsilon_{g2(s)} (1 - \tau_{gl(s)})}$$

$$R_{ps(s)} = \frac{1}{A_p F_{ps} \tau_{gl(s)}}$$

$$R_{gp(s)} = \frac{1}{A_g F_{gp} (1 - \tau_{gl(s)})}$$

$$R_{gs(s)} = \frac{1}{A_g F_{gs} (1 - \tau_{gl(s)})}$$

$$R_{p(r)} = \frac{\rho_{p(r)}}{\epsilon_{p(r)} A_p}$$

$$R_{gw(r)} = \frac{1}{A_g F_{gw} (1 - \tau_{gl(s)})}$$

$$R_{gl(r)} = \frac{\rho_{gl(r)}}{A_g \epsilon_{gl(r)} (1 - \tau_{gl(r)})}$$

$$R_{pw(r)} = \frac{1}{A_p F_{pw} \tau_{gl(r)}}$$

$$R_{g2(r)} = \frac{\rho_{g2(r)}}{A_g \epsilon_{g2(r)} (1 - \tau_{gl(r)})}$$

$$R_{ps(r)} = \frac{1}{A_p F_{ps} \tau_{gl(r)}}$$

$$R_{gp(r)} = \frac{1}{A_g F_{gp} (1 - \tau_{gl(r)})}$$

$$R_{gs(r)} = \frac{1}{A_g F_{gs} (1 - \tau_{gl(r)})}$$

In the equations the resistance, R_x , between $E_{g(s)}$ and $E_{g(r)}$ as shown in Figure 3-31 does not occur explicitly. This resistance is shown in the network only to indicate a potential difference between $E_{g(s)}$ and $E_{g(r)}$ and is never calculated.

The values of the radiative properties of the plate and shield, occurring in the resistances, depend upon the degree of dust coverage (X). For the S-13 plate this functional dependence can be obtained from Tables 2-4 and 2-9. For the shield some simple model must be established. In the present analysis, the following functional relationships between radiative properties of the shield and dust coverage (X) have been used:

$$\alpha_{gl(s)} = \alpha_{g(s)}(1-X) + \alpha_{d(s)}X$$

$$\alpha_{gl(r)} = \alpha_{g(r)}(1-X) + \alpha_{d(r)}X$$

$$\rho_{gl(s)} = \rho_{g(s)}(1-X) + \rho_{d(s)}X$$

$$\rho_{gl(r)} = \rho_{g(r)}(1-X) + \rho_{d(r)}X$$

$$\tau_{gl(s)} = \tau_{g(s)}(1-X) = \tau_{g2(s)}$$

$$\tau_{gl(r)} = \tau_{g(r)}(1-X) = \tau_{g2(r)}$$

$$\alpha_{g2(s)} = \alpha_{g(s)} + \alpha_{d(s)} \tau_{g(s)}X$$

$$\alpha_{g2(r)} = \alpha_{g(r)} + \alpha_{d(r)} \tau_{g(r)}X$$

$$\rho_{g2(s)} = \rho_{g(s)} + \rho_{d(s)} \tau_{g(s)}^X$$

$$\rho_{g2(r)} = \rho_{g(r)} + \rho_{d(r)} \tau_{g(r)}^X$$

These relationships are based on the assumption that the dust is opaque. They reduce to the uncontaminated values when $X = 0$, and also satisfy the basic requirement $\alpha + \rho + \tau = 1$. When the value of τ_g is set equal to unity, the resulting equations correspond to the case when the shield is not present.

In equations (3-1) through (3-6), the quantities $E_{s(s)}$, $E_{s(r)}$, $E_{w(s)}$, $E_{w(r)}$, and q_p'' have known values. In addition, $E_{g(s)}$ and $E_{p(s)}$ may be set equal to zero because plate and shield temperature never exceed 500°K. The shape factors may be calculated in the standard fashion. Thus, there remains six equations in six unknowns: $E_{p(r)}$, $J_{p(s)}$, $J_{p(r)}$, $E_{g(r)}$, $J_{gl(s)}$, and $J_{gl(r)}$. The equations can be solved by algebraic manipulation with the following solutions for the unknowns:

$$J_{gl(s)} = \frac{\left(\frac{E_{s(s)}}{R}\right)}{D_1} \quad (3-7)$$

$$J_{p(s)} = \frac{\left(\frac{E_{s(s)}}{R}\right)}{D_2} \quad (3-8)$$

$$J_p(r) = \frac{q_p + \frac{J_p(s)}{R_p(s)} + \frac{E_s(r)}{R_{ps}(r)} + \frac{E_w(r)}{R_{pw}(r)}}{D_6}$$

$$+ \frac{R_{g1}(r) \left[\frac{E_s(r)}{R_{gs}(r)} + D_4 R_{g1}(r) \left(\frac{J_{g1}(s)}{R_{g1}(r)} + \frac{J_p(s)}{R_{gp}(s) + R_{g2}(s)} \right) \right]}{\left[(R_{g1}(r))^2 D_3 D_4 - 1 \right] \left[R_{gp}(r) + R_{g2}(r) \right]} \quad (3-9)$$

$$E_g(r) = \frac{R_{g1}(r) \left[\frac{E_s(r)}{R_{gs}(r)} + D_4 R_{g1}(r) \left(\frac{J_p(r)}{R_{gp}(r) + R_{g2}(r)} + \frac{J_{g1}(s)}{R_{g1}(s)} + \frac{J_p(s)}{R_{gp}(s) + R_{g2}(s)} \right) \right]}{(R_{g1}(r))^2 D_3 D_4 - 1} \quad (3-10)$$

$$E_p(r) = R_p(r) \left(q_p + \frac{J_p(s)}{R_p(s)} + \frac{J_p(r)}{R_p(r)} \right) \quad (3-11)$$

$$J_{g1}(r) = \frac{\frac{E_g(r)}{R_{g1}(r)} + \frac{E_s(r)}{R_{gs}(r)}}{D_4} \quad (3-12)$$

where

$$D_1 = \frac{1}{R_{g1}(s)} + \frac{1}{R_{gs}(s)} + \frac{1}{R_{gw}(s)}$$

$$D_2 = \frac{1}{R_p(s)} + \frac{1}{R_{ps}(s)} + \frac{1}{R_{pw}(s)} + \frac{1}{R_{gp}(s) + R_{g2}(s)}$$

$$D_3 = \frac{1}{R_{g1}(r)} + \frac{1}{R_{gp}(r) + R_{g2}(r)}$$

$$D_4 = \frac{1}{R_{g1}(r)} + \frac{1}{R_{gs}(r)} + \frac{1}{R_{gw}(r)}$$

$$D_5 = \frac{1}{R_p(r)} + \frac{1}{R_{ps}(r)} + \frac{1}{R_{pw}(r)} + \frac{1}{R_{gp}(r) + R_{g2}(r)}$$

$$D_6 = D_5 - \frac{1}{R_{p(r)}} - \frac{D_4 (R_{g1(r)})^2 \left(\frac{1}{R_{gp(r)} + R_{g2(r)}} \right)}{\left[(R_{g1(r)})^2 D_3 D_4 - 1 \right] \left[R_{gp(r)} + R_{g2(r)} \right]}$$

The plate temperature can be calculated based on the Stefan-Boltzmann Law:

$$\begin{aligned} T_p &= \left(\frac{E_p}{\sigma} \right)^{\frac{1}{4}} \\ &= \left(\frac{E_{p(r)} + E_{p(s)}}{\sigma} \right)^{\frac{1}{4}} \\ &= \left(\frac{E_{p(r)}}{\sigma} \right)^{\frac{1}{4}} \end{aligned} \tag{3-13}$$

For purposes of data correlation, the use of dimensionless variables is useful. In the present case when the solar simulator is "on" the solutions expressed by equations (3-7) through (3-12) can be put in dimensionless form simply by dividing by $G_s (= E_s F_{gs})$, the solar constant. Dimensionless plate temperature θ_p can then be expressed as

$$\theta_p = \left(\frac{E_p}{G_s} \right)^{\frac{1}{4}} \tag{3-14}$$

The parameter θ_p is a function only of the dimensionless plate heat load, q_p''/G_s , and the degree of dust coverage, (X).

By means of the preceding equation the dimensionless plate temperature has been calculated for the various test runs for the case with the solar simulator "on". The results are plotted in terms of θ_p versus q_p''/G_s for various levels of dust contamination in Figures 3-32 through 3-36. Values of the radiative properties of

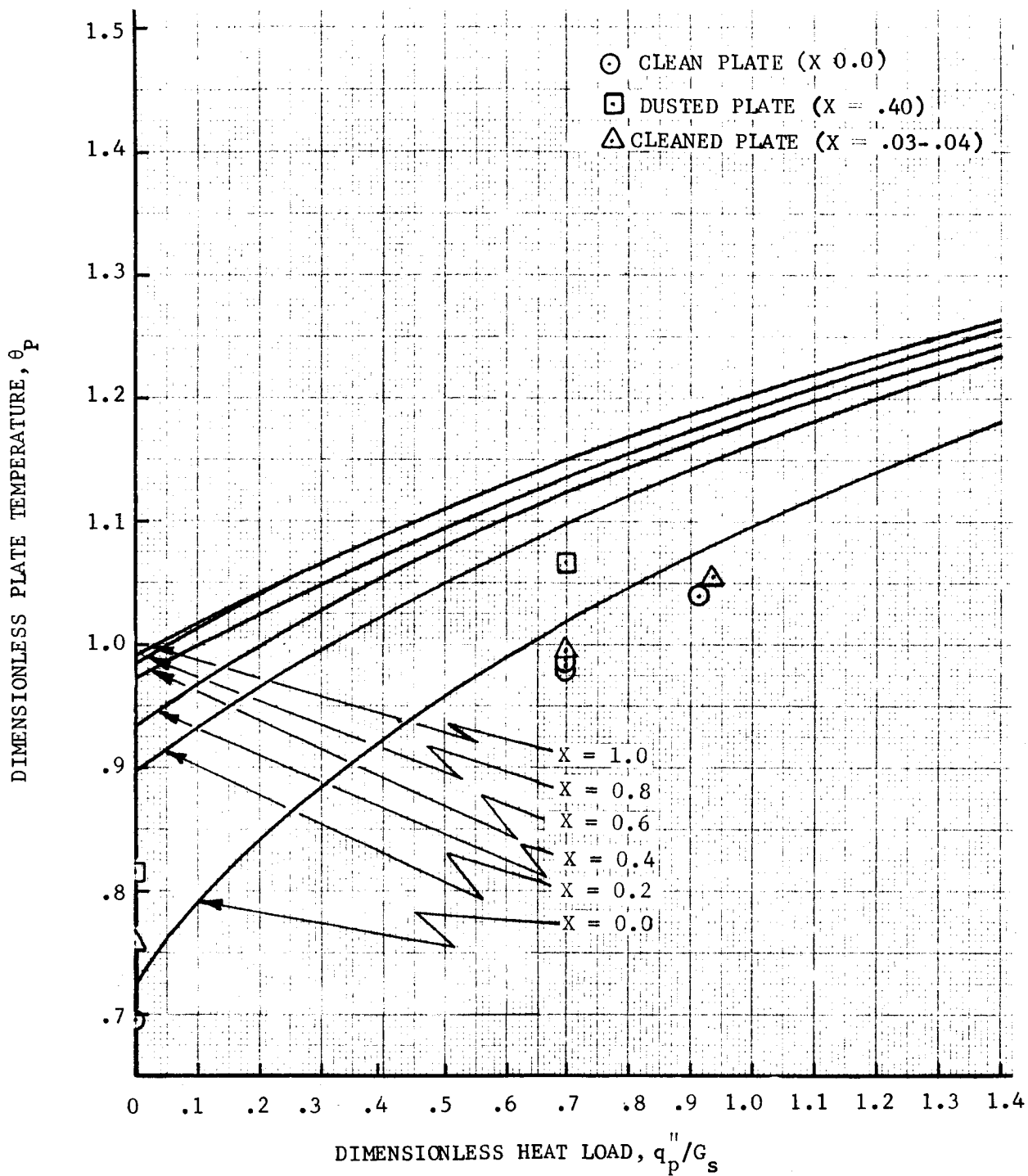


Figure 3-32. CORRELATION OF DIMENSIONLESS PLATE TEMPERATURE, θ_p , FOR CALIBRATION TEST RUN (SOLAR SIMULATOR ON)

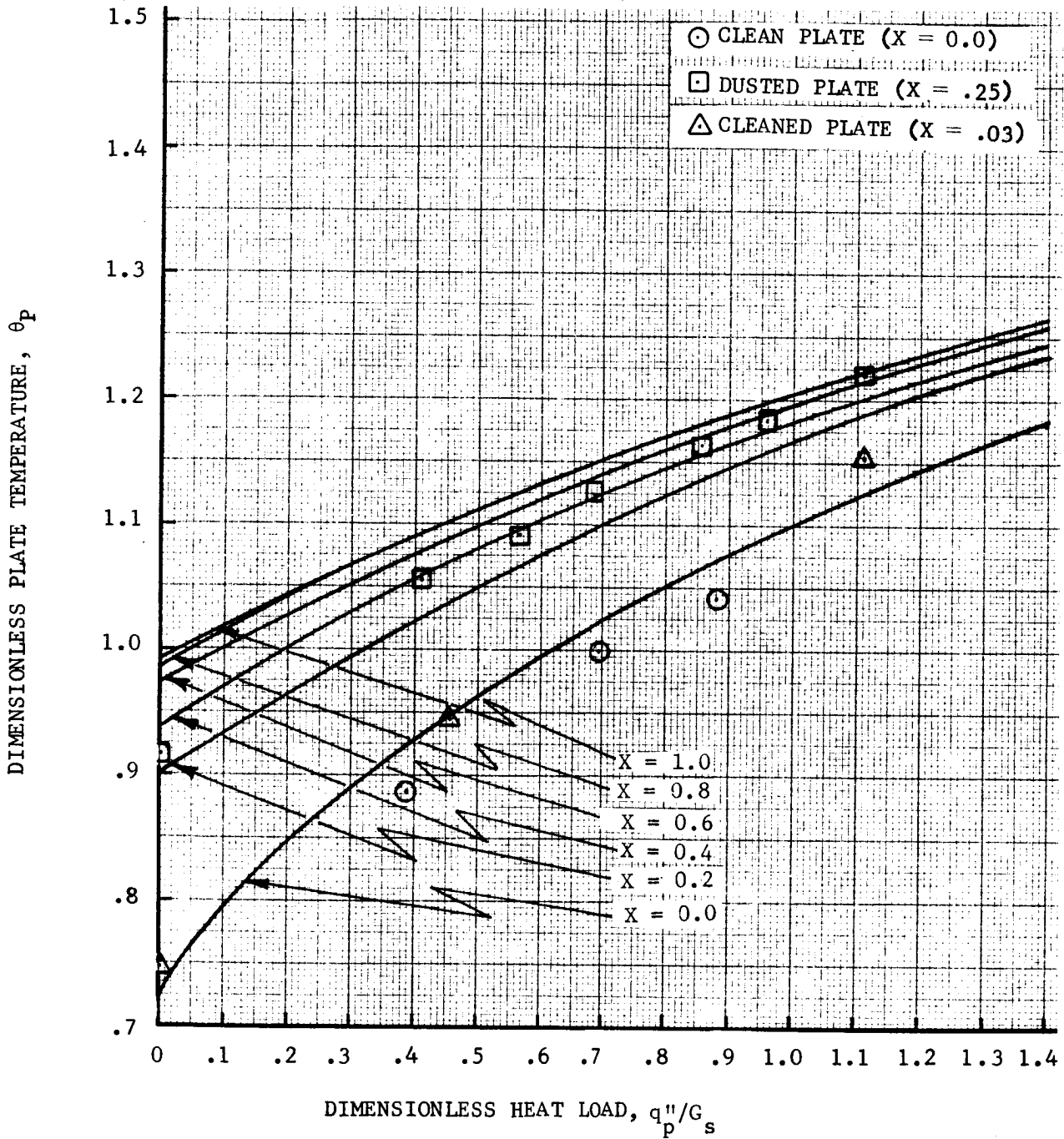


Figure 3-33. CORRELATION OF DIMENSIONLESS PLATE TEMPERATURE, θ_p FOR JET AND PLATE TEST RUNS WITH LIQUID INHIBISOL (SOLAR SIMULATOR ON)

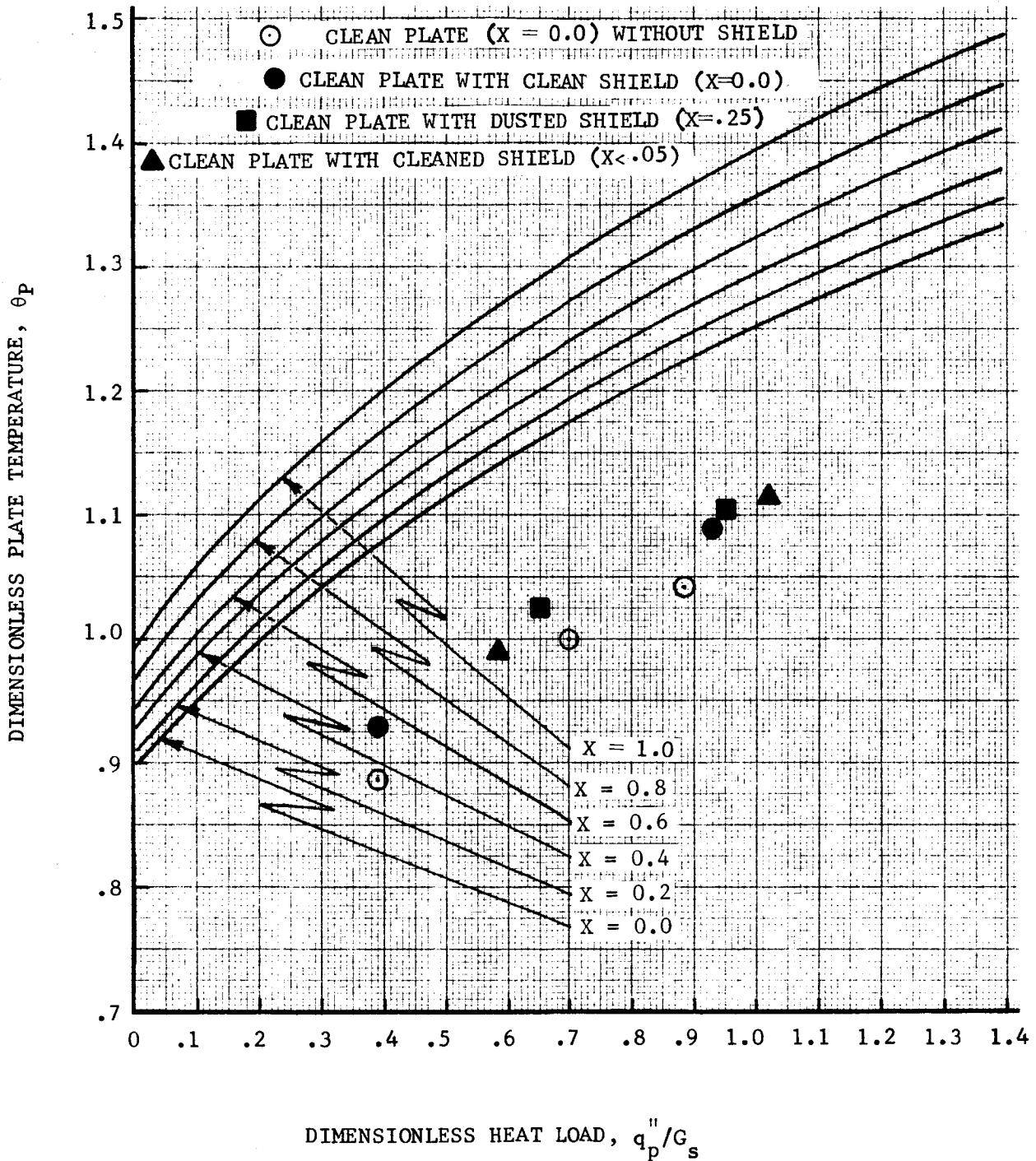


Figure 3-34. CORRELATION OF DIMENSIONLESS PLATE TEMPERATURE, θ_p FOR JET AND ARSENIC TRISULFIDE SHIELD TEST RUN (SOLAR SIMULATOR ON)

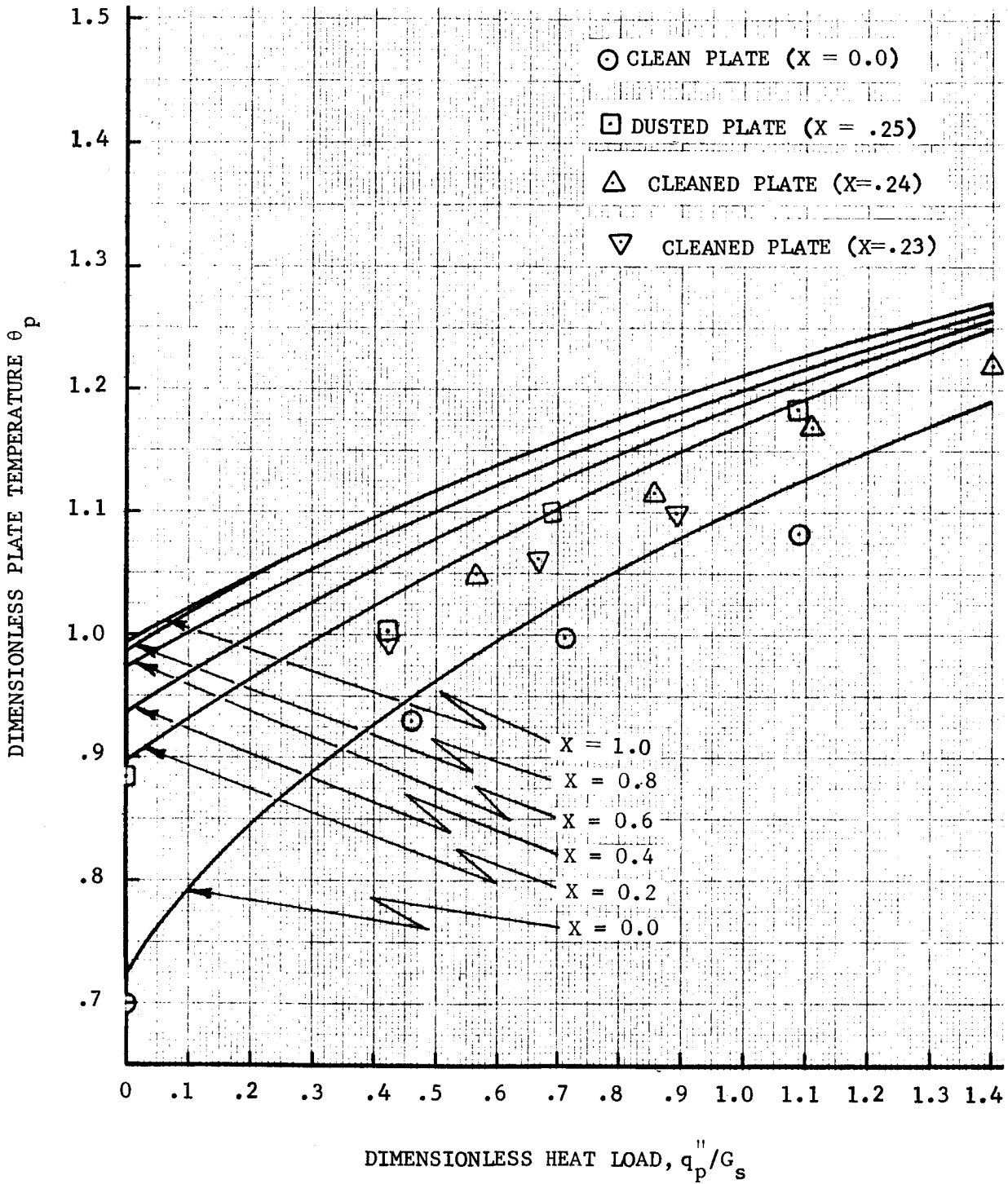


Figure 3-35. CORRELATION OF DIMENSIONLESS PLATE TEMPERATURE, θ_p FOR VIBRATING SURFACE TEST RUN (SOLAR SIMULATOR ON)

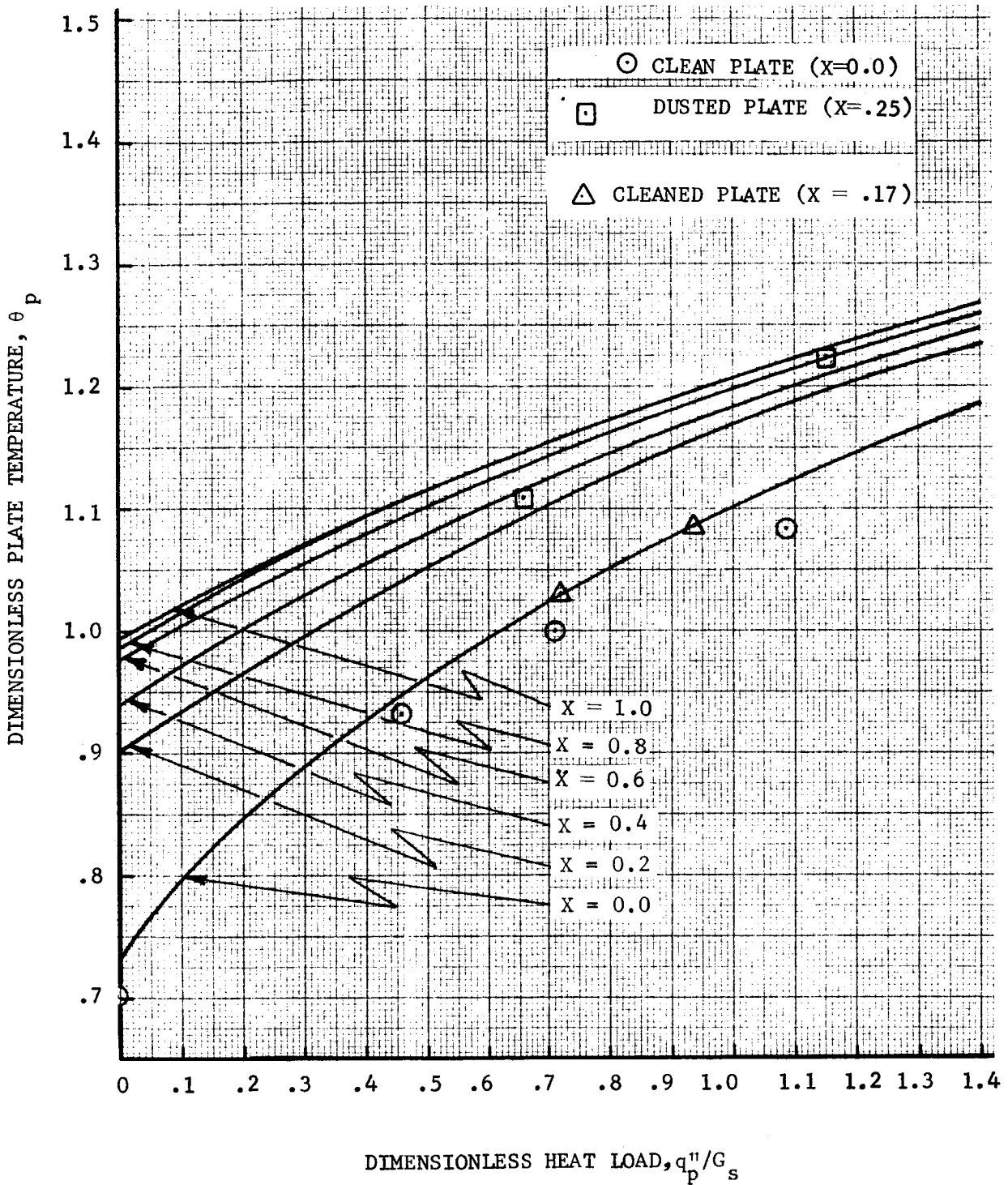


Figure 3-36. CORRELATION OF DIMENSIONLESS PLATE TEMPERATURE, θ_p FOR MECHANICAL BRUSH TEST RUN (SOLAR SIMULATOR ON)

7 June 1967

the dust, plate, and shield used in developing these figures are provided in Table 3-10.

Table 3-10. RADIATIVE PROPERTIES OF DUST, PLATE, AND SHIELD

Property	Basalt Dust	Material		
		S-13 Plate	As ₂ S ₃ Shield	
			Present	Not Present
Solar Absorptance	.84	.191	0.516	0
Solar Transmittance	0	0	0.245	1.0
Infrared Absorptance	.88	.83	.225	0
Infrared Transmittance	0	0	.515	1.0

This data for Table 3-10 for the basalt dust and the S-13 are based on the experimental results already reported. The As₂S₃ data is based on the manufacturer's specifications plus preliminary Northrop measurements.

The measured values of temperature expressed in terms of θ_p are also plotted in Figures 3-32 through 3-36. Correlation of data for the unshielded tests is generally good although there appears to be a consistent error for the uncontaminated plate temperature. This is probably due to a variation in the value of the solar absorptance of the S-13. For the case of the plate temperature with the arsenic trisulfide shield, good agreement between measurement and prediction is not indicated. The predicted values are consistently higher than measured values by ~20 percent. More significant is the fact that the measured temperatures display little or no spread due to dust contamination while the predicted values display a considerable spread. This disagreement between experiment and theory can be attributed to one of two causes:

- 1) The thermal network model may not provide a sufficiently accurate representation of the actual physical phenomena.
- 2) The radiative properties of the shield used in the calculation of predicted temperature may be inaccurate. (The cracking of the As_2S_3 shield during the tests may have resulted in a change in such properties.)

Only further study can establish which is the correct cause.

SECTION IV

CONCLUSIONS AND RECOMMENDATIONS

The objectives of the research effort have been:

- to determine the effect of dust on radiator surfaces and
- to develop methods for preventing or removing accumulations of dust from such surfaces.

The details of the results obtained have been provided in Sections II and III. Based on these results, certain conclusions and recommendations may be formulated.

The presence of basalt dust on either S-13 or aluminized Teflon thermal control coatings causes a general increase in spectral absorptance of the surface over all wavelengths in the solar spectrum. This in turn causes an increase in the total solar absorptance of the surface. The variation of total solar absorptance with dust contamination is nonlinear in nature. A relatively small degree of contamination (~10-percent dust coverage) can produce a large increase in solar absorptance (~90 percent). With dust present on the surface, the total solar absorptance of the surface tends to increase with angle of incidence. In general, if the increase in solar absorptance of the surface is to remain below 20 percent, the dust contamination must be kept below ~3 percent.

The infrared emittance of the basalt dust is very nearly equal to the infrared emittance of the thermal control coatings. For this reason dust contamination produces very little change in the value of this property of the surface.

The removal or prevention of dust accumulation on the thermal control surface under simulated lunar conditions proved to be a difficult task. For the devices tested, the jet and plate device proved most effective. The jet and shield device was second with the mechanical brush and vibratory surface devices third and fourth, respectively. None of the devices proved completely effective. Because of experimental considerations, the surface area cleaned by each was small.

With respect to specific working fluids or materials, for the jet the incompressible fluids proved more effective than the compressible fluids. Of the incompressible fluids tested, methyl chloroform (inhibisol) gave the best performance. For the shield material the arsenic-trisulfide shield gave the best results although the ordinary glass plate proved nearly as effective. For the brush material, the styrofoam proved to be the most promising.

The fact that the presence of the shield caused the plate temperature to become less sensitive to the level of dust contamination appears significant. For situations where dust cannot be prevented or removed, the use of a shield would tend to reduce the increase in plate temperature.

Prediction of plate surface temperature with dust contamination and without the shield appears to pose no problem provided accurate property data are available for the surface as a function of dust coverage. For the case involving the plate covered by the shield with dust on the latter, accurate prediction of plate temperature is more difficult and deserves further study. In this respect more accurate and complete values of the radiative properties of the shield material are desirable.

In the course of the research effort several new concepts were envisioned which appeared promising but were not adequately studied due to lack of time and funds. These included a transpiration cleaning action involving a porous thermal control coating, and a "peel-off" transparent sheet. These concepts, along with the electrostatic concept for which complete testing was not accomplished, appear worthy of further study.

The most general conclusion that can be reached based on the data collected would be that considerable work remains to be done before the optimum dust removal/prevention system can be established. Furthermore, for each lunar craft or lunar missions, a specialized dust removal/prevention system may be required. If, however, dust contamination proves to be a problem in lunar exploration, this research effort represents an initial step toward the solution of the problem.

SECTION V

REFERENCES

1. Jaffe, L. D., Shoemaker, E. M., Surveyor I Mission Report Part II Scientific Data and Results, Jet Propulsion Laboratory, California Institute of Technology, Pasadena, California, 10 September 1966.
2. Private Communication, Jet Propulsion Laboratory, May 1967.
3. Grannis, P. D., "Electrostatic Erosion Mechanism on the Moon," JGR, Vol. 66, No. 12, 1961, pp. 4293-4299.
4. Bennett, E. C., Wood, H. L., et al., "Thermal Properties of Simulated Lunar Material in Air or in Vacuum," AIAA Journal, Vol. 1, No. 6, 1963, pp. 1402-1407.
5. McCracken, C. W., Dubin, M., "Dust Bombardment on the Lunar Surface," NASA Technical Note NASA TN D-2100, 1963, 21 pages.
6. Salisbury, J. W., Glaser, P. E., et al., "Adhesive Behavior of Silicate Powders in Ultra High Vacuum," Journal of Geophysics Research, Vol. 69, No. 2, 15 January 1964.
7. Stein, B. A., Johnson, P. C., "Investigation of Soil Adhesion Under High Vacuum," The Lunar Surface Material and Charact., Academic Press, 1964, pp. 93-110, 532 pages.
8. Anon., "Study of Cryogenic Storage on the Moon," Contract NAS8-4377, Huntsville, Alabama, A. D. Little Inc., Cambridge, Mass., 1964.
9. Naughton, J. J., Barnes, I. L., Hammond, D. A., "Rock Degradation by Alkali Metal: A Possible Lunar Erosion Mechanism," Science, Vol. 149, 1965, pp. 630-631.
10. Ryan, J. A., "Experimental Investigation of Ultra-High Vacuum Adhesion as Related to Lunar Surface," OART Contract NAS7-307, 1965, 4th Qtly Rept.
11. Walker, E. H., "AGU Annual Mtg. Lunar Dust Clouds Produced by the Impact of Space Vehicles and Meteoric Bodies, 1965.
12. Stanley, Lucas, and Breazeale, "Interim Report - Lunar Environmental Analysis - A Survey of Lunar Surface Models," Tech. Memo. No. 293A, Northrop Corp., 15 March 1966.
13. Kopal, Zdenek, Physics and Astronomy of the Moon, Academic Press, New York, 1962.
14. Anon., "Radiators for Snap 50/SPUR," Tech. Report AF APL-TR-64-143, Airsearch Man. Co.
15. Anon., "Engineering Study of Multipurpose Engine/and Fuel System," LESA Final Report, Vol. V, WANL-PR(S)-006-B.

7 June 1967

16. Anon., "Engineering Study of Nuclear Power Plant," LESA Final Report, Vol. III, WANL-PR(S)-009A.
17. Hansen, R. H., and Kosfeld, O. R., "Apollo Logistic Support Systems Molab Studies," TM X-53032.6.
18. Anon., "Lunar Shelter/Rover Conceptual Design and Evaluation," NASA CR-60149.
19. Systems Section, "Development of a Deep Subsurface Lunar Drill for Post-Apollo Mission," (NAS8-20537) TR-293-6-061, Northrop Space Laboratories, Huntsville, Ala., 15 August 1966.
20. Anon., "Feasibility Investigation of a Moving Belt Radiator," ASD-TDR-63-551, Summary Report.
21. Anon., "Compact Lunar Power Station," MTP-ASTR-A-63-8.
22. Oppenheim, A. K., "The Network of Radiation Analysis," ASME Paper 54-A75, 1954.

SECTION VI

BIBLIOGRAPHY

1. Anderson, J. W., et al., "Experimental and Analytical Assessment of Space Thermal and Vacuum Environment Simulation Requirements," J. Spacecraft and Rockets, 3, (7), 976, 1966.
2. Anon., "An Introduction to the Geology of the Moon, AF-CRL-65-357.
3. Anon., "Classification of Methods for Determining Particle Size," Analyst 88, (1044), 1963, pp. 156-187.
4. Anon., "Experimental Investigation of Total Emittance and Solar Absorptance of Several Coatings Between 300° and 575°K," NASA TN D-3381.
5. Anon., "Good Degreases for Aluminum," Modern Metals, April 1959, p. 56.
6. Anon., "Lunar Dust - Bibliography," ARB-048386, 21 March 1966.
7. Anon., "Lunar Craters," Icarus, March 1966, pp. 130, 154, 165, 178, 190, 201.
8. Anon., "Lunar Photographs: Evidence for a Fragmental Surface Layer," Science, 26 August 1966, p. 985.
9. Anon., "Micrometeorite Experiment Planned for AS-205 Flight," Aviation Week, 29 August 1966, p. 75.
10. Anon., "NASA Contributions to the Technology of Inorganic Coatings," N-65-15535, OTS, Springfield, Virginia, p. 267.
11. Anon., "NASA 1965 Summer Conference on Lunar Exploration and Science," NASA SP-88, 1965, p. 448.
12. Anon., "Simulation of Albedo-Planetary Reflection and Emission--is Best Accomplished with a Baffled, Modular Radiation Array," Space/Aeron. 45 (4) 123, April 1966.
13. Anon., "Singer Considers the Old Lunar-Dust Question in the Light of Lunar G's Photos," Astron. & Aeron., 4 (5) 14, May 1966.
14. Anon., "NASA Thermal Protection Systems (U)," NASA TM-X650, February 1962.
15. Anon., "Proc. 6th Symposium on Hypervelocity Impact," Vol. 4, Applications (Secret), May 1963.
16. Aronson, J. R., et al., "Infrared Spectra from Fine Particulate Surfaces," Science 152 (3720) 345, 15 April 1966.

17. Avdeev, S. P. and Rinas, V. F., "A Method of Determining the Emittance of Partially Transparent Materials," Instr. & Exp. Tech. (6) 1462, 1965.
18. Babushkin, A. A., "Investigation of Formation of Polymer Coatings by the Method of IR Spectroscopy," Bull. Acad. Sci. USSR, Phys. Sci., 27 (7) (July 1965), 1964, pp. 856-957.
19. Bakker, W. T., "Particle Size Measurement of Aluminum by Centrifuging," Bell Amer. Ceram. Soc. Inc., 1966, p. 582.
20. Beer, Arthur, (Ed.), "Vistas in Astronomy," Vol. 1 (Astronautics, Astrophysics, Solar, Etc.), Vol. 2 (Photometry, Spectroscopy, Etc.), Pergamon Press, 1965.
21. Bell, P. R., "Vacuum Welding of Olivine," Science 153 (3734), 22 July 1966, p. 410.
22. Beller, W., "Soviet View of Lunar Surface Reported," Missiles & Rockets, 23 May 1966, p. 74.
23. Bendor, E., "Free Molecular Expansion of Initially Moving Gases into Vacuum," Quart. J. Mechan. & Appl. Mathem., 14 (4), 19 November 1966, pp. 497-509.
24. Bevans, J. T., "Prediction of Space Vehicle Thermal Characteristics," AFFDL-TR-65-139, August 1965.
25. Bonneville, J. M., "Techniques for Computing the Thermal Radiation Incident on Vehicles in Space," NAS-5-664, June 1962.
26. Boor, L., et al., "Hardness and Abrasion Resistance of Plastics," ASTM Bulletin No. 145, 1947, pp. 68-73.
27. Brown, H. and Murray, B. C., (Research), Annual Report (Grant NSG 56-60) Part II, Summary of Research, 31 January 1962.
28. Bryant, P. J., "Cohesion of Clean Surfaces and the Effect of Adsorbed Gases," Trans 9th Vac. Symp. (AVS), 1962.
29. Bucher, G. C., and Stern, H. E., "Physics of the Moon--Selected Topics Concerning Lunar Exploration," NASA TN D-2944, November 1965.
30. Buroulde, P., "The Lunar Environment," NASW-6, 28 October 1960.
31. Burns, G., "Reference Tables for the Pt (30% Rh) vs. Pt (6% Rh) Thermocouple," J. Res. NBS, Sect. C., April-June 1966, p. 89.
32. Cabannes, F. and Ch., "Facteurs de Reflexion et D'emission D'oxyde de Magnesium Fritte," Annales de Physique 10 (11-12), November-December 1965, p. 707.

33. Campanaro, T. Ricolji, "Effective Emissivity of a Spherical Cavity," Appl. Optics 5 (6), June 1966, p. 929.
34. Clausen, O. W., and Neu, J. T., "The Use of Directionally Dependent Radiation Properties for Spacecraft Thermal Control," Astron. Sct. 11 (5), September-October 1965, p. 328.
35. Cohn, C. C., "Chemical Polishing of Aluminum and its Alloys," Electroplate & Metal Finishing, November 1960, p. 421.
36. Corn, M., and Stein, F., "Adhesion of Atmospheric Dustfall Particles to a Glass Slide," Nature 211 (5044), 2 July 1966, p. 60.
37. Coulson, K. L., et al., "Effect of Surface Reflection on Planetary Albedo," Icarus 5 (2), March 1966, p. 139.
38. Curtis, H. B., "Measurement of Emittance and Absorptance of Selected Materials Between 280° and 600°K," J. Spacecraft & Rockets 3 (3), 1966, p. 383.
39. Damask, A. C., "Proton Irradiation from the Sun May Bond Dust Particles on the Surface of the Moon," C & EN, 20 June 1966, p. 43.
40. Dance, J. B., "Counting and Sizing Microscopic Particles," Industrial Electronics 4 (1), January 1966, p. 10.
41. Diedrich, J. H., and Curtis, H. B., "Experimental Investigation of Total Emittance and Solar Absorptance of Several Coatings Between 300° and 575°K," NASA TN D-3381, April 1966.
42. Divari, N. B., "Charged Dust Particles in Interplanetary Space," Sov. Astronomy 10 (1), July-August 1966, p. 151.
43. Eastman, D. W., and Bounema, J. P., "Flowfield of Highly Underexpanded Jet Impinging on a Surface," AIAA Jour. 4 (7), July 1966, p. 1302.
44. Edwards, D. K., and Hall, W. M., "Far Infrared Reflectance of Spacecraft Coatings," JPL-TR 32-873, NAS7-100, 31 January 1966.
45. Edwards, O. J., "Optical Absorption Coefficients of Fused Silica $\lambda = 0.17\mu$ to 35μ From Room Temperature to 980°C," NASA TN D-3257, February 1966.
46. Eubanks, A. G., and Moore, D. G., "Investigation of Aluminum Phosphate Coatings for Thermal Insulation of Airframes," NASA TN D-106, November 1959.

47. Fesenkov, V. G., "Photometric Peculiarities of the Moon," Sov. Astronomy 4 (3), November-December 1960, p. 468.
48. Fisher, D. E., "The Origin of Meteorites and Space Erosion and Cosmic Radiation Gases," J. Geophys. Res. 71 (13), 1 July 1966, p. 3251.
49. Fowle, A., "Thermal Scale Modeling of Spacecraft: An Experimental Investigation," J. Spacecraft & Rockets, April 1966, p. 577.
50. Francis, J. E., "Effect of Optical Thickness on the Directional Transmittance and Emittance of a Dielectric," J. Opt. Soc. Am., June 1966, p. 779.
51. Friedman, H., "Surfactants for use in Dispersing Pigment Throughout a Coating Material," IBM Tech Dis. Bull., March 1966, p. 1309.
52. Funsu, A. I., "Determination of the Thermal Emittance Stability of Spacecraft Radiator Coatings," ASD TDR-63-429.
53. Galitskayo, E., "Radiation Control of the Orientation of Space Probes," Cosmic Res. 3 (3), May-June 1965, p. 298.
54. Gault, D. E., et al., "Spray Ejected from the Lunar Surface by Meteoroid Impact," NASA TN D-1767, April 1963.
55. Geer, R. L., "Impact Studies on Lunar Dust Models at Various Vacuums," ASD TR 61-595, January 1962.
56. Gericke, O., "Experimental Data of Ultrasonic Transducer Frequency," Materials Evaluation, August 1966, p. 409.
57. Gilligan, J. E., "Stable White Coatings," IITRI-U6004-21, February 1966.
58. Glaser, P. E., et al., "Investigation of Materials for Vacuum Insulation up to 4000°F," ASD-TDR-62-88, January 1962.
59. Glaser, P. E., "Studies of the Physical Characteristics of Probable Lunar Surface Materials," AFCRL-64-970(II)N65-22451, 1964.
60. Glaser, P. E., et al., "Study of Cryogenic Storage on the Moon," 3rd Progress Report (NAS8-11377), 1 September to 1 October 1964.
61. Goetzl, C. G., Rittenhouse, J. B., and Singletary, John B., Space Materials Handbook, Addison-Wesley Publishing Co., Inc., Mass., 1965.
62. Godridge, A. M., "Particle Size Classifier," J. Sci. Instr. 39 (12), 1962, p. 611.
63. Gordon, A., "Emissivity of a Surface After Sandblasting," High Temp. 3 (6), November-December, 1965.

64. Green, J., "Moon's Surface," Int. Sci. & Tech., September 1966, p. 59.
65. Gubareff, G. G., et al., "Thermal Radiation Properties Survey," 2nd Ed., 1960.
66. Hapke, B., "Some Comments on Gehrel's Model of the Lunar Surface," Icarus 5 (2), March 1966, p. 154.
67. Hapke, B., "An Improved Theoretical Lunar Photometric Function," Astron. J., June 1966, p. 33.
68. Havry, G. L., "An Apparatus for the Measurement of Total Hemispherical Emmissivity and Thermal Conductivity Between Ambient and Liquid Nitrogen Temperatures," ASD TDR 63-146.
69. Hayre, H. S., and Moore, R. K., "Radar Backscatter Theories for Near Vertical Incidence and Their Application to an Estimate of the Lunar Surface Roughness," N-62 11754 EE 67, January 1962.
70. Hibben, R., "Micrometeorite Data Challenges Theories," Aviation Week, 5 September 1966, p. 54.
71. Hill, L. R., "The Effect of Vacuum on the Shear Strength of an Idealized Granular Medium," Astronaut. Act., July-August, 1965, p. 261.
72. Hormann, H. H., "Novel Ultraviolet Radiation Absorbers in Satellite Temperature Control Coatings," Industr. & Engng. Chem. 5 (1), March 1966, p. 92.
73. Hottel, H. C., et al., "The Role of Scatter in Determining the Radiative Properties of Surfaces," MIT-46, Special Printing 012, 1966.
74. Hovisjo, W. A., et al., "Infrared Reflectance Spectra of Igneous Rocks, Tuffs, and Red Sandstone from .5 to .22 μ ," J. Opt. Soc. Am. 56 (5), 1966, p. 639-643.
75. Howell, J., "Radiative Interactions Between Absorbing-Emitting and Flowing Media with Internal Energy Generation," AIAA Paper 66-434, 1966.
76. Hwang, Sun-tak, "Surface Diffusion in Microporous Media," Conrad, J. Chem. Eng., April 1966, p. 82.
77. IITRI, "Investigation of Environmental Effects of Coatings for Thermal Control of Large Space Vehicles," NASA Marshall Space Flight Center, Huntsville, Commerce Business Daily Notice, 15 April 1966.
78. Jack, J. R., "Techniques for Measuring Absorptance and Emittance by Using Cyclic Incident Radiation," AIAA Paper 66-416, 1966.
79. Jagger, R. M., "Spectrum Analysis of Terrain of Mare Cognitum," J. Geophys. Res., April 1966, p. 2023.

80. Jaffe, L. D., "The Lunar Program," NAS7-100, 1963.
81. Jaffe, L. D., "Depth of the Lunar Dust Strength of the Lunar Dust, Bearing Strength of Fairy Castle Structures, NAS7-100, JPL TR 32-856, 15 February 1966.
82. Jaffe, L. D., "Lunar Dust Depth in Mare Cognitum," JPL TR No. 32-896, J. Geophys. Res. 71 (4) 15 February 1966, p. 1095.
83. Jaffe, L. D., "Lunar Dust Depth in Mare Cognitum," NAS7-100, 30 March 1966.
84. Jaffe, L. D., and Scott, R. F., "Lunar Surface Strength: Implications of Luna 9 Landing," Science 153 (3734) 22 July 1966, p. 407.
85. Jurca, S., "A Note on Particle Size Determination," Int. J. of Powder Metal, 2 (3), 1966, p. 47.
86. Katzoff, S., "Symposium on Thermal Radiation of Solids," NASA-SP 55 (ML-TDR-64-159), 6 March 1964, p. 4.
87. Kaye, B. H., "Thermal Stability of Sedimenting Suspensions used to Measure Particle-Size Distributions," Material Research & Standards, November 1965.
88. Kendall, B.R.F., and Zabielski, M. F., "High-Temperature Insulating Adhesives for Vacuum Applications," J. Vac. Sci. Tech. 3 (3), May-June 1966, p. 114.
89. Kessler, J. N., "New Process Prepares Plastics for Stronger Adhesive Bonding," IITRI Industrial Research Newsletter, April 1966.
90. Kornhauser, M., "The Crater Contribution to Surface Roughness of the Moon," Astron. Sci. Rev., January-March 1962, p. 23.
91. Kingery, W.D., "Fundamental Study of Photoplate Sounding in Refractories," J. Amer. Ceram. Soc. 33 (8), August 1950, pp. 239-247.
92. Kramer, H. W., "Radioactivity of the Lunar Surface," Science 152 (3726), 27 May 1955, p. 1235.
93. Kroustein, M., "Investigations on Spectral Reflectance and Absorption Characteristics of Camouflage Paint Materials and Natural Objects," DA-44-009-ENG-1447, 1956.
94. Liebert, C. L., "Spectral Emittance of Al_2O_3 and ZnO on Opaque Substrates," NASA TN D-3115, November 1965.
95. Love, T. J., "Experimental Determination of Thermal Radiation Scattering by Small Particles," AF-33-657-8859, June 1965.
96. Lowe, H. J., and Lucas, D. H., "Static Electrification," Brit. J. Appl. Phys. Suppl. 2, S40, 1953.

97. Lowman, P. D., Jr., "Report on the Lunar Surface Materials Conference," Boston, May 1963.
98. Lowrance, D. T., and Cox, R. L., "Fundamental Studies of the Stability of Thermal-Control Coatings," AIAA Jour. 4 (5), 1966, p. 906.
99. Lundeberg, J. F., et al., "Meteoroid Protection for Spacecraft Structures," NASA CR-54201, October 1965.
100. Lyon, J. P., "Evaluation of Infrared Spectrophometry for Componential Analysis of Lunar and Planetary Soils," NASR-49-04; NASA CR-100, November 1964.
101. Lytheton, R. A., "The Effect of the Lunar Orbit of Meteoritic Accretion," JPL-TR-32-293, NAS7-100, March 1966.
102. Maiden, C. J., and McMillan, A. R., "An Investigation of the Protection Afforded a Spacecraft by a Thin Shield," AIAA Paper, 22 January 1964.
103. Martin Co., "Measurement of Thermal Radiation Characteristics," ER 13638, September 1964.
104. Mason, R. L., "Engineering Lunar Model Surface," NASA-TM-X54753 TR 83-D, 4 September 1964.
105. McCue, G., "A Note Concerning the Effective Emittance of Certain Grooved Surfaces," AIAA Journal, April 1966.
106. Miller, G. M., and Bratton, F. H., "The Effects of High Vacuum and Ultraviolet Radiation on Plastic Materials," NAS-5-2834, September 1964.
107. Mimura, T., "Thermal Radiation Absorptance and Vacuum Outgassing Characteristics of Several Metallic and Coated Surfaces," NASA TN D-3234, February 1966.
108. Mirtich, M. J., and Mark, H., "Feasibility of Accelerating Micron-Size Particles in Shock-Tube Flows for Hypervelocity Degradation of Reflective Surfaces," NASA TN D-3187, January 1966.
109. Nelson, K., "A Device for the Rapid Measurement of Total Emittance," J. Spacecraft & Rockets, May 1966, p. 758.
110. Nickols, L. D., "Surface Temperature Distribution on Thin-Walled Bodies Subjected to Solar Radiation in Interplanetary Space," NASA TN D-584, October 1961.
111. Nordwall, H. L., "Program for Determining Total Emissivity and Absorptivity," ASD TN 61-120, September 1963.
112. Oethking, P., "Photometric Studies of Difusely Reflecting Surfaces with Applications to the Brightness of the Moon," J. Geophys. Res. 71 (10), 15 May 1966, p. 2505.

113. Osgood, J. H., and Goen, J., "Sonic Velocity and Penetrability of Simulated Lunar Rock Dust," Geophysics 31 (3), June 1966.
114. Parmer, J. F., and Wiebelt, J. A., "The Thermal Radiation Characteristics of Specular Walled Grooves in the Solar Space Environment," AIAA Paper 66-459, 1966.
115. Parmer, J. F., "The Thermal Radiation Characteristics of Specular Walled Grooves in the Solar Space Environment," Dissert. 66-4053, 1966.
116. Pay, R., "Lunar Orbiter Reports Safe Atmosphere," Technology Week, 29 August 1966, p. 22.
117. Penn, S. H., et al., "Determination of the Coefficient of Friction of Metals and Non-Metals at Ultra-High Vacuum," NAS8-5415, May 1964.
118. Petroun, N. N., "A Spectrophotometric Study of the Lunar Surface," Sov. Astron. 10 (1), July-August 1966, p. 128.
119. Pilpel, N., "The Technology of Powders," Discovery 27 (7), 1966, p. 30.
120. Polyranskii, V., "On the Reflection of Light from Rough Surfaces," Optics & Spectro 12 (4), April 1966, p. 391.
121. Ramakrishna, K. V., "Prediction of the Lunar Surface Temperature, Phase 1," NAS8-20082, 15 March 1966.
122. Rauser, W. H., "Lunar Surface Luminance Prediction," NAS8-20082, March 1966.
123. Richmond, J. C., "Procedures for the Precise Determination of Thermal Radiation Properties," ML-TDR 64-257, Part 2, April 1965.
124. Rogers, R. N., and Morris, E. D., Jr., "Determination of Emissivities with a Differential Scanning Calorimeter," Anal. Chem. 38 (3), 1966, p. 410.
125. Rushol, E., "Physical Properties of the Lunar Surface," Cosmic Res. 3 (3), May-June 1965, p. 302.
126. Ryan, J. A., "Lunar Miscellany," AD 420980, April 1963.
127. Ryan, J. A., "Experimental Investigation of Ultra-High Vacuum Adhesion as Related to the Lunar Surface," NAS7-307, 30 June 1965.
128. Ryan, J. A., "Adhesion of Silicates in Space Environment," J. Geophys. Res. 71 (18), 15 September 1966, pp. 4413-4425.
129. Sackleh, F. J., "The Dustwall Concept of Meteoroid Protection," Res. & Techn. Briefs 4 (6), June 1966, p. 15.

130. Salisbury, J. W., and Van Tassel, R. A., "State of the Lunar Dust," Pub. Astr. Soc. Pacif. 74 (438), 1962, p. 245.
131. Salisbury, J. W., and Glaser, P. E. (Ed.), "Studies of the Characteristics of Probable Lunar Materials," P AFCRL-64-970, January 1964.
132. Savage, J. A., and Nielsen, S., "The Infrared Transmission of Telluride Glasses," Chem. & Phys. of Glasses, 7 (2), April 1966, pp. 56-59.
133. Shafer, C. F., and Bannister, T. C., "Pegasus Thermal Control Coatings Experiment," AIAA Paper 66-419, 28 June 1966.
134. Schatz, E. A., "Thermal Radiation Properties of Binary Mixtures," AIAA Paper 65-670.
135. Schmidt, W. F., and Olson, R. L., "Effects of Near-Ultraviolet Radiation on Thermal Control Surfaces at Cryogenic Temperatures," AIAA Paper 66-418.
136. Schutten, J., and Van Dyke, Th., "Luminescence Caused by Proton Impact with Special Reference to the Lunar Surface," Nature 211 (5048), 30 July 1966, p. 470.
137. Schwartz, H. S., and Farmer, R. W., "Thermal Irradiation of Plastic Materials," WADD-TR 67-647, August 1961.
138. Scully, J. C., "Hyproevents in Plastics Coatings on Metals: New Russian Advances," Light Metals & Metal Industry, March 1966, p. 53.
139. Setov, V. N., "Determination of Dust Cohesion to the Surface of Filters and Their Regeneration," Kolloid. Zh. 28 (2), March-April 1966, p. 275.
140. Shifrin, K. S., "Determination of the Particle Spectrum from the Scattering Function," Fiz. Atm. i Okeana 2 (2), 1966, p. 149.
141. Shilard, R., "Phenomenological Macrorheology in Lunar Soil Physics," AIAA Paper 66-516, 28 June 1966.
142. Shimaru, Y., "Survival Time of Lunar Surface Irregularities and Viscosity Distribution within the Moon," Icarus 5 (4), July 1966, p. 455.
143. Shoemaker, E. M., "Surveyor Found "Gritty" Moon That Can Support a Spacecraft," N. Y. Times, 17 June 1966.
144. Simmons, J. A., and Gift, R. D., "Some Difficulties of Operating Liquid Systems in a Vacuum," IAF-Intern. Astron. Congress, 9 through 15 October 1966.
145. Singer, S. F., and Walker, E. H., "Electrostatic Dust Transport on the Lunar Surface," Icarus 1, 1962, pp. 112-120.

146. Snisluchowski, R., "Structure and Coherency of the Lunar Dust Layer," J. Geophys. Res. 71, (6), 15 March 1966, p. 1569.
147. Sopp, Olav I., Moun, J., "Size Analysis in Sub-Sieve Range by Electronic Counter," Nature 210 (5037), 14 May 1966, p. 723.
148. Steere, R., "Thermal Properties of Thin-Film Polymers by Transient Heating," J. Appl. Phys., August 1966, p. 3338.
149. Stepka, F. S., et al., "Investigation of Characteristics of Pressure Waves Generated in Water Filled Tanks Impacted by High-Velocity Projectiles," NASA TN D-3143, December 1965.
150. Stierwalt, D. L., et al., "Measurement of the Infrared Spectral Absorptance of Optical Materials," J. Appl. Opt. 2, 1963, p. 1169.
151. Stierwalt, D. L., "Low-Temperature Spectral Emittance Measurements," AD 637, 15 August 1966, p. 742.
152. Tauaka, M., et al., "Direct Formation in Sheet Form of Arsenic-Sulfur Glasses by Distillation under Normal Pressure," J. Ceram. Assoc. Japan 73, 1965, pp. 51-55.
153. Trotskii, V. S., "Nature and Physical State of the Surface Layer of the Moon," Sov. Astron. J. 6 (1), July-August 1962, pp. 51-54.
154. Voyutskii, S. S., et al., "How Temperature Dependence and Activation Energy Affects the Adhesion of Polymers to Metals," Adhesives Age 8 (11), November 1965, p. 22.
155. Watkins, H. D., "Lunar Rocks Loom as Hazard to Apollo," Aviation Week, 13 June 1966, p. 27.
156. Wattson, R. B., Hapke, B. W., "A Comparison of the IR Spectra of the Moon and Simulated Lunar Surface Materials," Astrophys. J. 144 (1), April 1966, p. 364.
157. Wehner, et al., "Investigation of Sputtering Effects on the Moon's Surface," 4th Quart. Status Report, NASA(CR56292)N64-24023, 1964.
158. Wetmore, W., "Luna 9 Photos Indicate Surface Erosion," Aviation Week, 23 May 1966, p. 34.
159. Whipple, F. L., "Dust - Meteorites," Astronautics, August 1962, p. 40.
160. Winslow, P. M., "Study of Adhesion and Cohesion in Vacuum," NAS8-11006, NASA-CR-62595, 1 January 1965.
161. Winslow, P. M., "Adhesion of Metals in Space Environment," Vacuum Sci. Tech. 3 (2), April 1966, pp. 54-61.

165. Wittenberg, A. M., "Total Hemispherical Emissivity of Sapphire," J. Opt. Soc. Am. 55, 1965, p. 432.
166. Wood, W. D., and Coffin, C. L., "Hemispherical Total-Emittance Measurement in the Temperature Range 175° to 350°K for Selected Thermal-Control and Corrosion-Protection Coatings," AIAA Paper No. 66-18.
167. Zerlaut, Gene A., "Stable White Coatings," IITRI Report No. C207-25, 27 March 1963.
168. Zerlaut, Gene A., "Development of Space Stable Thermal Control Coating Paints with Low Solar Absorptance Emittance Ratios," NASA-CR-60355, 5 March 1965.
169. Zerlaut, G. A., and Rubin, G. A., "Development of Space Stable Thermal Control Coatings," NASA CR-74469, 21 February 1966.

APPENDIX A

EXPERIMENTAL DATA ASSOCIATED WITH MEASUREMENT OF SURFACE

SPECTRAL ABSORPTANCE OF DUST-CONTAMINATED THERMAL CONTROL COATINGS

A.1 S-13 Data

INTEGRATING SPHERE PROGRAMMED WORK SHEET

SAMPLE NO. 6

LEAD SULFIDE DETECTOR				
NO.	λ	DRUM	SLIT	ρ_s
1	2.45	7.48	2.00	47
2	2.05	8.58	2.00	73
3	1.82	9.05	2.00	69
4	1.67	9.40	2.00	67
5	1.54	9.65	2.00	76
6	1.44	9.88	2.00	77
7	1.36	10.10	1.74	78
8	1.29	10.23	1.52	80
9	1.23	10.33	1.42	80
10	1.17	10.44	1.16	80
11	1.12	10.55	1.12	82
12	1.08	10.63	1.06	82
13	1.04	10.71	1.02	83
14	1.00	10.83	1.02	84
15	0.96	10.96	0.92	85
16	0.93	11.00	0.86	85
17	0.90	11.08	0.84	85
18	0.87	11.14	0.80	85
19	0.84	11.20	0.80	86
20	0.81	11.29	0.76	86
21	0.79	11.34	0.74	87
22	0.77	11.40	0.74	88
23	0.75	11.46	0.72	88
24	0.72	11.55	0.72	88
25	0.70	11.65	0.70	88
26	0.69	11.69	0.70	88
27*	0.67	11.75	0.74	90
28*	0.65	11.86	0.74	89
29*	0.64	11.90	0.76	90
30*	0.62	12.03	0.78	91
31*	0.60	12.15	0.84	90
32*	0.59	12.20	0.90	91
33*	0.57	12.34	0.98	92

PHOTOMULTIPLIER DETECTOR				
NO.	λ	DRUM	SLIT	ρ_s
27*	0.67	11.75	0.74	90
28*	0.65	11.86	0.74	90
29*	0.64	11.90	0.76	90
30*	0.62	12.03	0.78	91
31*	0.60	12.15	0.84	91
32*	0.59	12.20	0.90	90
33*	0.57	12.34	0.98	92
34	0.56	12.45	1.00	91
35	0.55	12.49	1.08	92
36	0.53	12.65	1.16	91
37	0.52	12.72	1.24	90
38	0.50	12.90	1.24	92
39	0.49	13.00	1.30	93
40	0.48	13.10	1.44	92
41	0.47	13.20	1.58	93
42	0.46	13.31	1.70	95
43	0.44	13.60	1.90	91
44	0.43	13.80	2.00	89
#45	0.41	14.20	2.00	77
#46	0.39	14.58	2.00	39
#47	0.37	15.08	2.00	03
#48	0.34	16.02	2.00	02

$$\alpha_{\text{solar}} = \left[\sum_{m=1}^{m=48} (1-\rho_m) + \dots + (1-\rho_m) \right]_{m=48} = 48$$

$$\alpha_s = .195$$

* Overlap

Long Wavelength Filter In Beam

INTEGRATING SPHERE PROGRAMMED WORK SHEET

SAMPLE NO. 7

LEAD SULFIDE DETECTOR				
NO.	λ	DRUM	SLIT	ρ_s
1	2.45	7.48	2.00	45
2	2.05	8.58	2.00	65
3	1.82	9.05	2.00	65
4	1.67	9.40	2.00	62
5	1.54	9.65	2.00	68
6	1.44	9.88	2.00	69
7	1.36	10.10	1.74	70
8	1.29	10.23	1.52	72
9	1.23	10.33	1.42	72
10	1.17	10.44	1.16	72
11	1.12	10.55	1.12	73
12	1.08	10.63	1.06	74
13	1.04	10.71	1.02	74
14	1.00	10.83	1.02	75
15	0.96	10.96	0.92	75
16	0.93	11.00	0.86	75
17	0.90	11.08	0.84	76
18	0.87	11.14	0.80	76
19	0.84	11.20	0.80	76
20	0.81	11.29	0.76	76
21	0.79	11.34	0.74	78
22	0.77	11.40	0.74	78
23	0.75	11.46	0.72	78
24	0.72	11.55	0.72	78
25	0.70	11.65	0.70	78
26	0.69	11.69	0.70	80
27*	0.67	11.75	0.74	79
28*	0.65	11.86	0.74	78
29*	0.64	11.90	0.76	79
30*	0.62	12.03	0.78	78
31*	0.60	12.15	0.84	80
32*	0.59	12.20	0.90	80
33*	0.57	12.34	0.98	78

PHOTOMULTIPLIER DETECTOR				
NO.	λ	DRUM	SLIT	ρ_s
27*	0.67	11.75	0.74	80
28*	0.65	11.86	0.74	80
29*	0.64	11.90	0.76	80
30*	0.62	12.03	0.78	80
31*	0.60	12.15	0.84	80
32*	0.59	12.20	0.90	80
33*	0.57	12.34	0.98	81
34	0.56	12.45	1.00	81
35	0.55	12.49	1.08	80
36	0.53	12.65	1.16	79
37	0.52	12.72	1.24	81
38	0.50	12.90	1.24	81
39	0.49	13.00	1.30	81
40	0.48	13.10	1.44	82
41	0.47	13.20	1.58	80
42	0.46	13.31	1.70	80
43	0.44	13.60	1.90	81
44	0.43	13.80	2.00	78
#45	0.41	14.20	2.00	70
#46	0.39	14.58	2.00	38
#47	0.37	15.08	2.00	06
#48	0.34	16.02	2.00	04

$$\alpha_{\text{solar}} = \left[\sum_{m=1}^{m=48} (1-\rho_m) + \dots + (1-\rho_m) \right] : 48$$

$$\alpha_s = .245$$

* Overlap

Long Wavelength Filter In Beam

INTEGRATING SPHERE PROGRAMMED WORK SHEET

SAMPLE NO. 7-A

LEAD SULFIDE DETECTOR				
NO.	λ	DRUM	SLIT	ρ_s
1	2.45	7.48	2.00	48
2	2.05	8.58	2.00	70
3	1.82	9.05	2.00	69
4	1.67	9.40	2.00	65
5	1.54	9.65	2.00	73
6	1.44	9.88	2.00	74
7	1.36	10.10	1.74	75
8	1.29	10.23	1.52	76
9	1.23	10.33	1.42	76
10	1.17	10.44	1.16	77
11	1.12	10.55	1.12	78
12	1.08	10.63	1.06	78
13	1.04	10.71	1.02	79
14	1.00	10.83	1.02	79
15	0.96	10.96	0.92	80
16	0.93	11.00	0.86	79
17	0.90	11.08	0.84	80
18	0.87	11.14	0.80	80
19	0.84	11.20	0.80	82
20	0.81	11.29	0.76	82
21	0.79	11.34	0.74	82
22	0.77	11.40	0.74	83
23	0.75	11.46	0.72	83
24	0.72	11.55	0.72	83
25	0.70	11.65	0.70	82
26	0.69	11.69	0.70	85
27*	0.67	11.75	0.74	84
28*	0.65	11.86	0.74	85
29*	0.64	11.90	0.76	83
30*	0.62	12.03	0.78	84
31*	0.60	12.15	0.84	83
32*	0.59	12.20	0.90	83
33*	0.57	12.34	0.98	84

PHOTOMULTIPLIER DETECTOR				
NO.	λ	DRUM	SLIT	ρ_s
27*	0.67	11.75	0.74	84
28*	0.65	11.86	0.74	85
29*	0.64	11.90	0.76	83
30*	0.62	12.03	0.78	86
31*	0.60	12.15	0.84	86
32*	0.59	12.20	0.90	84
33*	0.57	12.34	0.98	84
34	0.56	12.45	1.00	88
35	0.55	12.49	1.08	85
36	0.53	12.65	1.16	85
37	0.52	12.72	1.24	85
38	0.50	12.90	1.24	88
39	0.49	13.00	1.30	88
40	0.48	13.10	1.44	86
41	0.47	13.20	1.58	86
42	0.46	13.31	1.70	87
43	0.44	13.60	1.90	84
44	0.43	13.80	2.00	81
#45	0.41	14.20	2.00	72
#46	0.39	14.58	2.00	37
#47	0.37	15.08	2.00	05
#48	0.34	16.02	2.00	04

$$\alpha_{\text{solar}} = \left[\sum_{m=1}^{m=48} (1-\rho_m) + \dots + (1-\rho_m) \right] : 48$$

$$\alpha_s = .239$$

* Overlap

Long Wavelength Filter In Beam

INTEGRATING SPHERE PROGRAMMED WORK SHEET

SAMPLE NO. 8

LEAD SULFIDE DETECTOR				
NO.	λ	DRUM	SLIT	ρ_s
1	2.45	7.48	2.00	40
2	2.05	8.58	2.00	61
3	1.82	9.05	2.00	61
4	1.67	9.40	2.00	58
5	1.54	9.65	2.00	63
6	1.44	9.88	2.00	65
7	1.36	10.10	1.74	66
8	1.29	10.23	1.52	67
9	1.23	10.33	1.42	67
10	1.17	10.44	1.16	67
11	1.12	10.55	1.12	68
12	1.08	10.63	1.06	69
13	1.04	10.71	1.02	68
14	1.00	10.83	1.02	69
15	0.96	10.96	0.92	68
16	0.93	11.00	0.86	69
17	0.90	11.08	0.84	68
18	0.87	11.14	0.80	69
19	0.84	11.20	0.80	68
20	0.81	11.29	0.76	69
21	0.79	11.34	0.74	70
22	0.77	11.40	0.74	70
23	0.75	11.46	0.72	71
24	0.72	11.55	0.72	70
25	0.70	11.65	0.70	70
26	0.69	11.69	0.70	71
27*	0.67	11.75	0.74	70
28*	0.65	11.86	0.74	69
29*	0.64	11.90	0.76	71
30*	0.62	12.03	0.78	70
31*	0.60	12.15	0.84	71
32*	0.59	12.20	0.90	70
33*	0.57	12.34	0.98	67

PHOTOMULTIPLIER DETECTOR				
NO.	λ	DRUM	SLIT	ρ_s
27*	0.67	11.75	0.74	71
28*	0.65	11.86	0.74	70
29*	0.64	11.90	0.76	71
30*	0.62	12.03	0.78	72
31*	0.60	12.15	0.84	71
32*	0.59	12.20	0.90	70
33*	0.57	12.34	0.98	71
34	0.56	12.45	1.00	70
35	0.55	12.49	1.08	71
36	0.53	12.65	1.16	67
37	0.52	12.72	1.24	68
38	0.50	12.90	1.24	70
39	0.49	13.00	1.30	70
40	0.48	13.10	1.44	70
41	0.47	13.20	1.58	69
42	0.46	13.31	1.70	69
43	0.44	13.60	1.90	66
44	0.43	13.80	2.00	65
#45	0.41	14.20	2.00	58
#46	0.39	14.58	2.00	32
#47	0.37	15.08	2.00	06
#48	0.34	16.02	2.00	06

$$\alpha_{\text{solar}} = \left[\sum_{m=1}^{m=48} (1-\rho_m) + \dots + (1-\rho_m) \right] \div 48$$

$$\alpha_s = .360$$

* Overlap

Long Wavelength Filter In Beam

INTEGRATING SPHERE PROGRAMMED WORK SHEET

SAMPLE NO. 9

LEAD SULFIDE DETECTOR				
NO.	λ	DRUM	SLIT	ρ_s
1	2.45	7.48	2.00	38
2	2.05	8.58	2.00	52
3	1.82	9.05	2.00	49
4	1.67	9.40	2.00	48
5	1.54	9.65	2.00	53
6	1.44	9.88	2.00	53
7	1.36	10.10	1.74	53
8	1.29	10.23	1.52	54
9	1.23	10.33	1.42	54
10	1.17	10.44	1.16	54
11	1.12	10.55	1.12	55
12	1.08	10.63	1.06	55
13	1.04	10.71	1.02	55
14	1.00	10.83	1.02	55
15	0.96	10.96	0.92	55
16	0.93	11.00	0.86	55
17	0.90	11.08	0.84	55
18	0.87	11.14	0.80	55
19	0.84	11.20	0.80	56
20	0.81	11.29	0.76	56
21	0.79	11.34	0.74	56
22	0.77	11.40	0.74	56
23	0.75	11.46	0.72	57
24	0.72	11.55	0.72	57
25	0.70	11.65	0.70	56
26	0.69	11.69	0.70	56
27*	0.67	11.75	0.74	56
28*	0.65	11.86	0.74	56
29*	0.64	11.90	0.76	56
30*	0.62	12.03	0.78	56
31*	0.60	12.15	0.84	55
32*	0.59	12.20	0.90	55
33*	0.57	12.34	0.98	55

PHOTOMULTIPLIER DETECTOR				
NO.	λ	DRUM	SLIT	ρ_s
27*	0.67	11.75	0.74	57
28*	0.65	11.86	0.74	56
29*	0.64	11.90	0.76	56
30*	0.62	12.03	0.78	55
31*	0.60	12.15	0.84	56
32*	0.59	12.20	0.90	55
33*	0.57	12.34	0.98	55
34	0.56	12.45	1.00	55
35	0.55	12.49	1.08	55
36	0.53	12.65	1.16	55
37	0.52	12.72	1.24	54
38	0.50	12.90	1.24	54
39	0.49	13.00	1.30	54
40	0.48	13.10	1.44	52
41	0.47	13.20	1.58	52
42	0.46	13.31	1.70	51
43	0.44	13.60	1.90	51
44	0.43	13.80	2.00	49
#45	0.41	14.20	2.00	42
#46	0.39	14.58	2.00	24
#47	0.37	15.08	2.00	07
#48	0.34	16.02	2.00	05

$$\alpha_{\text{solar}} = \left[\sum_{m=1}^{m=48} (1-\rho_m) + \dots + (1-\rho_m) \right] : 48$$

$$\alpha_s = .490$$

* Overlap

Long Wavelength Filter In Beam

INTEGRATING SPHERE PROGRAMMED WORK SHEET

SAMPLE NO. 14

LEAD SULFIDE DETECTOR				
NO.	λ	DRUM	SLIT	ρ_s
1	2.45	7.48	2.00	33
2	2.05	8.58	2.00	47
3	1.82	9.05	2.00	41
4	1.67	9.40	2.00	39
5	1.54	9.65	2.00	42
6	1.44	9.88	2.00	42
7	1.36	10.10	1.74	42
8	1.29	10.23	1.52	42
9	1.23	10.33	1.42	42
10	1.17	10.44	1.16	42
11	1.12	10.55	1.12	43
12	1.08	10.63	1.06	43
13	1.04	10.71	1.02	42
14	1.00	10.83	1.02	42
15	0.96	10.96	0.92	42
16	0.93	11.00	0.86	42
17	0.90	11.08	0.84	43
18	0.87	11.14	0.80	43
19	0.84	11.20	0.80	44
20	0.81	11.29	0.76	43
21	0.79	11.34	0.74	44
22	0.77	11.40	0.74	43
23	0.75	11.46	0.72	43
24	0.72	11.55	0.72	43
25	0.70	11.65	0.70	43
26	0.69	11.69	0.70	43
27*	0.67	11.75	0.74	43
28*	0.65	11.86	0.74	42
29*	0.64	11.90	0.76	43
30*	0.62	12.03	0.78	42
31*	0.60	12.15	0.84	42
32*	0.59	12.20	0.90	42
33*	0.57	12.34	0.98	42

PHOTOMULTIPLIER DETECTOR				
NO.	λ	DRUM	SLIT	ρ_s
27*	0.67	11.75	0.74	43
28*	0.65	11.86	0.74	43
29*	0.64	11.90	0.76	43
30*	0.62	12.03	0.78	41
31*	0.60	12.15	0.84	42
32*	0.59	12.20	0.90	42
33*	0.57	12.34	0.98	42
34	0.56	12.45	1.00	42
35	0.55	12.49	1.08	43
36	0.53	12.65	1.16	41
37	0.52	12.72	1.24	41
38	0.50	12.90	1.24	41
39	0.49	13.00	1.30	41
40	0.48	13.10	1.44	40
41	0.47	13.20	1.58	39
42	0.46	13.31	1.70	40
43	0.44	13.60	1.90	38
44	0.43	13.80	2.00	38
#45	0.41	14.20	2.00	33
#46	0.39	14.58	2.00	21
#47	0.37	15.08	2.00	08
#48	0.34	16.02	2.00	02

$$\alpha_{\text{solar}} = \left[\sum_{m=1}^{m=48} (1-\rho_m) + \dots + (1-\rho_{m=48}^m) \right] \div 48$$

$$\alpha_s = .603$$

* Overlap

Long Wavelength Filter In Beam

INTEGRATING SPHERE PROGRAMMED WORK SHEET

SAMPLE NO. 14

LEAD SULFIDE DETECTOR				
NO.	λ	DRUM	SLIT	ρ_s
1	2.45	7.48	2.00	46
2	2.05	8.58	2.00	65
3	1.82	9.05	2.00	64
4	1.67	9.40	2.00	61
5	1.54	9.65	2.00	66
6	1.44	9.88	2.00	68
7	1.36	10.10	1.74	68
8	1.29	10.23	1.52	70
9	1.23	10.33	1.42	70
10	1.17	10.44	1.16	69
11	1.12	10.55	1.12	70
12	1.08	10.63	1.06	71
13	1.04	10.71	1.02	72
14	1.00	10.83	1.02	71
15	0.96	10.96	0.92	72
16	0.93	11.00	0.86	72
17	0.90	11.08	0.84	73
18	0.87	11.14	0.80	73
19	0.84	11.20	0.80	74
20	0.81	11.29	0.76	73
21	0.79	11.34	0.74	73
22	0.77	11.40	0.74	74
23	0.75	11.46	0.72	74
24	0.72	11.55	0.72	75
25	0.70	11.65	0.70	75
26	0.69	11.69	0.70	75
27*	0.67	11.75	0.74	74
28*	0.65	11.86	0.74	75
29*	0.64	11.90	0.76	73
30*	0.62	12.03	0.78	73
31*	0.60	12.15	0.84	72
32*	0.59	12.20	0.90	75
33*	0.57	12.34	0.98	74

PHOTOMULTIPLIER DETECTOR				
NO.	λ	DRUM	SLIT	ρ_s
27*	0.67	11.75	0.74	75
28*	0.65	11.86	0.74	75
29*	0.64	11.90	0.76	75
30*	0.62	12.03	0.78	75
31*	0.60	12.15	0.84	74
32*	0.59	12.20	0.90	75
33*	0.57	12.34	0.98	76
34	0.56	12.45	1.00	77
35	0.55	12.49	1.08	76
36	0.53	12.65	1.16	76
37	0.52	12.72	1.24	75
38	0.50	12.90	1.24	75
39	0.49	13.00	1.30	74
40	0.48	13.10	1.44	74
41	0.47	13.20	1.58	73
42	0.46	13.31	1.70	73
43	0.44	13.60	1.90	72
44	0.43	13.80	2.00	69
#45	0.41	14.20	2.00	61
#46	0.39	14.58	2.00	34
#47	0.37	15.08	2.00	07
#48	0.34	16.02	2.00	05

$$\alpha_{\text{solar}} = \left[\sum_{m=1}^{m=48} (1-\rho_m) + \dots + (1-\rho_m) \right]_{m=48} = 48$$

$$\alpha_s = .321$$

* Overlap

Long Wavelength Filter In Beam

INTEGRATING SPHERE PROGRAMMED WORK SHEET

SAMPLE NO. 15

LEAD SULFIDE DETECTOR				
NO.	λ	DRUM	SLIT	ρ_s
1	2.45	7.48	2.00	30
2	2.05	8.58	2.00	40
3	1.82	9.05	2.00	39
4	1.67	9.40	2.00	37
5	1.54	9.65	2.00	40
6	1.44	9.88	2.00	40
7	1.36	10.10	1.74	40
8	1.29	10.23	1.52	41
9	1.23	10.33	1.42	41
10	1.17	10.44	1.16	40
11	1.12	10.55	1.12	41
12	1.08	10.63	1.06	41
13	1.04	10.71	1.02	41
14	1.00	10.83	1.02	41
15	0.96	10.96	0.92	41
16	0.93	11.00	0.86	41
17	0.90	11.08	0.84	42
18	0.87	11.14	0.80	41
19	0.84	11.20	0.80	43
20	0.81	11.29	0.76	42
21	0.79	11.34	0.74	43
22	0.77	11.40	0.74	42
23	0.75	11.46	0.72	43
24	0.72	11.55	0.72	42
25	0.70	11.65	0.70	43
26	0.69	11.69	0.70	43
27*	0.67	11.75	0.74	43
28*	0.65	11.86	0.74	42
29*	0.64	11.90	0.76	43
30*	0.62	12.03	0.78	43
31*	0.60	12.15	0.84	43
32*	0.59	12.20	0.90	42
33*	0.57	12.34	0.98	42

PHOTOMULTIPLIER DETECTOR				
NO.	λ	DRUM	SLIT	ρ_s
27*	0.67	11.75	0.74	42
28*	0.65	11.86	0.74	42
29*	0.64	11.90	0.76	42
30*	0.62	12.03	0.78	41
31*	0.60	12.15	0.84	41
32*	0.59	12.20	0.90	41
33*	0.57	12.34	0.98	41
34	0.56	12.45	1.00	41
35	0.55	12.49	1.08	41
36	0.53	12.65	1.16	41
37	0.52	12.72	1.24	40
38	0.50	12.90	1.24	40
39	0.49	13.00	1.30	40
40	0.48	13.10	1.44	39
41	0.47	13.20	1.58	39
42	0.46	13.31	1.70	38
43	0.44	13.60	1.90	38
44	0.43	13.80	2.00	36
#45	0.41	14.20	2.00	33
#46	0.39	14.58	2.00	20
#47	0.37	15.08	2.00	09
#48	0.34	16.02	2.00	07

$$\alpha_{\text{solar}} = \left[\sum_{m=1}^{m=48} (1-\rho_m) + \dots + (1-\rho_{\frac{m}{48}}) \right] \div 48$$

$$\alpha_s = .625$$

* Overlap

Long Wavelength Filter In Beam

INTEGRATING SPHERE PROGRAMMED WORK SHEET

SAMPLE NO. 15

LEAD SULFIDE DETECTOR				
NO.	λ	DRUM	SLIT	ρ_s
1	2.45	7.48	2.00	45
2	2.05	8.58	2.00	69
3	1.82	9.05	2.00	68
4	1.67	9.40	2.00	65
5	1.54	9.65	2.00	73
6	1.44	9.88	2.00	73
7	1.36	10.10	1.74	75
8	1.29	10.23	1.52	76
9	1.23	10.33	1.42	76
10	1.17	10.44	1.16	76
11	1.12	10.55	1.12	78
12	1.08	10.63	1.06	79
13	1.04	10.71	1.02	79
14	1.00	10.83	1.02	79
15	0.96	10.96	0.92	79
16	0.93	11.00	0.86	79
17	0.90	11.08	0.84	80
18	0.87	11.14	0.80	81
19	0.84	11.20	0.80	82
20	0.81	11.29	0.76	82
21	0.79	11.34	0.74	82
22	0.77	11.40	0.74	84
23	0.75	11.46	0.72	83
24	0.72	11.55	0.72	83
25	0.70	11.65	0.70	83
26	0.69	11.69	0.70	84
27*	0.67	11.75	0.74	83
28*	0.65	11.86	0.74	83
29*	0.64	11.90	0.76	82
30*	0.62	12.03	0.78	84
31*	0.60	12.15	0.84	84
32*	0.59	12.20	0.90	83
33*	0.57	12.34	0.98	84

PHOTOMULTIPLIER DETECTOR				
NO.	λ	DRUM	SLIT	ρ_s
27*	0.67	11.75	0.74	83
28*	0.65	11.86	0.74	84
29*	0.64	11.90	0.76	84
30*	0.62	12.03	0.78	86
31*	0.60	12.15	0.84	84
32*	0.59	12.20	0.90	84
33*	0.57	12.34	0.98	84
34	0.56	12.45	1.00	87
35	0.55	12.49	1.08	85
36	0.53	12.65	1.16	84
37	0.52	12.72	1.24	84
38	0.50	12.90	1.24	84
39	0.49	13.00	1.30	85
40	0.48	13.10	1.44	84
41	0.47	13.20	1.58	83
42	0.46	13.31	1.70	84
43	0.44	13.60	1.90	81
44	0.43	13.80	2.00	78
#45	0.41	14.20	2.00	70
#46	0.39	14.58	2.00	36
#47	0.37	15.08	2.00	06
#48	0.34	16.02	2.00	04

$$\alpha_{\text{solar}} = \left[\sum_{m=1}^{m=48} (1-\rho_m) + \dots + (1-\rho_m) \right] \div 48$$

$$\alpha_s = .246$$

* Overlap

Long Wavelength Filter In Beam

INTEGRATING SPHERE PROGRAMMED WORK SHEET

SAMPLE NO. 16

LEAD SULFIDE DETECTOR				
NO.	λ	DRUM	SLIT	ρ_s
1	2.45	7.48	2.00	19
2	2.05	8.58	2.00	21
3	1.82	9.05	2.00	21
4	1.67	9.40	2.00	20
5	1.54	9.65	2.00	21
6	1.44	9.88	2.00	20
7	1.36	10.10	1.74	21
8	1.29	10.23	1.52	21
9	1.23	10.33	1.42	21
10	1.17	10.44	1.16	21
11	1.12	10.55	1.12	22
12	1.08	10.63	1.06	21
13	1.04	10.71	1.02	22
14	1.00	10.83	1.02	22
15	0.96	10.96	0.92	22
16	0.93	11.00	0.86	22
17	0.90	11.08	0.84	22
18	0.87	11.14	0.80	22
19	0.84	11.20	0.80	23
20	0.81	11.29	0.76	23
21	0.79	11.34	0.74	23
22	0.77	11.40	0.74	23
23	0.75	11.46	0.72	23
24	0.72	11.55	0.72	23
25	0.70	11.65	0.70	23
26	0.69	11.69	0.70	22
27*	0.67	11.75	0.74	22
28*	0.65	11.86	0.74	22
29*	0.64	11.90	0.76	22
30*	0.62	12.03	0.78	22
31*	0.60	12.15	0.84	22
32*	0.59	12.20	0.90	22
33*	0.57	12.34	0.98	22

PHOTOMULTIPLIER DETECTOR				
NO.	λ	DRUM	SLIT	ρ_s
27*	0.67	11.75	0.74	22
28*	0.65	11.86	0.74	22
29*	0.64	11.90	0.76	22
30*	0.62	12.03	0.78	22
31*	0.60	12.15	0.84	22
32*	0.59	12.20	0.90	22
33*	0.57	12.34	0.98	21
34	0.56	12.45	1.00	21
35	0.55	12.49	1.08	21
36	0.53	12.65	1.16	21
37	0.52	12.72	1.24	21
38	0.50	12.90	1.24	21
39	0.49	13.00	1.30	20
40	0.48	13.10	1.44	20
41	0.47	13.20	1.58	20
42	0.46	13.31	1.70	20
43	0.44	13.60	1.90	19
44	0.43	13.80	2.00	19
#45	0.41	14.20	2.00	17
#46	0.39	14.58	2.00	13
#47	0.37	15.08	2.00	09
#48	0.34	16.02	2.00	08

$$\alpha_{\text{solar}} = \left[\sum_{m=1}^{m=48} (1-\rho_m) + \dots + (1-\rho_{m=48}) \right] : 48$$

$$\alpha_s = .795$$

* Overlap

Long Wavelength Filter In Beam

INTEGRATING SPHERE PROGRAMMED WORK SHEET

SAMPLE NO. 19

LEAD SULFIDE DETECTOR				
NO.	λ	DRUM	SLIT	ρ_s
1	2.45	7.48	2.00	26
2	2.05	8.58	2.00	35
3	1.82	9.05	2.00	35
4	1.67	9.40	2.00	34
5	1.54	9.65	2.00	37
6	1.44	9.88	2.00	37
7	1.36	10.10	1.74	37
8	1.29	10.23	1.52	37
9	1.23	10.33	1.42	38
10	1.17	10.44	1.16	38
11	1.12	10.55	1.12	39
12	1.08	10.63	1.06	39
13	1.04	10.71	1.02	39
14	1.00	10.83	1.02	40
15	0.96	10.96	0.92	40
16	0.93	11.00	0.86	40
17	0.90	11.08	0.84	41
18	0.87	11.14	0.80	40
19	0.84	11.20	0.80	41
20	0.81	11.29	0.76	41
21	0.79	11.34	0.74	41
22	0.77	11.40	0.74	41
23	0.75	11.46	0.72	41
24	0.72	11.55	0.72	41
25	0.70	11.65	0.70	41
26	0.69	11.69	0.70	43
27*	0.67	11.75	0.74	42
28*	0.65	11.86	0.74	42
29*	0.64	11.90	0.76	41
30*	0.62	12.03	0.78	42
31*	0.60	12.15	0.84	41
32*	0.59	12.20	0.90	41
33*	0.57	12.34	0.98	43

PHOTOMULTIPLIER DETECTOR				
NO.	λ	DRUM	SLIT	ρ_s
27*	0.67	11.75	0.74	42
28*	0.65	11.86	0.74	41
29*	0.64	11.90	0.76	42
30*	0.62	12.03	0.78	42
31*	0.60	12.15	0.84	42
32*	0.59	12.20	0.90	42
33*	0.57	12.34	0.98	42
34	0.56	12.45	1.00	42
35	0.55	12.49	1.08	43
36	0.53	12.65	1.16	42
37	0.52	12.72	1.24	42
38	0.50	12.90	1.24	41
39	0.49	13.00	1.30	41
40	0.48	13.10	1.44	40
41	0.47	13.20	1.58	40
42	0.46	13.31	1.70	40
43	0.44	13.60	1.90	40
44	0.43	13.80	2.00	39
#45	0.41	14.20	2.00	36
#46	0.39	14.58	2.00	20
#47	0.37	15.08	2.00	09
#48	0.34	16.02	2.00	06

$$\alpha_{\text{solar}} = \left[\sum_{m=1}^{m=48} (1-\rho_m) + \dots + (1-\rho_{\frac{m}{48}}) \right] \div 48$$

$$\alpha_s = .614$$

* Overlap

Long Wavelength Filter In Beam

INTEGRATING SPHERE PROGRAMMED WORK SHEET

SAMPLE NO. 20

LEAD SULFIDE DETECTOR				
NO.	λ	DRUM	SLIT	ρ_s
1	2.45	7.48	2.00	19
2	2.05	8.58	2.00	22
3	1.82	9.05	2.00	22
4	1.67	9.40	2.00	20
5	1.54	9.65	2.00	22
6	1.44	9.88	2.00	22
7	1.36	10.10	1.74	22
8	1.29	10.23	1.52	22
9	1.23	10.33	1.42	22
10	1.17	10.44	1.16	23
11	1.12	10.55	1.12	23
12	1.08	10.63	1.06	24
13	1.04	10.71	1.02	23
14	1.00	10.83	1.02	23
15	0.96	10.96	0.92	23
16	0.93	11.00	0.86	23
17	0.90	11.08	0.84	24
18	0.87	11.14	0.80	24
19	0.84	11.20	0.80	24
20	0.81	11.29	0.76	24
21	0.79	11.34	0.74	24
22	0.77	11.40	0.74	24
23	0.75	11.46	0.72	24
24	0.72	11.55	0.72	24
25	0.70	11.65	0.70	25
26	0.69	11.69	0.70	25
27*	0.67	11.75	0.74	25
28*	0.65	11.86	0.74	25
29*	0.64	11.90	0.76	24
30*	0.62	12.03	0.78	25
31*	0.60	12.15	0.84	24
32*	0.59	12.20	0.90	23
33*	0.57	12.34	0.98	24

PHOTOMULTIPLIER DETECTOR				
NO.	λ	DRUM	SLIT	ρ_s
27*	0.67	11.75	0.74	24
28*	0.65	11.86	0.74	24
29*	0.64	11.90	0.76	24
30*	0.62	12.03	0.78	24
31*	0.60	12.15	0.84	23
32*	0.59	12.20	0.90	23
33*	0.57	12.34	0.98	24
34	0.56	12.45	1.00	23
35	0.55	12.49	1.08	24
36	0.53	12.65	1.16	23
37	0.52	12.72	1.24	23
38	0.50	12.90	1.24	23
39	0.49	13.00	1.30	22
40	0.48	13.10	1.44	22
41	0.47	13.20	1.58	22
42	0.46	13.31	1.70	22
43	0.44	13.60	1.90	21
44	0.43	13.80	2.00	22
#45	0.41	14.20	2.00	20
#46	0.39	14.58	2.00	15
#47	0.37	15.08	2.00	10
#48	0.34	16.02	2.00	09

$$\alpha_{\text{solar}} = \left[\sum_{m=1}^{m=48} (1-\rho_m) + \dots + (1-\rho_m) \right] \div 48$$

$$\alpha_s = .778$$

* Overlap

Long Wavelength Filter In Beam

INTEGRATING SPHERE PROGRAMMED WORK SHEET

SAMPLE NO. 21

LEAD SULFIDE DETECTOR				
NO.	λ	DRUM	SLIT	ρ_s
1	2.45	7.48	2.00	26
2	2.05	8.58	2.00	32
3	1.82	9.05	2.00	32
4	1.67	9.40	2.00	30
5	1.54	9.65	2.00	32
6	1.44	9.88	2.00	32
7	1.36	10.10	1.74	32
8	1.29	10.23	1.52	32
9	1.23	10.33	1.42	32
10	1.17	10.44	1.16	32
11	1.12	10.55	1.12	32
12	1.08	10.63	1.06	32
13	1.04	10.71	1.02	32
14	1.00	10.83	1.02	32
15	0.96	10.96	0.92	31
16	0.93	11.00	0.86	32
17	0.90	11.08	0.84	31
18	0.87	11.14	0.80	32
19	0.84	11.20	0.80	32
20	0.81	11.29	0.76	31
21	0.79	11.34	0.74	32
22	0.77	11.40	0.74	32
23	0.75	11.46	0.72	31
24	0.72	11.55	0.72	33
25	0.70	11.65	0.70	32
26	0.69	11.69	0.70	31
27*	0.67	11.75	0.74	32
28*	0.65	11.86	0.74	31
29*	0.64	11.90	0.76	32
30*	0.62	12.03	0.78	31
31*	0.60	12.15	0.84	30
32*	0.59	12.20	0.90	31
33*	0.57	12.34	0.98	29

PHOTOMULTIPLIER DETECTOR				
NO.	λ	DRUM	SLIT	ρ_s
27*	0.67	11.75	0.74	31
28*	0.65	11.86	0.74	31
29*	0.64	11.90	0.76	31
30*	0.62	12.03	0.78	30
31*	0.60	12.15	0.84	30
32*	0.59	12.20	0.90	31
33*	0.57	12.34	0.98	30
34	0.56	12.45	1.00	30
35	0.55	12.49	1.08	30
36	0.53	12.65	1.16	30
37	0.52	12.72	1.24	29
38	0.50	12.90	1.24	28
39	0.49	13.00	1.30	28
40	0.48	13.10	1.44	28
41	0.47	13.20	1.58	27
42	0.46	13.31	1.70	27
43	0.44	13.60	1.90	26
44	0.43	13.80	2.00	26
#45	0.41	14.20	2.00	23
#46	0.39	14.58	2.00	16
#47	0.37	15.08	2.00	10
#48	0.34	16.02	2.00	09

$$\alpha_{\text{solar}} = \left[\sum_{m=1}^{m=48} (1-\rho_m) + \dots + (1-\rho_m) \right] \div 48$$

$$\alpha_s = .707$$

* Overlap

Long Wavelength Filter In Beam

INTEGRATING SPHERE PROGRAMMED WORK SHEET

SAMPLE NO. 21

LEAD SULFIDE DETECTOR				
NO.	λ	DRUM	SLIT	ρ_s
1	2.45	7.48	2.00	44
2	2.05	8.58	2.00	64
3	1.82	9.05	2.00	63
4	1.67	9.40	2.00	60
5	1.54	9.65	2.00	67
6	1.44	9.88	2.00	68
7	1.36	10.10	1.74	68
8	1.29	10.23	1.52	70
9	1.23	10.33	1.42	70
10	1.17	10.44	1.16	69
11	1.12	10.55	1.12	71
12	1.08	10.63	1.06	72
13	1.04	10.71	1.02	72
14	1.00	10.83	1.02	71
15	0.96	10.96	0.92	71
16	0.93	11.00	0.86	72
17	0.90	11.08	0.84	73
18	0.87	11.14	0.80	73
19	0.84	11.20	0.80	74
20	0.81	11.29	0.76	73
21	0.79	11.34	0.74	73
22	0.77	11.40	0.74	72
23	0.75	11.46	0.72	75
24	0.72	11.55	0.72	76
25	0.70	11.65	0.70	75
26	0.69	11.69	0.70	75
27*	0.67	11.75	0.74	74
28*	0.65	11.86	0.74	75
29*	0.64	11.90	0.76	72
30*	0.62	12.03	0.78	73
31*	0.60	12.15	0.84	73
32*	0.59	12.20	0.90	75
33*	0.57	12.34	0.98	73

PHOTOMULTIPLIER DETECTOR				
NO.	λ	DRUM	SLIT	ρ_s
27*	0.67	11.75	0.74	74
28*	0.65	11.86	0.74	74
29*	0.64	11.90	0.76	75
30*	0.62	12.03	0.78	74
31*	0.60	12.15	0.84	73
32*	0.59	12.20	0.90	74
33*	0.57	12.34	0.98	75
34	0.56	12.45	1.00	75
35	0.55	12.49	1.08	75
36	0.53	12.65	1.16	74
37	0.52	12.72	1.24	74
38	0.50	12.90	1.24	73
39	0.49	13.00	1.30	73
40	0.48	13.10	1.44	71
41	0.47	13.20	1.58	71
42	0.46	13.31	1.70	70
43	0.44	13.60	1.90	68
44	0.43	13.80	2.00	66
#45	0.41	14.20	2.00	58
#46	0.39	14.58	2.00	32
#47	0.37	15.08	2.00	07
#48	0.34	16.02	2.00	05

$$\alpha_{\text{solar}} = \left[\sum_{m=1}^{m=48} (1-\rho_m) + \dots + (1-\rho_{m=48}) \right] \div 48$$

$$\alpha_s = .330$$

* Overlap

Long Wavelength Filter In Beam

INTEGRATING SPHERE PROGRAMMED WORK SHEET

SAMPLE NO. 22

LEAD SULFIDE DETECTOR				
NO.	λ	DRUM	SLIT	ρ_s
1	2.45	7.48	2.00	15
2	2.05	8.58	2.00	16
3	1.82	9.05	2.00	16
4	1.67	9.40	2.00	16
5	1.54	9.65	2.00	16
6	1.44	9.88	2.00	16
7	1.36	10.10	1.74	15
8	1.29	10.23	1.52	15
9	1.23	10.33	1.42	16
10	1.17	10.44	1.16	15
11	1.12	10.55	1.12	16
12	1.08	10.63	1.06	15
13	1.04	10.71	1.02	16
14	1.00	10.83	1.02	15
15	0.96	10.96	0.92	16
16	0.93	11.00	0.86	16
17	0.90	11.08	0.84	16
18	0.87	11.14	0.80	16
19	0.84	11.20	0.80	17
20	0.81	11.29	0.76	16
21	0.79	11.34	0.74	16
22	0.77	11.40	0.74	16
23	0.75	11.46	0.72	16
24	0.72	11.55	0.72	16
25	0.70	11.65	0.70	16
26	0.69	11.69	0.70	16
27*	0.67	11.75	0.74	16
28*	0.65	11.86	0.74	16
29*	0.64	11.90	0.76	16
30*	0.62	12.03	0.78	16
31*	0.60	12.15	0.84	16
32*	0.59	12.20	0.90	16
33*	0.57	12.34	0.98	16

PHOTOMULTIPLIER DETECTOR				
NO.	λ	DRUM	SLIT	ρ_s
27*	0.67	11.75	0.74	15
28*	0.65	11.86	0.74	16
29*	0.64	11.90	0.76	16
30*	0.62	12.03	0.78	16
31*	0.60	12.15	0.84	16
32*	0.59	12.20	0.90	16
33*	0.57	12.34	0.98	16
34	0.56	12.45	1.00	16
35	0.55	12.49	1.08	15
36	0.53	12.65	1.16	15
37	0.52	12.72	1.24	15
38	0.50	12.90	1.24	15
39	0.49	13.00	1.30	14
40	0.48	13.10	1.44	14
41	0.47	13.20	1.58	14
42	0.46	13.31	1.70	13
43	0.44	13.60	1.90	13
44	0.43	13.80	2.00	13
#45	0.41	14.20	2.00	12
#46	0.39	14.58	2.00	12
#47	0.37	15.08	2.00	10
#48	0.34	16.02	2.00	10

$$\alpha_{\text{solar}} = \left[\sum_{m=1}^{m=48} (1-\rho_m) + \dots + (1-\rho_m) \right] \div 48$$

$$\alpha_s = .848$$

* Overlap

Long Wavelength Filter In Beam

INTEGRATING SPHERE PROGRAMMED WORK SHEET

SAMPLE NO. 29

LEAD SULFIDE DETECTOR				
NO.	λ	DRUM	SLIT	ρ_s
1	2.45	7.48	2.00	47
2	2.05	8.58	2.00	70
3	1.82	9.05	2.00	69
4	1.67	9.40	2.00	66
5	1.54	9.65	2.00	74
6	1.44	9.88	2.00	75
7	1.36	10.10	1.74	76
8	1.29	10.23	1.52	78
9	1.23	10.33	1.42	79
10	1.17	10.44	1.16	79
11	1.12	10.55	1.12	80
12	1.08	10.63	1.06	82
13	1.04	10.71	1.02	82
14	1.00	10.83	1.02	83
15	0.96	10.96	0.92	84
16	0.93	11.00	0.86	83
17	0.90	11.08	0.84	84
18	0.87	11.14	0.80	86
19	0.84	11.20	0.80	85
20	0.81	11.29	0.76	85
21	0.79	11.34	0.74	86
22	0.77	11.40	0.74	87
23	0.75	11.46	0.72	87
24	0.72	11.55	0.72	88
25	0.70	11.65	0.70	88
26	0.69	11.69	0.70	88
27*	0.67	11.75	0.74	89
28*	0.65	11.86	0.74	88
29*	0.64	11.90	0.76	89
30*	0.62	12.03	0.78	88
31*	0.60	12.15	0.84	88
32*	0.59	12.20	0.90	91
33*	0.57	12.34	0.98	89

PHOTOMULTIPLIER DETECTOR				
NO.	λ	DRUM	SLIT	ρ_s
27*	0.67	11.75	0.74	88
28*	0.65	11.86	0.74	88
29*	0.64	11.90	0.76	89
30*	0.62	12.03	0.78	89
31*	0.60	12.15	0.84	89
32*	0.59	12.20	0.90	91
33*	0.57	12.34	0.98	91
34	0.56	12.45	1.00	90
35	0.55	12.49	1.08	90
36	0.53	12.65	1.16	92
37	0.52	12.72	1.24	92
38	0.50	12.90	1.24	92
39	0.49	13.00	1.30	92
40	0.48	13.10	1.44	94
41	0.47	13.20	1.58	94
42	0.46	13.31	1.70	93
43	0.44	13.60	1.90	91
44	0.43	13.80	2.00	90
#45	0.41	14.20	2.00	78
#46	0.39	14.58	2.00	40
#47	0.37	15.08	2.00	05
#48	0.34	16.02	2.00	04

$$\alpha_{\text{solar}} = \left[\sum_{m=1}^{m=48} (1-\rho_m) + \dots + (1-\rho_{m=48}) \right] \div 48$$

$$\alpha_s = .201$$

* Overlap

Long Wavelength Filter In Beam

INTEGRATING SPHERE PROGRAMMED WORK SHEET

SAMPLE NO. 30

LEAD SULFIDE DETECTOR				
NO.	λ	DRUM	SLIT	ρ_s
1	2.45	7.48	2.00	42
2	2.05	8.58	2.00	60
3	1.82	9.05	2.00	59
4	1.67	9.40	2.00	56
5	1.54	9.65	2.00	62
6	1.44	9.88	2.00	63
7	1.36	10.10	1.74	63
8	1.29	10.23	1.52	65
9	1.23	10.33	1.42	65
10	1.17	10.44	1.16	64
11	1.12	10.55	1.12	66
12	1.08	10.63	1.06	66
13	1.04	10.71	1.02	66
14	1.00	10.83	1.02	66
15	0.96	10.96	0.92	67
16	0.93	11.00	0.86	67
17	0.90	11.08	0.84	66
18	0.87	11.14	0.80	68
19	0.84	11.20	0.80	68
20	0.81	11.29	0.76	68
21	0.79	11.34	0.74	67
22	0.77	11.40	0.74	67
23	0.75	11.46	0.72	68
24	0.72	11.55	0.72	68
25	0.70	11.65	0.70	68
26	0.69	11.69	0.70	68
27*	0.67	11.75	0.74	69
28*	0.65	11.86	0.74	67
29*	0.64	11.90	0.76	67
30*	0.62	12.03	0.78	66
31*	0.60	12.15	0.84	67
32*	0.59	12.20	0.90	68
33*	0.57	12.34	0.98	67

PHOTOMULTIPLIER DETECTOR				
NO.	λ	DRUM	SLIT	ρ_s
27*	0.67	11.75	0.74	67
28*	0.65	11.86	0.74	68
29*	0.64	11.90	0.76	67
30*	0.62	12.03	0.78	67
31*	0.60	12.15	0.84	67
32*	0.59	12.20	0.90	66
33*	0.57	12.34	0.98	66
34	0.56	12.45	1.00	66
35	0.55	12.49	1.08	65
36	0.53	12.65	1.16	65
37	0.52	12.72	1.24	65
38	0.50	12.90	1.24	66
39	0.49	13.00	1.30	65
40	0.48	13.10	1.44	65
41	0.47	13.20	1.58	64
42	0.46	13.31	1.70	63
43	0.44	13.60	1.90	61
44	0.43	13.80	2.00	60
#45	0.41	14.20	2.00	50
#46	0.39	14.58	2.00	29
#47	0.37	15.08	2.00	07
#48	0.34	16.02	2.00	05

$$\alpha_{\text{solar}} = \left[\sum_{m=1}^{m=48} (1-\rho_m) + \dots + (1-\rho_{\frac{m}{8}}) \right] \div 48$$

$$\alpha_s = .387$$

* Overlap

Long Wavelength Filter In Beam

INTEGRATING SPHERE PROGRAMMED WORK SHEET

SAMPLE NO. 31

LEAD SULFIDE DETECTOR				
NO.	λ	DRUM	SLIT	ρ_s
1	2.45	7.48	2.00	47
2	2.05	8.58	2.00	66
3	1.82	9.05	2.00	65
4	1.67	9.40	2.00	63
5	1.54	9.65	2.00	68
6	1.44	9.88	2.00	69
7	1.36	10.10	1.74	70
8	1.29	10.23	1.52	72
9	1.23	10.33	1.42	72
10	1.17	10.44	1.16	72
11	1.12	10.55	1.12	73
12	1.08	10.63	1.06	74
13	1.04	10.71	1.02	75
14	1.00	10.83	1.02	74
15	0.96	10.96	0.92	75
16	0.93	11.00	0.86	75
17	0.90	11.08	0.84	76
18	0.87	11.14	0.80	77
19	0.84	11.20	0.80	77
20	0.81	11.29	0.76	78
21	0.79	11.34	0.74	76
22	0.77	11.40	0.74	77
23	0.75	11.46	0.72	78
24	0.72	11.55	0.72	79
25	0.70	11.65	0.70	80
26	0.69	11.69	0.70	80
27*	0.67	11.75	0.74	80
28*	0.65	11.86	0.74	79
29*	0.64	11.90	0.76	80
30*	0.62	12.03	0.78	80
31*	0.60	12.15	0.84	81
32*	0.59	12.20	0.90	80
33*	0.57	12.34	0.98	80

PHOTOMULTIPLIER DETECTOR				
NO.	λ	DRUM	SLIT	ρ_s
27*	0.67	11.75	0.74	79
28*	0.65	11.86	0.74	80
29*	0.64	11.90	0.76	80
30*	0.62	12.03	0.78	79
31*	0.60	12.15	0.84	80
32*	0.59	12.20	0.90	80
33*	0.57	12.34	0.98	80
34	0.56	12.45	1.00	80
35	0.55	12.49	1.08	80
36	0.53	12.65	1.16	80
37	0.52	12.72	1.24	79
38	0.50	12.90	1.24	82
39	0.49	13.00	1.30	81
40	0.48	13.10	1.44	81
41	0.47	13.20	1.58	81
42	0.46	13.31	1.70	80
43	0.44	13.60	1.90	78
44	0.43	13.80	2.00	77
#45	0.41	14.20	2.00	68
#46	0.39	14.58	2.00	36
#47	0.37	15.08	2.00	07
#48	0.34	16.02	2.00	05

$$\alpha_{\text{solar}} = \left[\sum_{m=1}^{m=48} (1-\rho_m) + \dots + (1-\rho_{m=48}) \right] \div 48$$

$$\alpha_s = .281$$

* Overlap

Long Wavelength Filter In Beam

INTEGRATING SPHERE PROGRAMMED WORK SHEET

SAMPLE NO. 32

LEAD SULFIDE DETECTOR				
NO.	λ	DRUM	SLIT	ρ_s
1	2.45	7.48	2.00	46
2	2.05	8.58	2.00	63
3	1.82	9.05	2.00	63
4	1.67	9.40	2.00	60
5	1.54	9.65	2.00	65
6	1.44	9.88	2.00	66
7	1.36	10.10	1.74	67
8	1.29	10.23	1.52	68
9	1.23	10.33	1.42	68
10	1.17	10.44	1.16	68
11	1.12	10.55	1.12	69
12	1.08	10.63	1.06	70
13	1.04	10.71	1.02	70
14	1.00	10.83	1.02	70
15	0.96	10.96	0.92	71
16	0.93	11.00	0.86	71
17	0.90	11.08	0.84	71
18	0.87	11.14	0.80	73
19	0.84	11.20	0.80	72
20	0.81	11.29	0.76	73
21	0.79	11.34	0.74	72
22	0.77	11.40	0.74	71
23	0.75	11.46	0.72	72
24	0.72	11.55	0.72	74
25	0.70	11.65	0.70	75
26	0.69	11.69	0.70	74
27*	0.67	11.75	0.74	74
28*	0.65	11.86	0.74	73
29*	0.64	11.90	0.76	73
30*	0.62	12.03	0.78	72
31*	0.60	12.15	0.84	72
32*	0.59	12.20	0.90	71
33*	0.57	12.34	0.98	72

PHOTOMULTIPLIER DETECTOR				
NO.	λ	DRUM	SLIT	ρ_s
27*	0.67	11.75	0.74	73
28*	0.65	11.86	0.74	74
29*	0.64	11.90	0.76	74
30*	0.62	12.03	0.78	74
31*	0.60	12.15	0.84	73
32*	0.59	12.20	0.90	75
33*	0.57	12.34	0.98	74
34	0.56	12.45	1.00	74
35	0.55	12.49	1.08	72
36	0.53	12.65	1.16	73
37	0.52	12.72	1.24	73
38	0.50	12.90	1.24	76
39	0.49	13.00	1.30	73
40	0.48	13.10	1.44	73
41	0.47	13.20	1.58	73
42	0.46	13.31	1.70	72
43	0.44	13.60	1.90	71
44	0.43	13.80	2.00	69
#45	0.41	14.20	2.00	60
#46	0.39	14.58	2.00	32
#47	0.37	15.08	2.00	06
#48	0.34	16.02	2.00	05

$$\alpha_{\text{solar}} = \left[\sum_{m=1}^{m=48} (1-\rho_m) + \dots + (1-\rho_m) \right] \div 48$$

$$\alpha_s = .333$$

* Overlap

Long Wavelength Filter In Beam

INTEGRATING SPHERE PROGRAMMED WORK SHEET

SAMPLE NO. 34

LEAD SULFIDE DETECTOR				
NO.	λ	DRUM	SLIT	ρ_s
1	2.45	7.48	2.00	46
2	2.05	8.58	2.00	67
3	1.82	9.05	2.00	68
4	1.67	9.40	2.00	63
5	1.54	9.65	2.00	70
6	1.44	9.88	2.00	71
7	1.36	10.10	1.74	72
8	1.29	10.23	1.52	73
9	1.23	10.33	1.42	74
10	1.17	10.44	1.16	73
11	1.12	10.55	1.12	75
12	1.08	10.63	1.06	75
13	1.04	10.71	1.02	76
14	1.00	10.83	1.02	76
15	0.96	10.96	0.92	77
16	0.93	11.00	0.86	76
17	0.90	11.08	0.84	77
18	0.87	11.14	0.80	78
19	0.84	11.20	0.80	78
20	0.81	11.29	0.76	78
21	0.79	11.34	0.74	79
22	0.77	11.40	0.74	78
23	0.75	11.46	0.72	79
24	0.72	11.55	0.72	78
25	0.70	11.65	0.70	78
26	0.69	11.69	0.70	79
27*	0.67	11.75	0.74	80
28*	0.65	11.86	0.74	80
29*	0.64	11.90	0.76	80
30*	0.62	12.03	0.78	80
31*	0.60	12.15	0.84	79
32*	0.59	12.20	0.90	81
33*	0.57	12.34	0.98	80

PHOTOMULTIPLIER DETECTOR				
NO.	λ	DRUM	SLIT	ρ_s
27*	0.67	11.75	0.74	79
28*	0.65	11.86	0.74	80
29*	0.64	11.90	0.76	79
30*	0.62	12.03	0.78	79
31*	0.60	12.15	0.84	80
32*	0.59	12.20	0.90	80
33*	0.57	12.34	0.98	80
34	0.56	12.45	1.00	80
35	0.55	12.49	1.08	80
36	0.53	12.65	1.16	78
37	0.52	12.72	1.24	78
38	0.50	12.90	1.24	80
39	0.49	13.00	1.30	78
40	0.48	13.10	1.44	78
41	0.47	13.20	1.58	78
42	0.46	13.31	1.70	77
43	0.44	13.60	1.90	76
44	0.43	13.80	2.00	74
#45	0.41	14.20	2.00	65
#46	0.39	14.58	2.00	36
#47	0.37	15.08	2.00	06
#48	0.34	16.02	2.00	05

$$\alpha_{\text{solar}} = \left[\sum_{m=1}^{m=48} (1-\rho_m) + \dots + (1-\rho_m) \right]_{m=48} = 48$$

$$\alpha_s = .283$$

* Overlap

Long Wavelength Filter In Beam

INTEGRATING SPHERE PROGRAMMED WORK SHEET

SAMPLE NO. 36

LEAD SULFIDE DETECTOR				
NO.	λ	DRUM	SLIT	ρ_s
1	2.45	7.48	2.00	46
2	2.05	8.58	2.00	68
3	1.82	9.05	2.00	68
4	1.67	9.40	2.00	64
5	1.54	9.65	2.00	71
6	1.44	9.88	2.00	72
7	1.36	10.10	1.74	74
8	1.29	10.23	1.52	75
9	1.23	10.33	1.42	76
10	1.17	10.44	1.16	75
11	1.12	10.55	1.12	76
12	1.08	10.63	1.06	77
13	1.04	10.71	1.02	78
14	1.00	10.83	1.02	78
15	0.96	10.96	0.92	79
16	0.93	11.00	0.86	79
17	0.90	11.08	0.84	80
18	0.87	11.14	0.80	79
19	0.84	11.20	0.80	80
20	0.81	11.29	0.76	80
21	0.79	11.34	0.74	81
22	0.77	11.40	0.74	81
23	0.75	11.46	0.72	82
24	0.72	11.55	0.72	81
25	0.70	11.65	0.70	83
26	0.69	11.69	0.70	82
27*	0.67	11.75	0.74	83
28*	0.65	11.86	0.74	82
29*	0.64	11.90	0.76	84
30*	0.62	12.03	0.78	83
31*	0.60	12.15	0.84	83
32*	0.59	12.20	0.90	83
33*	0.57	12.34	0.98	83

PHOTOMULTIPLIER DETECTOR				
NO.	λ	DRUM	SLIT	ρ_s
27*	0.67	11.75	0.74	84
28*	0.65	11.86	0.74	83
29*	0.64	11.90	0.76	83
30*	0.62	12.03	0.78	83
31*	0.60	12.15	0.84	83
32*	0.59	12.20	0.90	82
33*	0.57	12.34	0.98	85
34	0.56	12.45	1.00	86
35	0.55	12.49	1.08	84
36	0.53	12.65	1.16	85
37	0.52	12.72	1.24	83
38	0.50	12.90	1.24	84
39	0.49	13.00	1.30	86
40	0.48	13.10	1.44	86
41	0.47	13.20	1.58	85
42	0.46	13.31	1.70	83
43	0.44	13.60	1.90	83
44	0.43	13.80	2.00	82
#45	0.41	14.20	2.00	80
#46	0.39	14.58	2.00	37
#47	0.37	15.08	2.00	06
#48	0.34	16.02	2.00	05

$$\alpha_{\text{solar}} = \left[\sum_{m=1}^{m=48} (1-\rho_m) + \dots + (1-\rho_m) \right] \div 48$$

$$\alpha_s = .250$$

* Overlap

Long Wavelength Filter In Beam

INTEGRATING SPHERE PROGRAMMED WORK SHEET

SAMPLE NO. 38

LEAD SULFIDE DETECTOR				
NO.	λ	DRUM	SLIT	ρ_s
1	2.45	7.48	2.00	44
2	2.05	8.58	2.00	68
3	1.82	9.05	2.00	67
4	1.67	9.40	2.00	62
5	1.54	9.65	2.00	70
6	1.44	9.88	2.00	70
7	1.36	10.10	1.74	72
8	1.29	10.23	1.52	74
9	1.23	10.33	1.42	74
10	1.17	10.44	1.16	74
11	1.12	10.55	1.12	76
12	1.08	10.63	1.06	76
13	1.04	10.71	1.02	76
14	1.00	10.83	1.02	77
15	0.96	10.96	0.92	76
16	0.93	11.00	0.86	77
17	0.90	11.08	0.84	77
18	0.87	11.14	0.80	78
19	0.84	11.20	0.80	78
20	0.81	11.29	0.76	78
21	0.79	11.34	0.74	79
22	0.77	11.40	0.74	81
23	0.75	11.46	0.72	79
24	0.72	11.55	0.72	79
25	0.70	11.65	0.70	80
26	0.69	11.69	0.70	81
27*	0.67	11.75	0.74	81
28*	0.65	11.86	0.74	80
29*	0.64	11.90	0.76	80
30*	0.62	12.03	0.78	81
31*	0.60	12.15	0.84	78
32*	0.59	12.20	0.90	79
33*	0.57	12.34	0.98	79

PHOTOMULTIPLIER DETECTOR				
NO.	λ	DRUM	SLIT	ρ_s
27*	0.67	11.75	0.74	80
28*	0.65	11.86	0.74	80
29*	0.64	11.90	0.76	81
30*	0.62	12.03	0.78	80
31*	0.60	12.15	0.84	81
32*	0.59	12.20	0.90	80
33*	0.57	12.34	0.98	81
34	0.56	12.45	1.00	82
35	0.55	12.49	1.08	82
36	0.53	12.65	1.16	81
37	0.52	12.72	1.24	82
38	0.50	12.90	1.24	82
39	0.49	13.00	1.30	81
40	0.48	13.10	1.44	81
41	0.47	13.20	1.58	79
42	0.46	13.31	1.70	79
43	0.44	13.60	1.90	79
44	0.43	13.80	2.00	77
#45	0.41	14.20	2.00	67
#46	0.39	14.58	2.00	35
#47	0.37	15.08	2.00	06
#48	0.34	16.02	2.00	05

$$\alpha_{\text{solar}} = \left[\sum_{m=1}^{m=48} (1-\rho_m) + \dots + (1-\rho_m) \right] : 48$$

$$\alpha_s = .274$$

* Overlap

Long Wavelength Filter In Beam

INTEGRATING SPHERE PROGRAMMED WORK SHEET

SAMPLE NO. 39

LEAD SULFIDE DETECTOR				
NO.	λ	DRUM	SLIT	ρ_s
1	2.45	7.48	2.00	34
2	2.05	8.58	2.00	50
3	1.82	9.05	2.00	50
4	1.67	9.40	2.00	47
5	1.54	9.65	2.00	52
6	1.44	9.88	2.00	53
7	1.36	10.10	1.74	53
8	1.29	10.23	1.52	54
9	1.23	10.33	1.42	55
10	1.17	10.44	1.16	54
11	1.12	10.55	1.12	55
12	1.08	10.63	1.06	56
13	1.04	10.71	1.02	56
14	1.00	10.83	1.02	56
15	0.96	10.96	0.92	56
16	0.93	11.00	0.86	56
17	0.90	11.08	0.84	57
18	0.87	11.14	0.80	57
19	0.84	11.20	0.80	57
20	0.81	11.29	0.76	57
21	0.79	11.34	0.74	58
22	0.77	11.40	0.74	58
23	0.75	11.46	0.72	58
24	0.72	11.55	0.72	57
25	0.70	11.65	0.70	56
26	0.69	11.69	0.70	57
27*	0.67	11.75	0.74	58
28*	0.65	11.86	0.74	57
29*	0.64	11.90	0.76	57
30*	0.62	12.03	0.78	56
31*	0.60	12.15	0.84	55
32*	0.59	12.20	0.90	57
33*	0.57	12.34	0.98	57

PHOTOMULTIPLIER DETECTOR				
NO.	λ	DRUM	SLIT	ρ_s
27*	0.67	11.75	0.74	57
28*	0.65	11.86	0.74	58
29*	0.64	11.90	0.76	57
30*	0.62	12.03	0.78	57
31*	0.60	12.15	0.84	57
32*	0.59	12.20	0.90	58
33*	0.57	12.34	0.98	58
34	0.56	12.45	1.00	57
35	0.55	12.49	1.08	58
36	0.53	12.65	1.16	58
37	0.52	12.72	1.24	58
38	0.50	12.90	1.24	58
39	0.49	13.00	1.30	57
40	0.48	13.10	1.44	56
41	0.47	13.20	1.58	56
42	0.46	13.31	1.70	56
43	0.44	13.60	1.90	55
44	0.43	13.80	2.00	52
#45	0.41	14.20	2.00	48
#46	0.39	14.58	2.00	27
#47	0.37	15.08	2.00	07
#48	0.34	16.02	2.00	05

$$\alpha_{\text{solar}} = \left[\sum_{m=1}^{m=48} (1-\rho_m) + \dots + (1-\rho_{m=48}) \right] \div 48$$

$$\alpha_s = .475$$

* Overlap

Long Wavelength Filter In Beam

INTEGRATING SPHERE PROGRAMMED WORK SHEET

SAMPLE NO. 39-A

LEAD SULFIDE DETECTOR				
NO.	λ	DRUM	SLIT	ρ_s
1	2.45	7.48	2.00	42
2	2.05	8.58	2.00	68
3	1.82	9.05	2.00	68
4	1.67	9.40	2.00	64
5	1.54	9.65	2.00	72
6	1.44	9.88	2.00	73
7	1.36	10.10	1.74	75
8	1.29	10.23	1.52	76
9	1.23	10.33	1.42	76
10	1.17	10.44	1.16	75
11	1.12	10.55	1.12	78
12	1.08	10.63	1.06	79
13	1.04	10.71	1.02	79
14	1.00	10.83	1.02	80
15	0.96	10.96	0.92	80
16	0.93	11.00	0.86	80
17	0.90	11.08	0.84	80
18	0.87	11.14	0.80	80
19	0.84	11.20	0.80	82
20	0.81	11.29	0.76	81
21	0.79	11.34	0.74	81
22	0.77	11.40	0.74	80
23	0.75	11.46	0.72	83
24	0.72	11.55	0.72	82
25	0.70	11.65	0.70	82
26	0.69	11.69	0.70	82
27*	0.67	11.75	0.74	82
28*	0.65	11.86	0.74	81
29*	0.64	11.90	0.76	82
30*	0.62	12.03	0.78	80
31*	0.60	12.15	0.84	82
32*	0.59	12.20	0.90	81
33*	0.57	12.34	0.98	84

PHOTOMULTIPLIER DETECTOR				
NO.	λ	DRUM	SLIT	ρ_s
27*	0.67	11.75	0.74	84
28*	0.65	11.86	0.74	83
29*	0.64	11.90	0.76	85
30*	0.62	12.03	0.78	84
31*	0.60	12.15	0.84	84
32*	0.59	12.20	0.90	85
33*	0.57	12.34	0.98	86
34	0.56	12.45	1.00	85
35	0.55	12.49	1.08	85
36	0.53	12.65	1.16	86
37	0.52	12.72	1.24	86
38	0.50	12.90	1.24	86
39	0.49	13.00	1.30	85
40	0.48	13.10	1.44	86
41	0.47	13.20	1.58	85
42	0.46	13.31	1.70	83
43	0.44	13.60	1.90	82
44	0.43	13.80	2.00	80
#45	0.41	14.20	2.00	70
#46	0.39	14.58	2.00	37
#47	0.37	15.08	2.00	06
#48	0.34	16.02	2.00	04

$$\alpha_{\text{solar}} = \left[\sum_{m=1}^{m=48} (1-\rho_m) + \dots + (1-\rho_{m=48}) \right] \div 48$$

$$\alpha_s = .249$$

* Overlap

Long Wavelength Filter In Beam

INTEGRATING SPHERE PROGRAMMED WORK SHEET

SAMPLE NO. 40

LEAD SULFIDE DETECTOR				
NO.	λ	DRUM	SLIT	ρ_s
1	2.45	7.48	2.00	29
2	2.05	8.58	2.00	41
3	1.82	9.05	2.00	41
4	1.67	9.40	2.00	39
5	1.54	9.65	2.00	42
6	1.44	9.88	2.00	42
7	1.36	10.10	1.74	43
8	1.29	10.23	1.52	44
9	1.23	10.33	1.42	44
10	1.17	10.44	1.16	43
11	1.12	10.55	1.12	44
12	1.08	10.63	1.06	45
13	1.04	10.71	1.02	44
14	1.00	10.83	1.02	44
15	0.96	10.96	0.92	44
16	0.93	11.00	0.86	44
17	0.90	11.08	0.84	44
18	0.87	11.14	0.80	44
19	0.84	11.20	0.80	44
20	0.81	11.29	0.76	45
21	0.79	11.34	0.74	47
22	0.77	11.40	0.74	45
23	0.75	11.46	0.72	47
24	0.72	11.55	0.72	46
25	0.70	11.65	0.70	45
26	0.69	11.69	0.70	46
27*	0.67	11.75	0.74	46
28*	0.65	11.86	0.74	45
29*	0.64	11.90	0.76	46
30*	0.62	12.03	0.78	45
31*	0.60	12.15	0.84	46
32*	0.59	12.20	0.90	45
33*	0.57	12.34	0.98	44

PHOTOMULTIPLIER DETECTOR				
NO.	λ	DRUM	SLIT	ρ_s
27*	0.67	11.75	0.74	47
28*	0.65	11.86	0.74	46
29*	0.64	11.90	0.76	47
30*	0.62	12.03	0.78	46
31*	0.60	12.15	0.84	47
32*	0.59	12.20	0.90	46
33*	0.57	12.34	0.98	47
34	0.56	12.45	1.00	45
35	0.55	12.49	1.08	46
36	0.53	12.65	1.16	46
37	0.52	12.72	1.24	45
38	0.50	12.90	1.24	46
39	0.49	13.00	1.30	44
40	0.48	13.10	1.44	44
41	0.47	13.20	1.58	44
42	0.46	13.31	1.70	44
43	0.44	13.60	1.90	43
44	0.43	13.80	2.00	41
#45	0.41	14.20	2.00	37
#46	0.39	14.58	2.00	21
#47	0.37	15.08	2.00	07
#48	0.34	16.02	2.00	06

$$\alpha_{\text{solar}} = \left[\sum_{m=1}^{m=48} (1-\rho_m) + \dots + (1-\rho_m) \right] \div 48$$

$$\alpha_s = .581$$

* Overlap

Long Wavelength Filter In Beam

INTEGRATING SPHERE PROGRAMMED WORK SHEET

SAMPLE NO. 40-A

LEAD SULFIDE DETECTOR				
NO.	λ	DRUM	SLIT	ρ_s
1	2.45	7.48	2.00	42
2	2.05	8.58	2.00	67
3	1.82	9.05	2.00	67
4	1.67	9.40	2.00	63
5	1.54	9.65	2.00	71
6	1.44	9.88	2.00	72
7	1.36	10.10	1.74	73
8	1.29	10.23	1.52	75
9	1.23	10.33	1.42	75
10	1.17	10.44	1.16	74
11	1.12	10.55	1.12	76
12	1.08	10.63	1.06	77
13	1.04	10.71	1.02	77
14	1.00	10.83	1.02	79
15	0.96	10.96	0.92	78
16	0.93	11.00	0.86	78
17	0.90	11.08	0.84	78
18	0.87	11.14	0.80	78
19	0.84	11.20	0.80	79
20	0.81	11.29	0.76	80
21	0.79	11.34	0.74	80
22	0.77	11.40	0.74	80
23	0.75	11.46	0.72	81
24	0.72	11.55	0.72	80
25	0.70	11.65	0.70	80
26	0.69	11.69	0.70	81
27*	0.67	11.75	0.74	80
28*	0.65	11.86	0.74	82
29*	0.64	11.90	0.76	80
30*	0.62	12.03	0.78	81
31*	0.60	12.15	0.84	81
32*	0.59	12.20	0.90	82
33*	0.57	12.34	0.98	81

PHOTOMULTIPLIER DETECTOR				
NO.	λ	DRUM	SLIT	ρ_s
27*	0.67	11.75	0.74	82
28*	0.65	11.86	0.74	81
29*	0.64	11.90	0.76	82
30*	0.62	12.03	0.78	82
31*	0.60	12.15	0.84	81
32*	0.59	12.20	0.90	81
33*	0.57	12.34	0.98	82
34	0.56	12.45	1.00	82
35	0.55	12.49	1.08	82
36	0.53	12.65	1.16	82
37	0.52	12.72	1.24	82
38	0.50	12.90	1.24	82
39	0.49	13.00	1.30	83
40	0.48	13.10	1.44	82
41	0.47	13.20	1.58	82
42	0.46	13.31	1.70	80
43	0.44	13.60	1.90	78
44	0.43	13.80	2.00	76
#45	0.41	14.20	2.00	66
#46	0.39	14.58	2.00	36
#47	0.37	15.08	2.00	05
#48	0.34	16.02	2.00	05

$$\alpha_{\text{solar}} = \left[\sum_{m=1}^{m=48} (1-\rho_m) + \dots + (1-\rho_m) \right] \div 48$$

$$\alpha_s = .267$$

* Overlap

Long Wavelength Filter In Beam

A.2 Aluminized Teflon Data

INTEGRATING SPHERE PROGRAMMED WORK SHEET

SAMPLE NO. 23

LEAD SULFIDE DETECTOR				
NO.	λ	DRUM	SLIT	ρ_s
1	2.45	7.48	2.00	93
2	2.05	8.58	2.00	91
3	1.82	9.05	2.00	91
4	1.67	9.40	2.00	91
5	1.54	9.65	2.00	92
6	1.44	9.88	2.00	91
7	1.36	10.10	1.74	90
8	1.29	10.23	1.52	90
9	1.23	10.33	1.42	90
10	1.17	10.44	1.16	90
11	1.12	10.55	1.12	89
12	1.08	10.63	1.06	89
13	1.04	10.71	1.02	87
14	1.00	10.83	1.02	85
15	0.96	10.96	0.92	83
16	0.93	11.00	0.86	82
17	0.90	11.08	0.84	80
18	0.87	11.14	0.80	79
19	0.84	11.20	0.80	78
20	0.81	11.29	0.76	78
21	0.79	11.34	0.74	77
22	0.77	11.40	0.74	78
23	0.75	11.46	0.72	80
24	0.72	11.55	0.72	78
25	0.70	11.65	0.70	79
26	0.69	11.69	0.70	80
27*	0.67	11.75	0.74	80
28*	0.65	11.86	0.74	81
29*	0.64	11.90	0.76	81
30*	0.62	12.03	0.78	78
31*	0.60	12.15	0.84	80
32*	0.59	12.20	0.90	79
33*	0.57	12.34	0.98	80

PHOTOMULTIPLIER DETECTOR				
NO.	λ	DRUM	SLIT	ρ_s
27*	0.67	11.75	0.74	80
28*	0.65	11.86	0.74	80
29*	0.64	11.90	0.76	79
30*	0.62	12.03	0.78	80
31*	0.60	12.15	0.84	79
32*	0.59	12.20	0.90	80
33*	0.57	12.34	0.98	80
34	0.56	12.45	1.00	81
35	0.55	12.49	1.08	80
36	0.53	12.65	1.16	80
37	0.52	12.72	1.24	78
38	0.50	12.90	1.24	80
39	0.49	13.00	1.30	78
40	0.48	13.10	1.44	78
41	0.47	13.20	1.58	77
42	0.46	13.31	1.70	76
43	0.44	13.60	1.90	74
44	0.43	13.80	2.00	74
#45	0.41	14.20	2.00	72
#46	0.39	14.58	2.00	71
#47	0.37	15.08	2.00	70
#48	0.34	16.02	2.00	66

$$\alpha_{\text{solar}} = \left[\sum_{m=1}^{m=48} (1-\rho_m) + \dots + (1-\rho_m) \right] \div 48$$

$$\alpha_s = .185$$

* Overlap

Long Wavelength Filter In Beam

INTEGRATING SPHERE PROGRAMMED WORK SHEET

SAMPLE NO. 24

LEAD SULFIDE DETECTOR				
NO.	λ	DRUM	SLIT	ρ_s
1	2.45	7.48	2.00	13
2	2.05	8.58	2.00	14
3	1.82	9.05	2.00	14
4	1.67	9.40	2.00	14
5	1.54	9.65	2.00	14
6	1.44	9.88	2.00	14
7	1.36	10.10	1.74	14
8	1.29	10.23	1.52	15
9	1.23	10.33	1.42	14
10	1.17	10.44	1.16	14
11	1.12	10.55	1.12	14
12	1.08	10.63	1.06	14
13	1.04	10.71	1.02	14
14	1.00	10.83	1.02	14
15	0.96	10.96	0.92	15
16	0.93	11.00	0.86	15
17	0.90	11.08	0.84	15
18	0.87	11.14	0.80	15
19	0.84	11.20	0.80	16
20	0.81	11.29	0.76	14
21	0.79	11.34	0.74	14
22	0.77	11.40	0.74	14
23	0.75	11.46	0.72	15
24	0.72	11.55	0.72	14
25	0.70	11.65	0.70	14
26	0.69	11.69	0.70	15
27*	0.67	11.75	0.74	15
28*	0.65	11.86	0.74	16
29*	0.64	11.90	0.76	14
30*	0.62	12.03	0.78	14
31*	0.60	12.15	0.84	15
32*	0.59	12.20	0.90	15
33*	0.57	12.34	0.98	14

PHOTOMULTIPLIER DETECTOR				
NO.	λ	DRUM	SLIT	ρ_s
27*	0.67	11.75	0.74	15
28*	0.65	11.86	0.74	14
29*	0.64	11.90	0.76	15
30*	0.62	12.03	0.78	14
31*	0.60	12.15	0.84	14
32*	0.59	12.20	0.90	13
33*	0.57	12.34	0.98	14
34	0.56	12.45	1.00	14
35	0.55	12.49	1.08	14
36	0.53	12.65	1.16	14
37	0.52	12.72	1.24	14
38	0.50	12.90	1.24	13
39	0.49	13.00	1.30	13
40	0.48	13.10	1.44	13
41	0.47	13.20	1.58	13
42	0.46	13.31	1.70	13
43	0.44	13.60	1.90	12
44	0.43	13.80	2.00	12
#45	0.41	14.20	2.00	11
#46	0.39	14.58	2.00	11
#47	0.37	15.08	2.00	10
#48	0.34	16.02	2.00	08

$$\alpha_{\text{solar}} = \left[\sum_{m=1}^{m=48} (1-\rho_m) + \dots + (1-\rho_m) \right] \div 48$$

$$\alpha_s = .864$$

* Overlap

Long Wavelength Filter In Beam

INTEGRATING SPHERE PROGRAMMED WORK SHEET

SAMPLE NO. 25

LEAD SULFIDE DETECTOR				
NO.	λ	DRUM	SLIT	ρ_s
1	2.45	7.48	2.00	91
2	2.05	8.58	2.00	92
3	1.82	9.05	2.00	91
4	1.67	9.40	2.00	92
5	1.54	9.65	2.00	92
6	1.44	9.88	2.00	91
7	1.36	10.10	1.74	91
8	1.29	10.23	1.52	91
9	1.23	10.33	1.42	91
10	1.17	10.44	1.16	90
11	1.12	10.55	1.12	89
12	1.08	10.63	1.06	89
13	1.04	10.71	1.02	88
14	1.00	10.83	1.02	87
15	0.96	10.96	0.92	84
16	0.93	11.00	0.86	84
17	0.90	11.08	0.84	81
18	0.87	11.14	0.80	81
19	0.84	11.20	0.80	81
20	0.81	11.29	0.76	79
21	0.79	11.34	0.74	79
22	0.77	11.40	0.74	79
23	0.75	11.46	0.72	80
24	0.72	11.55	0.72	80
25	0.70	11.65	0.70	81
26	0.69	11.69	0.70	80
27*	0.67	11.75	0.74	81
28*	0.65	11.86	0.74	81
29*	0.64	11.90	0.76	81
30*	0.62	12.03	0.78	81
31*	0.60	12.15	0.84	82
32*	0.59	12.20	0.90	82
33*	0.57	12.34	0.98	81

PHOTOMULTIPLIER DETECTOR				
NO.	λ	DRUM	SLIT	ρ_s
27*	0.67	11.75	0.74	81
28*	0.65	11.86	0.74	81
29*	0.64	11.90	0.76	81
30*	0.62	12.03	0.78	81
31*	0.60	12.15	0.84	81
32*	0.59	12.20	0.90	82
33*	0.57	12.34	0.98	82
34	0.56	12.45	1.00	82
35	0.55	12.49	1.08	81
36	0.53	12.65	1.16	81
37	0.52	12.72	1.24	80
38	0.50	12.90	1.24	81
39	0.49	13.00	1.30	81
40	0.48	13.10	1.44	81
41	0.47	13.20	1.58	80
42	0.46	13.31	1.70	79
43	0.44	13.60	1.90	75
44	0.43	13.80	2.00	77
#45	0.41	14.20	2.00	75
#46	0.39	14.58	2.00	72
#47	0.37	15.08	2.00	70
#48	0.34	16.02	2.00	64

$$\alpha_{\text{solar}} = \left[\sum_{m=1}^{m=48} (1-\rho_m) + \dots + (1-\rho_m) \right] \div 48$$

$$\alpha_s = .174$$

* Overlap

Long Wavelength Filter In Beam

INTEGRATING SPHERE PROGRAMMED WORK SHEET

SAMPLE NO. 26

LEAD SULFIDE DETECTOR				
NO.	λ	DRUM	SLIT	ρ_s
1	2.45	7.48	2.00	42
2	2.05	8.58	2.00	42
3	1.82	9.05	2.00	41
4	1.67	9.40	2.00	41
5	1.54	9.65	2.00	41
6	1.44	9.88	2.00	38
7	1.36	10.10	1.74	42
8	1.29	10.23	1.52	42
9	1.23	10.33	1.42	40
10	1.17	10.44	1.16	39
11	1.12	10.55	1.12	37
12	1.08	10.63	1.06	38
13	1.04	10.71	1.02	38
14	1.00	10.83	1.02	35
15	0.96	10.96	0.92	32
16	0.93	11.00	0.86	33
17	0.90	11.08	0.84	34
18	0.87	11.14	0.80	36
19	0.84	11.20	0.80	34
20	0.81	11.29	0.76	33
21	0.79	11.34	0.74	32
22	0.77	11.40	0.74	34
23	0.75	11.46	0.72	31
24	0.72	11.55	0.72	33
25	0.70	11.65	0.70	31
26	0.69	11.69	0.70	32
27*	0.67	11.75	0.74	34
28*	0.65	11.86	0.74	35
29*	0.64	11.90	0.76	32
30*	0.62	12.03	0.78	33
31*	0.60	12.15	0.84	33
32*	0.59	12.20	0.90	30
33*	0.57	12.34	0.98	32

PHOTOMULTIPLIER DETECTOR				
NO.	λ	DRUM	SLIT	ρ_s
27*	0.67	11.75	0.74	33
28*	0.65	11.86	0.74	33
29*	0.64	11.90	0.76	33
30*	0.62	12.03	0.78	33
31*	0.60	12.15	0.84	35
32*	0.59	12.20	0.90	30
33*	0.57	12.34	0.98	32
34	0.56	12.45	1.00	30
35	0.55	12.49	1.08	32
36	0.53	12.65	1.16	30
37	0.52	12.72	1.24	28
38	0.50	12.90	1.24	28
39	0.49	13.00	1.30	28
40	0.48	13.10	1.44	29
41	0.47	13.20	1.58	29
42	0.46	13.31	1.70	29
43	0.44	13.60	1.90	27
44	0.43	13.80	2.00	26
#45	0.41	14.20	2.00	26
#46	0.39	14.58	2.00	23
#47	0.37	15.08	2.00	22
#48	0.34	16.02	2.00	15

$$\alpha_{\text{solar}} = \left[\sum_{m=1}^{m=48} (1-\rho_m) + \dots + (1-\rho_m) \right] : 48$$

$$\alpha_s = .670$$

* Overlap

Long Wavelength Filter In Beam

INTEGRATING SPHERE PROGRAMMED WORK SHEET

SAMPLE NO. 26

LEAD SULFIDE DETECTOR				
NO.	λ	DRUM	SLIT	ρ_s
1	2.45	7.48	2.00	90
2	2.05	8.58	2.00	91
3	1.82	9.05	2.00	90
4	1.67	9.40	2.00	91
5	1.54	9.65	2.00	90
6	1.44	9.88	2.00	90
7	1.36	10.10	1.74	90
8	1.29	10.23	1.52	91
9	1.23	10.33	1.42	89
10	1.17	10.44	1.16	89
11	1.12	10.55	1.12	88
12	1.08	10.63	1.06	88
13	1.04	10.71	1.02	87
14	1.00	10.83	1.02	85
15	0.96	10.96	0.92	83
16	0.93	11.00	0.86	81
17	0.90	11.08	0.84	80
18	0.87	11.14	0.80	78
19	0.84	11.20	0.80	78
20	0.81	11.29	0.76	78
21	0.79	11.34	0.74	78
22	0.77	11.40	0.74	78
23	0.75	11.46	0.72	79
24	0.72	11.55	0.72	78
25	0.70	11.65	0.70	79
26	0.69	11.69	0.70	80
27*	0.67	11.75	0.74	80
28*	0.65	11.86	0.74	78
29*	0.64	11.90	0.76	80
30*	0.62	12.03	0.78	78
31*	0.60	12.15	0.84	79
32*	0.59	12.20	0.90	78
33*	0.57	12.34	0.98	80

PHOTOMULTIPLIER DETECTOR				
NO.	λ	DRUM	SLIT	ρ_s
27*	0.67	11.75	0.74	79
28*	0.65	11.86	0.74	79
29*	0.64	11.90	0.76	77
30*	0.62	12.03	0.78	79
31*	0.60	12.15	0.84	80
32*	0.59	12.20	0.90	81
33*	0.57	12.34	0.98	80
34	0.56	12.45	1.00	79
35	0.55	12.49	1.08	72
36	0.53	12.65	1.16	78
37	0.52	12.72	1.24	78
38	0.50	12.90	1.24	79
39	0.49	13.00	1.30	80
40	0.48	13.10	1.44	78
41	0.47	13.20	1.58	77
42	0.46	13.31	1.70	78
43	0.44	13.60	1.90	75
44	0.43	13.80	2.00	74
#45	0.41	14.20	2.00	73
#46	0.39	14.58	2.00	70
#47	0.37	15.08	2.00	69
#48	0.34	16.02	2.00	66

$$\alpha_{\text{solar}} = \left[\sum_{m=1}^{m=48} (1-\rho_m) + \dots + (1-\rho_m) \right] : 48$$

$$\alpha_s = .191$$

* Overlap

Long Wavelength Filter In Beam

INTEGRATING SPHERE PROGRAMMED WORK SHEET

SAMPLE NO. 27

LEAD SULFIDE DETECTOR				
NO.	λ	DRUM	SLIT	ρ_s
1	2.45	7.48	2.00	68
2	2.05	8.58	2.00	66
3	1.82	9.05	2.00	66
4	1.67	9.40	2.00	65
5	1.54	9.65	2.00	65
6	1.44	9.88	2.00	64
7	1.36	10.10	1.74	64
8	1.29	10.23	1.52	63
9	1.23	10.33	1.42	62
10	1.17	10.44	1.16	62
11	1.12	10.55	1.12	61
12	1.08	10.63	1.06	61
13	1.04	10.71	1.02	61
14	1.00	10.83	1.02	59
15	0.96	10.96	0.92	58
16	0.93	11.00	0.86	56
17	0.90	11.08	0.84	55
18	0.87	11.14	0.80	56
19	0.84	11.20	0.80	52
20	0.81	11.29	0.76	54
21	0.79	11.34	0.74	52
22	0.77	11.40	0.74	52
23	0.75	11.46	0.72	54
24	0.72	11.55	0.72	53
25	0.70	11.65	0.70	53
26	0.69	11.69	0.70	54
27*	0.67	11.75	0.74	54
28*	0.65	11.86	0.74	54
29*	0.64	11.90	0.76	52
30*	0.62	12.03	0.78	53
31*	0.60	12.15	0.84	52
32*	0.59	12.20	0.90	52
33*	0.57	12.34	0.98	51

PHOTOMULTIPLIER DETECTOR				
NO.	λ	DRUM	SLIT	ρ_s
27*	0.67	11.75	0.74	52
28*	0.65	11.86	0.74	50
29*	0.64	11.90	0.76	58
30*	0.62	12.03	0.78	57
31*	0.60	12.15	0.84	57
32*	0.59	12.20	0.90	56
33*	0.57	12.34	0.98	57
34	0.56	12.45	1.00	57
35	0.55	12.49	1.08	56
36	0.53	12.65	1.16	54
37	0.52	12.72	1.24	53
38	0.50	12.90	1.24	50
39	0.49	13.00	1.30	49
40	0.48	13.10	1.44	47
41	0.47	13.20	1.58	43
42	0.46	13.31	1.70	42
43	0.44	13.60	1.90	37
44	0.43	13.80	2.00	34
#45	0.41	14.20	2.00	24
#46	0.39	14.58	2.00	14
#47	0.37	15.08	2.00	08
#48	0.34	16.02	2.00	07

$$\alpha_{\text{solar}} = \left[\sum_{m=1}^{m=48} (1-\rho_m) + \dots + (1-\rho_{\frac{m}{8}}) \right] : 48$$

$$\alpha_s = .481$$

* Overlap

Long Wavelength Filter In Beam

INTEGRATING SPHERE PROGRAMMED WORK SHEET

SAMPLE NO. 28

LEAD SULFIDE DETECTOR				
NO.	λ	DRUM	SLIT	ρ_s
1	2.45	7.48	2.00	35
2	2.05	8.58	2.00	32
3	1.82	9.05	2.00	33
4	1.67	9.40	2.00	32
5	1.54	9.65	2.00	32
6	1.44	9.88	2.00	31
7	1.36	10.10	1.74	31
8	1.29	10.23	1.52	30
9	1.23	10.33	1.42	30
10	1.17	10.44	1.16	30
11	1.12	10.55	1.12	29
12	1.08	10.63	1.06	29
13	1.04	10.71	1.02	29
14	1.00	10.83	1.02	28
15	0.96	10.96	0.92	28
16	0.93	11.00	0.86	27
17	0.90	11.08	0.84	27
18	0.87	11.14	0.80	27
19	0.84	11.20	0.80	27
20	0.81	11.29	0.76	27
21	0.79	11.34	0.74	26
22	0.77	11.40	0.74	27
23	0.75	11.46	0.72	27
24	0.72	11.55	0.72	27
25	0.70	11.65	0.70	27
26	0.69	11.69	0.70	26
27*	0.67	11.75	0.74	27
28*	0.65	11.86	0.74	26
29*	0.64	11.90	0.76	25
30*	0.62	12.03	0.78	26
31*	0.60	12.15	0.84	25
32*	0.59	12.20	0.90	25
33*	0.57	12.34	0.98	25

PHOTOMULTIPLIER DETECTOR				
NO.	λ	DRUM	SLIT	ρ_s
27*	0.67	11.75	0.74	27
28*	0.65	11.86	0.74	26
29*	0.64	11.90	0.76	26
30*	0.62	12.03	0.78	25
31*	0.60	12.15	0.84	25
32*	0.59	12.20	0.90	24
33*	0.57	12.34	0.98	26
34	0.56	12.45	1.00	26
35	0.55	12.49	1.08	24
36	0.53	12.65	1.16	24
37	0.52	12.72	1.24	24
38	0.50	12.90	1.24	24
39	0.49	13.00	1.30	23
40	0.48	13.10	1.44	23
41	0.47	13.20	1.58	22
42	0.46	13.31	1.70	22
43	0.44	13.60	1.90	21
44	0.43	13.80	2.00	21
#45	0.41	14.20	2.00	18
#46	0.39	14.58	2.00	19
#47	0.37	15.08	2.00	17
#48	0.34	16.02	2.00	12

$$\alpha_{\text{solar}} = \left[\sum_{m=1}^{m=48} (1-\rho_m) + \dots + (1-\rho_m) \right] : 48$$

$$\alpha_s = .739$$

* Overlap

Long Wavelength Filter In Beam

INTEGRATING SPHERE PROGRAMMED WORK SHEET

SAMPLE NO. 28

LEAD SULFIDE DETECTOR				
NO.	λ	DRUM	SLIT	ρ_s
1	2.45	7.48	2.00	92
2	2.05	8.58	2.00	92
3	1.82	9.05	2.00	91
4	1.67	9.40	2.00	91
5	1.54	9.65	2.00	91
6	1.44	9.88	2.00	90
7	1.36	10.10	1.74	90
8	1.29	10.23	1.52	91
9	1.23	10.33	1.42	90
10	1.17	10.44	1.16	90
11	1.12	10.55	1.12	88
12	1.08	10.63	1.06	89
13	1.04	10.71	1.02	88
14	1.00	10.83	1.02	86
15	0.96	10.96	0.92	84
16	0.93	11.00	0.86	82
17	0.90	11.08	0.84	81
18	0.87	11.14	0.80	78
19	0.84	11.20	0.80	80
20	0.81	11.29	0.76	79
21	0.79	11.34	0.74	78
22	0.77	11.40	0.74	80
23	0.75	11.46	0.72	79
24	0.72	11.55	0.72	79
25	0.70	11.65	0.70	79
26	0.69	11.69	0.70	80
27*	0.67	11.75	0.74	81
28*	0.65	11.86	0.74	79
29*	0.64	11.90	0.76	82
30*	0.62	12.03	0.78	80
31*	0.60	12.15	0.84	81
32*	0.59	12.20	0.90	80
33*	0.57	12.34	0.98	80

PHOTOMULTIPLIER DETECTOR				
NO.	λ	DRUM	SLIT	ρ_s
27*	0.67	11.75	0.74	81
28*	0.65	11.86	0.74	80
29*	0.64	11.90	0.76	79
30*	0.62	12.03	0.78	84
31*	0.60	12.15	0.84	81
32*	0.59	12.20	0.90	83
33*	0.57	12.34	0.98	81
34	0.56	12.45	1.00	81
35	0.55	12.49	1.08	81
36	0.53	12.65	1.16	80
37	0.52	12.72	1.24	81
38	0.50	12.90	1.24	80
39	0.49	13.00	1.30	84
40	0.48	13.10	1.44	80
41	0.47	13.20	1.58	79
42	0.46	13.31	1.70	80
43	0.44	13.60	1.90	78
44	0.43	13.80	2.00	77
#45	0.41	14.20	2.00	75
#46	0.39	14.58	2.00	73
#47	0.37	15.08	2.00	72
#48	0.34	16.02	2.00	68

$$\alpha_{\text{solar}} = \left[\sum_{m=1}^{m=48} (1-\rho_m) + \dots + (1-\rho_{\frac{m}{8}}) \right] : 48$$

$$\alpha_s = .163$$

* Overlap

Long Wavelength Filter In Beam

INTEGRATING SPHERE PROGRAMMED WORK SHEET

SAMPLE NO. 33

LEAD SULFIDE DETECTOR				
NO.	λ	DRUM	SLIT	ρ_s
1	2.45	7.48	2.00	91
2	2.05	8.58	2.00	90
3	1.82	9.05	2.00	91
4	1.67	9.40	2.00	90
5	1.54	9.65	2.00	90
6	1.44	9.88	2.00	90
7	1.36	10.10	1.74	89
8	1.29	10.23	1.52	88
9	1.23	10.33	1.42	88
10	1.17	10.44	1.16	88
11	1.12	10.55	1.12	87
12	1.08	10.63	1.06	86
13	1.04	10.71	1.02	86
14	1.00	10.83	1.02	84
15	0.96	10.96	0.92	81
16	0.93	11.00	0.86	80
17	0.90	11.08	0.84	79
18	0.87	11.14	0.80	78
19	0.84	11.20	0.80	77
20	0.81	11.29	0.76	78
21	0.79	11.34	0.74	77
22	0.77	11.40	0.74	77
23	0.75	11.46	0.72	77
24	0.72	11.55	0.72	78
25	0.70	11.65	0.70	77
26	0.69	11.69	0.70	79
27*	0.67	11.75	0.74	80
28*	0.65	11.86	0.74	79
29*	0.64	11.90	0.76	79
30*	0.62	12.03	0.78	79
31*	0.60	12.15	0.84	80
32*	0.59	12.20	0.90	76
33*	0.57	12.34	0.98	80

PHOTOMULTIPLIER DETECTOR				
NO.	λ	DRUM	SLIT	ρ_s
27*	0.67	11.75	0.74	78
28*	0.65	11.86	0.74	78
29*	0.64	11.90	0.76	78
30*	0.62	12.03	0.78	78
31*	0.60	12.15	0.84	77
32*	0.59	12.20	0.90	79
33*	0.57	12.34	0.98	79
34	0.56	12.45	1.00	78
35	0.55	12.49	1.08	76
36	0.53	12.65	1.16	77
37	0.52	12.72	1.24	77
38	0.50	12.90	1.24	79
39	0.49	13.00	1.30	76
40	0.48	13.10	1.44	76
41	0.47	13.20	1.58	75
42	0.46	13.31	1.70	74
43	0.44	13.60	1.90	73
44	0.43	13.80	2.00	71
#45	0.41	14.20	2.00	70
#46	0.39	14.58	2.00	66
#47	0.37	15.08	2.00	64
#48	0.34	16.02	2.00	60

$$\alpha_{\text{solar}} = \left[\sum_{m=1}^{m=48} (1-\rho_m) + \dots + (1-\rho_{\frac{m}{8}}) \right] : 48$$

$$\alpha_s = .202$$

* Overlap

Long Wavelength Filter In Beam

INTEGRATING SPHERE PROGRAMMED WORK SHEET

SAMPLE NO. 35

LEAD SULFIDE DETECTOR				
NO.	λ	DRUM	SLIT	ρ_s
1	2.45	7.48	2.00	90
2	2.05	8.58	2.00	90
3	1.82	9.05	2.00	90
4	1.67	9.40	2.00	90
5	1.54	9.65	2.00	90
6	1.44	9.88	2.00	91
7	1.36	10.10	1.74	90
8	1.29	10.23	1.52	90
9	1.23	10.33	1.42	89
10	1.17	10.44	1.16	89
11	1.12	10.55	1.12	87
12	1.08	10.63	1.06	87
13	1.04	10.71	1.02	86
14	1.00	10.83	1.02	85
15	0.96	10.96	0.92	81
16	0.93	11.00	0.86	81
17	0.90	11.08	0.84	80
18	0.87	11.14	0.80	79
19	0.84	11.20	0.80	77
20	0.81	11.29	0.76	77
21	0.79	11.34	0.74	78
22	0.77	11.40	0.74	78
23	0.75	11.46	0.72	79
24	0.72	11.55	0.72	80
25	0.70	11.65	0.70	80
26	0.69	11.69	0.70	79
27*	0.67	11.75	0.74	80
28*	0.65	11.86	0.74	79
29*	0.64	11.90	0.76	80
30*	0.62	12.03	0.78	80
31*	0.60	12.15	0.84	80
32*	0.59	12.20	0.90	81
33*	0.57	12.34	0.98	81

PHOTOMULTIPLIER DETECTOR				
NO.	λ	DRUM	SLIT	ρ_s
27*	0.67	11.75	0.74	80
28*	0.65	11.86	0.74	79
29*	0.64	11.90	0.76	79
30*	0.62	12.03	0.78	79
31*	0.60	12.15	0.84	80
32*	0.59	12.20	0.90	78
33*	0.57	12.34	0.98	80
34	0.56	12.45	1.00	79
35	0.55	12.49	1.08	79
36	0.53	12.65	1.16	79
37	0.52	12.72	1.24	79
38	0.50	12.90	1.24	80
39	0.49	13.00	1.30	79
40	0.48	13.10	1.44	75
41	0.47	13.20	1.58	75
42	0.46	13.31	1.70	74
43	0.44	13.60	1.90	73
44	0.43	13.80	2.00	74
#45	0.41	14.20	2.00	73
#46	0.39	14.58	2.00	67
#47	0.37	15.08	2.00	68
#48	0.34	16.02	2.00	60

$$\alpha_{\text{solar}} = \left[\sum_{m=1}^{m=48} (1-\rho_m) + \dots + (1-\rho_{\frac{m}{8}}) \right] : 48$$

$$\alpha_s = .196$$

* Overlap

Long Wavelength Filter In Beam

INTEGRATING SPHERE PROGRAMMED WORK SHEET

SAMPLE NO. 37

LEAD SULFIDE DETECTOR				
NO.	λ	DRUM	SLIT	ρ_s
1	2.45	7.48	2.00	91
2	2.05	8.58	2.00	91
3	1.82	9.05	2.00	91
4	1.67	9.40	2.00	90
5	1.54	9.65	2.00	92
6	1.44	9.88	2.00	90
7	1.36	10.10	1.74	90
8	1.29	10.23	1.52	89
9	1.23	10.33	1.42	89
10	1.17	10.44	1.16	89
11	1.12	10.55	1.12	88
12	1.08	10.63	1.06	87
13	1.04	10.71	1.02	87
14	1.00	10.83	1.02	84
15	0.96	10.96	0.92	82
16	0.93	11.00	0.86	81
17	0.90	11.08	0.84	80
18	0.87	11.14	0.80	79
19	0.84	11.20	0.80	77
20	0.81	11.29	0.76	77
21	0.79	11.34	0.74	78
22	0.77	11.40	0.74	79
23	0.75	11.46	0.72	77
24	0.72	11.55	0.72	78
25	0.70	11.65	0.70	78
26	0.69	11.69	0.70	79
27*	0.67	11.75	0.74	80
28*	0.65	11.86	0.74	78
29*	0.64	11.90	0.76	79
30*	0.62	12.03	0.78	80
31*	0.60	12.15	0.84	80
32*	0.59	12.20	0.90	79
33*	0.57	12.34	0.98	80

PHOTOMULTIPLIER DETECTOR				
NO.	λ	DRUM	SLIT	ρ_s
27*	0.67	11.75	0.74	79
28*	0.65	11.86	0.74	79
29*	0.64	11.90	0.76	80
30*	0.62	12.03	0.78	79
31*	0.60	12.15	0.84	79
32*	0.59	12.20	0.90	78
33*	0.57	12.34	0.98	80
34	0.56	12.45	1.00	80
35	0.55	12.49	1.08	80
36	0.53	12.65	1.16	79
37	0.52	12.72	1.24	78
38	0.50	12.90	1.24	79
39	0.49	13.00	1.30	78
40	0.48	13.10	1.44	78
41	0.47	13.20	1.58	75
42	0.46	13.31	1.70	74
43	0.44	13.60	1.90	74
44	0.43	13.80	2.00	72
#45	0.41	14.20	2.00	69
#46	0.39	14.58	2.00	68
#47	0.37	15.08	2.00	66
#48	0.34	16.02	2.00	62

$$\alpha_{\text{solar}} = \left[\sum_{m=1}^{m=48} (1-\rho_m) + \dots + (1-\rho_m) \right] : 48$$

$$\alpha_s = .194$$

* Overlap

Long Wavelength Filter In Beam

7 June 1967

APPENDIX B

Northrop Space Laboratories

Presentation

Lunar Dust Removal/Prevention Concept

Contract NAS8-20116

29 June 1966

7 June 1967

APPENDIX B

As part of the conceptual design process, the necessity arose for establishing some systematic process for comparing and evaluating the eight concepts envisioned for removing or preventing dust accumulation. Such a comparison and evaluation procedure would be useful in establishing a priority for fabrication and testing. The process developed and the resulting comparisons, evaluations, and priorities of the different concepts are summarized in Charts 1 through 10 of this appendix. These charts were used as part of a presentation to NASA on 29 June 1966.

Chart 1 reflects the basic philosophy or objective under consideration: Either the dust must be removed by some means from the radiator surface after it has accumulated, or some method must be devised to prevent its accumulation.

Chart 2 presents a listing of the most significant forces available for removing the dust. The forces are divided into two categories, body and surface. Body forces act upon each individual particle of matter and result from the basic nature of matter itself. No physical contact between particles of matter is necessary for body forces to occur. Surface forces act upon the surface of particles and only occur when physical contact between particles of matter exists.

Each of the eight concepts is based on the use of one of the forces already discussed. The matching of force with concept is presented in Chart 3. It should be noted that of the forces listed in Chart 2, only gravitational and magnetic body forces, and normal surface forces were not utilized by one of the concepts. Actually any concept involving a tilted surface would use a gravitational body force.

7 June 1967

The dust removal/prevention concepts under consideration were to lead initially to experimental apparatus suitable for testing in a space chamber. For this reason a number of experimental factors had to be considered. These factors, as shown in Chart 4, were weighted from 0.5 to 1.0 according to their relative importance. The basic thinking behind the formulation of these factors was that a removal/prevention concept which was difficult to test experimentally was less desirable from a practical research standpoint than a concept for which experimental testing was relatively straightforward.

Although no operational systems were to be the result of the research effort, some attention was also given to the formulation of operational parameters, which would be important for an operational system operating in the lunar environment. These parameters, which were assigned equal weight, as shown in Chart 5 were divided into two categories: operational factors and operational considerations. The factors were those items for which some kind of a numerical grade could be assigned. The considerations were more qualitative in nature, with an adjective (excellent, good, fair, or poor) being used for evaluation purposes. The reason behind the development of the operational factors and considerations was simply that any concept, which was completely impractical from an operational standpoint, should not be seriously considered for experimental testing. Notice should be taken that astronaut maintenance, implying astronautical extravehicular activity (EVA), was one of the operational factors. One of the basic guidelines for the entire research effort was the avoidance of astronaut EVA.

Based on the experimental factors presented in Chart 4, each of the eight devices was graded based on all available information. The resulting performance matrix is shown in Chart 6. For each concept, the upper row of numbers represents

7 June 1967

the unweighted grades for each factor, while the lower row are the weighted values in accordance with Chart 4. The total grade based on the weighted number is presented in the right-hand column of Chart 6. The vibrating surface received the highest grade based on the experimental factors. The vibrating shield was second, the jet and surface third, the electrostatic surface fourth, and the electrostatic curtain fifth. The brush concept was ranked sixth, the jet and shield seventh, and the spinning shield eighth.

Each concept was also evaluated based on the operational factors and considerations presented in Chart 5. The resulting performance matrices are presented in Charts 7 and 8. The alternate scores presented in Chart 7 for the electrostatic surface reflect the fact that the power requirements for this concept were difficult to define because of uncertainties associated with the voltage requirements. Based on the operational factors, the electrostatic surface received the highest grade; the vibrating surface and the jet and surface were tied for second; the jet and shield was fourth; the vibrating shield fifth; the electrostatic curtain sixth; the brush seventh; and the spinning shield eighth. With respect to operational considerations, the following order of ranking from highest to lowest occurred: (1) electrostatic surface, (2) jet and surface, (3) jet and shield, (4) vibrating shield, (5) spinning shield, and vibrating surface (tie), (7) electrostatic curtain, and (8) brush.

Because of the special significance of mass and power requirements, which were used as inputs to Chart 7, a separate chart (Chart 9) was developed to provide mass and power values. The data presented in this chart were based on the mass or power associated with shielding or cleaning one square meter of radiator surface in one second. A 3.04- by 3.04-meter surface was used in those cases where the size of the radiator surface affected the calculations. The powerplant mass-per-power-produced

was assumed to be 0.00159 kg/watt, and the power requirement for each system multiplied by this factor provided a value for "mass for power" for each concept. In every case, this "mass for power" was small in comparison with the mass-per-unit-area of the system. Notice should be taken that the mass expended per unit area for jet concepts, while significant, was not considered part of the total mass of the system. This resulted from the fact that the working fluid for the jet concepts, as originally conceived, was to be a gas obtained from cryogenic boiloff.

In terms of power requirements per unit area, the two jet concepts had the lowest requirements. The electrostatic surface was third or fifth lowest, depending upon the electrostatic voltage required. The electrostatic curtain was fourth (or third depending on the ranking of the electrostatic surface), the vibrating surface fifth (or fourth), the vibrating shield sixth, the spinning shield seventh, and the brush eighth.

With regard to total mass requirements per unit area, the electrostatic surface required the least mass. The electrostatic curtain was second lowest, the brush third, and the vibrating surface fourth. The last four in order were the jet and surface, the vibrating shield, the spinning shield, and the jet and shield.

Chart 10 presents a summary of the rankings of each device as previously indicated in Charts 6, 7, and 8. Northrop's original recommendation for order of fabrication is also presented along with final order jointly agreed upon by NASA and Northrop. The vibrating surface was to be first, the jet and shield second, the brush and shield third, the electrostatic curtain fourth, the electrostatic surface fifth, the brush and surface sixth, and the jet and shield seventh. Only the first three concepts were definitely to be tested; the fourth concept was

7 June 1967

desirable but not necessary. There were no definite plans for testing the remaining four concepts.

As the final order of fabrication would indicate, the concept with the highest rankings did not necessarily receive the highest priority for fabrication and test. This situation resulted from a number of reasons. First, it should be realized that the ranking system was not intended as an absolute rule but instead was to serve only as a guide for establishing a priority. Furthermore, it was desirable to cover as broad a field as possible, and thereby extract a maximum amount of information from a limited number of tests. Finally, the affinity of the S-13 thermal control coating for dust made it desirable to test the shielded version of those devices involving dust removal by means of surface forces (jet and brush concepts). Those concepts employing body forces (vibrating and electrostatic) appeared less sensitive to the S-13 affinity for dust, and thus the unshielded version of these concepts was favored.

Chart 1

Basic Philosophy

1. Prevent dust accumulating
or
2. Remove accumulated dust

Chart 2

Available Forces

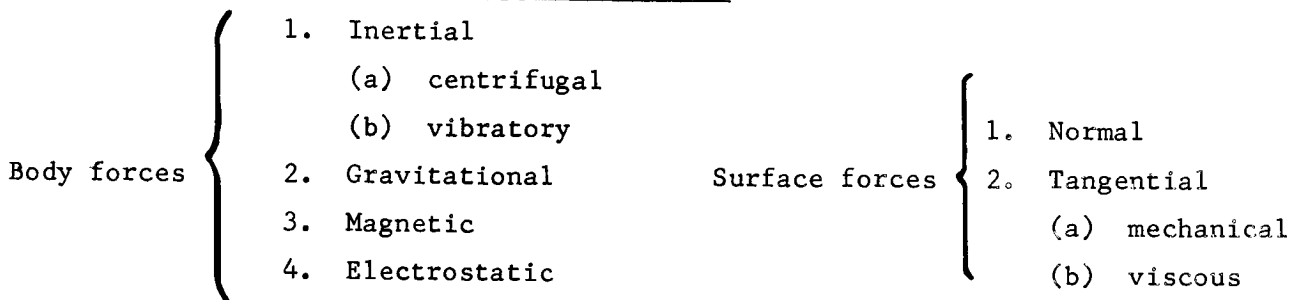


Chart 3

Concepts

<u>Device</u>	<u>Force Employed</u>
Brush	mechanical shear
Electrostatic Curtain	electrostatic
Electrostatic Surface	electrostatic
Jet and Shield	viscous shear
Jet and Surface	viscous shear
Spinning Shield	centrifugal
Vibrating Shield	vibratory
Vibrating Surface	vibratory

Chart 4

Experimental Factors*

<u>Factor</u>	<u>Weight</u>
Theoretically Sound	1.0
System Simulation	.9
State-of-the-Art	.9
Cost	.8
Environmental Simulation	.8
Ease of Measurements	.7
Simplicity	.6
Adaptability	.6
Ease of Fabrication	.5

Chart 5

Operational Factors (Equal Weight)*

Total Mass
Mass Expenditure
Power Requirements
Simplicity
Astronaut Maintenance

Operational Consideration (Equal Weight)**

Practicality
Reliability
Structural Integrity
Systems Compatibility
System Performance Improvements
Space Requirements
Cost

* For each device a grade from 1 to 10 is to be assigned pertaining to each factor.

** For each device, a grade of Excellent, Good, Fair, or Poor should be assigned relating to each consideration.

EXPERIMENTAL FACTORS

PERFORMANCE MATRIX

CONCEPTS	EXPERIMENTAL FACTORS									
	THEORETICALLY SOUND (1.0)	SYSTEM SIMULATION (.9)	STATE-OF-THE-ART (.9)	COST (.8)	ENVIRONMENTAL SIMULATION (.8)	EASE OF MEASUREMENTS (.7)	SIMPLICITY (.6)	ADAPTABILITY (.6)	EASE OF FABRICATION (.5)	GRADE
BRUSH	6	10	7	7	7	7	4	4	4	
	6.0	9.0	6.3	5.6	5.6	4.9	2.4	2.4	2.0	44.2
ELECTROSTATIC CURTAIN	9	9	8	8	7	7	3	4	4	
	9.0	8.1	7.2	6.4	5.6	5.6	1.8	2.4	2.0	48.1
ELECTROSTATIC SURFACE	8	8	3	8	10	7	6	8	6	
	8.0	7.2	2.7	6.4	8.0	4.9	3.6	4.8	3.0	48.6
JET & SHIELD	7	6	8	5	3	6	7	8	7	
	7.0	5.4	7.2	4.0	2.4	4.2	4.2	4.8	3.5	42.7
JET & SURFACE	7	7	10	8	3	7	9	9	8	
	7.0	6.3	9.0	6.4	2.4	4.9	5.4	5.4	4.0	50.8
SPINNING SHIELD	2	3	8	3	5	9	5	5	5	
	2.0	2.7	7.2	2.4	4.0	6.3	3.0	3.0	2.5	33.1
VIBRATING SHIELD	10	6	9	3	10	10	8	9	8	
	10.0	5.4	8.1	2.4	8.0	7.0	4.8	5.4	4.0	55.1
VIBRATING SURFACE	10	4	10	10	10	8	10	10	10	
	10.0	3.6	9.0	8.0	8.0	5.6	6.0	6.0	5.0	61.2

OPERATIONAL FACTORS

PERFORMANCE MATRIX

CONCEPTS	OPERATIONAL FACTORS					GRADE
	TOTAL MASS	MASS EXPENDITURE	POWER REQUIREMENTS	SIMPLICITY	ASTRONAUT MAINTENANCE	
BRUSH	8	10	2	3	2	25
ELECTROSTATIC CURTAIN	9	10	8	2	1	30
ELECTROSTATIC SURFACE	10	10	9	6	10	9
JET & SHIELD	1	5	10	8	10	34
JET & SURFACE	5	5	10	9	10	39
SPINNING SHIELD	2	10	3	5	3	23
VIBRATING SHIELD	3	10	5	8	7	33
VIBRATING SURFACE	6	10	7	9	7	39

Chart 8

OPERATIONAL CONSIDERATIONS

PERFORMANCE MATRIX

CONCEPTS	OPERATIONAL CONSIDERATION							GRADE
	PRACTICALITY	RELIABILITY	STRUCTURAL INTEGRITY	SYSTEM COMPATIBILITY	SYSTEM PERFORMANCE IMPROVEMENT	SPACE REQUIREMENTS	COST	
BRUSH	F	P	F	P	P	F	F	FAIR ⁻
ELECTROSTATIC CURTAIN	F	P	F	G	P	F	F	FAIR
ELECTROSTATIC SURFACE	G	E	E	G	P	E	E	GOOD ⁺
JET & SHIELD	G	E	G	E	G	F	G	GOOD
JET & SURFACE	G	E	E	G	P	G	E	GOOD
SPINNING SHIELD	P	F	P	E	G	F	P	FAIR
VIBRATING SHIELD	G	G	F	E	G	G	F	GOOD
VIBRATING SURFACE	P	G	P	P	P	E	G	FAIR

Chart 9

Operational Mass and Power Requirements Performance Matrix

Concepts	Mass Per Unit Area ($\frac{kg}{m^2}$)	Mass Expended Per Unit Area ($\frac{kg}{m^2}$)	Power Per Unit Area ($\frac{watts}{m^2}$)	Mass for Power Per Unit Area ($\frac{kg}{m^2}$)	Total Mass Per Unit Area ($\frac{kg}{m^2}$)
Brush	.478	0	29.066	.0462	.524
Electrostatic Curtain	.209	0	2.691	.00418	.213
Electrostatic Surface	.161	0	.1249 17.224	.000199 .0274	.161 .188
Jet & Shield	15.1	3.12	0	0	15.1
Jet & Surface	5.36	3.12	0	0	5.36
Spinning Shield	14.1	0	28.204	.0449	14.1
Vibrating Shield	13.7	0	19.377	.0308	13.7
Vibrating Surface	3.71	0	5.329	.00846	3.72

Chart 10

Summary of Matrix Results

CONCEPTS	PERFORMANCE STANDINGS			ORDER OF FABRICATION	
	EXPERIMENTAL FACTORS	OPERATIONAL FACTORS	OPERATIONAL CONSIDERATIONS	RECOMMENDED	APPROVED
BRUSH	6	6	8	4a*	3/6 **
ELECTROSTATIC CURTAIN	5	5	7	4	4
ELECTROSTATIC SURFACE	4	1	1	3	5
JET & SHIELD	7	3	3	2a*	2
JET & SURFACE	3	2	2	2	7
SPINNING SHIELD	8	7	5	5	---
VIBRATING SHIELD	2	4	4	1a*	---
VIBRATING SURFACE	1	2	5	1	1

* The letter "a" indicates an alternate selection

** The brush and shield are third in order while the brush and surface are sixth.

APPENDIX C

ORIGINAL TEST DATA FOR
DUST REMOVAL/PREVENTION DEVICES

7 June 1967

C.4 VIBRATING SURFACE DEVICE

Solar Simulator	Power (Watts)	S-13 Temp (°K)	Shield Temp (°K)	R/M	Condition
OFF	40	416	-	-.80	Clean
OFF	25	372	-	-.80	Clean
OFF	16	337	-	-.80	Clean
OFF	6	275	-	-.85	Clean
ON	40	431	-	2.05	Clean
ON	25	393	-	1.93	Clean
ON	16	365	-	1.91	Clean
ON	0	275	-	1.90	Clean
OFF	40	438	-	-.80	Dusted
OFF	25	370	-	-.80	Dusted
OFF	16	352	-	-.80	Dusted
ON	0	348	-	1.92	Dusted
ON	40	472	-	2.05	Dusted
ON	25	437	-	2.02	Dusted
ON	16	413	-	2.15	Dusted
OFF	50	447	-	-.82	Cleaned
OFF	40	422	-	-.80	Cleaned
OFF	29	390	-	-.82	Cleaned
OFF	20	359	-	-.77	Cleaned
ON	50	482	-	1.98	Cleaned
ON	40	462	-	1.98	Cleaned
ON	30	446	-	1.93	Cleaned
ON	20	415	-	1.95	Cleaned
OFF	40	417	-	-.79	Cleaned
OFF	32	395	-	-.80	Cleaned
OFF	25	372	-	-.80	Cleaned
ON	32	436	-	1.99	Cleaned
ON	23.5	419	-	1.95	Cleaned
ON	15	396	-	2.00	Cleaned

APPENDIX D

INDEX OF ENGINEERING DRAWINGS

CONTRACT NAS8-20116

<u>Drawing No.</u>	<u>Title</u>
T-23000	Shaft, Lower
T-23001	Adapter Support
T-23002	Head
T-23003	Upper Support Pincher
T-23004	Lower Support Pincher
T-23005	Shaft
T-23006	Holder (Sample)
T-23007	Train
T-23008	Shaft, Upper
T-23009	Coupling
T-23010	Locking, Plate
T-23011	Plate Motor Mount
T-23012	Hanger Bracket Lunar Dust Removal
T-23013	Head Leveler
T-23014	Shield Support
T-23015	Shaft Support
T-23016	Shield Holder
T-33000	Brush Holder
T-33001	Brush Track
T-33002	Brush Blank
T-33003	Motor Support Plate

INDEX OF ENGINEERING DRAWINGS (Concluded)

<u>Drawing No.</u>	<u>Title</u>
T-33004	Bracket Supports
T-33005	Brush Guide
T-33006	Shield
T-33007	Train Housing
T-33008	Mount Pedestal
T-33009	Sample Plate
T-43000	Base
T-43001	Brush
T-53000	Spray Nozzle
T-53001	Jet
T-53002	Lunar Dust Removal Vibrating Surface